

THE VASCULATURE AND IMMUNE SYSTEM
IN MODELS OF GLAUCOMA

By THOMAS F. SABLJIC, B.H.Sc. (HONOURS), M.Sc.

A Thesis Submitted to the School of Graduate Studies in Partial Fulfilment of the
Requirements for the Degree Doctor of Philosophy

McMaster University © Copyright by Thomas F. Sabljic June 2016

McMaster University DOCTOR OF PHILOSOPHY (2016) Hamilton, Ontario
(Neuroscience)

TITLE: The Role of the Vasculature and Immune System in Models of Glaucoma

AUTHOR: Thomas F. Sabljic, B.H.Sc. (Honours, McMaster University), M.Sc.
(McMaster University)

SUPERVISOR: Dr. Alexander K. Ball

NUMBER OF PAGES: xv, 206

LAY ABSTRACT

Glaucoma is a disease that affects the eyes, leading initially to the loss of parts of vision, and ultimately to blindness. The immune system and blood vessels (vasculature) play a role in glaucoma. Different animal models, surgical and genetic, of this disease will be used to study the involvement of the immune response and changes in the structure of the vasculature. Understanding how these affect the progress of disease can assist in the development of treatments that can prevent and/or reverse blindness. The immune system and vasculature do not play an important role early after optic nerve crush surgery. A genetic model with high pressure in the eye shows that the immune system plays an important role and that the structure of the vasculature changes late after injury. Understanding these changes can help create treatments for glaucoma to prevent the loss of vision from this disease.

ABSTRACT

Purpose: The purpose of this study was to investigate the role of the vasculature and immune system in models of glaucoma. Vascular changes have been implicated in glaucoma. As well there is mounting evidence that the immune system plays a role in the disease. It is my hypothesis that the vasculature and immune system play a role in the retinal response to injury in models of glaucoma.

Methods: Immunohistochemistry, *in vivo* retinal imaging (Bright field, fluorescent, optical coherence tomography), Slit2 injections and Evan's blue labeling were used to investigate vascular and immune changes associated with retinal ganglion cell death after optic nerve crush up to 28 days after injury. Histology, immunohistochemistry, and intravascular labeling were utilized to investigate the role of the vascular degeneration and the systemic immune response to elevated intraocular pressure in 8-16 week old AP-2 β Neural Crest Cell Knockout (AP-2 β NCC KO) mice.

Results: The vascular and immune responses to optic nerve crush were not found to play a significant role in the response to retinal ganglion cell death. Conversely the role of vascular degeneration and immune cell recruitment to the retinas of

AP-2 β NCC KO mice demonstrated that these factors played a significant role in the retinal response to injury.

Conclusion: The vasculature and immune system play a varied role in the response to retinal injury and neurodegeneration depending on the model being studied. The vascular and immune changes were of minimal significance in acute optic nerve crush injury. On the other hand, the chronic injury associated with elevated intraocular pressure in AP-2 β NCC KO mice was associated with significant vascular degeneration and systemic immune cell infiltration.

ACKNOWLEDGEMENTS

Thank you to Dr. Alexander Ball for supervising me. I would also like to acknowledge my supervisory committee members, Dr. Jane Foster and Dr. Elyanne Ratcliffe for their help and guidance.

I truly appreciate Dr. Judith West-Mays for supplying me with discarded mice as well as AP-2B Neural Crest Cell Knockout Mice and allowing me to perform experiments on her animals. I am very grateful for the help of Paula Deschamps, who helped me obtain these animals from the lab of Dr. West-Mays.

Thank you Dr. Lisa Robinson for providing me with reagents. Thank you to the Marta and Owen Boris Foundation (Hamilton, ON, Canada) for their generous donation of equipment (Phoenix Micron) that allowed me to perform *in vivo* imaging studies. I would also like to acknowledge Dr. Laurie Doering for allowing me to use the fluorescence microscope in his laboratory.

TABLE OF CONTENTS

LAY ABSTRACT	iii
ABSTRACT	v
ACKNOWLEDGMENTS	vi
TABLE OF CONTENTS	vii
LIST OF FIGURES	xi
LIST OF ABBREVIATIONS	xiv
DECLARATION OF ACADEMIC ACHIEVEMENT	xv
CHAPTER 1: INTRODUCTION	1
<i>1.1 Anatomy of the Eye and Retina</i>	1
<i>1.2 Retinal Glial Cells</i>	4
<i>1.3 Blood Supply of the Eye</i>	10
<i>1.4 Ocular Immune Privilege</i>	13
<i>1.5 Blood Brain Barrier</i>	15
<i>1.6 Blood Retinal Barrier</i>	16
<i>1.7 Glaucoma</i>	21
<i>1.8 Experimental Models of Glaucoma</i>	24
<i>1.9 Genetic Models of Glaucoma</i>	25
<i>1.10 The Immune System and Glaucoma</i>	28
<i>1.11 Slit2, Neuronal Guidance Cue and Immunomodulator</i>	31
<i>1.12 The Vascular Theory of Glaucoma</i>	33
<i>1.13 Vascular Changes Associated with Glaucoma</i>	35
<i>1.14 Figures</i>	39
CHAPTER 2: RATIONALE & HYPOTHESIS	44
2.1 Objective 1: To determine the role of the immune system and vasculature after optic nerve crush in mice	44
<i>2.1.1 Specific Aim 1: To determine the effect of Slit2 on retinal ganglion cell death after optic nerve crush</i>	45
<i>2.1.2 Specific Aim 2: To determine the role of vascular and systemic immune changes in the retinal response to optic nerve crush injury</i>	48
2.2 Objective 2: To determine the role of the immune system and vascular degeneration in the retina of AP-2β neural crest cell knockout mice (AP-2β NCC KO)	49
<i>2.2.1 Specific Aim 1: Characterization of retinal remodeling in the cohort of AP-2β NCC KO mice studied</i>	49
<i>2.2.2 Specific Aim 2: To determine the role of vascular degeneration in the retinas of AP-2β NCC KO mice</i>	50
<i>2.2.3 Specific Aim 3: To determine the role of the immune system in the retina of AP-2β NCC KO mice</i>	50

2.3 Objective 3: To determine the role of the optic nerve head in AP-2β NCC KO mice.....	51
2.3.1 <i>Specific Aim 1: To determine the structural changes associated with chronic elevated intraocular pressure.....</i>	51
2.3.2 <i>Specific Aim 2: To determine the glial reactions in the optic nerve head of AP-2β NCC KO mice.....</i>	51
CHAPTER 3: EXPERIMENTAL METHODS.....	53
3.1 The role of the vasculature and immune system after optic nerve crush in mice.....	53
3.1.1 <i>Animals.....</i>	53
3.1.2 <i>Optic Nerve Crush Injury.....</i>	53
3.1.3 <i>Slit2 Tail Vein Injections.....</i>	55
3.1.4 <i>Tissue Preparation.....</i>	55
3.1.5 <i>Brn-3a Whole Mount Immunohistochemistry.....</i>	55
3.1.6 <i>Whole Mounts.....</i>	56
3.1.7 <i>Evan's blue injection.....</i>	56
3.1.8 <i>Frozen Sections.....</i>	57
3.1.9 <i>Fluorescent Microscopy.....</i>	58
3.1.10 <i>In vivo Retinal Imaging.....</i>	58
3.1.11 <i>Acridine Orange Leukocyte Fluorography.....</i>	59
3.1.12 <i>Fluorescein Angiography.....</i>	59
3.2 The role of the immune system and vascular degeneration in the retina of AP-2β NCC KO mice.....	60
3.2.1 <i>Generation of AP-2β NCC KO Animals.....</i>	60
3.2.2 <i>Retinal Measurements.....</i>	60
3.2.3 <i>Brn3a Retinal Section Immunohistochemistry.....</i>	61
3.2.4 <i>Neurobiotin Labeling.....</i>	62
3.2.5 <i>Retro-orbital FITC-Dextran Injections.....</i>	63
3.2.6 <i>Tissue Processing.....</i>	63
3.2.7 <i>Capillary Measurement.....</i>	64
3.3 The role of the optic nerve head in AP-2β NCC KO mice.....	65
3.3.1 <i>Frozen Sections Through The Optic Nerve Head.....</i>	65
3.3.2 <i>Toluidine Blue Staining.....</i>	66
3.3.3 <i>Optic Nerve Head Measurements.....</i>	66
3.3.4 <i>Immunohistochemistry.....</i>	66
3.3.5 <i>Fluorescent Imaging.....</i>	68
3.3.6 <i>Image Analysis.....</i>	68
3.4 Statistical Analysis.....	68
3.5 <i>Figures.....</i>	69

CHAPTER 4: THE ROLE OF THE IMMUNE SYSTEM AND VASCULATURE AFTER OPTIC NERVE CRUSH IN MICE.....	72
<i>4.1 Results.....</i>	<i>72</i>
4A. The effect of Slit2 on retinal ganglion cell death after optic nerve crush.....	72
<i>4.1.1 Retinal ganglion cell density decreases over 28 days after optic nerve crush injury.....</i>	<i>72</i>
<i>4.1.2 Slit2 does not affect retinal ganglion cell survival 7 days after optic nerve crush.....</i>	<i>73</i>
4B. The role of vascular changes in the retinal response to optic nerve crush injury.....	74
<i>4.1.3 The retinal vasculature does not leak after optic nerve crush.....</i>	<i>74</i>
<i>4.1.4 The optic nerve vasculature leaks at the crush site after optic nerve crush.....</i>	<i>75</i>
<i>4.1.5. The area of the crush site does not change over 24 hours after optic nerve crush.....</i>	<i>76</i>
<i>4.1.6 The diameter of retinal arterioles and venules does not change after optic nerve crush.....</i>	<i>76</i>
<i>4.1.7 Retinal thickness does not change over 7 days after optic nerve crush...</i>	<i>77</i>
<i>4.1.8 Retinal blood flow is unaffected by optic nerve crush injury.....</i>	<i>77</i>
<i>4.1.9 Leukocyte speed does not change after optic nerve crush.....</i>	<i>77</i>
<i>4.2 Discussion.....</i>	<i>78</i>
<i>4.3 Figures.....</i>	<i>86</i>
CHAPTER 5: THE ROLE OF THE IMMUNE SYSTEM AND VASCULAR DEGENERATION IN THE RETINA OF AP-2β NCC KO MICE.....	106
<i>5.1 Results.....</i>	<i>106</i>
5A. Characterization of retinal remodeling in the cohort of AP-2β NCC KO mice studied.....	106
<i>5.1.1 Retinal remodeling in AP-2β NCC KO mice.....</i>	<i>106</i>
5B. The role of vascular degeneration in the retinas of AP-2β NCC KO mice.....	108
<i>5.1.2 Decreases in capillary area in AP-2β NCC KO mice.....</i>	<i>108</i>
<i>5.1.3 Changes in capillary diameter in AP-2β NCC KO mice.....</i>	<i>109</i>
<i>5.1.4 Changes in capillary density in AP-2β NCC KO mice.....</i>	<i>109</i>
<i>5.1.5 Changes in intercapillary distance in AP-2β NCC KO mice.....</i>	<i>110</i>
<i>5.1.6 Correlation between the thickness of the inner plexiform layer and intercapillary distance in the intermediate capillary plexus.....</i>	<i>111</i>
5C. The role of the immune system in the retina of AP-2β NCC KO mice.....	111
<i>5.1.7 Immune cells are adherent to vitreal surface of AP-2β NCC KO retinas</i>	<i>111</i>
<i>5.2 Discussion.....</i>	<i>112</i>
<i>5.3 Figures.....</i>	<i>121</i>

CHAPTER 6: THE ROLE OF THE OPTIC NERVE HEAD IN AP-2β NCC KO MICE.....	135
<i>6.1 Results.....</i>	135
6A: Structural changes in the optic nerve head of AP-2β NCC KO mice...	135
<i>6.1.1 Retinal thickness at the optic disc decreases in AP-2β NCC KO.....</i>	135
<i>6.1.2 The optic nerve is displaced below the level of the sclera in AP-2β NCC KO mice.....</i>	135
<i>6.1.3 The optic nerve head is excavated below the level of the sclera in AP-2β NCC KO mice.....</i>	136
6B: Glial reactivity in the optic nerve head of AP-2β NCC KO mice.....	136
<i>6.1.4 Iba-1 expression in the retinas and optic nerve head of AP-2β NCC KO mice.....</i>	136
<i>6.1.5 GFAP expression in the retinas and optic nerve head of AP-2β NCC KO mice.....</i>	137
<i>6.2 Discussion.....</i>	138
<i>6.3 Figures.....</i>	146
CHAPTER 8: CONCLUSION.....	158
REFERENCES.....	160

LIST OF FIGURES

Figure 1.1	Anatomy of the retina	39
Figure 1.2	Anatomy of the eye	40
Figure 1.3	Impairment of aqueous outflow leads to elevated intraocular pressure	41
Figure 1.4	The ocular gating system	42
Figure 1.5	The structure of Slit and Robo	43
Figure 3.1	Optic nerve crush results in the death of retinal ganglion cells	69
Figure 3.2	Generation of AP-2 β NCC KO mice	70
Figure 3.3	Quantification of optic nerve head changes	71
Figure 4.1	Whole-mounted retinas with immunohistochemical labeling of Brn3a	86
Figure 4.2	Retinal ganglion cell counts 7, 14, and 28 days after optic nerve crush	87
Figure 4.3	Percentage of retinal ganglion cell loss compared to uninjured animals over 28 days in three retinal sectors	88
Figure 4.4	Whole-mounted retinas were immunohistochemically labeled for Brn3a in the central, midperipheral, and peripheral retina.	89
Figure 4.5	Retinal ganglion cell counts (cells/mm ²) in the central, mid-peripheral, and peripheral retina	90
Figure 4.6	12 μ m thick frozen transverse retinal sections of mice intravenously injected with Evan's Blue (labeling in red) and perfused with PBS	91
Figure 4.7	Staining intensity in frozen transverse retinal sections of mice intravenously injected with Evan's Blue and perfused with PBS	92
Figure 4.8	Whole mounted retinas of mice intravenously injected with Evan's Blue (labeling in red) and perfused with PBS	93
Figure 4.9	Standardized staining intensity whole mounted retinas of mice intravenously injected with Evan's Blue and perfused with PBS	94
Figure 4.10	12 μ m thick frozen transverse optic nerve head sections of mice intravenously injected with Evan's Blue (labeling in red) and perfused with PBS	95
Figure 4.11	Staining intensity of the crush site of mice intravenously injected with Evan's Blue and perfused with PBS	96
Figure 4.12	Crush site area of mice intravenously injected with Evan's Blue and perfused with PBS	97
Figure 4.13	<i>In vivo</i> retinal imaging after optic nerve crush injury	98
Figure 4.14	Change in retinal arteriolar and venular diameter after optic nerve crush over 7 days measured using bright field retinal	

	microscopy.	99
Figure 4.15	Retinal thicknesses in the mid-periphery after optic nerve crush measured using optical coherence tomography.	100
Figure 4.16	Retinal fluorescein angiograms after optic nerve crush injury in mice.	101
Figure 4.17	Fluorescein fill time during retinal fluorescein angiography	102
Figure 4.18	Blood smear stained with acridine orange.	103
Figure 4.19	Images of acridine orange leukocyte fluorography after optic nerve crush injury	104
Figure 4.20	Leukocyte transit time after optic nerve crush injury	105
Figure 5.1	Retinal layer thicknesses in control and AP-2 β NCC KO retinas.	121
Figure 5.2	Nuclear density of the inner and outer nuclear layers in control mice and AP-2 β NCC KOs	122
Figure 5.3	Quantification of Brn3a cell density in control and AP-2 β NCC KO retinas	123
Figure 5.4	Fluorescent immune cells on the vitreal surface of the retina of controls versus AP-2 β NCC KOs	124
Figure 5.5	Quantification of fluorescent cells on the retinal surface	125
Figure 5.6	Fluorescent cells based on location on the retina.	126
Figure 5.7	Fluorescent cell density on the retinal surface of AP-2 β NCC KOs	127
Figure 5.8	DAPI labeled nuclei and FITC-Dextran filled blood vessels in control and AP-2 β NCC KO retinas	128
Figure 5.9	Whole mounts of retinas labeled intravascularly with FITC-Dextran in control and AP-2 β NCC KO mice.	129
Figure 5.10	Change in capillary plexus areas in control mice versus AP-2 β NCC KOs	130
Figure 5.11	Capillary diameter in the capillary plexuses of control versus AP-2 β NCC KO mice	131
Figure 5.12	Capillary density in the capillary plexuses of control versus AP-2 β NCC KO mice	132
Figure 5.13	Intercapillary distance in the capillary plexuses of control and AP-2 β NCC KO mice	133
Figure 5.14	Correlation between inner plexiform layer thickness and intercapillary distance in the intermediate capillary plexus	134
Figure 6.1	Toluidine blue staining of the optic nerve head in control and AP-2 β NCC KO mice.	146
Figure 6.2	Retinal thicknesses at the optic disc in control versus AP-2 β NCC KO mice	147
Figure 6.3	Tissue displacement from the sclera at the optic nerve head in control and AP-2 β NCC KO mice	148

Figure 6.4	Area of optic nerve head excavation below the level of the sclera in control and AP-2 β NCC KO mice	149
Figure 6.5	Iba-1 cell density in the retinas of AP-2 β NCC KO and control mice	150
Figure 6.6	Iba-1 fluorescence intensity in the retinas of control mice versus AP-2 β NCC KOs	151
Figure 6.7	Iba-1 fluorescence in the optic nerve heads of control and mice	152
Figure 6.8	Iba-1 cell density in the optic nerve head of AP-2 β NCC KO and control mice.	153
Figure 6.9	GFAP fluorescence intensity of the retinal ganglion cell layer in control versus AP-2 β NCC KO mice	154
Figure 6.10	GFAP expression in Müller cells in control mice versus AP-2 β NCC KOs	155
Figure 6.11	GFAP staining in the optic nerve head of control versus AP-2 β NCC KO mice	156
Figure 6.12	GFAP fluorescence intensity in the optic nerve head of control versus AP-2 β NCC KO mice	157

LIST OF ABBREVIATIONS

AP-2	Activating Protein-2
AREB	Animal Research Ethics Board
ARVO	Association for Research in Vision and Ophthalmology
CCAC	Canadian Council of Animal Care
GFAP	Glial Fibrillary Acidic Protein
HMVEC	Human Microvascular Endothelial Cell
HUVEC	Human Umbilical Vein Endothelial Cell
IBA-1	Ionizing Calcium-Binding Adaptor Molecule 1
PEDF	Pigment Epithelium Derived Growth Factor
NCC KO	Neural Crest Cell Knockout
RPE	Retinal Pigmented Epithelium
VEGF	Vascular Endothelial Growth Factor
ZO	Zonula Occludens

DECLARATION OF ACADEMIC ACHIEVEMENT

Vanessa Martino performed polymerase chain reaction to genotype all AP-2 β Neural Crest Cell Knockout mice and their control littermates.

The Neurobiotin labeling experiment was a collaborative experiment performed by Thomas Sabljic and Vanessa Martino. Thomas Sabljic performed all: anaesthesia of animals, enucleation, retinal/optic nerve dissection, and whole-mounting of retinas. Vanessa Martino applied the Neurobiotin tracer, performed the retinal fixation, incubation with fluorophore-conjugated Streptavidin, and all associated washes. The imaging and analysis of the particular data (leukocyte adhesion) presented in this study was also performed by Thomas Sabljic.

CHAPTER 1: INTRODUCTION

1.1 Anatomy of the Eye and Retina

The vertebrate eye is a complex organ used for vision. It collects light from the environment, converts the light into electrical signals, and transmits them to the brain through the optic nerve. The components of the eye arise from parts of the mesodermal and ectodermal layers in embryogenesis (Kivelä & Uusitalo, 1998). The mesoderm gives rise to the corneoscleral and uveal tunics, while the lens arises from the ectoderm (Oliver & Gruss, 1997). The retina is an extension of the central nervous system that originates from forebrain ectoderm (Oliver & Gruss, 1997). The evagination of the diencephalon gives rise to the optic vesicles that invaginate and form a bilayered optic cup (Lamb, Collin, & Pugh, 2007). The outer layer of the optic cup differentiates into the retinal pigmented epithelium after thinning into a monolayer of cells. While the inner layer is initially a monolayer, it proliferates into a neuroepithelium of multiple layers and proceeds to form the neural retina (Mey & Thanos, 2000).

The eye has an anterior and posterior segment (Smerdon, 2000) (**Figure 1.2**). The anterior segment is comprised of the cornea, lens, and iris (Smerdon, 2000). These structures control the amount of light entering the eye and focus light appropriately to form an image on the retina (Smerdon, 2000). Aqueous humor fills the anterior chamber of the eye and is separated from the posterior segment by the ciliary body and lens (Smerdon, 2000). Located behind the iris and in front of the suspensory ligament of the lens and ciliary processes is the

posterior chamber of the eye. The lens is a transparent and elastic biconcave disc that maintains its shape as a result of tension provided by the zonular fibres attached to the ciliary body (Smerdon, 2000). When the ciliary muscle in the ciliary body contracts, the tension on the zonular fibres is reduced, causing the lens to assume its more natural, spherical shape (Smerdon, 2000). The iris is located in front of the ciliary body and forms an angle with the cornea (Smerdon, 2000). The iridocorneal angle is also called the drainage angle (Gong, Tripathi, & Tripathi, 1996). Aqueous humor produced by the ciliary body flows from the posterior chamber between the lens and posterior iris, exiting the pupil to enter the anterior chamber (Gong et al., 1996). It travels towards the iridocorneal angle and through the spongy trabecular meshwork into Schlemm's canal to exit the eye into venous circulation (Gong et al., 1996).

The pupil is the central aperture through which light enters the eye is focused by the lens and projected to the posterior segment (Shastry, 1997). The structures located in the posterior segment of the eye are the retina, choroid, and sclera. The vitreous humor fills the space between the lens and the retina, maintaining the shape of the eye (Reddy & Kinsey, 1960). It is a transparent gelatinous mass that is comprised of mostly water (Reddy & Kinsey, 1960). Light travels through the vitreous humor to reach the retina (Shastry, 1997). The retina transduces the energy from light into an electrical signal that encodes visual information that is then conveyed to the brain (Shastry, 1997). The electrical signal from the retina travels via the optic nerve through four separate pathways.

These pathways are highly conserved among mammals and are the: central visual pathway (lateral geniculate nucleus) (Hickey & Spear, 1976), tectal pathway (superior colliculus) (Hayhow, Sefton, & Webb, 1962), retinohypothalamic pathway (hypothalamus) (Mason, Sparrow, & Lincoln, 1977), and pretectal pathway (nucleus of Edinger-Westphal) (Hayhow et al., 1962).

The retina is an organized multilayered structure consisting of three layers of neuronal and glial cell bodies that sandwich two synaptic layers (Malhotra, Minja, Crum, & Burrowes, 2011) (**Figure 1.1**). The innermost layers are the nerve fibre layer and retinal ganglion cell layer (Malhotra et al., 2011). Moving outwards are the inner plexiform layer, the inner nuclear layer, the outer plexiform layer, and the outer nuclear layer (photoreceptor nuclei) (Malhotra et al., 2011). The outer segments of the photoreceptors are associated with the retinal pigmented epithelium, the outermost layer of the retina (Malhotra et al., 2011). Lying between the retina and sclera is the choroid, the vascular layer of the eye (Malhotra et al., 2011).

The cells that make up the retina are neurons and glial cells. The five types of neurons in the retina are the photoreceptors, bipolar cells, horizontal cells, amacrine cells, and ganglion cells. The glial cells in the retina are the Müller cells, astrocytes, microglia. Oligodendrocytes are glial cells that myelinate the retinal ganglion cell axons in the optic nerve and are not seen in the retina, although exceptions exist in some species (Vecino, Rodriguez, Ruzafa, Pereiro, & Sharma, 2016). Glial cells are distinct from neurons in that they do not participate directly

in synaptic interactions and electrical signaling, but do provide supportive functions to maintain homeostasis, help to define synaptic contacts, and maintain neuronal signaling (Vecino et al., 2016). With regard to the functional connectivity of the retinal cells, the photoreceptors synapse with the processes of horizontal cells and bipolar cell dendrites in the outer plexiform layer (Palczewski, 2012). The somas of bipolar cells, horizontal cells, Müller cells, and amacrine cells comprise the inner nuclear layer (Palczewski, 2012). The inner plexiform layer is a synaptic network of amacrine cells and bipolar cells converging with the dendritic fields of retinal ganglion cells (Palczewski, 2012). The ganglion cell layer contains the cell bodies of retinal ganglion cells as well as amacrine cells (Palczewski, 2012). The axons of the retinal ganglion cells project through the nerve fibre layer towards the optic disc and into the optic nerve (Palczewski, 2012). Astrocytes are restricted to the nerve fibre layer and associate with retinal blood vessels (Nakahara, Mori, Kurauchi, Sakamoto, & Ishii, 2013). Müller cell basal end feet contribute to the inner limiting membrane of the retina (Berry, Ahmed, Lorber, Douglas, & Logan, 2008). Microglial cells are found in the ganglion cell layer, the inner plexiform layer, and the outer plexiform layer (Diaz-Araya, Provis, Penfold, & Billson, 1995).

1.2 Retinal Glial Cells

The idea of glial cells, as the cells making up the connective material of the brain between neurons, was first proposed by Rudolf Virchow in 1858

(Kettenmann & Verkhratsky, 2008). The retinal glia are multifunctional, adaptable cells that mediate normal retinal functions through close interactions with one another as well as retinal neurons (Chong & Martin, 2015). They play a role in the maintenance of the brain architecture, maintaining homeostasis, regulating neuronal communication, and nutrition (Vecino et al., 2016). Glia influence synaptic connectivity by controlling synaptic generation and maintenance as well as modulating the strength of synapses and plasticity (Vecino et al., 2016). They are also a source of progenitor cells in the brain (Vecino et al., 2016). Glial cells have intrinsic signalling systems that spread as Ca^{2+} waves and are correlated with the release of glutamate (Vecino et al., 2016). This signalling plays a role in immunity, angiogenesis, and neuroprotection (Vecino et al., 2016). Although glial cells initially respond to injury in an effort to restore homeostasis, their response can become such that it can be considered a primary pathogenic element (Vecino et al., 2016). More research is necessary to fully understand the important role of Müller cells, astrocytes, and microglia and their interactions with one another as well as neurons in the retina in both health and disease (Vecino et al., 2016).

Heinrich Müller first described the Müller cell as a radial fibre in the retina in 1851 (Kettenmann & Verkhratsky, 2008). It is now known that Müller cells are the predominant glial element, representing over 90% of glial cells, in the retina (Vecino et al., 2016). They are oriented radially, and cross the retina from its vitreal border through the layers to the distal end of the outer nuclear layer

(Vecino et al., 2016). The retina can be envisioned as a collection of functional units comprised of Müller cells and their immediate neighbouring retinal neurons (Reichenbach et al., 1993). Müller cells support the requirements of their neighbours and perform ionic, metabolic, and extracellular buffering to maintain stability in the retina (Vecino et al., 2016). There are a number of Müller cell characteristics that many species share in common. At the level of the external limiting membrane, Müller cells extend apical microvilli between the photoreceptor inner segments (Uga & Smelser, 1973). At the opposite end, Müller cells contribute to the inner limiting membrane by forming endfeet against the basal lamina that borders the vitreous body (Uga & Smelser, 1973). The lamellar processes of Müller cells ensheath the neuronal cell bodies and processes (Dreher, Robinson, & Distler, 1992; Hernández, Pearce-Kelling, Rodriguez, Aguirre, & Vecino, 2010; Reichenbach et al., 1988). Müller cells are involved in the structural organization of the inner blood retinal barrier by ensheathing retinal capillaries with their processes (Reichenbach et al., 1995). This close contact allows for metabolic exchange between the retinal vasculature and neurons (Sarthy & Ripps, 2002).

In response to almost all pathological challenges to the retina, Müller cells undergo reactive gliosis (Bringmann et al., 2009). Reactive gliosis is thought to be a result of a molecular cascade in response to signals received from injured or diseased retinal tissue (Fischer & Bongini, 2010). Features of Müller cell gliosis are cellular hypertrophy, increased rates of proliferation, loss of function,

inflammation, upregulation of intermediate filament expression, and tissue and vascular remodeling (Belecky-Adams, Chernoff, & Wilson, 2013).

The reactive gliosis observed in Müller cells is similar to the response to injury in astrocytes. Astrocytes are glial cells found in the inner retina as well as the major glial cell of the optic nerve head (Chong & Martin, 2015). The term astrocyte, in reference to the stellate morphology of the cells, was first used by Michael von Lenhossek in 1893 to name the cells previously seen in the nervous system by Camillo Golgi (Kettenmann & Verkhratsky, 2008). Astrocytic processes envelop blood vessels with no perivascular space between the adventitia of the vessels and the astrocytes (Hogan & Feeney, 1963; Hogan, Moschini, & Zardi, 1971). Astrocytes contribute structurally and participate in the maintenance of the inner blood-retinal barrier (Chan-Ling, 2006). Astrocytes play a role in ion homeostasis, participate in the uptake of neurotransmitters, and communicate by gap junctions (Newman, Frambach, & Odette, 1984; Ridet, Privat, Malhotra, & Gage, 1997). Glial fibrillary acidic protein (GFAP) is the predominant astrocytic intermediate filament and it is a reliable marker for the localization of astrocytes in the mammalian retina (Bignami, Eng, Dahl, & Uyeda, 1972). Studies of transgenic mice have revealed that GFAP plays a crucial role in the function of astrocytes under physiological as well as pathological conditions (Pekny & Nilsson, 2005). Quiescent astrocytes react to elevated intraocular pressure, ischemia, and excitotoxicity (Hernández, Urcola, & Vecino, 2008). When they become reactive, astrocytes hypertrophy, enlarge their soma, and develop thicker

processes (Vecino et al., 2016). GFAP immunoreactivity becomes enhanced in reactive gliosis and it is thought that these intermediate filaments help to maintain the mechanical integrity of the astrocytes themselves as well as the central nervous system tissue, but the understanding of this phenomenon is incomplete (Vecino et al., 2016). Astrocytes are implicated in retinal vascularization as they are the main producers of vascular endothelial growth factor (VEGF) during vessel formation under normal and pathological conditions (Ozaki et al., 2000; Stone et al., 1995). While astrocytes can be helpful in injury by providing neurotrophic support, mechanical support, and blood-retinal barrier maintenance, they can also be detrimental (Buffo, Rolando, & Ceruti, 2010). Astrocytes are able to express proteins that compromise the blood-retinal barrier, can promote retinal degeneration, and express genes encoding inflammatory mediators (Anderson, Hoyt, & Hogan, 1967; Kim et al., 2006).

The microglial cells fulfill the important role of controlling immune responses in the eye (Carson, Doose, & Melchior, 2006). In 1919, microglia were recognised as a separate cell type and glial cell by Pio del Rio-Hortega, who first suggested that they could migrate and act as phagocytes (Kettenmann & Verkhratsky, 2008). It is believed that the precursor cells of microglia are the primitive myeloid progenitors of the egg sac and not the bone marrow, although this is controversial (Ginhoux et al., 2010; Schulz et al., 2012). Microglia act as the resident macrophages in the central nervous system (Fernandes, Miller-Fleming, & Pais, 2014). They have immunological activity but also participate in

tissue homeostasis, as well as neural network development and maintenance (Gertig & Hanisch, 2014; Ransohoff & Brown, 2012). Microglia are differentiated histologically based on their ramified, process-bearing resting morphology, or amoeboid, rounded activated morphology (Streit, Walter, & Pennell, 1999; Zhang & Tso, 2003). Resting microglia are not inactive and are thought to be constantly screening central nervous system tissue, continually rebuilding and withdrawing their processes (Nimmerjahn, Kirchhoff, & Helmchen, 2005). Activation of microglia occurs when they sense a pathologic change in the retina and there are typically changes in cell morphology, size, number, cytokine and growth factor production as well as cell-surface molecule expression (Streit et al., 1999). Activated microglia can be helpful in injury and disease by clearing cellular debris, destroying invading pathogens, and promoting tissue repair (Kreutzberg, 1996). They can also be neurotoxic and exacerbate cell death by releasing nitric oxide, reactive oxygen species, and tumor necrosis factor-alpha (Hanisch & Kettenmann, 2007). Ionized calcium binding adaptor molecule-1 (Iba-1) is a common marker used to identify microglial cells (Ito et al., 1998). Iba-1 is a small EF hand protein consisting of 147 amino acids that functions as an adapter molecule mediating calcium signals and is upregulated in microglial activation (Ito et al., 1998). Understanding of the role of activated microglia in the pathogenesis of neurodegenerative diseases has increased and modulating their responses may be an effective therapeutic strategy (Ebnetter, Casson, & Wood, 2010).

1.3 Blood Supply of the Eye

The eye receives its arterial input from several branches of the ophthalmic artery, which is derived from the internal carotid artery (Kiel, 2011). The branches off the ophthalmic artery include the central retinal artery, the long and short posterior ciliary arteries, as well as the anterior ciliary arteries (Kiel, 2011).

The retina obtains its blood supply from the central retinal artery as well as the posterior ciliary arteries (Kiel, 2011). The central retinal artery travels in the optic nerve, piercing the sclera and branching to supply the inner layers of the retina (Kiel, 2011). Inner retinal vascularization varies among species (Kiel, 2011). In primates, the vasculature can be divided into four zones: an avascular zone at the fovea, the temporal region, a superonasal region, and a peripapillary region (Snodderly, Weinhaus, & Choi, 1992). Lagomorphs, small four-legged herbivorous vertebrates including rabbits, have a narrow band of superficial vessels, while rodents have a spoke-like arrangement. The inner retinal vessels are completely absent in guinea pigs (Kiel, 2011).

The retina is supplied by the choroid and the hyaloidal vessels during early eye development (Dorrell, Friedlander, & Smith, 2007). As the hyaloidal vasculature regresses and the retina thickens due to the final development and differentiation of the neuronal layers, a vascular system must develop to supply the hypoxic retina (Ritter et al., 2005). Mice are born with an avascular retina that fully vascularizes in the first few weeks of life (Ritter et al., 2005). Blood vessels

grow radially from the optic nerve head to the retinal periphery (Ritter et al., 2005). This process is analogous to human fetal retinal blood vessel development that occurs during the third trimester of gestation (Hughes, Yang, & Chan-Ling, 2000). There are three parallel planar vascular networks that develop within different layers of the retina over time. These are the superficial plexus within the ganglion cell layer during the first week following birth, the intermediate plexus at the inner edge of the inner nuclear layer by the second week after birth, and the deep plexus at the outer edge of the inner nuclear layer by the third week after birth (Dorrell, Aguilar, & Friedlander, 2002). These retinal vessels supply the inner two thirds of the retina and the outer third is nourished by the choroidal circulation that lies beneath the retina (Ritter et al., 2005).

Six to twelve short posterior ciliary arteries enter the sclera around the optic nerve and branch to form the arterioles of the dense outer layer of choroidal conduit vessels (Kiel, 2011). These arterioles give rise to terminal arterioles supplying lobules of the choriocapillaris comprising the layer of choriocapillaris adjacent to Bruch's membrane, the retinal pigmented epithelium, and the photoreceptor outer segments. The lobules of the choriocapillaris drain into venules that enter the outer conduit layer, coalescing into the four to five vortex veins piercing the sclera at the equator (Kiel, 2011).

The vascular supply of the optic nerve supplies three zones that are delineated by their location with reference to the lamina cribosa (Kiel, 2011). The prelaminar region of the optic nerve receives its blood supply by collateral vessels

from the choroid and retinal circulations (Kiel, 2011). The laminar zone receives blood from the short posterior ciliary and pial arteries (Kiel, 2011). The posterior laminar zone is supplied by the pial arteries (Kiel, 2011). The lamina cribrosa demarcates the transition of blood vessel exposure from intraocular pressure to the cerebral fluid pressure within the optic sheath (Hayreh, 1978).

The ciliary body and iris are nourished by the anterior ciliary arteries, the long posterior ciliary arteries, and anastomoses from the anterior choroid (Kiel, 2011). The anterior ciliary arteries follow the extraocular muscles and pierce the sclera to reach the major arterial circle of the iris. The long posterior ciliary arteries penetrate the sclera near the posterior pole of the eye and travel anteriorly between the sclera and choroid to join the major arterial circle of the iris (Kiel, 2011). The major arterial circle of the iris branches to supply the iris and ciliary body (Kiel, 2011).

Venous outflow from the eye is accomplished primarily by the vortex veins that merge with the superior and inferior ophthalmic veins, draining into the cavernous sinus, the pterygoid venous plexus and the facial vein (Kiel, 2011). In rodents, the orbital veins form a sinus (Kiel, 2011).

Autonomic innervation of the ocular vasculature is restricted to uveal blood vessels (choroid, ciliary body, and iris) and optic nerve (Ehinger, 1966; Ye, Laties, & Stone, 1990). Parasympathetic innervation originates from the pterygopalatine ganglion. The sympathetic nerves originate from the superior cervical ganglion. The retina lacks sympathetic and parasympathetic innervation

(Laties, 1967). A network of ganglion cells, similar to the enteric nervous system in the gut, has been identified in the choroid of primates and some birds species, but the functional significance of this network is not understood (Lütjen-Drecoll, 2006; May & Lütjen-Drecoll, 2004).

1.4 Ocular Immune Privilege

Immune privilege was discovered when allogeneic skin grafts were placed into the anterior chamber of the eye and the brains of rabbits (Medawar, 1948). While skin grafts placed at other body sites, including the skin, were rejected, grafts in the eye and the brain survived for long periods of time after placement (Medawar, 1948). Leukocytes perform constant immunological surveillance and are recruited to tissue when needed (Ley, Laudanna, Cybulsky, & Nourshargh, 2007). Several tissues such as the brain, eye, testis, and implanted uterus are considered immune-privileged sites (Shechter, London, & Schwartz, 2013). Immune privilege was initially thought to exist as a restrictive blockade of leukocyte entry into tissue through physical barriers (Shechter et al., 2013). Immune privilege is now envisioned as an active process facilitating immune tolerance and ignorance at privileged sites (Shechter et al., 2013). In immune-privileged sites, transplanted foreign organs and tissues survive for prolonged, or indefinite periods of time (Streilein, 2003). Non-privileged tissues result in the acute rejection of foreign tissue (Streilein, 2003). Allogeneic tumour cell implants into the anterior chamber of the eye, the vitreous cavity, and the subretinal space

result in progressive tumour growth, whereas they would normally be rejected at non-privileged sites (Hazlett & Stein-Streilein, 2012).

The visual axis of the eye precisely focuses light on the retina (Streilein, 2003). It is very delicate and would be distorted by inflammatory processes (Streilein, 2003). Distortion of the visual axis and the loss of ocular cells causes blindness (Streilein, 2003). Ocular immune privilege provides the eye with immunological protection that poses the smallest risk to the integrity of vision (Streilein, 2003). The eye and the immune system achieve ocular immune privilege using a number of separate but related strategies to modify immune responses in the eye (Streilein, 2003). These include the development of an immunosuppressive intraocular microenvironment, immunological ignorance, and peripheral tolerance of antigens derived from the eye (Streilein, 2003). Blood-ocular barriers are not completely impenetrable, so innate and adaptive immune cells and molecules are able to enter the internal compartments of the eye (Streilein, 2003). The eye has soluble and membrane-bound immunomodulatory factors that suppress the cellular and molecular mediators of innate and adaptive inflammatory immune responses (Streilein, 2003). Aqueous humor contains neuropeptides, cytokines, growth factors, and soluble cell-surface receptors that modulate immune activity (Taylor, 2007). Although the ocular microenvironment acts to dampen destructive immune responses, physical barriers act to prevent breaches by pathogens into the central nervous system (Kim et al., 2006).

1.5 Blood Brain Barrier

In 1885 Paul Ehrlich first described the concept of the blood brain barrier when he noticed that the peripheral injection of water soluble dyes did not result in the staining of the brain or cerebrospinal fluid (Ehrlich, 1885). In 1913 Goldman injected trypan blue intravenously and observed staining of all tissues except the brain. While these animals survived, those animals injected directly into the subarachnoid space with a small amount of trypan blue died in a few minutes after having convulsions (Cunha-Vaz, 1976). The rates of exchange and concentrations of many substances in the brain are different when compared to other organs as a result of the distinct differences in permeability at the blood-brain interface (Cunha-Vaz, 1976). The blood-brain barrier effectively protects the brain from pathogens while allowing the entry of essential nutrients (Nag, 2011). This is accomplished by the selectivity of tight junctions between vascular endothelial cells in the central nervous system (Balda et al., 1991). A similar barrier function in the retina was described by Schnaudigel (1913) and Palm (1947) who repeated Goldman's experiments but their work did not impact ophthalmic literature until 1965. Ashton and Cunha-Vaz examined the permeability of the blood vessels to histamine in the eye and discovered that it increased the vascular permeability of various ocular tissues except the retina. This finding suggested the existence of a barrier in the retina similar to the blood-brain barrier and was it confirmed by studying the penetration of a variety of substances into the retina and vitreous (Cunha-Vaz, 1976). The blood-retinal

barrier is now regarded as a critical factor in the development of retinal vascular disease as well as macular pathology (Cunha-Vaz, 1976).

1.6 Blood Retinal Barrier

The blood retinal barrier (**Figure 1.4**) plays an important role in the regulation of the retinal microenvironment (Kaur, Foulds, & Ling, 2008). An intact blood-retinal barrier is critical for normal vision as its breakdown results in clinical conditions where vision is affected adversely (Kaur et al., 2008). The blood retinal barrier is comprised of inner and outer components, preventing the leakage of macromolecules and potentially harmful agents and regulating the movement of fluid and molecules between the ocular vascular beds and retinal tissue (Kaur et al., 2008).

Tight junctions between adjacent capillary endothelial cells form the inner blood-retinal barrier. The endothelial cells rest on a basal lamina that is covered by the foot processes of Müller cells and astrocytes. Pericytes are found separated from the endothelial cells by the basal lamina. The astrocytes, Müller cells, and pericytes are all believed to contribute to the function of the inner blood retinal barrier. The blood vessels in the retina are distributed into the superficial, intermediate, and deep plexuses. The endothelial cells of the retinal capillaries lack fenestrations and have few vesicles (Bernstein & Hollenberg, 1965). The paucity of vesicles in the retinal capillary endothelium is thought to contribute to the inner blood-retinal barrier integrity (Sagaties Farmer, Schwartz, & Takamoto,

1997) as increases in endocytic vesicle formation occur in pathological inner blood-retinal barrier disruption (Vinores, Derevjanić, Ozaki, Okamoto, & Campochiaro, 1999). Fusion of the outer leaflets of adjacent endothelial cell membranes form the tight junctions of the retinal vascular endothelium (Sagaties, Raviola, Schaeffer, & Miller, 1987). The interendothelial space is obliterated by the tight junction, conferring selective barrier properties upon the retinal capillaries (Kaur et al., 2008). Molecular diffusion from the vascular lumen into the tissue is extremely restricted by the retinal vascular endothelial tight junctions (Sagaties et al., 1987). The tight junctions are composed of the zonula occludens 1-3 (ZO-1, ZO-2, ZO-3), cingulin, 7H6 antigen, occludin, symplekin (Mitic & Anderson, 1998), claudins (Furuse, Fujita, Hiiragi, Fujimoto, & Tsukita, 1998), and cadherin-5 (Russ, Davidson, Hoffman, & Haselton, 1998). ZO-1, ZO-2, and ZO-3, symplekin, 7H6 and cingulin are proteins that organize the tight junction and are located in the cytoplasm (Kaur et al., 2008). The absence of ZO-1 immunoreactivity in retinal blood vessels indicates a disruption of the tight junction (Dallasta et al., 1999). The flow of vascular fluid is regulated by occludin and claudin (Kaur et al., 2008). Cell-cell adhesion of neighbouring cells is maintained by the transmembrane glycoproteins of the cadherin superfamily (Petty & Lo, 2002). Pericytes are phagocytic cells that play an important role in the retinal vasculature regulating vascular tone, supporting the capillary wall, and secreting extracellular molecules (Shepro & Morel, 1993; Sims, 1991). The ratio of pericytes to vascular endothelial cells, 1:1 in humans, is greater than in any

other bed of vasculature (Balabanov & Dore-Duffy, 1998). In many animal models, pericyte coverage of retinal capillaries has been reported to be more extensive than in the cerebral cortex (Frank, Turczyn, & Das, 1990).

Müller cells are closely associated with retinal blood vessels, playing an important role in the formation and upkeep of the blood-retinal barrier, the absorption of nutrients, and the clearance of metabolites (Distler & Dreher, 1996; Tout, Chan-Ling, Holländer, & Stone, 1993). Müller cells support neuronal activity (Reichenbach et al., 2007), are involved in the control and homeostasis of ions, signaling molecules, and in the regulation of extracellular pH (Bringmann et al., 2000). Dysfunction of Müller cells is associated with blood-retinal barrier break down in pathological conditions including diabetes (Tretiach, Madigan, Wen, & Gillies, 2005). Whereas Müller cells secrete pigment epithelium derived growth factor (PEDF) under normal conditions, in conditions of hypoxia and inflammation Müller cells enhance vascular endothelial growth factor (VEGF) secretion (Eichler, Kuhrt, Hoffmann, Wiedemann, & Reichenbach, 2000; Kaur, Sivakumar, & Foulds, 2006). PEDF antagonizes the action of VEGF (Eichler et al., 2001), which has been showed to increase vascular permeability in nearly all of the tissues in the body (Kaur et al., 2008). PEDF expression decreases in hypoxic conditions resulting in a rise of VEGF production and a consequent increase in vascular permeability (Duh et al., 2002). Matrix metalloproteinase production by Müller cells can impair blood-retinal barrier function (Tretiach et

al., 2005), as these enzymes result in the proteolytic destruction of the tight junction protein occludin (Giebel, Woenckhaus, Fabian, & Tost, 2005).

Astrocytes migrate to the nerve fibre layer from the optic nerve during development (Watanabe & Raff, 1988) and closely associate with the retinal vessels (Schnitzer, 1987), helping to maintain their structural integrity (Zhang & Stone, 1997). Astrocytes enhance the expression of the tight junction protein ZO-1 and modify endothelial morphology, increasing the barrier properties of the retinal vascular endothelium (Gardner, 1995). Contact between astrocytes and blood vessels has been shown to play a primary role in the expression of occludin, claudin-5, and ZO-1 in the vasculature of the brain *in vivo* (Willis, Leach, Clarke, Nolan, & Ray, 2004). Astrocytic dysfunction has been reported to play a crucial role in the breakdown of the inner blood retinal barrier and the production of vasogenic oedema (Chan-Ling & Stone, 1992; Gardner et al., 1997; Rungger-Brändle, Dosso, & Leuenberger, 2000). Breakdown of the inner blood-retinal barrier has been demonstrated in cases of acute distension of the vessel wall, ischemia, biochemical influences, inflammation, defects in endothelial membrane, and the failure of organic anion active transport (Cunha-Vaz, 1976).

The outer blood-retinal barrier is formed by tight junctions between the retinal pigmented epithelial cells (Cunha-Vaz, 1976). The retinal pigmented epithelium rests upon Bruch's membrane, separating the neural retina from the choriocapillaris (Kaur et al., 2008). Occludin-1, claudins, and ZO-1 have been reported at the tight junctions between adjacent retinal pigmented epithelial cells

(Tserentsoodol, Shin, Suzuki, & Takata, 1998; Williams & Rizzolo, 1997). The retinal pigmented epithelium (RPE) plays an important role in transporting nutrients from the blood to the outer retina (Kaur et al., 2008). There is both transcellular and paracellular molecular movement across the retinal pigmented epithelium (Kaur et al., 2008). The transport of substances outward from the subretinal space consists of hydrostatic and osmotic forces moving small molecules through the paracellular inter-RPE cellular clefts, and active transport transcellularly (Pederson, 2006). The tight junctions between epithelial cells restrict the paracellular movement of larger molecules (Kaur et al., 2008). The tight junctions of the retinal pigmented epithelium are attached to the actin cytoskeleton of retinal pigmented epithelial cells, interacting with cellular signaling molecules and establishing cellular polarity (Tsukita, Furuse, & Itoh, 2001). The polarized asymmetrical distribution of the RPE membrane proteins is plastic, varying with environmental changes (Drubin & Nelson, 1996; Eaton & Simons, 1995) and contributing to the outer blood-retinal barrier (Rizzolo, 1997; Rodriguez-Boulan & Nelson, 1989). Local environmental factors also affect the permeability of the retinal pigmented epithelium by causing structural and functional changes in the tight junctions. For example, the tight junctions of the RPE are affected by diffusible factors such as hepatocyte growth factor (HGF) from the outer retina or the RPE (Balda et al., 1991). The structure and function of tight junctions can be modified by the presence of HGF from the RPE (Jin, Barron, He, Ryan, & Hinton, 2002). HGF overexpression results in blood-retinal

barrier breakdown and chronic retinal detachment (Jin, Chen, He, Ryan, & Hinton, 2004).

The circulation of blood in the fenestrated capillaries of the choriocapillaris nourishes the outer layers of the retina. To facilitate this function there is a large movement of molecules in a baso-apical direction from the choroid to the retina (Kaur et al., 2008). Retinal metabolic waste products in the subretinal space, localized between the retina and the retinal pigmented epithelium, are transported in an apico-basal direction towards the choroid (Kaur et al., 2008). Breakdown of the outer blood retinal barrier is observed in ischemia, mechanical distension of the pigmented epithelium layer, defective pigment epithelium, inflammation, and failure of the active transport system (Do Carmo, Ramos, Reis, Proenca, & Cunha-Vaz, 1998).

1.7 Glaucoma

Glaucoma is the leading cause of blindness worldwide (Tham et al., 2014). Over 111.8 million people are expected to be affected by 2040 with a disproportion in prevalence predominantly affecting populations in Asia and Africa (Tham et al., 2014). Approximately half of individuals with glaucoma are unaware of their affliction because irreversible damage precedes the perception of visual deficits (Liesegang, 1996). The deterioration or loss of any of the senses can result in a decrease in quality of life, but the loss of vision can be particularly

devastating, making the accomplishment of the activities of daily living and self-care difficult or impossible without assistance.

Glaucoma is a chronic, multifactorial group of ocular disorders that are united by clinically characteristic optic neuropathy related to intraocular pressure (Casson, Chidlow, Wood, Crowston, & Goldberg, 2012). The optic neuropathy leads to thinning of the neuroretinal rim and visible enlargement of the optic cup (Casson et al., 2012). These changes occur as a result of the death of retinal ganglion cells and deformation of the lamina cribosa (Casson et al., 2012). Initial defects in specific visual fields may not be detectable, but the disease can be progressive, ultimately leading to complete blindness (Casson et al., 2012). Increased intraocular pressure, age, race, and genetics are all risk factors for glaucoma (Quigley & Broman, 2006). Intraocular pressure is the only modifiable risk factor and is the focus of clinical therapeutic strategies (Quigley & Broman, 2006). Treatment focuses on the prevention of further vision loss, but the ultimate goal is to rescue injured retinal ganglion cells, encourage the re-establishment of functional connections to the brain, and restore lost vision (Moore & Goldberg, 2010).

Glaucoma is comprised of a family of diseases resulting in the death of retinal ganglion cells that have been categorized according to the origin of, and specific characteristics associated with the disease. These types include developmental glaucomas, primary open-angle glaucoma, normal tension/pressure glaucoma, secondary open-angle glaucoma, primary angle-closure glaucoma, and

secondary angle-closure glaucoma. Developmental glaucomas arise congenitally and will be discussed in detail later. Open-angle and angle-closure refer to the appearance of the iridocorneal angle (**Figure 1.3**). Where an open-angle allows for the unobstructed flow of aqueous humor out of the eye, angle closure refers to an obstruction of the flow of aqueous humor caused by iridotrabeular contact that leads to an elevation of intraocular pressure. Primary open-angle glaucoma is a singular subtype of glaucoma with an open angle and an unknown etiology if intraocular pressure is found to be elevated. Normal-tension glaucoma is a subtype of primary open-angle glaucoma where elevated intraocular pressure is never observed (Casson et al., 2012). The existence of normal-tension glaucoma as a disease entity separate from primary open-angle glaucoma is disputed (Wilson, 1997). Secondary open-angle glaucoma refers to collective conditions where the iridocorneal angle is unobstructed, but intraocular pressure is elevated and the cause of this elevation is known (Casson et al., 2012). Primary angle-closure glaucoma is one subtype of glaucoma with confirmed iridotrabeular contact and elevated intraocular pressure (Casson et al., 2012). Secondary angle-closure glaucoma is a collective subtype of glaucoma where iridotrabeular contact arises from pathological mechanisms not associated with anatomical predisposition and intraocular pressure is elevated (Casson et al., 2012). The commonality among these conditions is the cupping of the optic nerve head, thinning of the neuroretinal rim, and loss of vision (Quigley, 1999). Aside from

these signs, there is variability in the presentation of individual patients (Quigley, 1999).

1.8 Experimental Models of Glaucoma

There are a variety of experimental models of glaucoma (Goldblum & Mittag, 2002). Each of these models has its limitations because glaucoma is predominantly a disease associated with old age in humans (Goldblum & Mittag, 2002). This significant time and expense associated with aging animals has led to the creation of experimental models that cause optic nerve injury or accelerate the death of retinal ganglion cells. These models include ischemia/reperfusion injury (Hayreh & Weingeist, 1980), excitotoxic damage (Sisk & Kuwabara, 1985), a variety of methods to experimentally elevate intraocular pressure (Laquis, Chaudhary, & Sharma, 1998; Morrison et al., 1997), *in vitro* neural injury studies (Levin, 2001), and optic nerve axotomy or crush injury (Berkelaar, Clarke, Wang, Bray, & Aguayo, 1994).

Optic nerve axotomy or crush is a relatively simple procedure compared to other models, involving the direct surgical lesion of the optic nerve using forceps. The advantages of this model are a shortened timecourse and specific and widespread retinal ganglion cell loss (Berkelaar et al., 1994). Optic nerve axotomy or transection results in the death of 90% of retinal ganglion cells within 2 weeks of injury (Koeberle & Ball, 1998). Optic nerve crush results in a slower timecourse of death compared to axotomy, but in both of these acute injury

models, retinal ganglion cells degenerate and die by apoptosis (Garcia-Valenzulela, Gorczyca, Darzynkiewicz, & Sharma, 1994). Data collected from acute optic nerve injury models provide insight into the mechanisms associated with cell death in glaucoma as well as other traumatic injuries in the central nervous system (Duvdevani et al., 1990).

1.9 Genetic Models of Glaucoma

A number of genetic models of glaucoma have been developed over the years. Many forms of glaucoma are associated with a defined genetic component (Wiggs, 2013). Specific genes have been identified for primary-open angle glaucoma (Stone et al., 1997), normal tension glaucoma (Rezaie et al., 2002), and developmental glaucomas (Gould & John, 2002). For example, primary open-angle glaucoma models include modifications of genes known to cause primary open-angle glaucoma in humans including myocilin, connective tissue growth factor, and optineurin (Junglas et al., 2012; Liu & Vollrath, 2004; Rezaie et al., 2002). There are also models of primary angle-closure glaucoma including those that involve changes in the expression of guanine nucleotide exchange factors for Rho guanosine triphosphatases and the glaucoma relevant mutant 4 gene (Fujikawa et al., 2010; Nair et al., 2011).

One extensively studied genetic model of glaucoma involves pigmentary dispersion in the anterior chamber of the eye. The DBA/2 lineage of mice that includes DBA/2J (Anderson, Smith, Hawes, et al., 2001a; Chang et al., 1999;

John et al., 1998; Mo et al., 2003), DBA/2NNia (Bayer et al., 2001; Danias et al., 2003; May & Mittag, 2004), and AKXD-28/TyJ (Anderson, Smith, Savinova, et al., 2001b) mice that all develop age-related forms of glaucoma. These mice develop iris disease, an elevation in intraocular pressure, and retinal ganglion cell loss (Wiggs, 2013). Eyes of DBA/2J resemble human pigment dispersion syndrome and pigmentary glaucoma and are useful models for these conditions. It has been determined that the glaucomatous iris disease of DBA/2J results from a digenic interaction of mutations in *Tyrp1* and *Gpnmb*, two genes encoding for melanosomal proteins (Lynch, Yanagi, DelBono, & Wiggs, 2002). The association of mutations in human *GPNMB* and *TYRP1* and inherited glaucomatous conditions remains to be accomplished (Anderson, Smith, Hawes, et al., 2001a; Lynch et al., 2002).

Developmental glaucomas are associated with malformations of the anterior segment of the eye (Gould & John, 2002). Multiple tissues including the iris, cornea, lens, Schlemm's canal and trabecular meshwork may be affected by anterior segment dysgenesis (Gould & John, 2002). Although primary congenital glaucoma is not traditionally classified as an example of anterior segment dysgenesis, it does involve abnormal development of the drainage structures in the anterior segment of the eye (Gould & John, 2002). The abnormalities observed in anterior segment dysgenesis are believed to result from primary defects in the migration and/or differentiation of the mesenchymal cells that are involved in the proper development of the cornea, iris, and drainage structures

(Kupfer & Kaiser-Kupfer, 1977; Kupfer & Kaiser-Kupfer, 1979; Trainor & Tam, 1995). Given the importance of the lens in anterior segment formation, the developmental abnormalities in anterior segment dysgenesis may also result from primary defects in the lens (Jamieson et al., 2002).

Severe anterior segment dysgenesis results in readily apparent phenotypes including iris hypoplasia, irregular and misplaced pupils, hazy corneas, and adhesion of the iris to the cornea (Gould & John, 2002). These phenotypic abnormalities can result in impediments to vision, cosmetic irregularities, and subsequent psychological consequences (Gould & John, 2002). Historically, physicians have distinguished anterior segment dysgenesis into subtypes based on the clinical phenotype presented by patients (Gould & John, 2002). These subtypes have included Axenfeld's anomaly, Rieger's anomaly, aniridia, iridogoniodysgenesis, Peter's anomaly, and posterior embryotoxon (Gould & John, 2002). This classification based on phenotype may be inappropriate given that these anomalies, such as misplaced pupils, vary significantly between patients, and even among patients in the same family (Gould & John, 2002). It is now understood that these disorders exist as part of a spectrum of expressivity of disease phenotypes (Alward, 2000; Shields, Buckley, Klintworth, & Thresher, 1985; Waring, Rodrigues, & Laibson, 1975).

Factors such as mutations in different genes, allelic heterogeneity, and genetic modifiers that differ between patients are believed to contribute to phenotypic variability and incomplete penetrance (Gould & John, 2002). Several

genes (PAX6, PITX2, PITX3, FOXC1, EYA1, CYP1B1, LMX1B, and MAF) are known to cause anterior segment dysgenesis in humans (Ito & Walter, 2013).

More genes are thought to be involved as some families of genes show linkage to other loci and some patients do not have mutations in any of the genes known to be associated with anterior segment dysgenesis (Ito & Walter, 2013).

AP-2 β neural crest cell knockout (AP-2 β NCC KO) mice exhibit anterior segment dysgenesis (Martino et al., 2016). One observed change in the anterior chamber is the adherence of the iris to the cornea (Martino et al., 2016). This disrupts the iridocorneal angle and is likely to impede the outflow of aqueous humor. Such an obstruction of the aqueous outflow pathway is expected to lead to elevations in intraocular pressure (Mao, Hedberg-Buenz, Koehn, John, & Anderson, 2011). Using a TonoLab Rebound tonometer the mutant mice were shown to have a significantly higher IOP than their littermate controls (Martino et al., 2016). Raised intraocular pressure is one of the main risk factors in glaucoma (Quigley & Broman, 2006) and these animals were expected to have retinal ganglion cell loss. Indeed, mutants had a significant loss of retinal ganglion cells compared to control animals (Martino et al., 2016). The AP-2 β NCC KO mouse is thus a novel model of closed angle glaucoma that warrants further study.

1.10 The Immune System and Glaucoma

Evidence has accumulated to suggest the involvement of immune system regulation in the events leading to glaucomatous optic nerve degeneration (Tezel

& Wax, 2004). Retinal cells and glia respond early to glaucomatous insults (Soto et al., 2008). Astrocytes become enlarged and upregulate cytoskeletal proteins as well as extracellular matrix proteins in both the retina and optic nerve head in human glaucoma (Nikolskaya et al., 2009; Wang, Cioffi, Cull, Dong, & Fortune, 2002). Studies in experimental glaucoma models have demonstrated that these changes occur in the early stages of disease, before retinal ganglion cell axon damage (Qu & Jakobs, 2013). Just a short term elevation of intraocular pressure results in rapid and reversible changes in astrocyte morphology in the optic nerve head (Sun, Qu, & Jakobs, 2013). The upregulation of extracellular matrix proteins may function to prevent damage to the blood-retinal barrier in response to intraocular pressure induced damage (Sofroniew & Vinters, 2010). The inhibition of reactive gliosis by the conditional deletion of signal transducer and activator of transcription 3 protein results in the massive infiltration of leukocytes after spinal cord injury (Herrmann et al., 2008). This is accompanied by increased neurodegeneration suggesting astrocytes play an important protective role in response to damage in the central nervous system (Herrmann et al., 2008). On the other hand, the overexpression of integrins by astrocytes may promote the adhesion and migration of leukocytes into the damaged optic nerve head (Tanigami, Okamoto, Yasue, & Shimaoka, 2012). As well, tenascin-C, that supports proinflammatory responses, is upregulated in astrocytes in human glaucoma as well as experimental models (Midwood et al., 2009). This suggests

that glaucomatous damage can elicit both helpful and destructive inflammatory responses from astrocytes (Soto et al., 2008).

Microglial activation in the retina and optic nerve head plays a role in the response to injury in experimental models of glaucoma (Bosco, Steele, & Vetter, 2011; Taylor, Calder, Albon, & Erichsen, 2011). The response is characterised by an increase in proliferation, changes in morphology, and increased phagocytic activity (Ebnetter et al., 2010). Activated microglia express proinflammatory molecules such as major histocompatibility complex class I, major histocompatibility complex class II, and members of the complement cascade (Bosco et al., 2012; Ebnetter et al., 2010; Howell et al., 2011).

Complement acts as an immune surveillance system and orchestrates inflammatory processes (Ricklin, Hajishengallis, Yang, & Lambris, 2010). It exists as a collection of approximately 25 plasma and membrane-bound proteins that protect against bacterial and parasitic infection. It has been reported that complement protein synthesis also occurs in glia and neurons (Nataf, Stahel, Davoust, & Barnum, 1999). The presence of low levels of complement regulatory proteins in the normal rat eye suggests that the complement system is continuously active (Sohn, Kaplan, Suk, Bora, & Bora, 2000). Retinal cells and the optic nerve head have been shown to increase the expression of complement after crush injury (Bora, Gobleman, Atkinson, Pepose, & Kaplan, 1993; Ohlsson, Bellander, Langmoen, & Svensson, 2003). Complement is activated by a number of different pathways, but they ultimately generate enzymatic complexes that

cause the formation of the membrane attack complex (MAC). The MAC creates transmembrane channel that allows the free diffusion of molecules resulting in cell lysis (Kuehn et al., 2006). Complement activation is an important component of the innate immune activities in a number of neuroinflammatory conditions including glaucoma (Tezel et al., 2012). Complement expression has been demonstrated in a number of experimental models of glaucoma (Ahmed et al., 2004; Kuehn et al., 2006; Miyahara et al., 2003; Stasi et al., 2006). There is also evidence that a deficiency in intrinsic complement regulation may lead to uncontrolled complement attack in glaucoma (Tezel et al., 2010).

The systemic immune system has been implicated in the response to glaucomatous injury. The entry of monocyte-derived cells into the optic nerve head has been reported to occur as a very early process in DBA/2J mice (Howell et al., 2012). B cells have been detected in human glaucomatous retinas (Gramlich et al., 2013). The effect of circulating immune cells on the fate of retinal ganglion cells in glaucoma is unclear and further studies are necessary to understand their involvement (Soto & Howell, 2014).

1.11 Slit2, Neuronal Guidance Cue and Immunomodulator

During central nervous system (CNS) development, neurons migrate and project their axons over great distances to reach their appropriate targets (Nadarajah, 2003). The guidance and patterning of axons relies on cell-surface receptors and ligands (Dickson, 2002). These extracellular molecules provide

directional cues by promoting or inhibiting the migration of developing axons (Dickson, 2002). The Slit family of secreted proteins and their cell-surface receptor Roundabout (Robo) were first described for their role in the repulsion of migrating growth cones (Kidd, Bland, & Goodman, 1999). Slit protein (**Figure 1.5**) family members contain a signal peptide, four tandem leucine-rich repeats, several epidermal growth factor (EGF) repeats, a conserved LNS spacer, and a carboxy-terminal cysteine knot (Rothberg & Artavanis-Tsakonas, 1992; Rothberg, Hartley, Walther, & Artavanis-Tsakonas, 1988; Rothberg, Jacobs, Goodman, & Artavanis-Tsakonas, 1990). Proteolytic processing of Slit2 protein gives rise to an N-terminal fragment and a C-terminal fragment (Brose et al., 1999). Both full length Slit and C-terminal fragments are secreted extracellularly, though the N-terminal fragment appears to associate tightly with the cellular membrane (Brose et al., 1999). Slit2 and Slit2-N both bind Robo receptors, repelling axons and migrating cells (Nguyen-Ba-Charvet, 2001). Knockout studies in developing *Drosophila* CNS demonstrated that Slit/Robo interactions prevented axons from repeatedly crossing the midline at random (Brose & Tessier-Lavigne, 2000). Retinal ganglion cell growth cones were shown to collapse when incubated with Slit2 *in vitro* (Niclou, Jia, & Raper, 2000). Slit proteins been implicated in retinal ganglion cell guidance (Thompson, Camand, Barker, & Erskine, 2006).

The effect of Slit depends on the particular peptide expressed, the specific interacting Robo receptor and cell type expressing that receptor (Weitzman, Bayley, & Naik, 2008). Four Robo genes have been identified in a number of

species (K. W. Park et al., 2003). Robo (**Figure 1.5**) is a single pass transmembrane receptor with its extracellular region containing five immunoglobulin domains and three fibronectin type III repeats (Kidd et al., 1998; Zallen, Yi, & Bargmann, 1998). Although Slit was first described in the developing CNS, it has become apparent that Slit and Robo have important functions in different organs and systems in adult animals (Yuen and Robinson 2013). It has been discovered that Slit proteins play an important role in the migration of immunological cells (Wu et al., 2001). Slit has significant anti-inflammatory properties as demonstrated by in vitro and in vivo experiments (Kanellis et al., 2004; Zhao, Anand, & Ganju, 2014). Additionally, it was discovered Slit plays an important role in regulating vascular permeability (Jones et al., 2008).

1.12 The Vascular Theory of Glaucoma

Glaucomatous optic neuropathy is characterized by atrophy of the optic nerve and visual field deterioration that corresponds to optic nerve head damage (Nakazawa, 2016). Historically, a bitter controversy has existed between the mechanical and vasogenic theories of the pathogenesis of glaucoma (Hayreh, 1994). The ophthalmoscope was first invented in the 1850s, leading to the first descriptions of optic nerve cupping that were obtained by observing the posterior segment of the eye in glaucoma patients. In 1857, Graefe promoted the idea that glaucoma was of mechanical origin, caused by the posterior displacement of the

lamina cribosa by elevated intraocular pressure (Gräfe, 1857). A competing theory was put forth by Jaeger who postulated that glaucoma was caused by an impairment of circulation in the posterior ciliary arteries (Jaeger, 1858). Histological evidence gathered by Schnabel in 1905 led to the suggestion that glaucoma was primarily a disease of the optic nerve, and that elevated intraocular pressure was not a direct cause of nerve fibre degeneration (Schnabel, 1905). In 1910 von Hippel buttressed the hypotheses of Schnabel but suggested that elevated intraocular pressure could affect the optic nerve in manners beyond the simple mechanical displacement of the lamina cribosa (Hippel, 1910). Similarities among the cavernous degeneration seen in glaucoma and the lacunar atrophy seen in ischemic disorders of the brain were noted by Lagrange and Beauvieux (LaGrange & Beauvieux, 1925). It was their hypothesis that in the presence of arteriosclerosis, elevated intraocular pressure would result in focal optic nerve damage by interfering with the short posterior ciliary artery supply in the choroid and lamina cribosa (LaGrange & Beauvieux, 1925). Since these early observations, a growing body of evidence indicates that the pathogenesis of glaucoma is a complex process that is influenced by factors beyond elevated intraocular pressure and the mechanical displacement of the lamina cribosa (Hayreh, 1994). There is remarkable individual variability in the vulnerability of the optic nerve head to elevated intraocular pressure-induced damage (Hayreh, 1994). Patients with ocular hypertension can have high intraocular pressure for many years without any demonstrable optic nerve head damage or changes in

visual acuity (Hollows & Graham, 1966). The existence of normal-tension glaucoma demonstrates that even patients with seemingly normal intraocular pressure can develop glaucoma (Sommer et al., 1991). Clinicians treating glaucoma patients are very familiar with the fact that the normalization of intraocular pressure using medical or surgical interventions does not necessarily halt the progression of visual loss (Kidd & O'Connor, 1985; Werner, Drance, & Schulzer, 1977). Despite extensive research of ocular blood flow, its role as a cause or consequence of glaucomatous optic neuropathy, remains unclear (Nakazawa, 2016).

1.13 Vascular Changes Associated with Glaucoma

It is commonly thought that in patients with glaucoma there is less demand for blood in the optic nerve head, resulting in the loss of capillaries in accordance with the progressive loss of axons (Nakazawa, 2016). This theory is supported by evidence that correlates alteration in ocular blood flow to structural vascular changes (Harris, Lerner, Costa, Martinez, & Siesky, 2013). Capillary loss in the optic disc of glaucomatous eyes has been documented in several studies (Harris et al., 2013). Early studies of histological specimens from glaucomatous eyes revealed a globally reduced capillary network in the optic disc (Cristini, 1951; Elschmig, 1928). Studies using fluorescein angiography have demonstrated that capillary dropout occurs in glaucoma (Plange, Kaup, Huber, Remky, & Arend, 2006; Plange, Kaup, Weber, Remky, & Arend, 2004). The optic discs of

patients with primary open-angle glaucoma, normal-tension glaucoma, ocular hypertension, and without glaucoma were evaluated using video fluorescein angiograms captured on a scanning laser ophthalmoscope (Plange et al., 2006). Patients with open-angle glaucoma and normal-tension glaucoma had larger and more numerous absolute filling defects than patients with ocular hypertension and normal controls (Plange et al., 2006). Absolute filling defects in blood vessels are associated with capillary non-perfusion and indicate capillary dropout (Harris et al., 2013). In a study examining post-mortem eyes in patients with primary open angle glaucoma and pseudoexfoliation glaucoma, capillary and axon loss was documented in both conditions (Gottanka, Kuhlmann, Scholz, Johnson, & Lütjen-Drecoll, 2005). There was a difference in capillary density in the optic nerve between primary open angle glaucoma and pseudoexfoliation glaucoma (Gottanka et al., 2005). Despite the loss of axons in pseudoexfoliation glaucoma, the capillary density remained constant (Gottanka et al., 2005). This is similar to findings observed in monkeys with laser-induced ocular hypertension (Furuyoshi et al., 2000; Quigley, Hohman, Addicks, & Green, 1984). The capillary density in the prelaminar optic nerves was the same in monkeys with induced ocular hypertension as well as in control animals (Furuyoshi et al., 2000; Quigley et al., 1984). These observations suggest that pseudoexfoliation glaucoma exemplifies a secondary glaucoma with retinal ganglion cell loss as a result of pressure-induced optic nerve damage, rather than primarily ischemic or other factors (Gottanka et al., 2005). Unlike pseudoexfoliation glaucoma, the optic nerves of patients with

primary open angle glaucoma were observed to have a loss of axons with an associated loss of capillary density (Gottanka et al., 2005). This suggests that the loss of capillary density cannot be explained by axon loss alone (Gottanka et al., 2005). Based on these findings, other factors, in addition to elevated intraocular pressure, are likely involved in the optic nerve degeneration observed in primary open angle glaucoma (Gottanka et al., 2005). These undetermined factors are postulated to contribute to the optic neuropathy of eyes in the absence of elevated intraocular pressure (Gottanka et al., 2005).

According to the vascular theory of glaucoma, chronic ischemia contributes to the loss of retinal ganglion cells and their axons (Harris et al., 2013). There is evidence obtained from prospective analysis of retinal blood vessels suggesting that a decrease in ocular blood flow precedes the onset of glaucomatous optic neuropathy and plays a role in disease progression (Nakazawa, 2016).

In an older Australian cohort followed up over a 10-year period, the narrowing of retinal arteriolar caliber measured quantitatively from photographs taken at baseline was associated with a greater long-term risk of developing primary open angle glaucoma (Kawasaki et al., 2013). The Beijing eye study showed an association between thinner retinal arterioles, but not venules, and glaucomatous optic nerve damage (Wang, Xu, Wang, Wang, & Jonas, 2007). The Rotterdam study determined that both retinal arteriolar and venular diameters were not related to an increased risk of open angle glaucoma (Ikram et al., 2005).

Although the data examining retinal arterioles and venules is not conclusive it is anticipated that advances in imaging technology along with further epidemiological studies will bring a resolution to the true role of retinal vessels in glaucomatous disease.

1.14 Figures

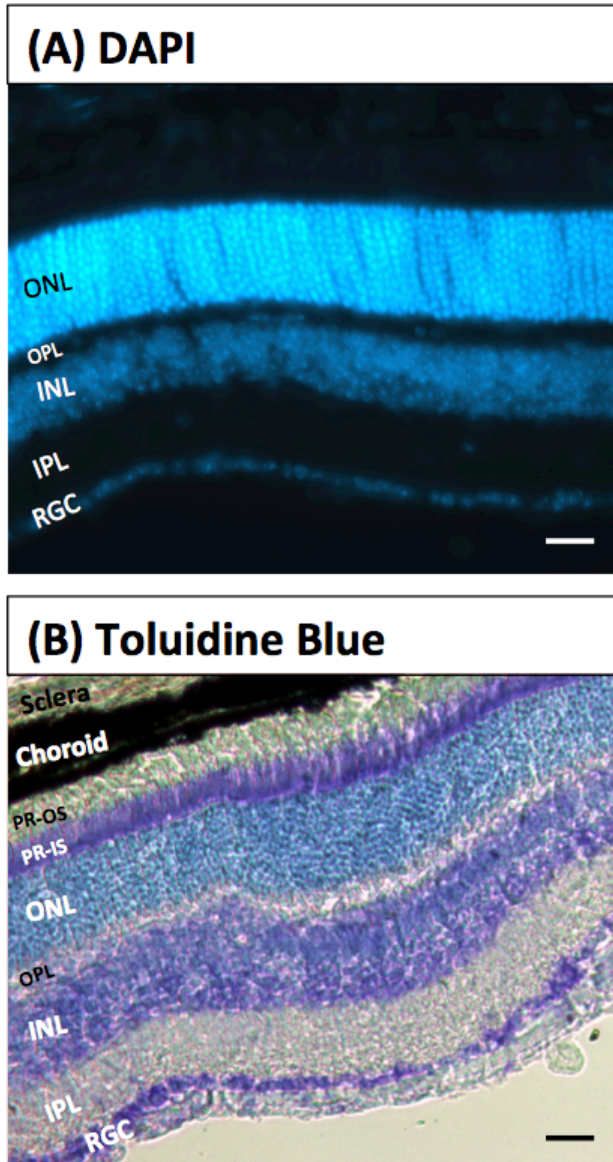


Figure 1.1 Anatomy of the retina. Frozen 12 μm transverse sections stained with (A) DAPI and (B) Toluidine Blue. DAPI (A) staining shows the layers of nuclei in the retina: the retinal ganglion cell layer (RGC), inner nuclear layer (INL) and outer nuclear layer (ONL). Toluidine Blue (B) staining reveals the inner plexiform layer (IPL), outer plexiform layer (OPL), photoreceptor inner segments (PR-IS) and outer segments (PR-OS). The choroid underlies the retina. The outer coat of the eye, the sclera, lies beneath the choroid.

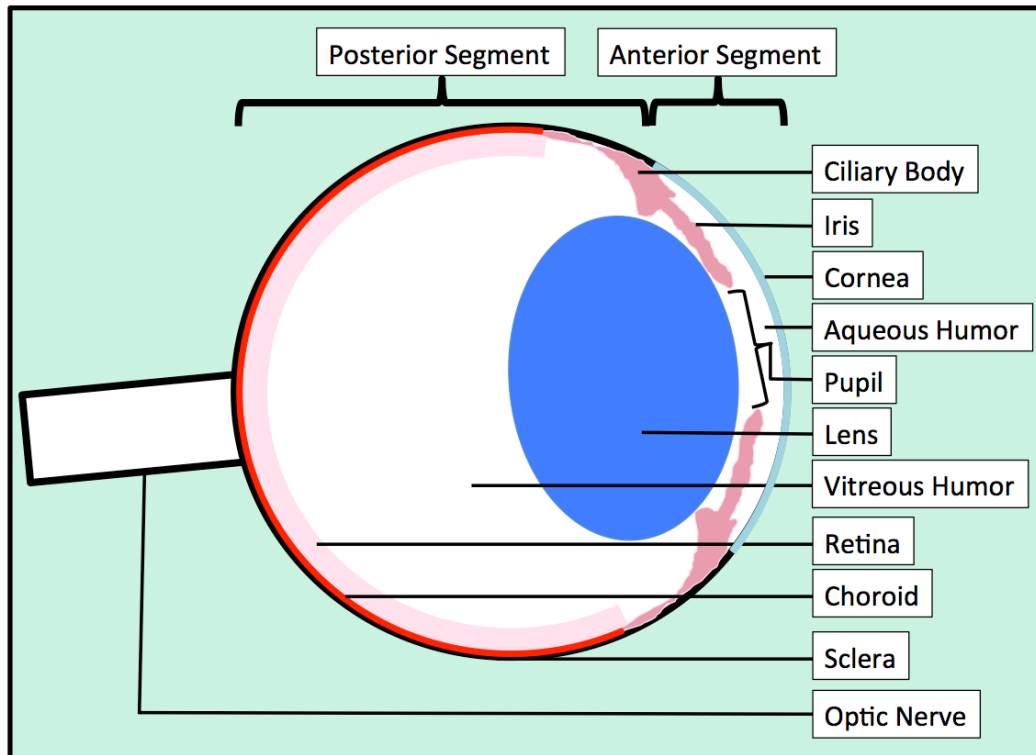


Figure 1.2 Anatomy of the eye. The eye is divided into the anterior and posterior segments. The posterior segment of the eye is comprised of the vitreous humor, retina, choroid, and optic nerve. The anterior segment includes the cornea, iris, ciliary body, and lens. The anterior segment consists of two fluid-filled spaces called the anterior chamber and posterior chamber. The anterior chamber is located between the posterior surface of the cornea and the iris. The posterior chamber is located between the iris and the anterior portion of the vitreous. The aqueous humor fills the spaces of the anterior and posterior chamber, draining through the trabecular meshwork and Schlemm's canal. Light enters the eye through the transparent cornea and focused on the retina by the lens. The retina transduces the light into an electrical signal that travels to the brain through the optic nerve that contains retinal ganglion cell axons. The posterior coat of the eye is the sclera. It is opaque and fibrous, maintaining the shape of the globe.

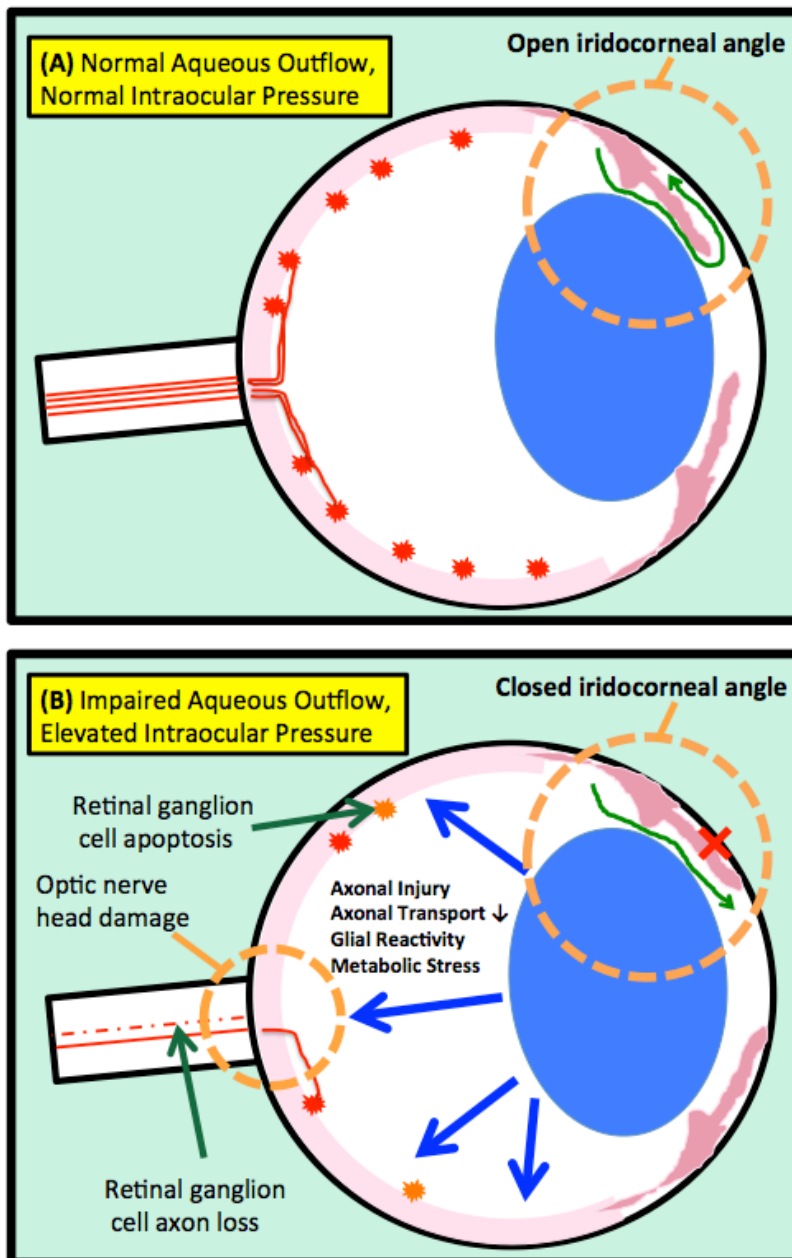


Figure 1.3 Impairment of aqueous outflow leads to elevated intraocular pressure. (A) Aqueous humor is produced by the ciliary body and flows into the anterior chamber through the pupil towards the trabecular meshwork and Schlemm's canal where it exits into venous circulation. (B) Closure of the iridocorneal disrupts the flow of aqueous humor and its ability to exit the eye causing a rise in intraocular pressure. Raised intraocular pressure can cause retinal ganglion cell axonal injury at the optic nerve head, disrupt axonal transport, cause metabolic stress, and glial reactivity. Together these factors cause retinal ganglion cell death.

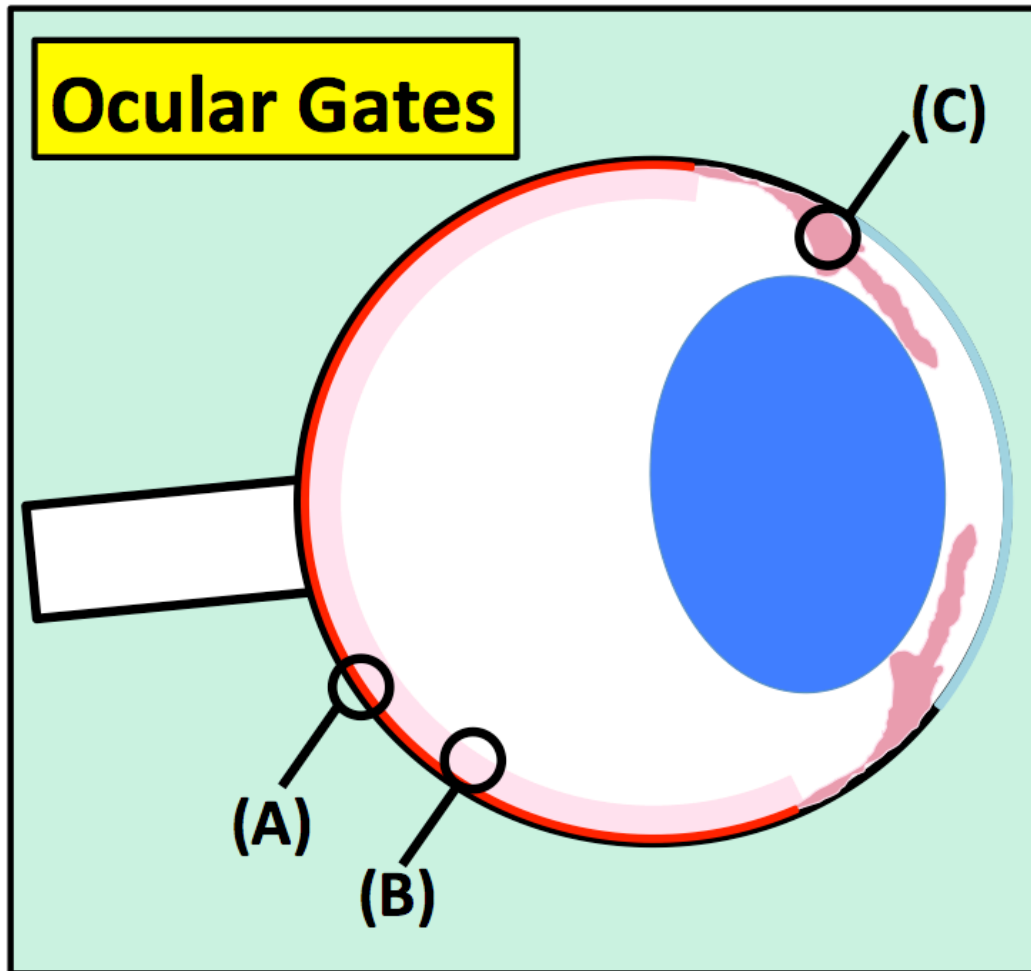


Figure 1.4 The ocular gating system. (A) The outer blood-retinal barrier is exterior to the retina. It consists of retinal pigmented epithelial cells interconnected with tight junctions and fenestrated choriocapillaries. (B) The inner blood-retinal barrier consists of tight junctions interconnecting endothelium and covered by astrocytes. (C) The blood-aqueous barrier is located in the ciliary body. It consists of non-pigmented epithelium interconnected by tight junctions and fenestrated endothelial cells (Shechter et al., 2013).

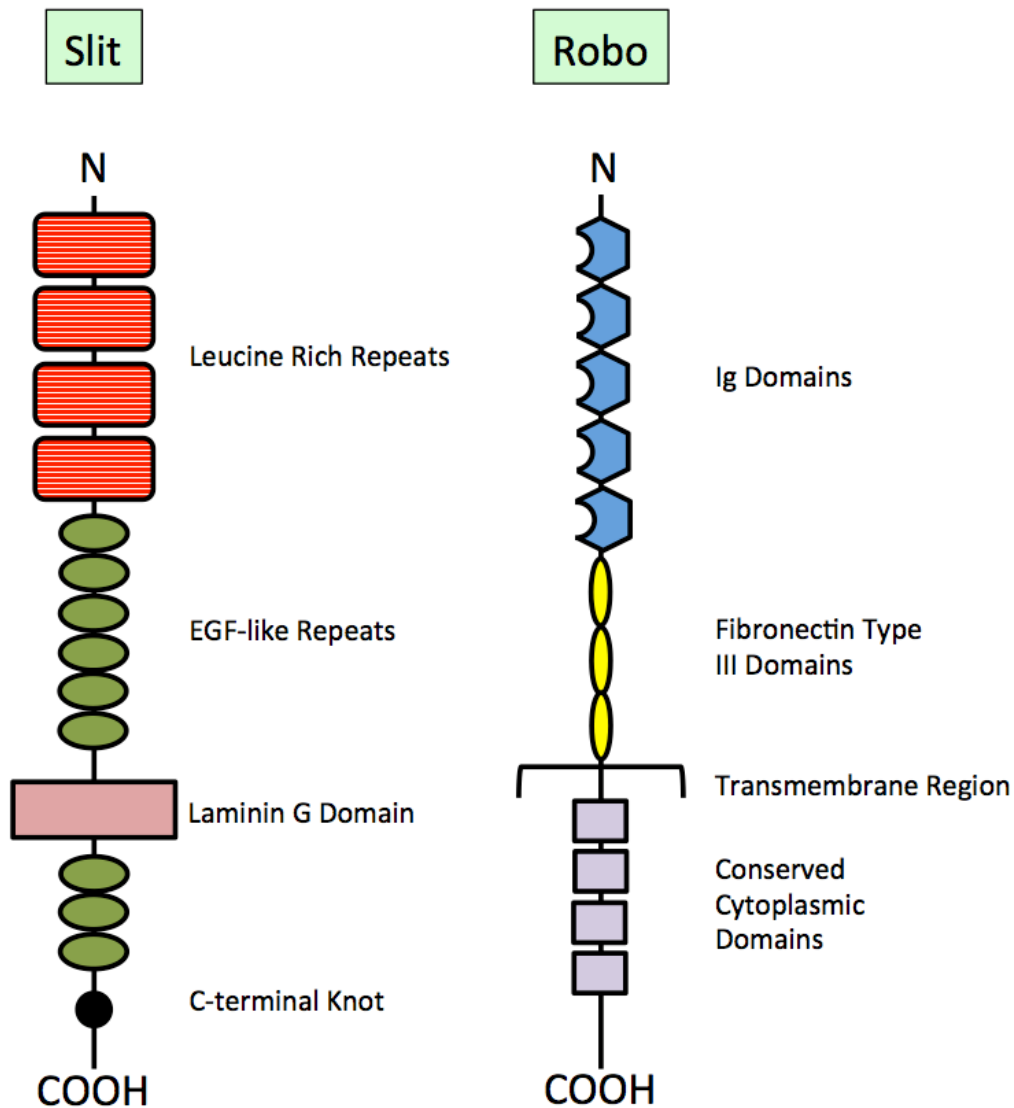


Figure 1.5 The Structure of Slit and Robo. Slit protein possesses multiple protein-binding motifs. It consists of four leucine-rich repeats, nine epidermal growth factor (EGF)-like repeats, a laminin G domain, and a cysteine-rich C-terminal domain. The Robo receptor has five immunoglobulin (Ig) domains, three fibronectin type III motifs, a transmembrane region and four conserved cytoplasmic domains (Adapted from(Piper & Little, 2003)).

CHAPTER 2: RATIONALE & HYPOTHESIS

Glaucoma is a complex multifactorial disease whose etiology remains incompletely understood. While the vascular theory of glaucoma suggests that vascular changes lead to glaucomatous changes, it remains unclear whether vascular changes are a cause or consequence of glaucoma. As well, accumulating evidence implicates the systemic immune system in the response to glaucomatous neurodegeneration, but its exact role is not well understood. **It is my overall hypothesis that the immune system and vasculature play a role in the retinal response to injury in models of glaucoma.**

2.1 Objective 1: To determine the role of the immune system and vasculature after optic nerve crush in mice

Optic nerve crush injury is a traumatic injury that triggers an immune response from resident microglia as well as blood-borne leukocytes (Battisti, Wang, Bozek, & Murray, 1995). The role of the immune response subsequent to optic nerve crush injury remains an area of controversy. Injection of pro-inflammatory cytokines into the optic nerve after crush injury is associated with conflicting results (Lotan, Solomon, Ben-Bassat, & Schwartz, 1994). While both TNF- α and CSF-1 increase the invasion of macrophages into the injury site, only TNF- α appears to increase the permissiveness of the environment to neuronal adhesion and thus regeneration (Lotan et al., 1994). Inflammatory stimulation

using lens injury (Leon, Yin, Nguyen, Irwin, & Benowitz, 2000), intravitreal application of crystallins (Fischer, Hauk, Müller, & Thanos, 2008), or Toll-like receptor 2 agonists (Hauk et al., 2009) all exert neuroprotective effects mediated by astrocyte-derived ciliary neurotrophic factor and leukemia inhibitory factor (Leino, Gerhart, Duelli, Enerson, & Drewes, 2001) . The use of the anti-inflammatory corticosteroid methylprednisolone has not proven to be a useful intervention to promote retinal ganglion cell survival after optic nerve crush (Huang, Chang, Lin, Sheu, & Tsai, 2011; Ohlsson, Westerlund, Langmoen, & Svensson, 2004; Steinsapir, Goldberg, Sinha, & Hovda, 2000). On the other hand, the use of anti-inflammatory granulocyte colony-stimulating factor results in significantly less retinal ganglion cell apoptosis 2 weeks after injury (Tsai, Chang, and Wang 2008; Tsai et al. 2010). As well, the anti-inflammatory drug minocycline has been shown to be neuroprotective in optic nerve transection injury (Levkovitch-Verbin et al. 2006; Abcouwer et al. 2013). The conflicting results of using immunomodulatory therapies following optic nerve crush injury suggest that more research is necessary to fully understand the role of the immune system.

2.1.1 Specific Aim 1: To determine the effect of Slit2 on retinal ganglion cell death after optic nerve crush

Slit/Robo signaling has classically been associated with the guidance of migrating axons in the developing nervous system (Guthrie, 2004). Investigation

into the role of Slit in fully developed animals has uncovered its potent anti-inflammatory properties (Kanellis et al., 2004) and its ability to regulate vascular permeability (Jones et al., 2009). Slit2 is a useful tool to study the role of the immune response after optic nerve injury. It has been shown that Slit2 decreases the recruitment of inflammatory cells including monocytes (Wu et al., 2001), dendritic cells (Guan et al., 2003), T cells (Prasad, Qamri, Wu, & Ganju, 2007), and neutrophils (Tole et al., 2009) by inhibiting their migration towards inflammatory stimuli (Yuen and Robinson 2013). In an *in vivo* model of crescentic glomerulonephritis in rats, Slit2 ameliorated renal function by inhibiting leukocyte recruitment to the site of injury (Kanellis et al., 2004). In an oxygen-glucose deprivation experiment in mixed neuronal-glia cultures, Slit dramatically attenuated neuronal death after insult (Altay, McLaughlin, Wu, Park, & Gidday, 2007). Slit may thus also have a direct neuroprotective effect or improve the glial response to ischemic injury (Altay et al., 2007). In a model of mouse global ischemia, three days of continuous systemic Slit administration significantly attenuated the death of hippocampal CA1 pyramidal cells (Altay et al., 2007). Slit2N potently inhibits ICAM-1 expression in HMVEC (human microvascular endothelial cells) and inhibits monocyte adhesion through the Robo4 receptor (Zhao et al., 2014). The inhibitory effect on leukocyte migration is of interest in optic nerve crush because systemic macrophages are found to invade the retinal nerve fiber layer and clear axonal debris after optic nerve axotomy (Garcia-Valenzuela & Sharma, 1999). Since Slit2 has a significant effect

on the migration and recruitment of leukocytes, this study was necessary to understand whether Slit2 had a neuroprotective effect on retinal ganglion cells, specifically by modulating the immune response to retinal ganglion cell death.

In mouse models of retinal and choroidal disease, oxygen-induced retinopathy and laser-induced choroidal neovascularization, respectively, Slit2 inhibits angiogenesis and vascular leak through a Robo4 dependent mechanism (Jones et al., 2008). Slit2N significantly reduces vascular leak in the lungs of LPS-treated mice by promoting the expression of VE-cadherin at the endothelial cell surface (London et al., 2010). By enhancing vascular stability, Slit2N significantly increased the survival of mice during the systemic inflammatory response triggered in a model of polymicrobial sepsis (London et al., 2010). Following H5N1 influenza infection in mice, Slit2N significantly inhibited endothelial cell hyperpermeability and reduced mortality (London & Li, 2011). *In vitro* experiments using HUVECs (human umbilical vein endothelial cells) demonstrated that Slit2N inhibits LPS-induced cytokine expression (Zhao et al., 2014). Given the potent effect of Slit2 on endothelial cells and consequently vascular permeability (London & Li, 2011), further investigation into the effect of Slit2 administration on the retinal vasculature following optic nerve crush injury is warranted. It was hypothesized that Slit2 would be neuroprotective to retinal ganglion cells after optic nerve crush through both its anti-inflammatory properties and the modulation of vascular stability after injury.

2.1.2 Specific Aim 2: To determine the role of vascular and systemic immune changes in the retinal response to optic nerve crush injury

The traumatic nature of optic nerve crush results in a mechanical interruption of blood flow through the optic nerve. A number of retinal diseases including retinal ischemia (Abcouwer et al., 2013), diabetic retinopathy (Mathews et al. 1997), retinopathy of prematurity (Sonmez et al. 2008) and age-related macular degeneration (Lip et al. 2001) are associated with increases in retinal vascular permeability (Erickson, Sundstrom, and Antonetti 2007). The precise effect of the interruption of blood flow on retinal ganglion cell death after optic nerve crush is unclear. It was hypothesized that the ischemic event induced by optic nerve crush would result in vascular leakage in the retina after injury.

Evidence obtained clinically and experimentally suggests that the immune system is involved in glaucoma (Ramírez et al., 2015). Monoclonal gammopathy has been observed to occur with an increased prevalence in glaucoma patients (Wax, Barrett, & Pestronk, 1994). Higher autoantibody levels are reported in blood serum as well as in the aqueous humor (Wax et al., 1994). In addition, immunoglobulin and plasma cell deposition in the retina has been observed (Wax et al., 1994). In a model of optic nerve crush, the adhesion of macrophages in the retinal vasculature as well as infiltration into the nerve fibre layer was observed (Garcia-Valenzuela & Sharma, 1999). The hypothesis regarding the systemic immune system after optic nerve crush was that systemic immune cells would be involved early on in the response to injury.

2.2 Objective 2: To determine the role of the immune system and vascular degeneration in the retina of AP-2 β NCC KO mice

2.2.1 Specific Aim 1: Characterization of retinal remodeling in the cohort of AP-2 β NCC KO mice studied

Martino et al. (2016) characterized retinal changes in a study of AP-2 β NCC KO mice. Martino et al. found a decrease in total retinal thickness in AP-2 β NCC KO mice compared to control littermates that was attributed to the thinning of the inner plexiform layer. A significant loss of retinal ganglion cells was observed in knockout mice as well. Intraocular pressure was measured in separate a cohort of AP-2 β NCC KO mice. Martino et al. reported that the intraocular pressure of these animals was 28.87 ± 5.19 mmHg, compared to control littermates that measured 9.76 ± 1.88 mmHg. Taken together these observations suggested that the eyes of AP-2 β NCC KO mice had undergone glaucomatous changes. The cohort of animals determined to have elevated intraocular pressure, along with their control littermates, were utilized in the present study to investigate retinal vascular changes. In order to study and correlate vascular changes with retinal changes, measurements of retinal thickness, retinal ganglion cell survival, and nuclear layer densities were performed in this cohort. These experiments were performed to ensure that the association of vascular changes to the glaucomatous retinal changes originally documented by Martino et al. was

appropriate. Additionally, these experiments were repeated to allow for the comparison of retinal remodeling and vascular changes within the same animal.

2.2.2 Specific Aim 2: To determine the role of vascular degeneration in the retinas of AP-2 β NCC KO mice

The role of the vasculature in glaucoma is unclear. AP-2 β NCC KO mice represent a novel model of early-onset glaucoma that may provide insight into the vascular mechanisms underlying disease or in response to disease. AP-2 β NCC KO mice exhibit high intraocular pressure that may have a significant impact on blood flow to the eye. Ischemia is thought to be an important factor involved in the pathogenesis of glaucoma. It was hypothesized that there would be vascular changes in response to the conditions within the eye due to elevated intraocular pressure.

2.2.3 Specific Aim 3: To determine the role of the immune system in the retina of AP-2 β NCC KO mice

Mounting evidence suggests that the immune system plays a role in the pathogenesis of glaucoma. AP-2 β NCC KO mice provide a convenient model of spontaneously induced elevated intraocular pressure to examine the role of systemic immune cells in the retinal response to retinal ganglion cell neurodegeneration. It was hypothesized that the systemic immune system would

mount a response to the death of retinal ganglion cells and the damage induced by elevated intraocular pressure.

2.3 Objective 3: To determine the role of the optic nerve head in AP-2 β NCC

KO mice

2.3.1 Specific Aim 1: To determine the structural changes associated with chronic elevated intraocular pressure

The optic nerve head is thought to be the site of damage that leads to glaucoma. Structural changes in the optic nerve head support this notion, including excavation of the optic nerve head and thinning of the neuroretinal rim. AP-2 β NCC KO mice represent a model of glaucoma with the potential to reveal new insights into the changes at the optic nerve head induced by high intraocular pressure. Martino et al. previously showed structural changes in the retinas of these mice. It was hypothesized that there would be structural changes at the site of the optic nerve head in AP-2 β NCC KO mice that resembled glaucomatous changes.

2.3.2 Specific Aim 2: To determine the glial reactions in the optic nerve head of AP-2 β NCC KO mice

Martino et al. originally performed immunohistochemistry on the retinas of a group of 8-12 week old AP-2 β NCC KO mice to visualize retinal GFAP and Iba-1 expression. An upregulation of both GFAP and Iba-1 in the retina were

observed in AP-2 β NCC KO mice compared to controls. The optic nerve head is the suspected site of axonal damage (Lye-Barthel, Sun, & Jakobs, 2013) in glaucoma and studying the changes in these mice that are associated with RGC loss may provide a greater understanding of the mechanisms that lead to glaucoma and how to improve upon current treatments.

In the following experiments, a separate group of AP-2 β NCC KO mice and their control littermates, aged 12-16 weeks, were used to examine changes at the optic nerve head. In order to compare and contrast optic nerve head changes with retinal changes, immunohistochemistry was performed on both the optic nerve head and retina, as was done previously, to visualize and quantify GFAP expression, and Iba-1 expression. It was hypothesized that there would be changes in both Iba-1 and GFAP expression in the optic nerve head corresponding to the changes observed in the retinas of AP-2 β NCC KO mice.

CHAPTER 3: EXPERIMENTAL METHODS

3.1 The role of the vasculature and immune system after optic nerve crush in mice

3.1.1 Animals

Animals used in optic nerve crush experiments were 8-10 week old phenotypically wild-type C57BL/6 mice free of common pathogens. Animals were obtained in kind from Dr. Jane Foster or Dr. Judith West-Mays. The animals were kept on a 12-hour light cycle and had access to water and food ad libitum. The use and care of mice were in accordance with the guidelines of the CCAC (Canadian Council of Animal Care) and approved by the McMaster AREB (Animal Research Ethics Board). All animal procedures were performed in accordance with the ARVO (Association for Research in Vision and Ophthalmology) Statement for the Use of Animals in Ophthalmic and Vision Research.

3.1.2 Optic Nerve Crush Injury

Mice were anaesthetized using intraperitoneal injections of 2.5% avertin (250 mg/kg of body mass). The mice were restrained onto a heating blanket using Velcro tape, making sure to have the eye protrude. Refresh Lacri-Lube lubricating ophthalmic ointment (Allergan, Markham, ON) was applied to both eyes to ensure that they did not dry out during the surgical procedure. Before beginning the

surgery, the Lacri-Lube was wiped off of the left eye and a few drops of 1% Xylocaine was applied to anaesthetize the area locally and minimize discomfort after the surgery. The optic nerve crush procedure was performed using a binocular operating microscope. The surgical procedure was performed according to the protocol developed by Templeton and Geisert (2012) (**Figure 3.1**). The surgery was performed only on the left eyes to standardize the injuries. A small incision was made in the conjunctiva beginning inferior to the globe and around the eye temporally. Micro-forceps were used to grasp the edge of the conjunctiva next to the globe and retracted to rotate the globe nasally. The optic nerve was visualized at the exposed posterior aspect of the globe. In the sham surgery condition, the procedure ended here and the eye was allowed to rotate back into place. The sham surgery was performed to control for the trauma that occurs when performing the surgery to access the optic nerve. In the optic nerve injury condition, the optic nerve was grasped approximately 1-3 mm from the globe with cross-action forceps for 10 seconds. The only pressure applied to the nerve resulted from the self-clamping mechanism of the cross-action forceps. Mydriasis was observed during the clamping of the optic nerve. After 10 seconds the optic nerve was released and the eye was allowed to rotate back into place after removing the forceps (Templeton & Geisert, 2012). The animals received subcutaneous injections of 1-2 ml of a 0.9% saline solution to prevent dehydration and were placed with their bodies half on, half off of a heating blanket for recovery. Animals were monitored for several hours after surgery.

3.1.3 Slit2 Tail Vein Injections

Animals received systemic intravenous tail vein injections in some experimental conditions. 0.2 ml of sodium phosphate buffered saline (PBS; 0.1 M, pH 7.3, 0.9% NaCl) or 0.2 ml of full length Slit2 (0.72 μ g), obtained in kind from Dr. Lisa Robinson, in PBS was injected immediately after anesthesia and 5 minutes before any surgical incisions were made and the optic nerve injury was performed. Frozen Slit2 was thawed on ice before use.

3.1.4 Tissue Preparation

Mice were euthanized 7, 14, and 28 days after injury using an overdose of isoflurane. The eyes were enucleated and placed in 4% paraformaldehyde, 2% sucrose in Sorensen's phosphate buffer (0.1M, pH 7.3) for 15 minutes. The cornea and lens were dissected away and the eyecup was replaced in the fixative solution for a total fixation time of 2 hours. The eyecups were then rinsed in PBS 3 times for 10 minutes each wash. The neural retinas were dissected away from the underlying retinal pigment epithelium and sclera. Any remaining vitreous humor was carefully removed from the retinal surface. Retinas were stored in PBS at 4°C until immunohistochemistry was performed.

3.1.5 Brn-3a Whole Mount Immunohistochemistry

Whole retinas were washed in a solution of 1% Triton X-100 in PBS 3 times for 10 minutes each time. They were then covered with 1% Triton X-100 in PBS and frozen at -80°C for 20 minutes, then allowed to fully thaw to room temperature for 30 minutes. The retinas were then incubated in a blocking solution overnight at 4°C. The blocking solution consisted of PBS with 2% normal donkey serum and 1% Triton-X 100. The retinas were then incubated in primary antibody (Goat α Brn3a; 1:200; Santa Cruz SC-31984 (C20); class IV POU domain-containing transcription factor) in blocking solution overnight at room temperature. To detect the primary antibody, retinas were incubated in Donkey α Goat Alexa 488 (1:200; Molecular Probes A-11055, Life Technologies) in blocking solution for 8 hours at room temperature. The tissue was then washed in PBS 3 times for 10 minutes each wash.

3.1.6 Whole Mounts

Whole retinas were mounted on slides between two coverslips that were used to elevate the coverslip placed on top of the retina to ensure that the retina was not flattened and that the retinal ganglion cell density was not distorted. A drop of Vectashield fluorescent mounting medium (H1000; Vector Labs, Burlington, ON) was applied to the slide before the final coverslip was placed.

3.1.7 Evan's blue injection

Retro-orbital injections of 0.3 ml of 20% Evan's blue in PBS filtered with a 0.22 µm syringe filter were performed on uninjured animals and animals 1 hour, 6 hours, and 24 hours after optic nerve crush. The animals were then perfused with PBS through the left atrium after being deeply anaesthetized with 2.5% avertin (250 mg/kg of body mass). The line was then switched to a solution of 4% paraformaldehyde, 2% sucrose in Sorensen's phosphate buffer (0.1M, pH 7.3) to fix the animal. Eyecups with attached optic nerves were dissected from the animal and fixed for an additional 1.5 hours in PBS.

3.1.8 Frozen Sections

Fixed eyecups were incubated in 30% sucrose in PBS overnight to cryoprotect the tissue. Eyecups were removed from the cryoprotectant and excess solution was removed using a cotton swab taking care to ensure the tissue never dried out. Any vitreous humor remaining on the retina was brushed away with a fine paintbrush. Eyecups were coated in Tissue-Tek Optimal Cutting Temperature compound (Sakura Finetek USA, Inc, CA, USA) and placed inside the cryostat (Leica CM1900) at -17°C. 12 µm transverse sections were taken of the retinas and collected on Superfrost Plus slides (Fisher Scientific, PA, USA). The slides were labeled and allowed to dry for at least one hour before storage in -20°C until needed. The remaining tissue was thawed, washed in PBS, and stored in PBS until whole mounted.

3.1.9 Fluorescent Microscopy

Slides were visualized under an epifluorescence microscope (Zeiss Axioplan 2, Carl Zeiss, Toronto, ON) using Zeiss Axiovision software. Images were taken at high power (40X) in the central (approximately 0.416 mm from the optic nerve head), mid-peripheral (approximately 1.25 mm from the optic nerve head), and peripheral (approximately 2 mm from the optic nerve head) retina in each of the four retinal quadrants (nasal, temporal, inferior, and superior). In total there were 12 sampling fields per retina. To determine the density of cells in the central, mid-peripheral, and peripheral retina, fluorescent retinal ganglion cells were manually counted in each image with ImageJ software (National Institutes of Health, version 1.5i) using the Cell Counter plugin. The cell density was calculated by dividing the total number of cells by the area of the field of view as measured by ImageJ.

3.1.10 In vivo Retinal Imaging

A Phoenix Micron IV Rodent Retinal Imaging Microscope (Phoenix Research Labs, CA, USA) was used for *in vivo* bright field imaging, fluorescent imaging, and optical coherence tomography. Mice were anaesthetized using 2.5% Avertin (250 mg/kg of body mass). The left pupils were dilated with one drop of 0.5% Tropicamide Ophthalmic Solution, USP (Akorn, IL, USA) and one drop of 2.5% Phenylephrine Hydrochloride Ophthalmic Solution, USP (Akorn, IL, USA). Both eyes were hydrated periodically with TearGel (Alcon Canada Inc., ON,

Canada) to prevent corneal desiccation.

3.1.11 Acridine Orange Leukocyte Fluorography

The mouse was positioned under the Micron Retinal Imaging Microscope and the retina was visualized under brightfield illumination. Acridine orange (Life Technologies, Burlington, Canada (10 mg/ml)) was injected (0.05 ml/min) intraperitoneally or intravenously (retro-orbital). Acridine orange is used as a fluorescent probe of nucleic acids. It fluoresces by interacting with DNA by intercalation and RNA by electrostatic attractions. When injected intravenously it labels leukocytes in circulation as well as vascular endothelial cells. Acridine orange fluorography has been used to study changes in leukocyte behaviour in the retina and other organs in vivo (Cahoon et al., 2014). Acridine orange fluorescence in the retina was visualized by using a 435–469 nm excitation filter and 520–530 nm barrier filter. A 5 minute video was recorded using Streampix software (NorPix Inc., Quebec, Canada).

3.1.12 Fluorescein Angiography

Fluorescein angiography was completed using intraperitoneal injection of 1% Fluorescein (AK-Fluor 10%, AKORN, Lake Forest, IL, USA) and visualization under the Phoenix Micron rodent imaging microscope in animals anaesthetized with 2.5% Avertin (250 mg/kg of body mass). A 2 minute video was recorded using Streampix software (NorPix Inc., Quebec, Canada).

3.2 The role of the immune system and vascular degeneration in the retina of AP-2 β NCC KO mice

3.2.1 Generation of AP-2 β NCC KO Mutant Animals

Tfap2b was conditionally deleted from neural crest cells by generating offspring from *Wnt1-Cre* mice heterozygous for a *Tfap2b* allele bred with homozygous floxed *Tfap2b* mice. Van Otterloo and Williams are preparing a manuscript that will detail the generation of *Tfap2b* floxed mice. PCR was performed using DNA extracted from ear clippings using the EZNA Tissue DNA Kit (Omega Bio-Tek) with the appropriate primer sequences for *Tfap2b* null, *Tfap2b* flox and *Wnt1-Cre* alleles. Mice identified as *Wnt1-Cre Tfap2b^{null/flox}* are referred to as AP-2 β NCC KO mice in the manuscript (**Figure 3.2**). All AP-2 β NCC KO mice used experimentally were 8-12 weeks old or 12-16 weeks old and matched to control littermates that maintained at least one functional copy of the *Tfap2b*.

3.2.2 Retinal Measurements

Frozen sections were collected as detailed in section 3.1.8. Slides of frozen sections were thawed from storage at -20°C to room temperature. Slides were washed three times in PBS for ten minutes each wash. Vectashield with DAPI was applied to the sections on the slide and a coverslip was placed on top. Images

of DAPI labeled retinas were captured at high magnification. The density of the nuclei was calculated by measuring the total number of nuclei in each of the DAPI labeled retinal layers. All the DAPI labeled nuclei in the retinal ganglion cell layer were counted and the length of the retinal ganglion cell layer was measured in three high magnification images. The retinal ganglion cell layer density was calculated by dividing the average number of nuclei by the average length of the layer and expressed as the average number of nuclei per mm. The density of the nuclei in the inner nuclear layer and outer nuclear layer was calculated by counting the number of DAPI labeled nuclei in the layer and dividing the value by the average total area occupied by the layer from three high magnification images. The value of the nuclear density in the inner nuclear layer and the outer nuclear layer is expressed as the average number of nuclei per mm². Using ImageJ, the thickness of the retinas was measured from the retinal ganglion cell layer to the retinal pigmented epithelium layer, along with the individual thicknesses of the retinal ganglion cell layer, the inner plexiform layer, the inner nuclear layer, the outer plexiform layer, the outer nuclear layer, and the photoreceptors, all in three high magnification retinal images and averaged.

3.2.3 Brn3a Retinal Section Immunohistochemistry

Slides with retinal sections were washed in PBS 3 times for 10 minutes each time. The retinas were then incubated in a blocking solution for 30 minutes at room temperature. The blocking solution consisted of PBS with 1% normal

donkey serum, 1% DMSO, and 0.1% Triton-X 100. The retinas were then incubated in primary antibody (Goat α Brn3a; 1:200; Santa Cruz SC-31984 (C20); class IV POU domain-containing transcription factor) overnight at room temperature. To detect the primary antibody, retinas were incubated in Donkey α Goat Texas Red (1:200; Jackson ImmunoResearch; 705-075-147) in blocking solution for 4 hours at room temperature. The tissue was then washed in PBS 3 times for 10 minutes each wash, and coverslipped with Vectashield Mounting Medium.

3.2.4 Neurobiotin Labeling

Mice were deeply anaesthetized. Both eyes were enucleated with attached optic nerves. Retrobulbar tissue was dissected away. The eyeballs were placed cornea side down in a moist, heated (37°C), oxygenated chamber. Gelfoam was soaked in 8% Neurobiotin (Vector Laboratories, Inc. Burlington, CA 94010) and placed on the remaining end of the optic nerve attached to the eye. The eyeballs were incubated for approximately one hour, and subsequently fixed in 4% phosphate buffered PFA. After 30 minutes the corneas were dissected away and the eyecups were fixed for an additional 90 minutes. Following 3 washes with PBS, retinas were removed from the eyecup and incubated in Texas Red Conjugated Streptavidin (Jackson ImmunoResearch Laboratories, Inc.) overnight on a rotator at room temperature. The retinas were then washed 3 times in PBS and mounted onto slides and coverslipped with Vectashield containing DAPI

(Vector Laboratories, Inc., Burlington, CA). The total number of fluorescent cells on the surface of whole mounted retinas was quantified for each retina examined. The retina was divided into thirds based on the distance from the optic nerve head and the fluorescent cells were quantified based on their location (central, mid-peripheral, or peripheral) with relation to the optic nerve head. Fluorescent cell density was calculated by dividing the total number of cells by the area they occupied, as calculated by ImageJ.

3.2.5 Retro-orbital FITC-Dextran Injections

The corneas of AP-2 β NCC KO mice are cloudy, preventing live imaging of the retina. To examine vascular changes in the AP-2 β NCC KO mouse, intravenous Fluorescein Isothiocyanate-Dextran (2,000,000 MW, Sigma-Aldrich Canada Ltd., Oakville, Ontario) was used. FITC-Dextran was injected retroorbitally after mice were anaesthetized using intraperitoneal injections of 2.5% avertin (250 mg/kg of body mass). After waiting five minutes, animals were sacrificed using an overdose of Avertin.

3.2.6 Tissue Processing

Eyes and optic nerves were dissected from the animals and fixed in 4% phosphate-buffered paraformaldehyde for 2 hours. After three washes for 10 minutes in PBS, retinas were dissected out of the eye cups, whole mounted on a

glass slide, and covered in Vectashield Mounting Medium (Vector Laboratories Canada Inc, Burlington, Ontario)

3.2.7 Capillary Measurement

A 20X image of each of the three dextran labeled capillary plexuses was captured in the midperiphery of four retinal quadrants using a Zeiss Imager.M2 microscope with AxioCam 506 mono. All measurements were completed manually using ImageJ software, with the measurer blinded to the condition of the animal. Changes in capillary area were calculated by measuring the area occupied by the fluorescent vessels in each image. Capillary density was measured in each of the three microvascular plexuses. A 500 μm line perpendicular to the orientation of the retinal capillaries was drawn on each image in five locations on the image, approximately the same distance apart. The number of intersecting capillaries was quantified for each line and averaged among the five lines. Capillary density was expressed as the average number of intersecting capillaries per 500 μm . The inter-capillary distance was also calculated by dividing the total distance measured by the number of intersecting capillaries and expressed in micrometers. Capillary diameter was calculated by measuring the perpendicular distance across the maximum chord axis of ten blood vessels in each of the capillary plexuses in the midperiphery of four retinal quadrants and expressed in micrometers.

3.3 The role of the optic nerve head in AP-2 β NCC KO mice

3.3.1 Frozen Sections Through The Optic Nerve Head

Fixed eyecups with attached optic nerves were incubated in 30% sucrose in PBS overnight to cryoprotect the tissue. Eyecups were removed from the cryoprotectant and excess solution was removed using a cotton swab taking care to ensure the tissue never dried out. Any vitreous humor remaining on the retina was brushed away with a fine paintbrush. Eyecups were coated in Tissue-Tek Optimal Cutting Temperature compound (Sakura Finetek USA, Inc, CA, USA) and placed inside an open plastic cylinder with one end in contact with the cryostat at -17°C. The plastic cylinder was created by cutting off the lid and conical tip of a 1.5 ml eppendorf vial. The eyecup was manipulated with forceps as it froze so that the optic nerve was centered on one end of the cylinder and the open face of the eyecup was centered at the other end of the cylinder. The specimen in frozen OCT was removed from the plastic cylinder and mounted on a frozen block, oriented to obtain transverse sections. 12 μ m transverse sections were taken of the retinas until reaching and cutting through the optic nerve head. Sections were collected on Superfrost Plus slides (Fisher Scientific, PA, USA). The slides were labeled and allowed to dry for at least one hour before storage in -20°C until needed for immunohistochemistry. The remaining tissue was thawed, washed in PBS, and stored in PBS until whole mounted.

3.3.2 Toluidine Blue Staining

Frozen slides were allowed to come to room temperature for at least 30 minutes. Slides were washed in PBS 3 times to remove OCT compound. A 1% Toluidine Blue, 1% Borax solution was applied to the sections for 30 seconds. The slides were washed and coverslipped in 50% PBS/50% glycerol.

3.3.3 Optic Nerve Head Measurements

The thickness of the retina was measured in the mid-periphery and at the point in the optic nerve head immediately before the retinal ganglion cell axons dive into the optic nerve, referred to as the optic disc, using ImageJ (**Figure 3.3**). The level of the sclera was used as a reference point for quantification of tissue displacement in the optic nerve head. The displacement of tissue from the level of the sclera was calculated by measuring from the level of the sclera to the point of maximum displacement above or below the sclera using ImageJ. The area of excavation was calculated by tracing the excavated area below the level of the sclera (μm^2) using ImageJ.

3.3.3 Immunohistochemistry

Slides with retinal sections were washed in PBS 3 times for 10 minutes each time. The retinas were then incubated in a blocking solution for 30 minutes at room temperature. The blocking solution consisted of PBS with 1% normal donkey serum, 1% DMSO, and 0.1% Triton-X 100. The retinas were then

incubated in primary antibodies: (Rabbit α Iba-1; 1:200, WAKO; #019-19741, ionized calcium-binding adapter molecule 1) or (Rabbit α GFAP; 1:200, Dako; Z 0334, glial fibrillary acidic protein) overnight at room temperature. To detect the primary antibody, retinas were incubated in Donkey α Rabbit Alexa 568 (1:200; Molecular Probes A-10042, Life Technologies) in blocking solution for 4 hours at room temperature. The tissue was then washed in PBS 3 times for 10 minutes each wash.

3.3.4 Fluorescent Imaging

Images were captured a Zeiss Imager.M2 microscope with AxioCam 506 mono. All images of immunohistochemistry were performed using standardized settings. Images of GFAP fluorescence were captured with the light source set at 10% brightness and with an exposure setting of 480 ms. Images of Iba-1 fluorescence were captured with the light source set at 40% and an exposure setting of 700 ms.

3.3.5 Image Analysis

Cell counts of Müller cells and microglial cells were performed using ImageJ software using the Cell Counter Plugin. GFAP fluorescence in the retinal ganglion cell layer was measured by tracing around the retinal ganglion cell layer and recording the calculated mean gray value. Mean gray value is the sum of all the gray values of the pixels contained in a selection, divided by the total number

of pixels. Optic nerve head GFAP fluorescence was calculated by tracing around the optic nerve head and measuring the mean gray value. Fluorescence of Iba-1 in the retina was calculated by tracing around the retina from the retinal ganglion cell layer to the photoreceptor layer and measuring the mean gray value.

3.4 Statistical Analysis

All Statistical analyses were performed using GraphPad Prism 6 (La Jolla, CA). Significance was determined by t-test or ANOVA analysis ($\alpha = 0.05$) followed by Tukey's post-hoc test. All values were reported as 95% confidence intervals.

3.5 Figures

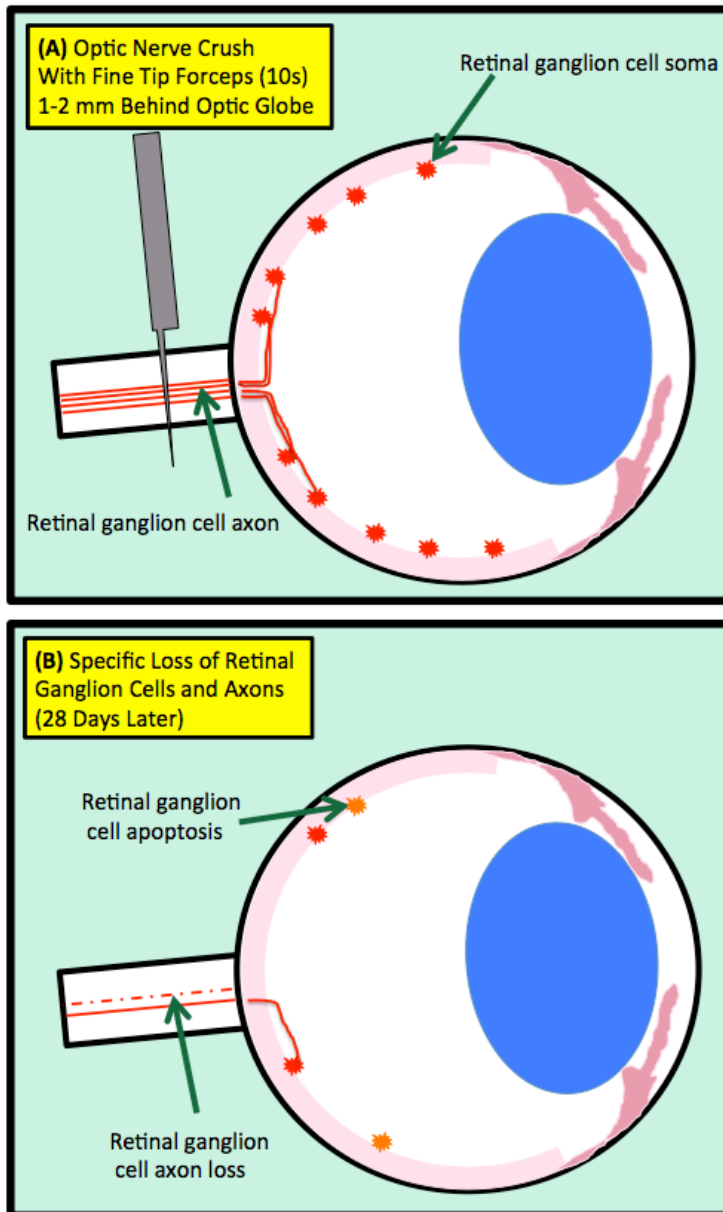


Figure 3.1 Optic nerve crush results in the death of retinal ganglion cells. (A) Mice were anesthetized and underwent optic nerve crush surgery. The optic nerve was crushed 1-2 mm behind the optic globe for 10s. The mouse was allowed to recover. **(B)** By 28 days most of the retinal ganglion cells have undergone apoptosis and the axons are lost from the optic nerve. This specific loss of retinal ganglion cells is a characteristic of glaucoma and this model is used to study neuron degeneration and the processes associated with it.

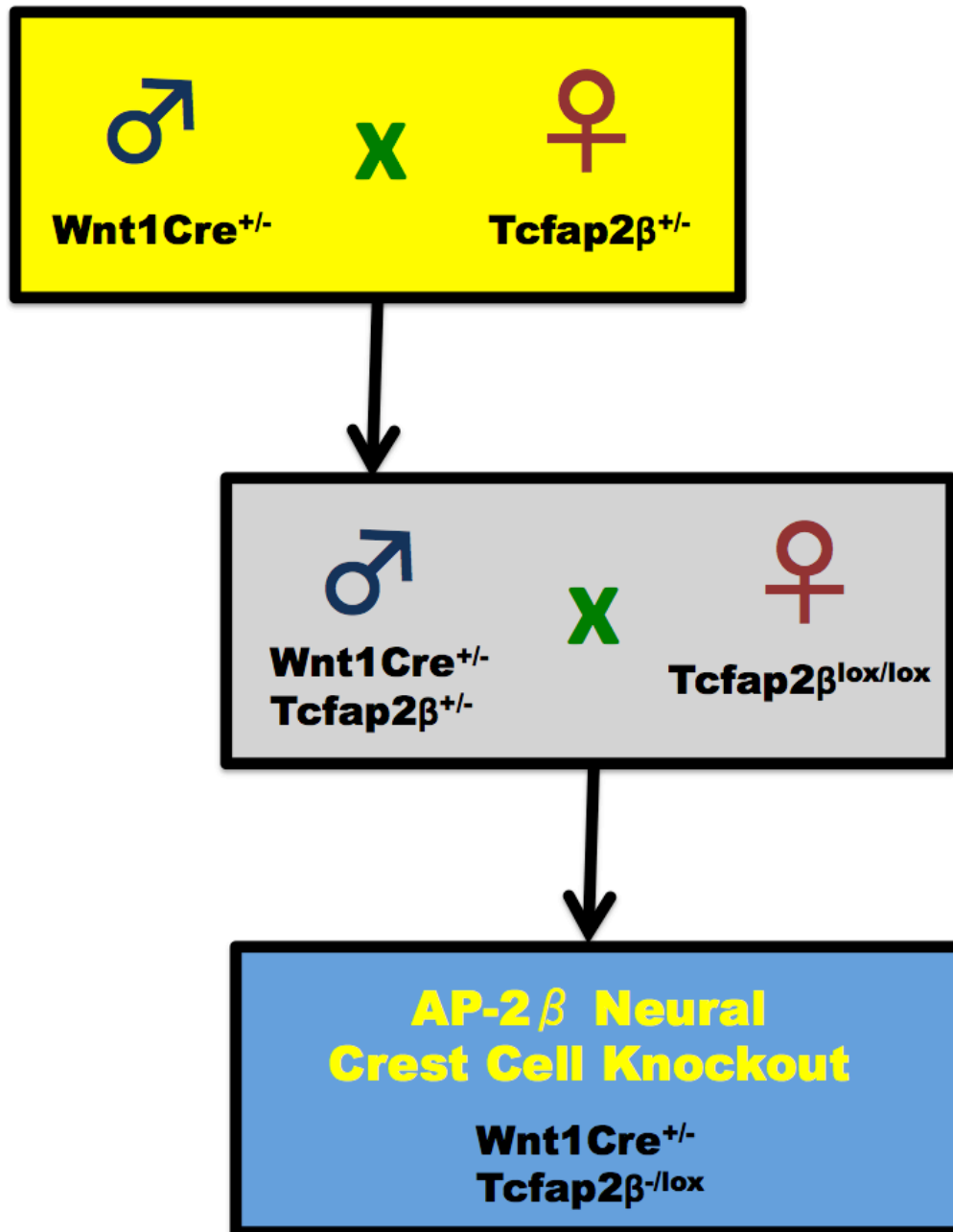


Figure 3.2 Generation of AP-2 β NCC KO mice. Female mice heterozygous for $Tcfap2\beta$ (null allele) were bred with male mice heterozygous for Cre recombinase expression directed by $Wnt1$ regulatory sequences that limit expression to the neural crest cells. Male offspring of this cross with a genotype of $Wnt1Cre^{+/-} Tcfap2\beta^{+/-}$ were bred with $Tcfap2\beta^{lox/lox}$. This generated mice with a heterozygous for $Tcfap2\beta$ null alleles but with a conditional disruption of $Tcfap2\beta$ limited to the neural crest cells mediated by Cre recombinase excision at the loxP site (Martino et al., 2016).

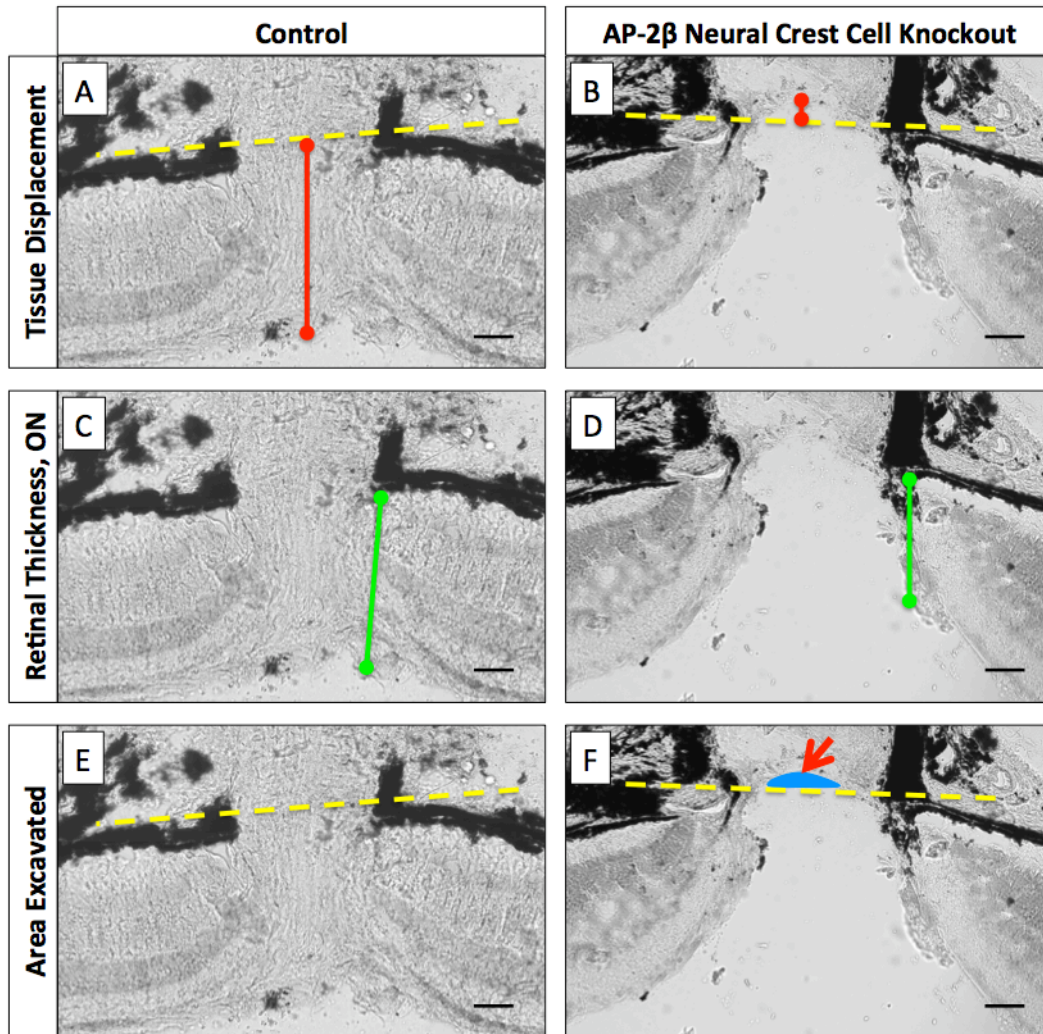


Figure 3.3 Quantification of optic nerve head changes. The optic nerve head undergoes remodelling in response to elevated intraocular pressure. A number of measures were used to quantify these changes in control versus AP-2 β NCC KO mice. (A)(B) Tissue displacement from the optic nerve head was quantified to obtain a numerical measure of the cupping of the optic nerve in affected mice. The level of the sclera was used as a reference point and the maximum displacement of tissue from the reference point was measured. (C)(D) The thickness of the retina at the optic nerve head was measured from the retinal pigmented epithelium to the nerve fibre layer to evaluate changes in thickness. (E)(F) The area excavated beneath the level of the sclera was quantified to create a measure of the degree of optic nerve cupping exhibited in affected animals.

CHAPTER 4: THE ROLE OF THE IMMUNE SYSTEM AND VASCULATURE AFTER OPTIC NERVE CRUSH IN MICE

4.1 Results

4A. The effect of Slit2 on retinal ganglion cell death after optic nerve crush

4.1.1 Retinal ganglion cell density decreases over 28 days after optic nerve crush injury

Immunofluorescence of Brn3a labeling was used to calculate retinal ganglion cell survival (**Figure 4.1**). In uninjured animals (n=4) there were 4404 ± 442 cells/mm in the central retina, 3700 ± 547 cells/mm in the mid-peripheral retina, and 2239 ± 723 in the retinal periphery (**Figure 4.2**). 7 days after optic nerve crush (n=4) there was a significant loss in Brn3a cell density in each of the retinal sectors (ANOVA/Tukey's post-hoc test; $p < 0.001$). There were 1466 ± 292 cells/mm in the central retina, 1250 ± 270 cells/mm in the mid-peripheral retina, and 937.2 ± 298.2 cells/mm in the retinal periphery of mice that received an optic nerve crush injury. The significant loss of retinal ganglion cells continued at 14 days compared to 7 days after optic nerve crush injury (n=4; ANOVA/Tukey's post-hoc test) in the central ($p = 0.0011$) and mid-peripheral ($p = 0.0117$) retina, but not the retinal periphery. There were 740 ± 105.8 cells/mm centrally in the retina, 646 ± 86.2 cells/mm in the midperiphery, and 428.6 ± 150.6 cells/mm in the periphery. 28 days after optic nerve crush injury (n=4) retinal ganglion cell loss

continued, but it was not statistically significant (ANOVA/Tukey's post-hoc test) in any of the retinal sectors. There were 417.7 ± 101.9 cells/mm in the central retina, 400.4 ± 168.8 cells/mm in the mid-periphery, and 256.6 ± 46.6 cells/mm in the retinal periphery in mice 28 days after optic nerve crush. In the central retina, 66.7%, 83.1%, and 90.5% of retinal ganglion cells were lost after 7 days, 14 days, and 28 days, respectively, after optic nerve crush compared to uninjured animals (**Figure 4.3**). In the mid-peripheral retina, 66.2%, 82.5%, and 89.2% of retinal ganglion cells were lost after 7 days, 14 days, and 28 days, respectively, after optic nerve crush compared to uninjured animals. In the peripheral retina, 58.1%, 80.9%, and 88.5% of retinal ganglion cells were lost after 7 days, 14 days, and 28 days, respectively, after optic nerve crush compared to uninjured animals. There were no significant differences in percentage of retinal ganglion cell loss after optic nerve crush injury between retinal sectors.

4.1.2 Slit2 does not affect retinal ganglion cell survival 7 days after optic nerve crush

Animals received a sham optic nerve crush surgery, or received an optic nerve crush injury plus intravenous PBS or Slit2 and were labeled for Brn3a (**Figure 4.4**). In mice receiving sham surgery (n=3), there were 4888 ± 941 cells/mm expressing Brn3a in central retina, 4586 ± 942 cells/mm in the midperiphery, and 2589 ± 1027 cells/mm in the peripheral retina (**Figure 4.5**). In mice that were injected with PBS and had their optic nerve crushed (n=4), there

were 1305 ± 169 cells/mm centrally, 1275 ± 219 cells/mm in the midperiphery, and 847.8 ± 117.7 cells/mm in the retinal periphery. Mice that were injected with Slit2 and had their optic nerve crushed (n=4) had 1373 ± 249 cells/mm in the central retina, 1400 ± 159 cells/mm in the mid-peripheral retina, and 990.2 ± 345.5 cells/mm in the periphery. There was a statistically significant difference in each of the retinal sectors between sham surgeries and both conditions undergoing optic nerve crush (ANOVA/Tukey's post-hoc test; $p < 0.001$). Mice with sham surgeries did not lose their retinal ganglion cells. There were no significant differences (ANOVA/Tukey's post-hoc test) in retinal ganglion cell death between animals injected with PBS and those injected with Slit2. Slit2 injected intravenously before injury did not have an effect on retinal ganglion cell death.

4B. The role of vascular changes in the retinal response to optic nerve crush injury

4.1.3 The retinal vasculature does not leak after optic nerve crush

Evan's blue fluorescence was expressed as mean gray value. In retinal sections (**Figure 4.6**), Evan's blue fluorescence was 3583 ± 1837 , 3858 ± 1236 , and 4334 ± 1736 , in mice undergoing sham optic nerve crush surgery and then injected with Evan's blue and perfused 1 hour (n=3), 6 hours (n=3), and 24 hours (n=3) after surgery, respectively (**Figure 4.7**). Animals that received an optic nerve crush and then Evan's blue injection and perfusion 1 hour (n=3), 6 hours (n=3), and 24 hours (n=3) after injury had Evan's blue fluorescence of $3296 \pm$

2701.2, 4597 ± 1489 , 3781 ± 2636 , respectively, in retinal sections. Evan's blue extravasation was not detected in retinal sections after sham surgery or optic nerve crush (ANOVA). Whole mounts were also examined for Evan's blue extravasation (**Figure 4.8**). Evan's blue fluorescence in mice that received sham surgery, Evan's blue injection and then perfusion after 1 hour, 6 hours, and 24 hours after the operation was 4074 ± 1499 , 3728 ± 2923.4 , and 3733 ± 2336 , respectively (**Figure 4.9**). Evan's blue fluorescence in mice that received optic nerve crush, and then Evan's blue injection and perfusion after 1 hour, 6 hours, and 24 hours after the operation was 4065 ± 2021 , 3362 ± 1677 , 3179 ± 1533 , respectively. Evan's blue extravasation was not detected in retinal whole mounts after sham surgery or optic nerve crush (ANOVA).

4.1.4 The optic nerve vasculature leaks at the crush site after optic nerve crush

Evan's blue fluorescence was expressed as the mean gray value. At the optic nerve crush site (**Figure 4.10**) Evan's blue fluorescence intensity was 3497 ± 825 , 3422 ± 965 , 4297 ± 1210 in animals that received a sham surgery and then Evan's blue injection plus perfusion 1 hour (n=3), 6 hours (n=3), and 24 hours (n=3) (**Figure 4.11**). In animals that received an optic nerve crush injury and then Evan's blue injection plus perfusion 1 hour (n=3), 6 hours (n=3), and 24 hours (n=3) later, the fluorescence intensity was 7892 ± 543 , 7219 ± 2279 , 8375 ± 2661 , respectively. There was a significant increase (ANOVA/Tukey's post hoc test; $p < 0.0001$) in the fluorescence of Evan's blue at the crush site in animals that

received an injury. There were no significant differences in the fluorescence at the crush site measured over 24 hours.

4.1.5. The area of the crush site does not change over 24 hours after optic nerve crush

The area of extravasated Evan's blue after Evan's blue injection and perfusion was 0 in all mice that received sham surgeries and were examined at 1 hour (n=3), 6 hours (n=3), and 24 hours (n=3) after sham surgery. The crush site as visualized by Evan's blue fluorescence (**Figure 4.10**) was $138447 \pm 62363 \mu\text{m}^2$, $135656 \pm 36973 \mu\text{m}^2$, $180214 \pm 84345 \mu\text{m}^2$, at 1 hour, 6 hours, and 24 hours after optic nerve crush, respectively (**Figure 4.12**). There were no significant differences in crush site among injured animals over a period of 24 hours (ANOVA).

4.1.6 The diameter of retinal arterioles and venules does not change after optic nerve crush

The change in diameter of all retinal arterioles and venules (**Figure 4.13**) was measured before optic nerve crush injury, immediately after, as well as 1 day, 3 days, and 7 days after injury. The mean diameter of retinal arterioles and venules in uninjured animals was 27.4736 ± 1.7791 . Immediately after optic nerve crush the diameter was $28.7828 \pm 2.3864 \mu\text{m}$, while it was $28.199 \pm 2.5546 \mu\text{m}$ 1 day after crush injury, $27.7567 \pm 2.1002 \mu\text{m}$ 3 days after injury, and $28.221 \pm$

2.2936 μm 7 days after injury. A frequency distribution was plotted with a bin centre of 15 μm . (**Figure 4.14**). There were no significant differences in arteriolar and venular diameter detected (ANOVA) after optic nerve crush, up to 7 days.

4.1.7 Retinal thickness does not change over 7 days after optic nerve crush

As measured using optical coherence tomography (**Figure 4.13**), the thickness of the retina was $218.6 \pm 7 \mu\text{m}$, $218.2 \pm 7.5 \mu\text{m}$, $216.6 \pm 9 \mu\text{m}$, $215.2 \pm 10.3 \mu\text{m}$, $217.4 \pm 5.1 \mu\text{m}$ in uninjured mice, immediately after optic nerve crush, 1 day after optic nerve crush, 3 days after optic nerve crush, and 7 days after optic nerve crush, respectively (**Figure 4.15**). There were no significant differences in retinal thickness between any of the experimental groups. The thickness of the retina does not change over 7 days following optic nerve crush.

4.1.8 Retinal blood flow is unaffected by optic nerve crush injury

The time to illuminate 250 μm of the retinal arterioles with intraperitoneally injected FITC (**Figure 4.16**) was 2.11 ± 1.3 seconds, 2.05 ± 1.82 seconds, and 1.94 ± 1.02 seconds in uninjured animals (n=4), 1 day after optic nerve crush (n=4), and 3 days after optic nerve crush (n=4), respectively (**Figure 4.17**). There were no measurable differences in retinal blood flow as visualized by fluorescein angiography (ANOVA).

4.1.9 Leukocyte speed does not change after optic nerve crush

The number of frames required for leukocytes labeled with acridine orange (**Figure 4.18**) to travel the length of retinal arterioles (**Figure 4.19**) in the field of view was 2.89 ± 0.48 frames, 2.78 ± 0.48 frames, 2.89 ± 0.48 frames, and 2.78 ± 0.48 frames, in uninjured animals (n=3), 1 day after optic nerve crush (n=3), 3 days after optic nerve crush (n=3) and 7 days after optic nerve crush (n=3), respectively (**Figure 4.20**). The number of frames required for leukocytes labeled with acridine orange to travel the length of retinal venules was 2.89 ± 0.48 frames, 3 ± 0.83 frames, 2.89 ± 0.48 frames, and 3.11 ± 0.48 frames, in uninjured animals (n=3), 1 day after optic nerve crush (n=3), 3 days after optic nerve crush (n=3) and 7 days after optic nerve crush (n=3), respectively. The rate of leukocyte travel was not significantly different in any of the studied experimental conditions (ANOVA). Leukocyte adherence and rolling was not observed in any of the experimental conditions.

4.2 Discussion

Acute optic nerve injury results in the apoptosis of retinal ganglion cells (Berkelaar et al., 1994; Rosenzweig et al., 2010). In this study, optic nerve crush resulted in the progressive death of retinal ganglion cells over 28 days as indicated by labeling of Brn3a. The loss of cell density was consistent throughout all areas of the retina studied. This type of widespread cell loss is unlike that typified in glaucoma that results in sectorial loss of retinal ganglion cells (Jakobs, Libby, Ben, John, & Masland, 2005), but is consistent with ganglion cell loss after acute

optic nerve injury (Nadal-Nicola s et al., 2009). This suggests that the sampling of retinal ganglion cells in section after optic crush injury can be restricted to a selected area of the retina and that this sampling would give an adequate representation of retinal ganglion cell density loss throughout the retina.

Slit2, initially discovered as a neuronal repellent in development (Shiau & Bronner-Fraser, 2009; Ye, Geng, Ma, & Geng, 2010; Zhao et al., 2014), is now understood to play an important role in modulating inflammation in the adult organism (Ye et al., 2010; Zhao et al., 2014). The neuroprotective mechanisms of Slit2 have been attributed to its ability to modulate inflammation by preventing the migration of immune cells to the site of injury (Wu et al., 2001), as well as decreasing the permeability of endothelial cells in models of injury associated with vascular leakage (Jones et al., 2008). The injection of Slit2 before optic nerve crush injury was expected to protect retinal ganglion cells from death after axonal injury as its neuroprotective abilities have been documented in a number of different models of neuronal death (Altay et al., 2007; Kanellis et al., 2004; Sherchan et al., 2016). Additionally, an *in vitro* mixed neuronal-glia coculture study using oxygen-glucose deprivation/reoxygenation injury found that Slit2 protected neurons from cell death suggesting that Slit2 may be directly neuroprotective to neurons (Altay et al., 2007). Slit2 did not have any measurable effect on the survival of retinal ganglion cells following optic nerve crush injury and their survival was no different from animals injected with vehicle, PBS, only. This indicates that Slit2 is not directly neuroprotective to retinal ganglion cells in

a model of retinal ganglion cell death caused by optic nerve crush injury. Additionally it suggests that the known targets of Slit2 in neuroprotection, immune cell recruitment and endothelial cell permeability, are not directly involved in the mechanisms leading to cell death after optic nerve crush injury. Although optic nerve crush results in a short-lived interruption in blood flow by the mechanical disruption of the vessels in the optic nerve, this transient change in perfusion may not be sufficient to induce vascular permeability or result in the recruitment of immune cells as observed in models of sustained ischemia. For example, in a model of ischemia in rabbits, the threshold for blood retinal barrier damage occurred between 20 and 40 minutes of sustained ischemia (Wilson et al., 1995). The absence of vascular permeability following optic nerve crush injury is thus consistent with previous these observations.

To clarify the involvement of the vascular response following optic nerve crush and gather definitive evidence regarding vascular permeability, Evan's blue injections followed by perfusion with PBS were used after injury. Evan's blue binds irreversibly to albumin and stains the CNS when the blood brain barrier is breached (Xu, Qaum, & Adamis, 2001). It was anticipated that vascular leakage would be observed in the retina as a response to axonal injury. When examining both retinal sections as well as whole mounted retinas of animals that received optic nerve crush, there was no evidence of Evan's blue extravasation up to 24 hours after injury. 24 hours after injury is sufficient to observe retinal vascular permeability after ischemic injury (Wilson et al., 1995). The absence of Evan's

blue extravasation indicates that the contribution of retinal vascular permeability to the death of retinal ganglion cells is negligible. There were no signs of disruption of the outer blood retinal barrier when examining sections. In whole-mounted retinas, with the choroid and pigmented epithelium dissected away, there were no visible disruptions of the inner blood-retinal barrier. When sections through the optic nerve head were examined after Evan's blue injection and PBS perfusion, there was a clear indication of Evan's blue extravasation, and blood-brain barrier disruption, as indicated by fluorescence at the crush site when examined by fluorescent microscopy. The fluorescence exhibited at the crush site demonstrated that there was a definite disruption of the vessels injured at the crush site and leakage into the parenchyma. The leakage was restricted to the crush site and did not extend into the retina. The distance between the crush site and retinal ganglion cell bodies reveals that beyond the fact that the crush site is the area where retinal ganglion cell axons are disrupted, there is likely no relationship between the leakage at the crush site does and the death of retinal ganglion cells. The size of the crush site, as visualized by Evan's blue leakage and fluorescence does not change over 24 hours, showing that the vascular disruption persists over this period of time and indicates that repair of the damaged vessels does not occur 24 hours.

Although there was no retinal vascular leakage observed after optic nerve crush injury, other changes in the retinal vasculature might have occurred. Studies of the retinal vasculature in human glaucoma have shown that, although

inconsistent, changes in the diameter of retinal arterioles and venules are associated with glaucoma (Jonas, Nguyen, & Naumann, 1989; Zhao, 2002). *In vivo* bright field imaging was used to visualize and measure any possible alterations in the structure of the retinal vasculature. It was expected that there would be measurable changes in the diameter of the vessels, potentially arising from alterations in the volume of blood contained in the vessels, whether through a decrease in blood flow resulting in a decreased diameter, or a backup of blood flow, resulting in an increased diameter. When measuring the diameter of the retinal arterioles and venules after optic nerve crush, there were no significant changes observed when a frequency distribution was plotted. This is further evidence of a lack of vascular reactivity in the retina following optic nerve crush injury. Although studies of human glaucoma have shown alterations in vascular diameter (Kawasaki et al., 2013), these may be associated with chronic changes in the vasculature associated with the aging body (Leung et al., 2003), rather than an acute injury like optic nerve crush.

Changes in retinal thickness have been documented in human glaucoma, particularly the retinal nerve fibre layer/ganglion cell layer and inner plexiform layer (de A Moura, Raza, Lazow, De Moraes, & Hood, 2012). *In vivo* retinal imaging using optical coherence tomography was used to quantify retinal thickness over 7 days after optic nerve crush injury. As demonstrated by Brn3a labeling, the optic nerve crush injury inflicted in these studies results in approximately 60% of retinal ganglion cell loss by 7 days. Since retinal thinning

is a characteristic of retinal remodeling in models of retinal ganglion cell loss, this experiment demonstrates that significant retinal ganglion cell loss precedes retinal remodeling and that remodeling is a late event in the retinal response to retinal ganglion cell loss.

Evan's blue injection and perfusion after optic nerve crush demonstrated a clear disruption of the vessels in the optic nerve as evidenced by Evan's blue extravasation. The degree to which retinal circulation was impaired by this disruption was unclear. In order to understand the implications of the disruption of the optic nerve vasculature on the retinal vasculature, fluorescein angiography was used to visualize retinal blood flow. The time required to illuminate 250 μ m of the retinal arterioles was measured and there were no differences observed between uninjured animals or animals up to 3 days after optic nerve crush. This evidence further supports the notion that the contribution of vascular disruption to retinal ganglion cell death is not significant. Additionally, this in vivo imaging reaffirms the evidence obtained using Evan's blue that vascular leakage is not a consequence of optic nerve crush injury. The integrity of the retinal arterioles, venules, and capillaries is not disrupted subsequent to optic nerve crush injury. As mentioned earlier, sustained ischemia would likely lead to blood-retinal barrier breakdown, but this is clearly not a characteristic of acute optic nerve crush (Wilson et al., 1995).

Although there was no evidence of vascular leakage or variation in the diameter of the retinal blood vessels, this does not rule out changes in the

endothelial cells of retinal blood vessels (Tsujikawa & Ogura, 2012). As seen in models of diabetic retinopathy, the endothelial cells of blood vessels may become activated and “sticky” to leukocytes (Cahoon et al., 2014). Potential changes in the activation of the endothelial cells lining retinal blood vessels was examined after optic nerve crush. It was expected that reactivity of the blood vessels would be observed through their interactions of systemic immune cells in circulation. Acridine orange leukocyte fluorography was used to track the flow of leukocytes in retinal arterioles and venules (Miyamoto, Hiroshiba, Tsujikawa, & Ogura, 1998). The number of frames required for leukocytes to traverse the length of retinal arterioles and venules was calculated from videos captured *in vivo*. The number of frames (0.07 seconds/frame) required for leukocytes to travel the length of visible arterioles and venules was approximately 3 frames in uninjured mice and in all mice examined up to 7 days after optic nerve crush. Following each optic nerve crush procedure performed, animals were examined using bright field and optical coherence tomography *in vivo*. It is important to note that some injured animals sustained a more severe optic nerve crush injury that resulted in retinal detachment near the optic nerve and the accumulation of fluid beneath the detached retina. Each of these animals with severe injury was excluded from analysis. As a positive control, some of these animals were examined using acridine leukocyte fluorography. Mice with detached retinas clearly exhibited changes in the flow of leukocytes. In areas of retinal detachment, the flow of leukocytes was slowed as they as they passed through the associated retinal

vessels. These types of changes in leukocyte flow and adhesion to retinal vessels have been documented in models with definite vascular reactivity, such as diabetic retinopathy (Tsujikawa & Ogura, 2012). These experiments solidify the fact that the role of the retinal vasculature in response to optic nerve crush is negligible. With regard to the retinal vasculature following optic nerve crush, there are no changes in permeability, no changes in vessel diameter, and no remarkable changes in blood or leukocyte flow.

4.3 Figures

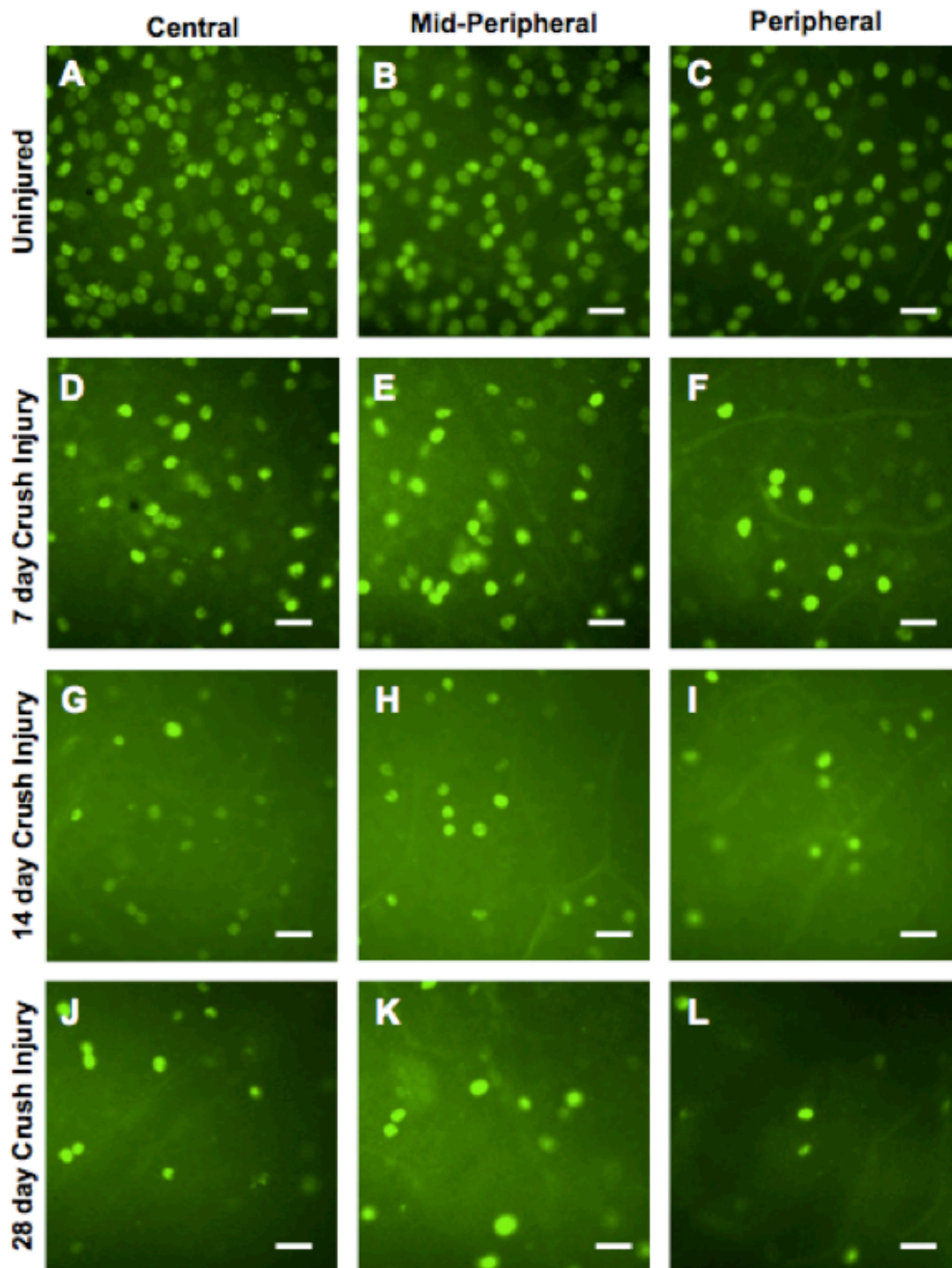


Figure 4.1 Whole-mounted retinas with immunohistochemical labeling of Brn3a (green), a marker of retinal ganglion cells, in the central, mid-peripheral, and peripheral retina in (A,B,C) uninjured mice (n=4), (D,E,F) 7 days after optic nerve crush (n=4), (G,H,I) 14 days after optic nerve crush (n=4), and 28 days after optic nerve crush (n=4) (J,K,L). Scale bar = 20 μ m

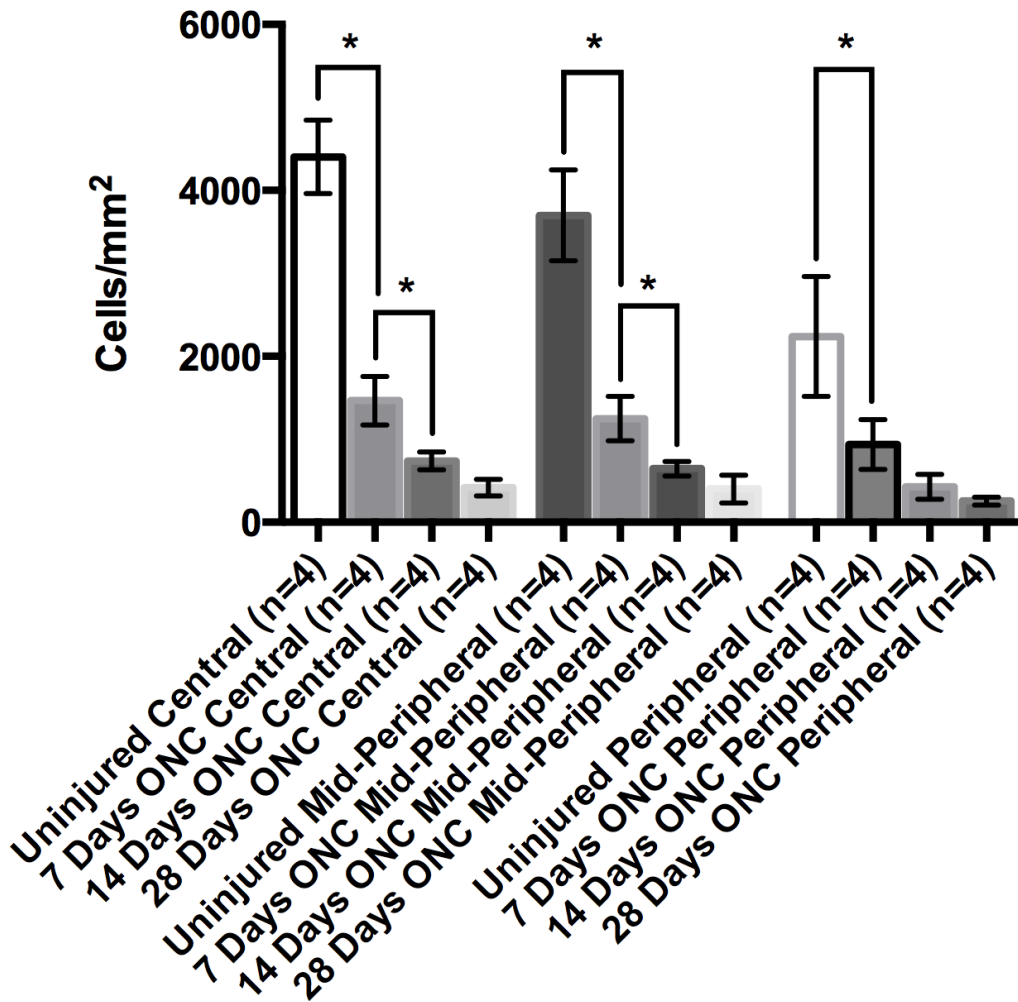


Figure 4.2 Retinal ganglion cell counts (cells/mm²) quantified by counting Brn3a+ cells labeled by immunohistochemistry in the whole mounted retinas of uninjured mice, and mice 7, 14, and 28 days after optic nerve crush. There was a loss of retinal ganglion cells over 28 days. (Central retina, uninjured (n=4) = 4404 ± 442 cells/mm, 7 days (n=4) after optic nerve crush = 1466 ± 292 cells/mm [uninjured versus 7 days, p<0.001], 14 days (n=4) after optic nerve crush = 740 ± 105.8 cells/mm [7 days versus 14 days, p=0.0011], 28 days (n=4) after optic nerve crush = 417.7 ± 101.9 cells/mm), (Mid-peripheral retina, uninjured (n=4) = 3700 ± 547 cells/mm, 7 days (n=4) after optic nerve crush = 1250 ± 270 cells/mm [uninjured versus 7 days, p<0.001], 14 days (n=4) after optic nerve crush = 646 ± 86.2 cells/mm [7 days versus 14 days, p=0.0117], 28 days (n=4) after optic nerve crush = 400.4 ± 168.8 cells/mm), (Peripheral retina, uninjured (n=4) = 2239 ± 723, 7 days (n=4) after optic nerve crush = 937.2 ± 298.2 cells/mm [uninjured versus 7 days, p<0.001], 14 days (n=4) after optic nerve crush = 428.6 ± 150.6 cells/mm, 28 days (n=4) after optic nerve crush = 256.6 ± 46.6 cells/mm)

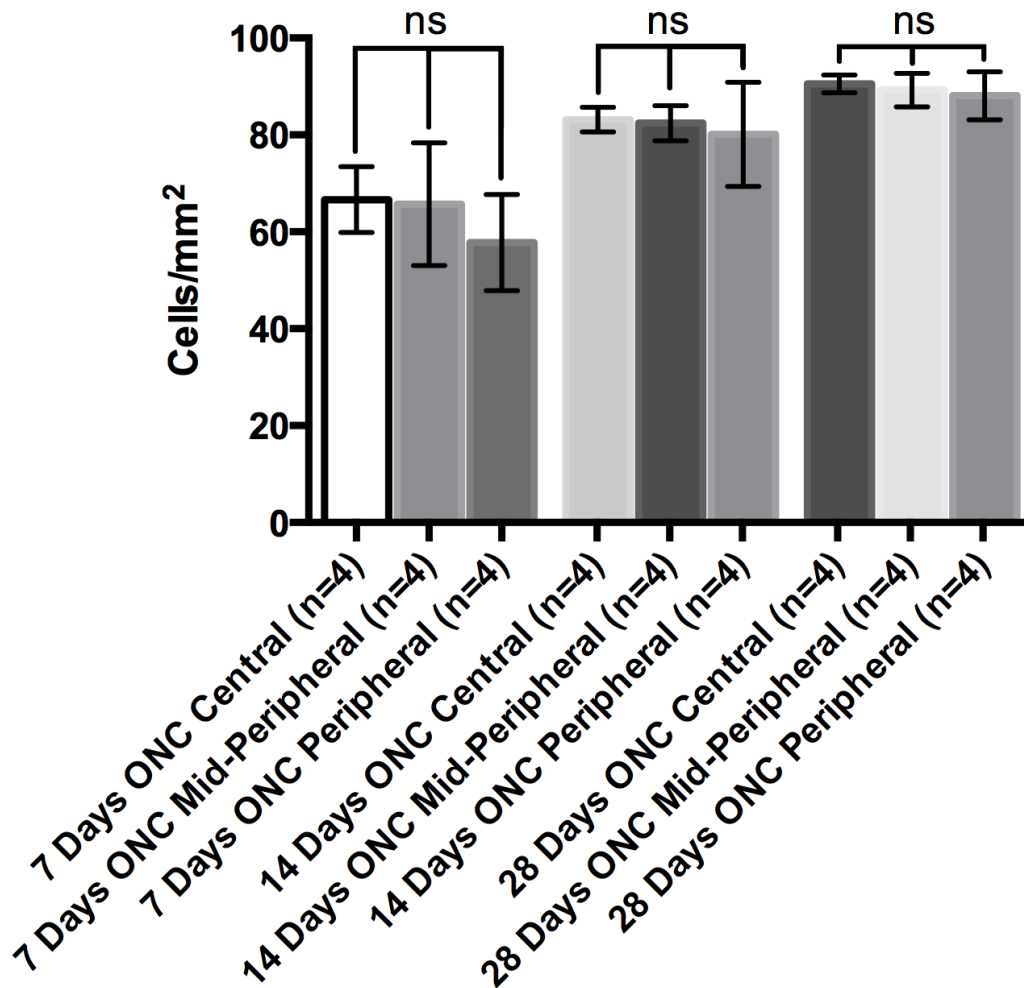


Figure 4.3 Percentage of retinal ganglion cell loss compared to uninjured animals over 28 days in three retinal sectors. There were no significant differences in percentage cell loss of retinal ganglion cells compared to controls in the central, mid-peripheral, and peripheral retina. The rate of RGC loss was consistent throughout the retina at 7, 14, and 28 days after optic nerve crush. (Retinal ganglion cell loss in the central retina, 7 days (n=4) after optic nerve crush = 66.7%, 14 days (n=4) after optic nerve crush = 83.1%, 28 days (n=4) after optic nerve crush = 90.5%) (Retinal ganglion cell loss in the mid-peripheral retina, 7 days (n=4) after optic nerve crush = 66.2%, 14 days (n=4) after optic nerve crush = 82.5%, 28 days (n=4) after optic nerve crush = 89.2%) (Retinal ganglion cell loss in the peripheral retina, 7 days (n=4) after optic nerve crush = 58.1%, 14 days (n=4) after optic nerve crush = 80.9%, 28 days (n=4) after optic nerve crush = 88.5%)

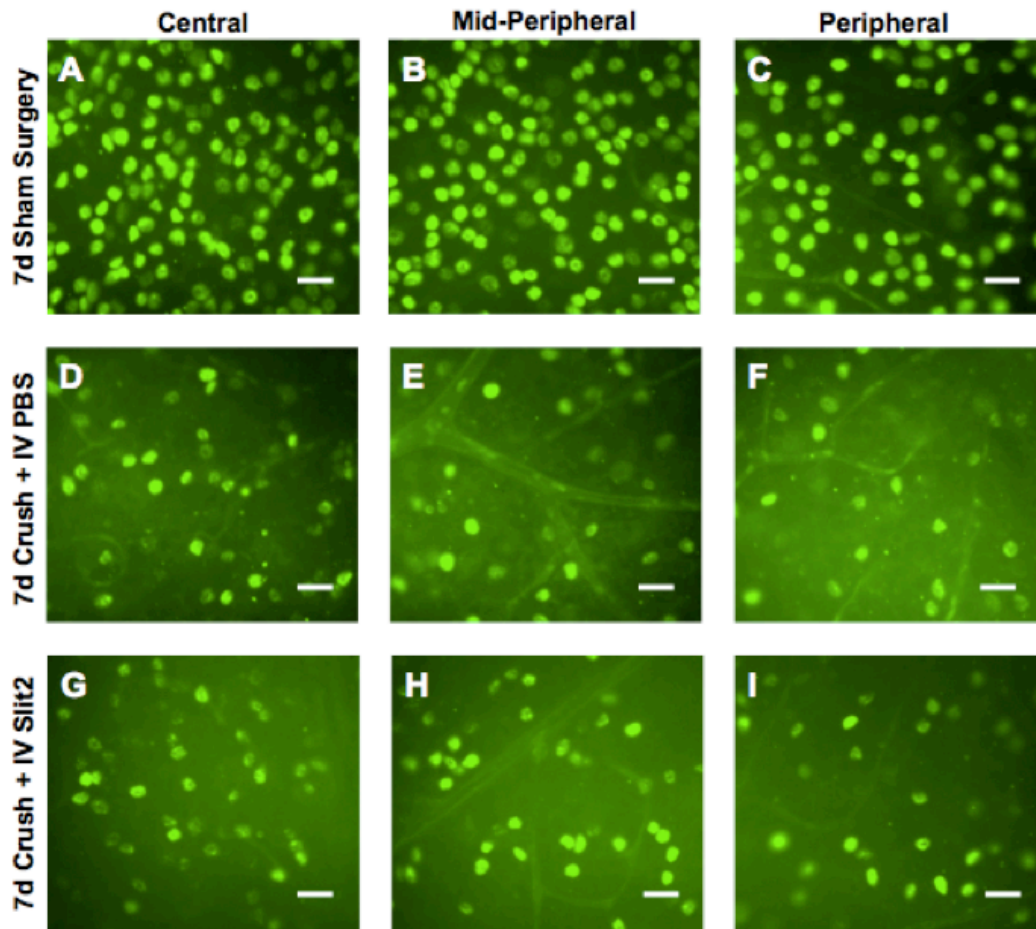


Figure 4.4 Whole-mounted retinas were immunohistochemically labeled for **Brn3a** in the central, midperipheral, and peripheral retina. (A,B,C) Brn3a (green) 7 days after sham surgery, (D,E,F) 7 days after optic nerve crush and intravenous (IV) PBS injection, or (G,H,I) 7 days after optic nerve crush and intravenous Slit2 injection. Scale bar = 20 μ m.

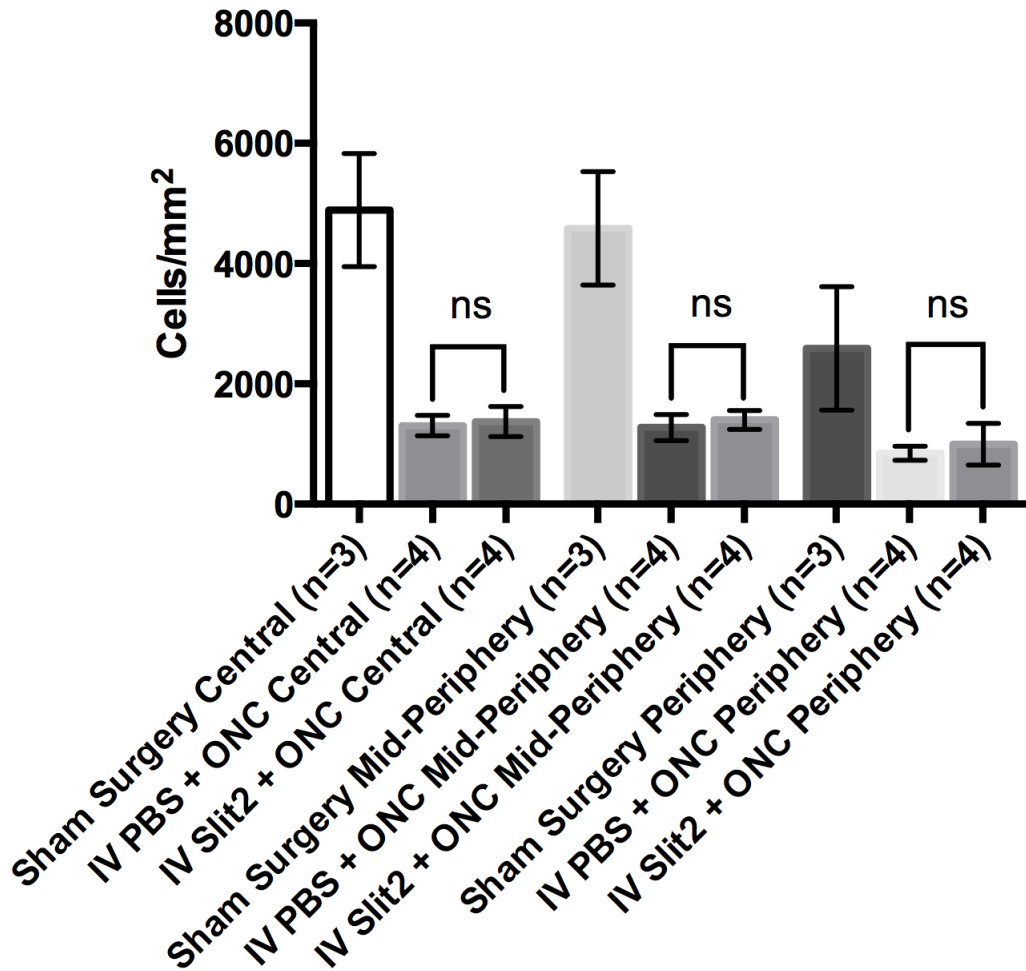


Figure 4.5 Retinal ganglion cell counts (cells/mm²) in the central, mid-peripheral, and peripheral retina quantified by counting Brn3a+ cells labeled by immunohistochemistry in the whole mounted retinas of mice 7 days receiving sham optic nerve crush surgeries, or receiving intravenous PBS or Slit2 injections before optic nerve crush injuries. There were no significant differences in retinal ganglion cell density between animals receiving optic nerve crush and injected with PBS versus Slit2. (Sham surgery after 7 days (uninjured), central retina = 4888 ± 941 cells/mm, mid-peripheral retina = 4586 ± 942 cells/mm, peripheral retina = 2589 ± 1027 cells/mm) (Optic nerve crush after 7 days with intravenous PBS injection, central retina = 1305 ± 169 cells/mm, mid-peripheral retina = 1275 ± 219 cells/mm, peripheral retina = 847.8 ± 117.7 cells/mm) (Optic nerve crush after 7 days with intravenous Slit2 injection, central retina = 1373 ± 249 cells/mm, mid-peripheral retina = 1400 ± 159 cells/mm, peripheral retina = 990.2 ± 345.5 cells/mm)

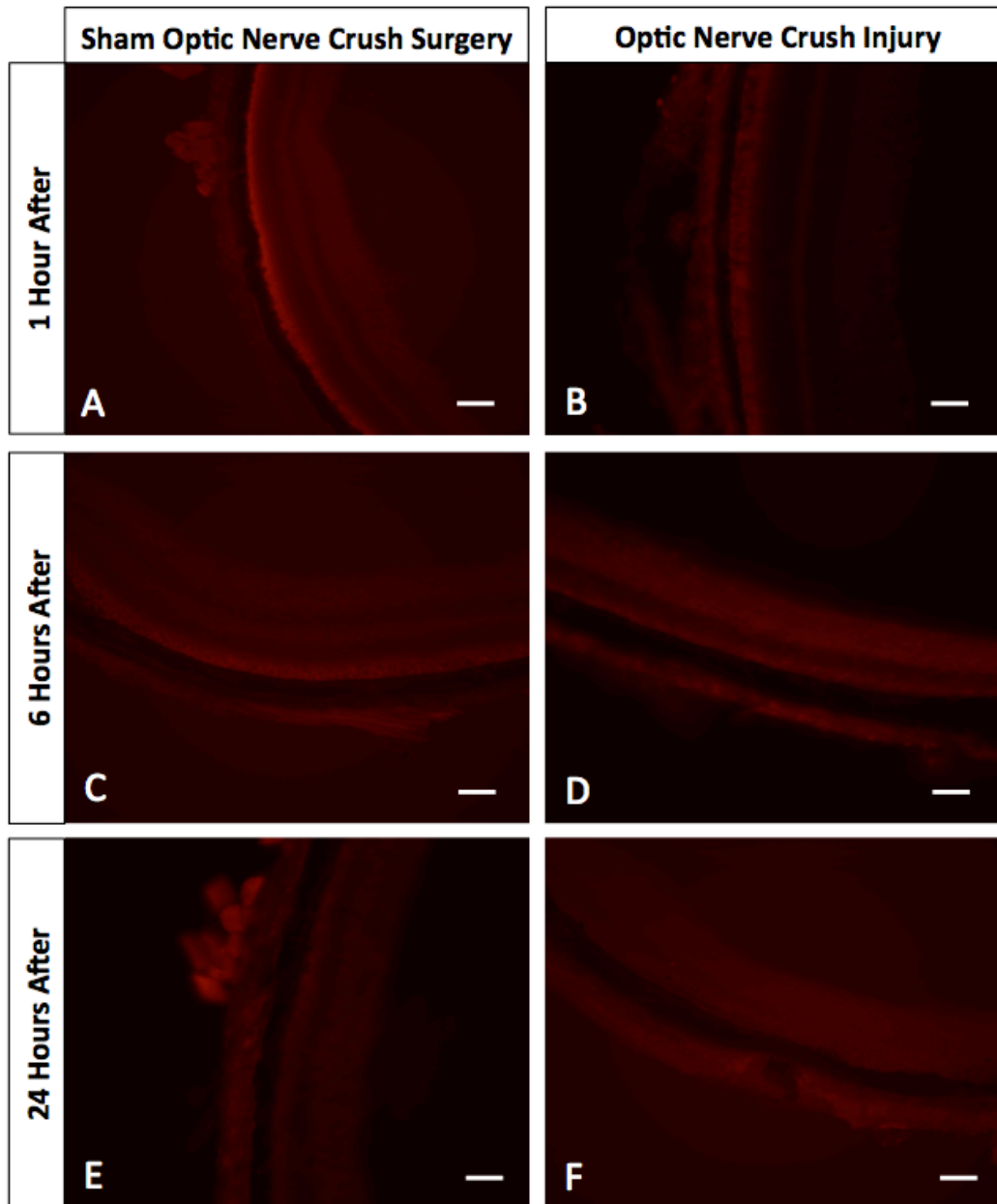


Figure 4.6 12 μm thick frozen transverse retinal sections of mice intravenously injected with Evan's Blue (labeling in red) and perfused with PBS (**A**) 1 hour after sham optic nerve crush surgery (n=3) (**B**) 1 hour after optic nerve crush injury (n=3) (**C**) 6 hours after sham optic nerve crush surgery (n=3) (**D**) 6 hours after optic nerve crush injury (n=3) (**E**) 24 hours after sham optic nerve crush surgery (n=3) (**F**) 24 hours after optic nerve crush injury (n=3). Evan's blue extravasation was not observed in any experimental condition. Scale = 50 μm .

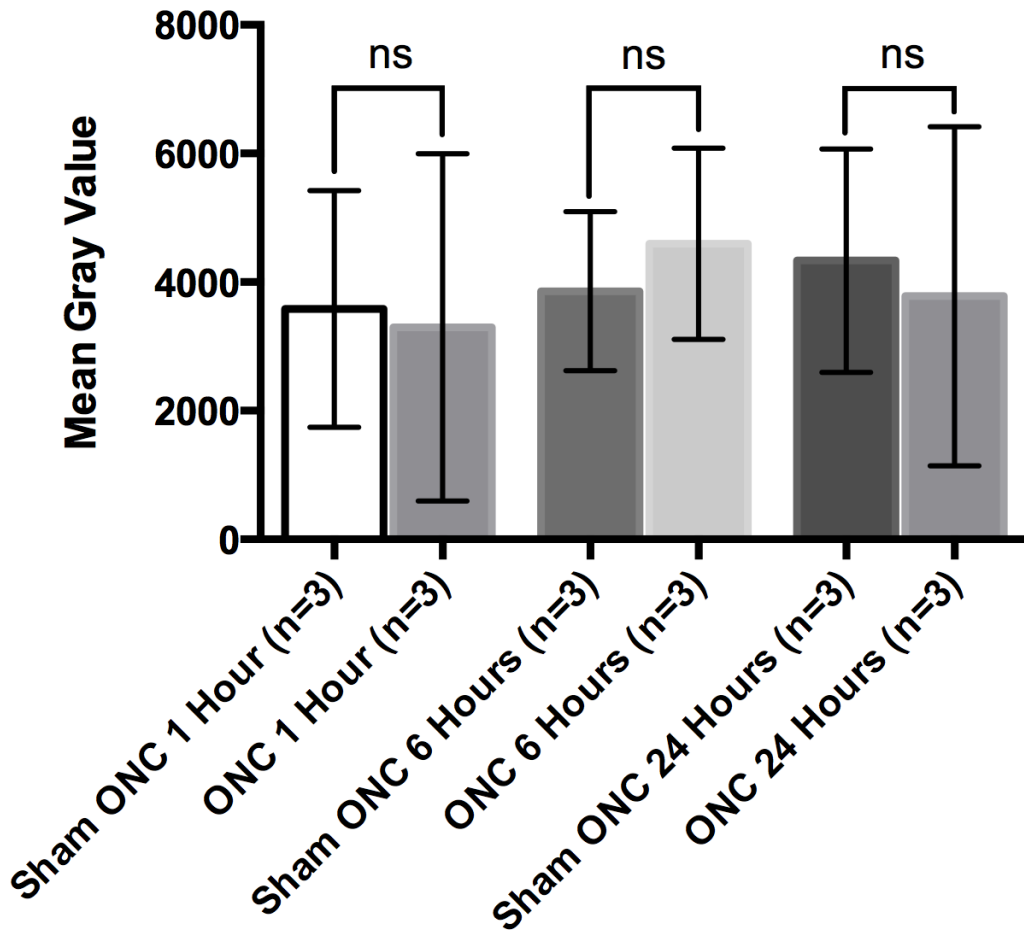


Figure 4.7 Staining intensity in frozen transverse retinal sections of mice intravenously injected with Evan’s Blue and perfused with PBS. There are no significant differences in staining intensity in retinal sections among mice receiving sham optic nerve crush surgery (1 hour after surgery, n=3, mean gray value = 3583 ± 1837; 6 hours after surgery, n=3, mean gray value = 3858 ± 1236; 24 hours after surgery, n=3, mean gray value = 4334 ± 1736), or optic nerve crush injury (1 hour after crush, n=3, mean gray value = 3296 ± 2701; 6 hours after crush, n=3, mean gray value = 4597 ± 1489; 24 hours after crush, n=3, mean gray value = 3781 ± 2636).

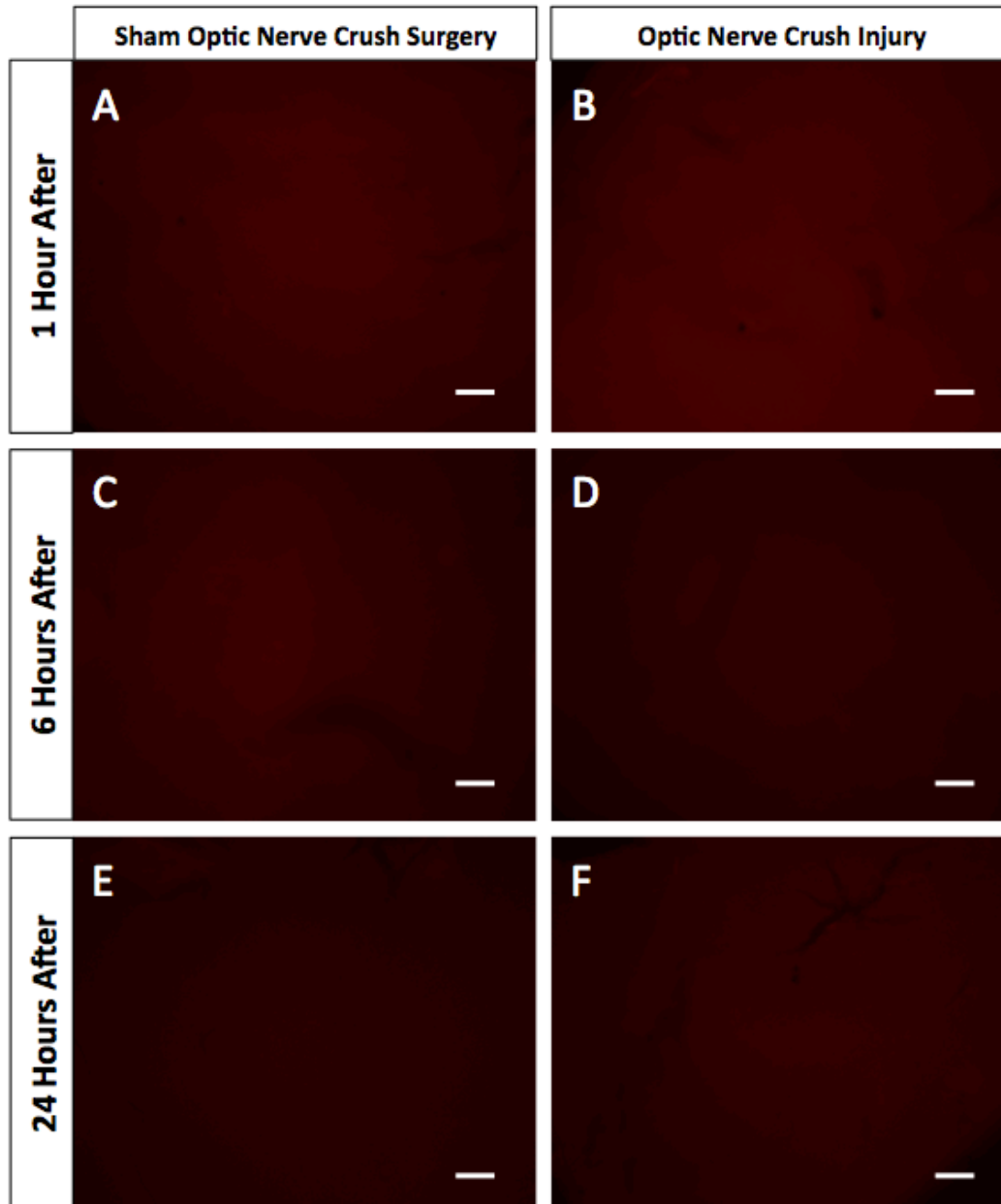


Figure 4.8 Whole mounted retinas of mice intravenously injected with Evan's Blue (labeling in red) and perfused with PBS (**A**) 1 hour after sham optic nerve crush surgery (n=3) (**B**) 1 hour after optic nerve crush injury (n=3) (**C**) 6 hours after sham optic nerve crush surgery (n=3) (**D**) 6 hours after optic nerve crush injury (n=3) (**E**) 24 hours after sham optic nerve crush surgery (n=3) (**F**) 24 hours after optic nerve crush injury (n=3). Evan's blue extravasation was not observed in any of the experimental conditions. Scale bar = 50 μ m.

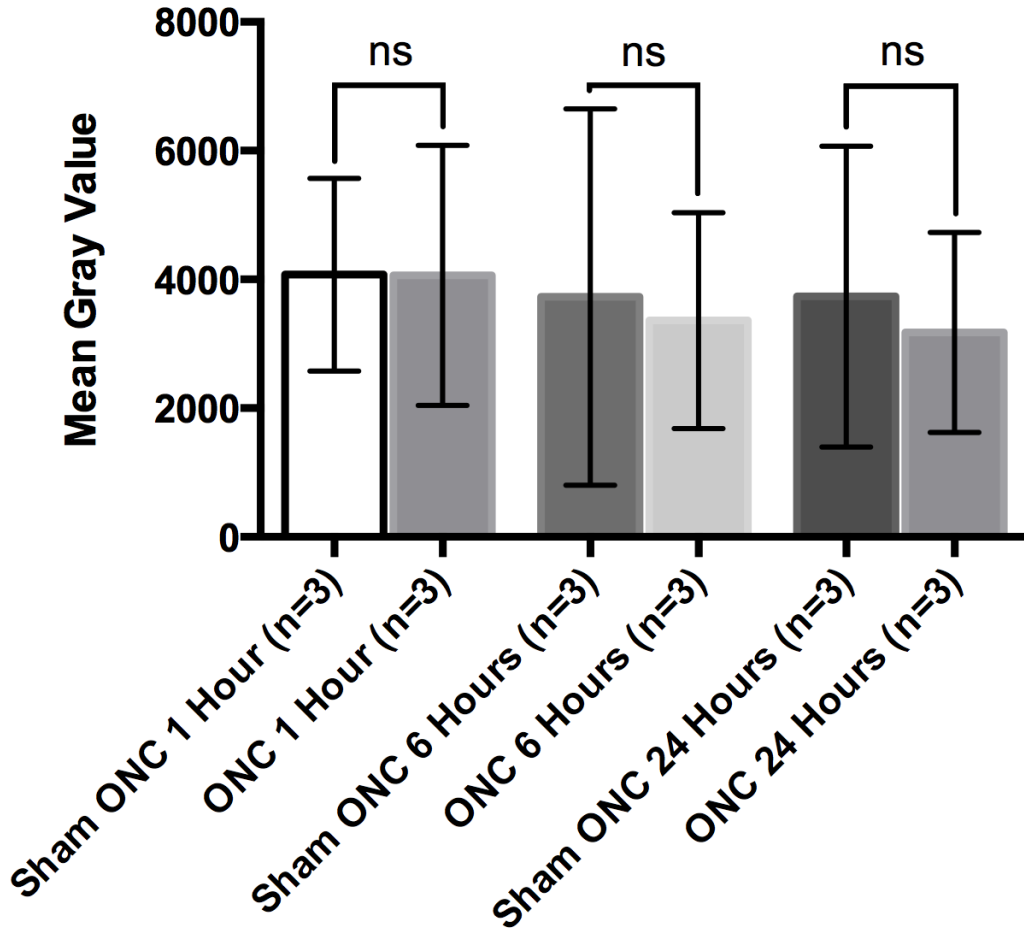


Figure 4.9 Standardized staining intensity whole mounted retinas of mice intravenously injected with Evan’s Blue and perfused with PBS. There are no significant differences in staining intensity in retinal whole mounts among mice receiving sham optic nerve crush surgery (1 hour after surgery, n=3, mean gray value = 4074 ± 1499; 6 hours after surgery, n=3, mean gray value = 3728 ± 2923; 24 hours after surgery, n=3, mean gray value = 3733 ± 2336), or optic nerve crush injury (1 hour after crush, n=3, mean gray value = 4065 ± 2021; 6 hours after crush, n=3, mean gray value = 3362 ± 1677; 24 hours after crush, n=3, mean gray value = 3179 ± 1533).

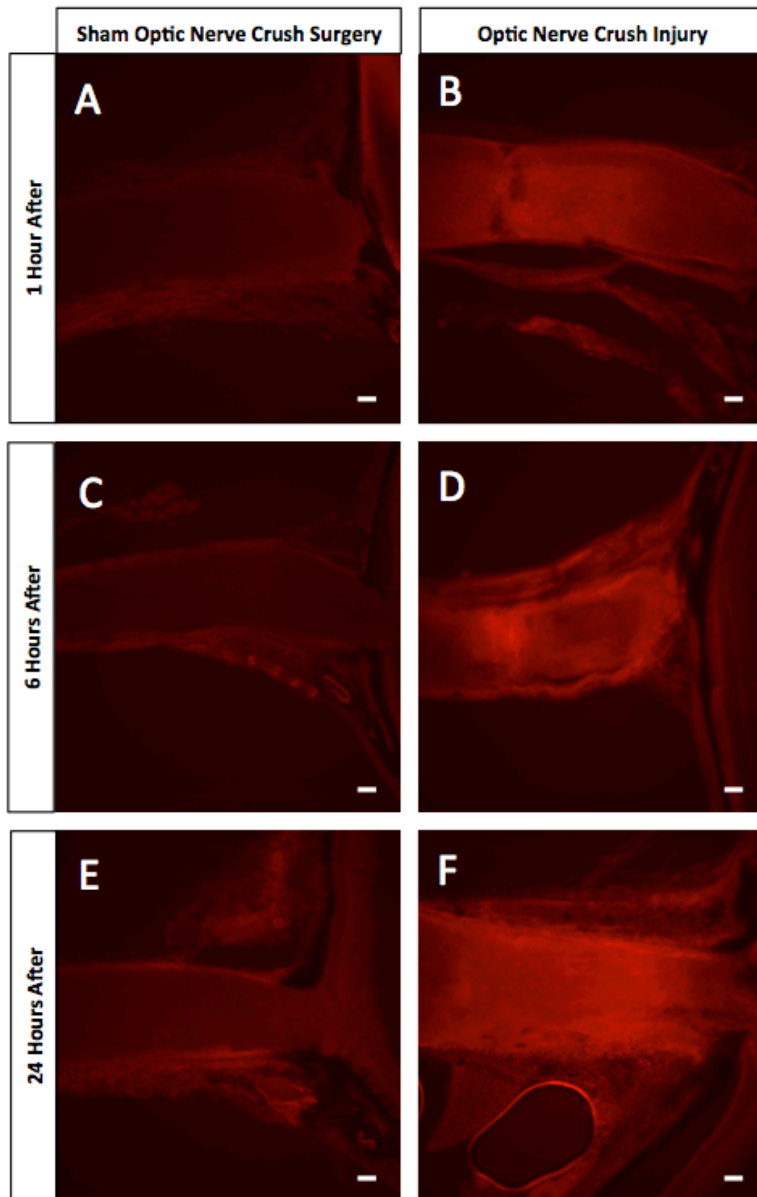


Figure 4.10 12 μm thick frozen transverse optic nerve head sections of mice intravenously injected with Evan's Blue (labeling in red) and perfused with PBS (A) 1 hour after sham optic nerve crush surgery (n=3) (B) 1 hour after optic nerve crush injury (n=3) (C) 6 hours after sham optic nerve crush surgery (n=3) (D) 6 hours after optic nerve crush injury (n=3) (E) 24 hours after sham optic nerve crush surgery (n=3) (F) 24 hours after optic nerve crush injury (n=3). Evan's blue extravasation was observed at the crush site in mice receiving optic nerve crush injury 1, 6, and 24 hours after the surgery. No crush site was observed in mice receiving a sham surgery. Scale bar = 50 μm .

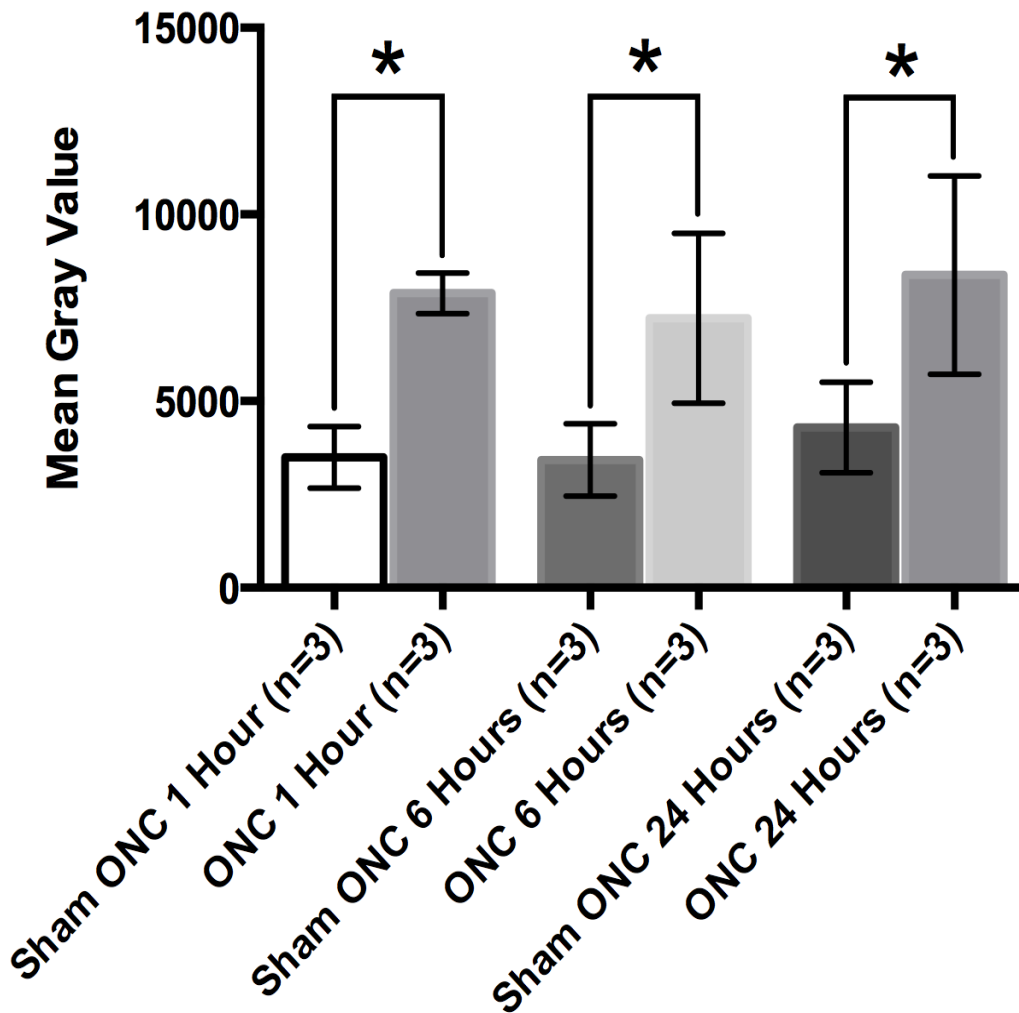


Figure 4.11 Staining intensity of the crush site of mice intravenously injected with Evan’s Blue and perfused with PBS 1, 6, and 24 hours after optic nerve crush injury or optic nerve crush sham surgery. There was a significant increase in the fluorescence of Evan’s blue in injured mice compared to animals receiving sham surgery (ANOVA/Tukey’s post hoc test’ $p < 0.001$). (1 hour after surgery, $n=3$, mean gray value = 3497 ± 825 , 6 hours after surgery, $n=3$, mean gray value = 3422 ± 965 ; 24 hours after surgery, $n=3$, mean gray value = 4297 ± 1210), or optic nerve crush injury (1 hour after crush, $n=3$, mean gray value = 7892 ± 543 , 6 hours after crush, $n=3$, mean gray value = 7219 ± 2279 ; 24 hours after crush, $n=3$, mean gray value = 8375 ± 2661). There were no significant differences in staining intensity at the crush site of injured mice between 1 hour, 6 hours, and 24 hours.

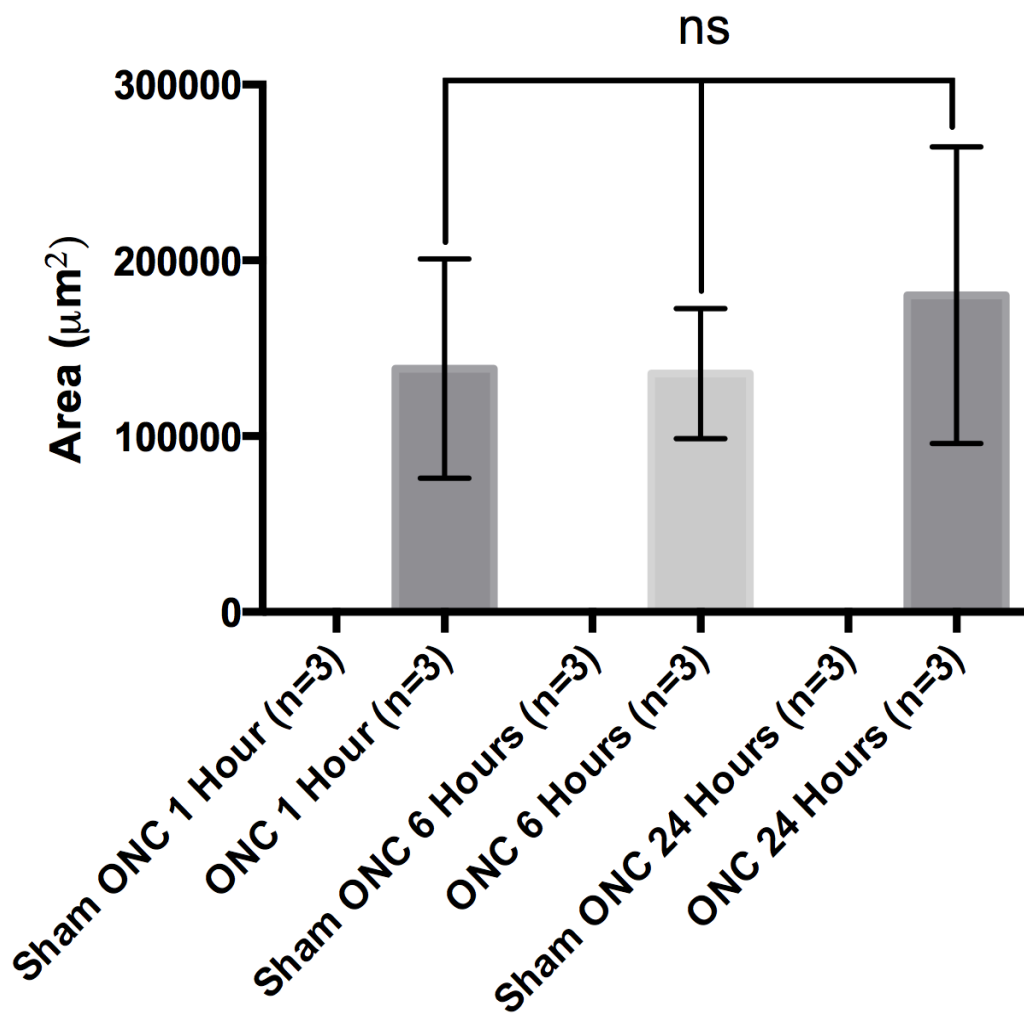


Figure 4.12 Crush site area of mice intravenously injected with Evan’s Blue and perfused with PBS 1, 6, and 24 hours after optic nerve crush injury or optic nerve crush sham surgery.. There were no significant differences in crush site area of injured mice between 1 hour, 6 hours, and 24 hours (1 hour after crush, n=3, 138447 ± 62363 µm², 6 hour after crush, n=3, 135656 ± 36973 µm², 24 hours after crush, n=3, 180214 ± 84345 µm²).

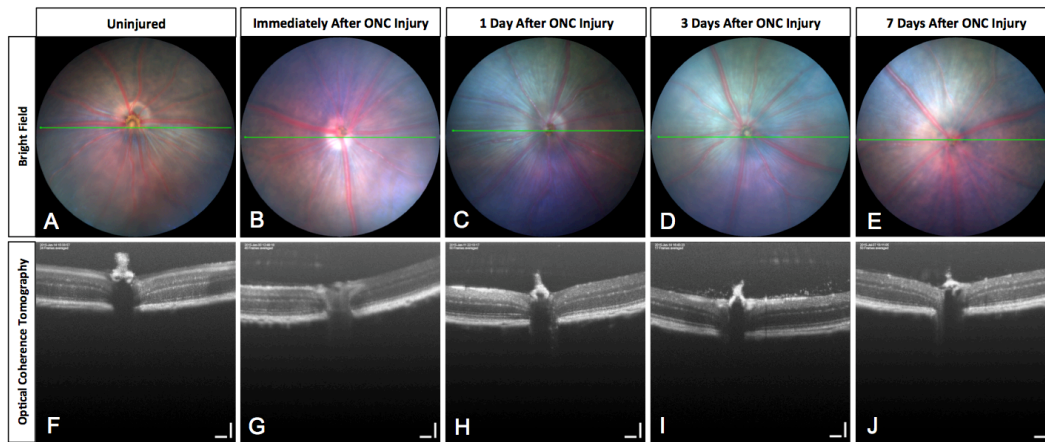


Figure 4.13 *In vivo* retinal imaging after optic nerve crush injury. Bright field retinal images in (A) uninjured mice, (B) immediately after optic nerve crush, (C) 1 day after optic nerve crush, (D) 3 days after optic nerve crush, (E) 7 days after optic nerve crush. The green line in images (A-E) corresponds to the area scanned using optical coherence tomography and visualized in the images underneath each bright field image. Optical coherence tomography scans in (F) uninjured mice, (G) immediately after optic nerve crush, (H) day after optic nerve crush, (I) 3 days after optic nerve crush, (J) 7 days after optic nerve crush.

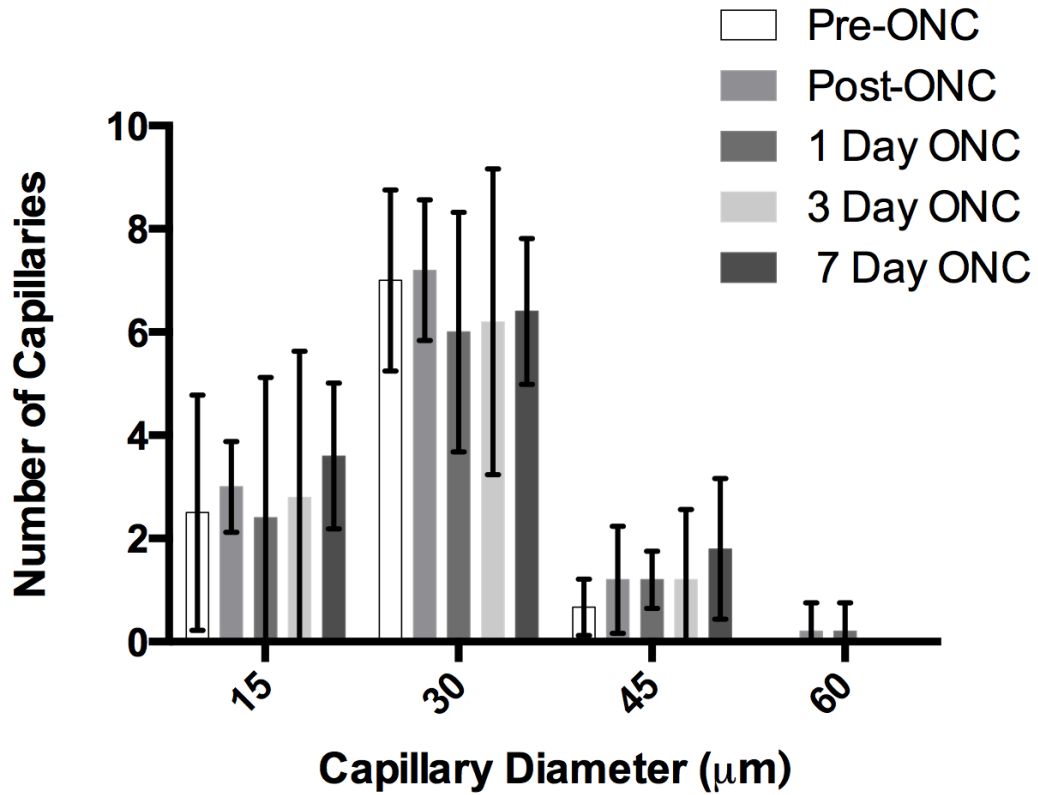


Figure 4.14 Change in retinal arteriolar and venular diameter after optic nerve crush over 7 days measured using bright field retinal microscopy. There were no significant changes in frequency distribution detected among arteriolar and venular diameters.

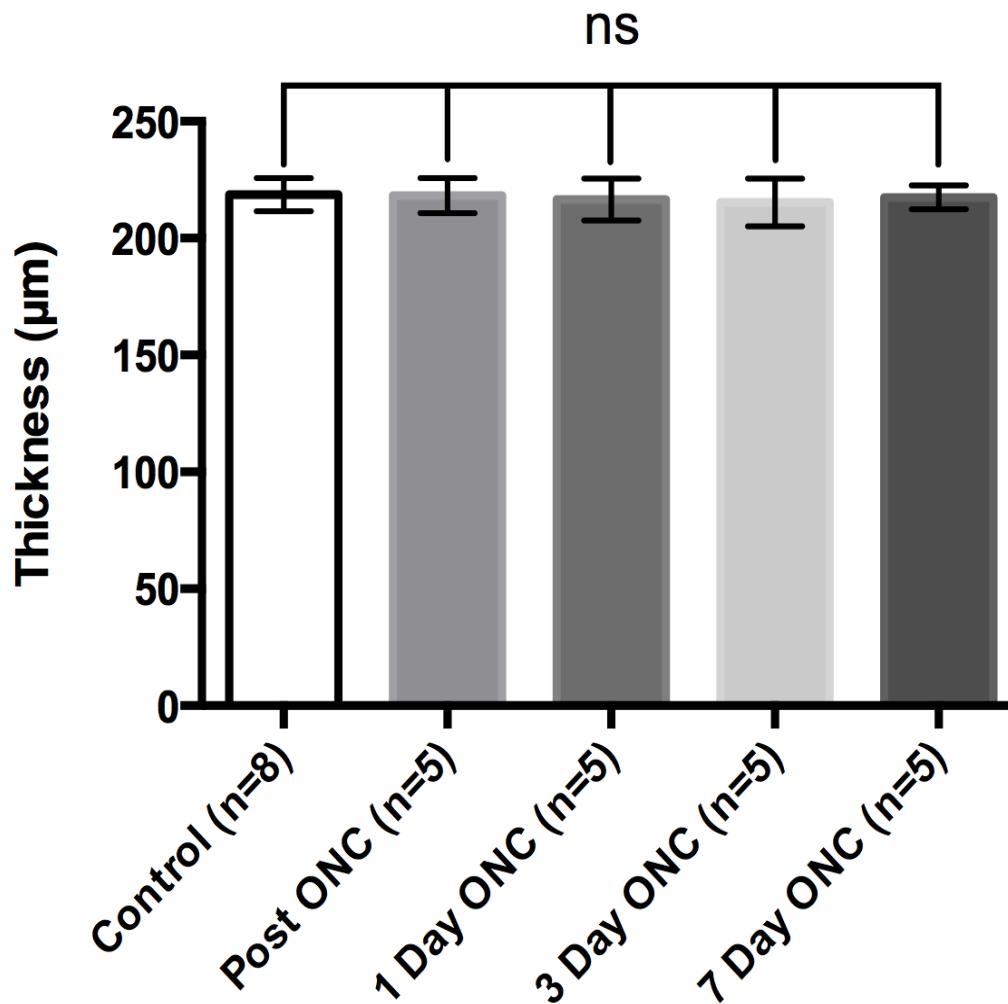


Figure 4.15 Retinal thicknesses in the mid-periphery after optic nerve crush measured using optical coherence tomography. Retinal thickness in uninjured mice (n=5, $218.6 \pm 7 \mu\text{m}$), immediately after optic nerve crush (n=5, $218.2 \pm 7.5 \mu\text{m}$), 1 day after optic nerve crush (n=5, $216.6 \pm 9 \mu\text{m}$), 3 days after optic nerve crush (n=5, $215.2 \pm 10.3 \mu\text{m}$), 7 days after optic nerve crush (n=5, $217.4 \pm 5.1 \mu\text{m}$). There were no significant changes in retinal thickness over 7 days after optic nerve crush (ANOVA).

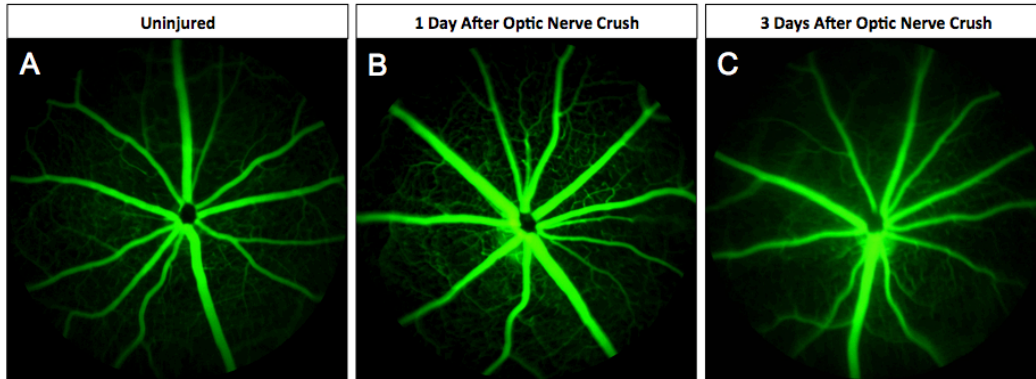


Figure 4.16 Retinal fluorescein angiograms after optic nerve crush injury in mice. Fluorescent images of intraperitoneally injected fluorescein (green) in (A) uninjured mice (n=4), (B) 1 day after optic nerve crush (n=4), (C) 3 days after optic nerve crush (n=4).

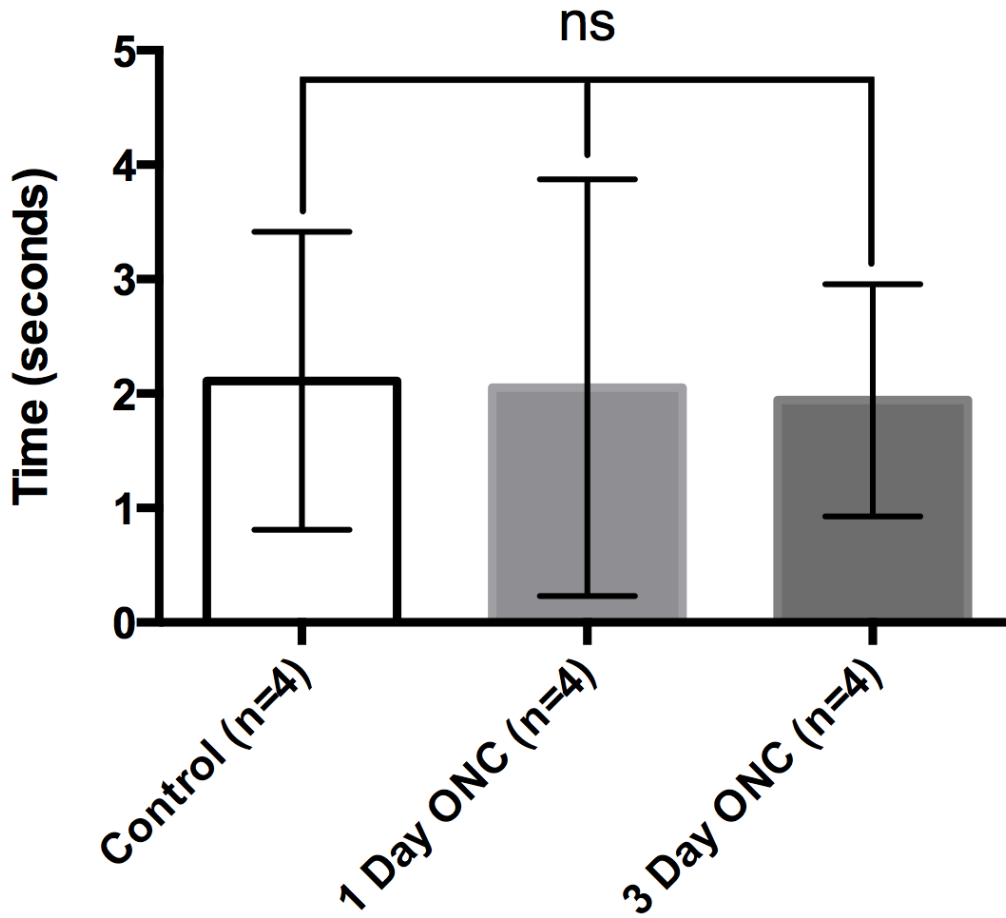


Figure 4.17 Fluorescein fill time during retinal fluorescein angiography.

There are no significant differences in fluorescein fill time when comparing uninjured mice (n=4, 2.11 ± 1.3 seconds), mice 1 day after optic nerve crush (n=4, 2.05 ± 1.82 seconds), and 3 days after optic nerve crush (n=4, 1.94 ± 1.02 seconds).

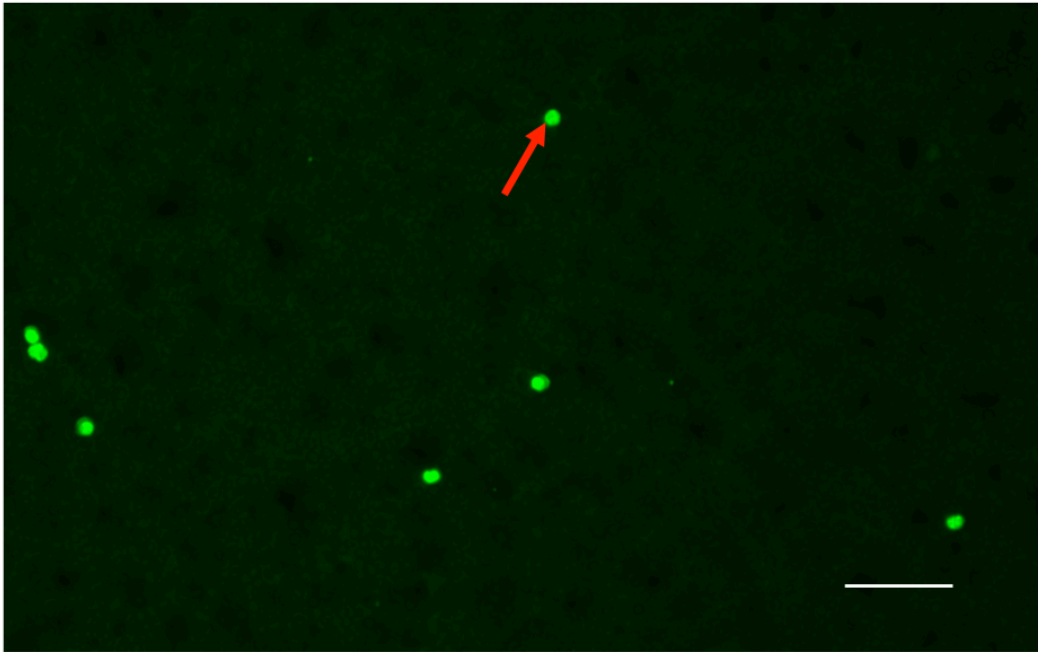


Figure 4.18 Blood smear stained with acridine orange. Acridine orange (green) staining on a mouse blood smear. Labeling is present in leukocytes, but not erythrocytes (n=3).

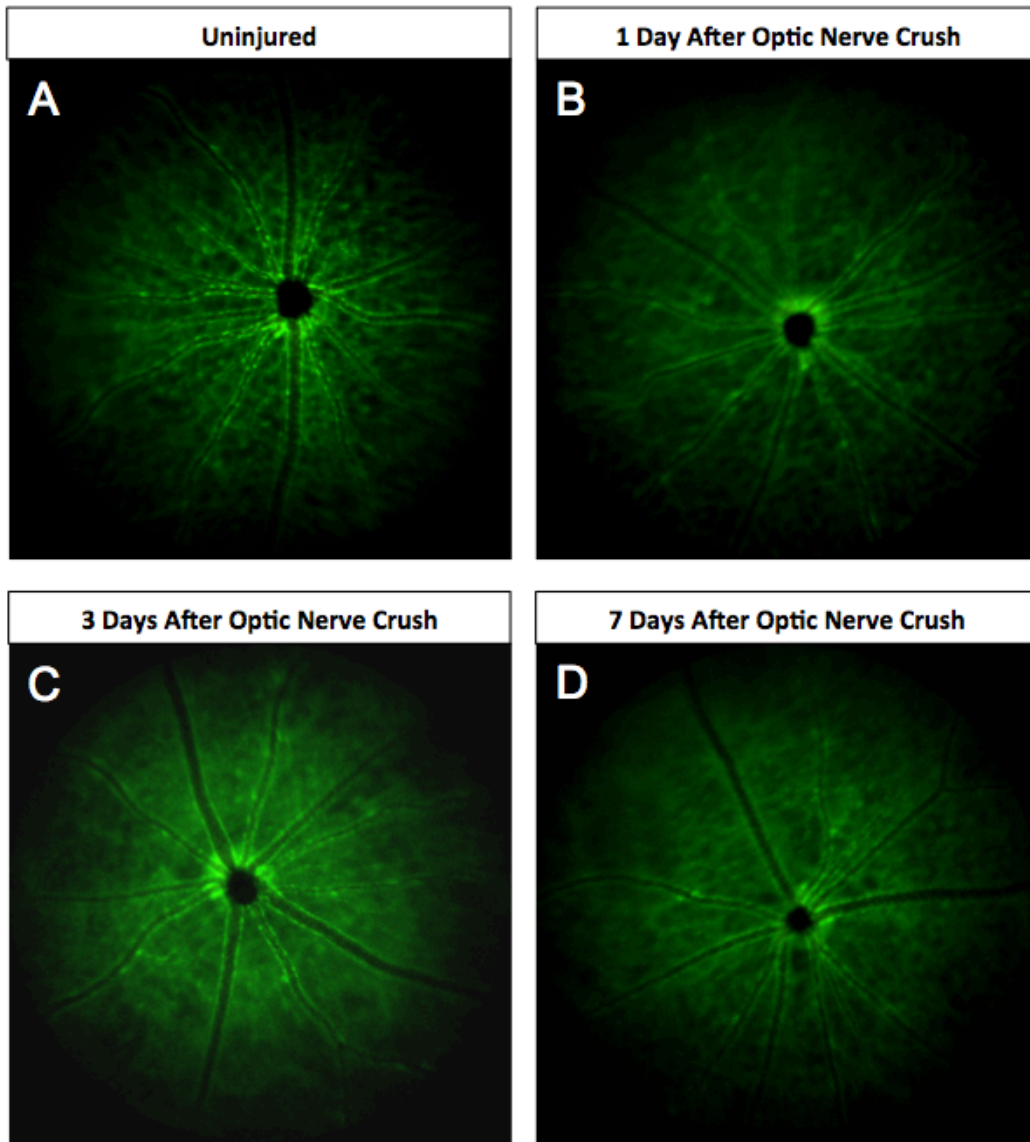


Figure 4.19 Images of acridine orange leukocyte fluorography after optic nerve crush injury. Acridine orange binds to DNA dyeing endothelial cells and leukocytes green. Acridine orange was injected in (A) uninjured mice (n=3), (B) 1 day after optic nerve crush (n=3), (C) 3 days after optic nerve crush (n=3), and (D) 7 days after optic nerve crush (n=3).

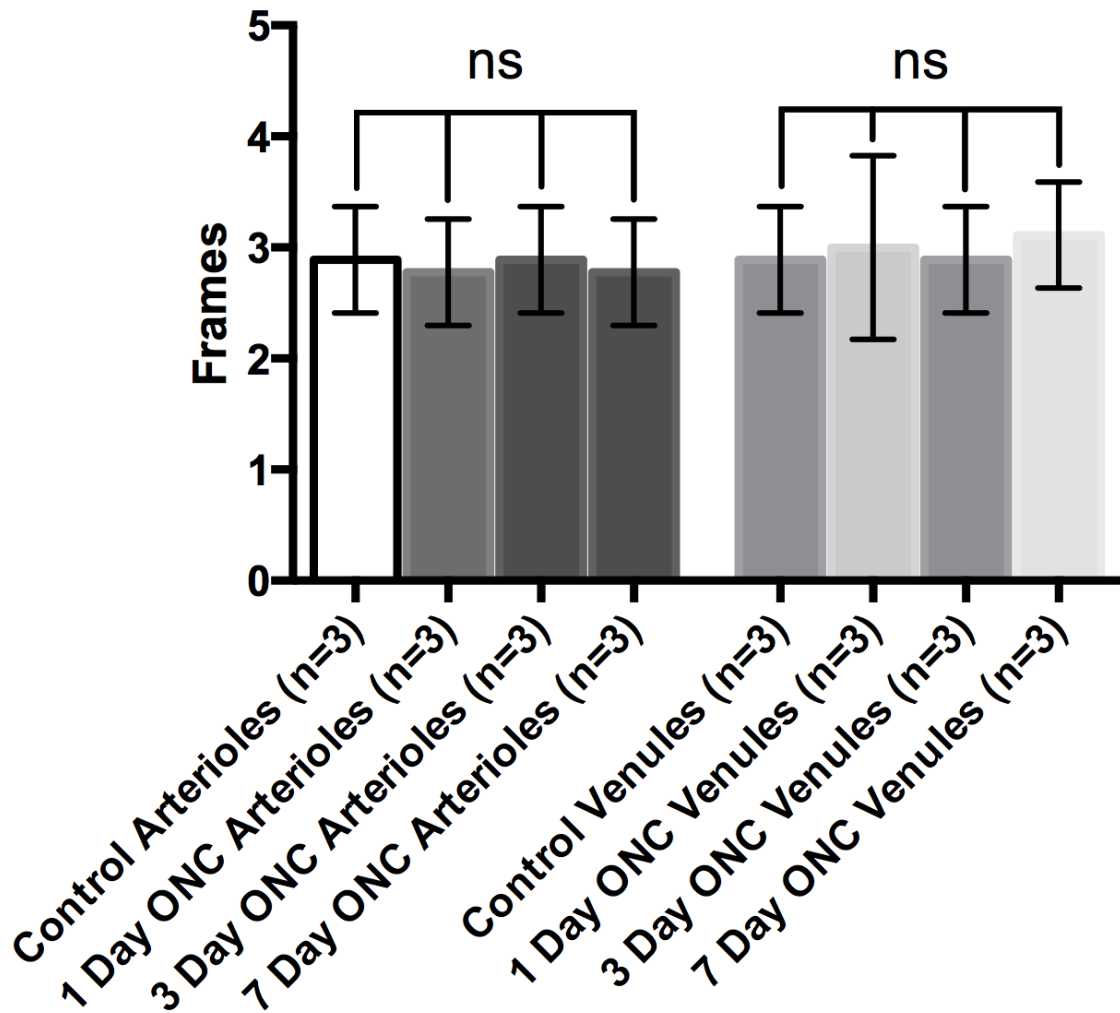


Figure 4.20 Leukocyte transit time after optic nerve crush injury. Leukocytes were tracked in retinal arterioles (uninjured animals (n=3), 2.89 ± 0.48 frames; 1 day after crush (n=3), 2.78 ± 0.48 frames; 3 days after crush (n=3), 2.89 ± 0.48 frames; 7 days after crush (n=3), 2.78 ± 0.48 frames) and venules (uninjured animals (n=3), 2.89 ± 0.48 frames; 1 day after crush (n=3), 3 ± 0.83 frames; 3 days after crush (n=3), 2.89 ± 0.48 frames; 7 days after crush (n=3), 3.11 ± 0.48 frames) using acridine orange leukocyte fluorography. There were no significant changes in leukocyte speed observed over 7 days after optic nerve crush injury.

CHAPTER 5: THE ROLE OF THE IMMUNE SYSTEM AND VASCULAR DEGENERATION IN THE RETINA OF AP-2 β NCC KO MICE

5.1 Results

5A. Characterization of retinal remodeling in the cohort of AP-2 β NCC KO mice studied

5.1.1 Retinal remodeling in AP-2 β NCC KO mice

The thickness of control retinas (n=5) was $189.3 \pm 29.1 \mu\text{m}$, while the thickness of AP-2 β NCC KO retinas (n=6) was $139.3 \pm 20.3 \mu\text{m}$. There was a significant decrease in the thickness of AP-2 β NCC KO retinas compared to controls (t test, p=0.0037). These findings are consistent with the findings of Martino et al. that there is an overall decrease in the thickness of the retina in AP-2 β NCC KO mice compared to control littermates.

The thickness of each of the retinal layers was quantified (**Figure 5.1**). There were no significant differences in thickness observed between controls (n=5) and AP-2 β NCC KOs (n=6) in the retinal ganglion cell layer, the inner nuclear layer, the outer nuclear layer, and the photoreceptor layer. The thickness of the retinal ganglion cell layer was $7.608 \pm 0.87 \mu\text{m}$ in control animals while it was $7.097 \pm 1.0 \mu\text{m}$ in AP-2 β NCC KOs. The inner nuclear layer was $33.81 \pm 5.28 \mu\text{m}$ in thickness in control animals, and $37.24 \pm 12.82 \mu\text{m}$ in AP-2 β NCC KO animals. In AP-2 β NCC KOs, the outer plexiform layer was $5.74 \pm 4.306 \mu\text{m}$ in thickness. In control animals the outer plexiform layer had a thickness of $10.66 \pm$

2.48 μm . In control animals, the outer nuclear layer measured $51.9 \pm 10.05 \mu\text{m}$ in thickness and was $52.2 \pm 7.09 \mu\text{m}$ in AP-2 β NCC KOs. The thickness of the photoreceptor layer did not change significantly in AP-2 β NCC KOs, $24.63 \pm 5.92 \mu\text{m}$, compared to $31.57 \pm 6.01 \mu\text{m}$ in control animals. There was a significant decrease (ANOVA/Tukey's post-hoc test, $p=0.0005$) in the thickness of the inner plexiform layer. The inner plexiform layer in control animals was found to be $36.63 \pm 4.74 \mu\text{m}$. Compared to controls, there was a 47% decrease in the thickness of the inner plexiform layer in AP-2 β NCC KOs that measured $19.39 \pm 4.62 \mu\text{m}$. Martino et al. also determined that only the inner plexiform layer decreases in AP-2 β NCC KOs. This reaffirms the consistency in the retinal changes affecting AP-2 β NCC KO mice previously reported.

The density of cells in the inner nuclear layer was $24145 \pm 3414 \text{ cells}/\text{mm}^2$ in control animals ($n=5$), while it was $22137 \pm 4034 \text{ cells}/\text{mm}^2$ in AP-2 β NCC KOs ($n=5$) (**Figure 5.2**). There were no statistically significant differences (ANOVA) between the values obtained for controls and AP-2 β NCC KOs in the inner nuclear layer. The density of the cells in the outer nuclear layer did not significantly vary between control animals and AP-2 β NCC KOs as well. There were $55592 \pm 8201 \text{ cells}/\text{mm}^2$ in control animals, while there were $50709 \pm 4988 \text{ cells}/\text{mm}^2$ in AP-2 β NCC KO animals.

There was a statistically significant (t test, $p<0.0001$) loss of DAPI labeled cells in the retinal ganglion cell layer in AP-2 β NCC KOs compared to controls. While there were an average of $121.9 \pm 3.8 \text{ cells}/\text{mm}$ in control animals ($n=6$),

there were 80.26 ± 10.18 cells/mm in AP-2 β NCC KO animals (n=6). There were 85.1 ± 9.66 cells/mm labeled with Brn3a in control animals (n=5), while there were 4.089 ± 2.968 cells/mm in AP-2 β NCC KOs (n=5) (**Figure 5.3**). There was a statistically significant decrease in Brn3a cell density in AP-2 β NCC KOs compared to controls (t test, $p < 0.0001$). These measurements align with the data obtained by Martino et al. and demonstrate that there is a specific loss of retinal ganglion cells, supporting the notion that the retinas of AP-2 β NCC KO mice have undergone glaucomatous changes.

5B. The role of vascular degeneration in the retinas of AP-2 β NCC KO mice

5.1.2 Decreases in capillary area in AP-2 β NCC KO mice

There was a significant decrease in capillary area in the superficial, intermediate, and deep retinal capillary plexuses in AP-2 β NCC KO mice compared to control littermates (**Figure 5.8, Figure 5.9**). All area values are expressed as area per 20X field of view. The area of the superficial capillary plexus was $24550 \pm 2729 \mu\text{m}^2$ in control animals, and $16619 \pm 2239 \mu\text{m}^2$ in AP-2 β NCC KOs (n=5) ($p = 0.0334$) (**Figure 5.10**). In controls the area of the intermediate capillary plexus was $18084 \pm 5401 \mu\text{m}^2$ and $5396 \pm 1862 \mu\text{m}^2$ in AP-2 β NCC KOs ($p = 0.0005$). The area of the deep capillary plexus was $58919 \pm 5636 \mu\text{m}^2$ in control animals while in AP-2 β NCC KOs it was $40433 \pm 7662 \mu\text{m}^2$ ($p < 0.001$).

5.1.3 Changes in capillary diameter in AP-2 β NCC KO mice

The average capillary diameter in the superficial capillary plexus of the retina was $4.114 \pm 0.567 \mu\text{m}$ in wild-type animals, while it was $3.949 \pm 0.507 \mu\text{m}$ in AP-2 β NCC KO animals (**Figure 5.11**). In the intermediate capillary plexus, wild-type animals had capillaries with an average diameter of $3.084 \pm 0.31 \mu\text{m}$ while AP-2 β NCC KO capillaries measured $2.943 \pm 0.475 \mu\text{m}$. The deep plexus was measured to be $4.161 \pm 0.404 \mu\text{m}$ in diameter in wild-type animals while it was $3.806 \pm 0.35 \mu\text{m}$ in AP-2 β NCC KOs. There were no significant differences when comparing plexuses in the same location between AP-2 β NCC KOs and controls. When comparing the superficial, intermediate, and deep plexuses within AP-2 β NCC KOs or controls only, the diameter of the capillaries in the intermediate plexus was significantly smaller when compared to the diameters of the superficial capillaries and deep capillaries among both groups. In wild type animals, the diameter of the capillaries of the intermediate plexus was smaller than the superficial capillaries ($p=0.0016$), as well as the deep capillaries ($p=0.0010$). In AP-2 β NCC KO animals the diameter of the intermediate plexus of capillaries was also significantly smaller than the superficial ($p=0.0021$) and deep plexuses ($p=0.0096$).

5.1.4 Changes in capillary density in AP-2 β NCC KO mice

There were significant changes in capillary density in the intermediate and deep capillary plexuses, but no significant changes in the superficial plexus. There

were an average of 5.547 ± 0.246 capillaries/500 μm in the superficial plexus of wild-type animals, while there were an average of 4.353 ± 1.188 capillaries/500 μm in AP-2 β NCC KO animals (**Figure 5.12**). In the intermediate plexus, while wild type animals had an average of 6.240 ± 1.025 capillaries/500 μm , AP-2 β NCC KO animals had 1.302 ± 1.412 capillaries/500 μm , significantly less in comparison (ANOVA/Tukey's post hoc test, $p < 0.0001$). The deep capillary plexus had an average capillary density of 9.237 ± 0.342 capillaries/500 μm in wild-type animals and there was a significant decrease (ANOVA/Tukey's post hoc test, $p < 0.0001$) in AP-2 β NCC KO animals that had an average density of 5.623 ± 1.35 capillaries/500 μm .

5.1.5 Changes in intercapillary distance in AP-2 β NCC KO mice

The distance between capillaries increased in the deep retinal plexus of AP-2 β NCC KO animals when compared to wild-type animals, while there were no significant changes in the superficial and deep plexuses (**Figure 5.13**). The intercapillary distance in the superficial capillary plexus was 90.60 ± 6.71 μm in wild-type animals, while in AP-2 β NCC KO animals it was 121.1 ± 43.27 μm . There was a significant increase ($p < 0.0001$) in intercapillary distance in the intermediate plexus of AP-2 β NCC KO animals at an average of 547.6 ± 309.3 μm compared to 81.41 ± 13.27 μm in controls. The intercapillary distance did not significantly differ in the deep vascular plexus in AP-2 β NCC KOs, at an average

of $91.86 \pm 22.43 \mu\text{m}$, compared to control animals that averaged an intercapillary distance of $54.28 \pm 2.04 \mu\text{m}$.

5.1.6 Correlation between the thickness of the inner plexiform layer and intercapillary distance in the intermediate capillary plexus

The correlation between the thickness of the inner plexiform layer and the intercapillary distance of the intermediate capillary plexus was analyzed. There was a strong correlation between inner plexiform layer thickness and intercapillary distance of the intermediate capillary plexus $r(8) = -0.9583$, $p < 0.0001$. (**Figure 5.14**)

5C. The role of the immune system in the retina of AP-2 β NCC KO mice

5.1.7 Immune cells are adherent to vitreal surface of AP-2 β NCC KO retinas

There were 113.3 ± 63.43 cells on the vitreal surface of whole mounted AP-2 β NCC KO retinas (n=6). The cells on the vitreal surface of the retina were immunoreactive for Iba-1, revealing their identity as macrophages. (**Figure 5.4, Figure 5.5**) There were 0 cells observed on the surface of wild-type retinas (n=6). There was a statistically significant increase (t test, $p=0.001$) in the number of cells on the surface of the AP-2 β NCC KO retinas compared to the controls.

The retina was divided into thirds based on the distance from the optic nerve head and adherent cells were quantified according their location on the retinal surface in AP-2 β NCC KOs (n=6) (**Figure 5.6**). Adherent cells were

predominantly found on the surface of the retinal periphery. There were 71.5 ± 56.31 cells in the periphery of whole mounted AP-2 β NCC KO retinas. In the mid-periphery there were 26.83 ± 7.28 cells, while there were 15 ± 8.95 cells in the periphery. The only significant difference observed was between the number of cells in the central versus peripheral retina (ANOVA/Tukey's post-hoc test; $p=0.0191$)

The density of cells on the vitreal surface of the AP-2 β NCC KO retinas ($n=5$) was calculated. There were 7.48 ± 5.89 cells/mm² in the periphery, 3.82 ± 1.04 cells/mm² in the mid-periphery, and 6.312 ± 3.77 cells/mm² in the central retina (**Figure 5.7**). There were no significant differences (ANOVA; $p=0.2798$) in cell density on the vitreal surface of the retina. The fluorescent cell density was approximately equal across all the retinal sectors.

5.2 Discussion

Martino et al. examined retinal changes in AP-2 β NCC KO mice and concluded that these animals developed early-onset glaucoma. A thinning of the retinal tissue was observed and of the layers measured in that study, it was concluded that only the inner plexiform layer thinned. In this study, the thickness of the retina was analyzed in a cohort of mice with an intraocular pressure of 28.87 ± 5.19 mmHg as determined by Martino et al. The findings in this cohort of 8-12 week old mice align exactly with the previous findings reported. There was an overall decrease in the thickness of the retina and the only retinal layer

associated with a significant decrease in thickness was the inner plexiform layer. In order to visualize the retinal ganglion cell loss originally observed by Martino et al., Brn3a immunohistochemistry was used to quantify retinal ganglion cell loss. The findings previously reported directly coincide with the observations in this study. Almost all retinal ganglion cells were lost in the cohort of AP-2 β NCC KO mice studied, confirming the expectation that there were glaucomatous changes in these mice. Retinal ganglion cells form synaptic connections with bipolar cells in the inner plexiform layer (Kolb, 1979). The loss of retinal ganglion cells is accompanied loss of thickness of the inner plexiform layer because of changes in the dendritic projections of the retinal ganglion cells (Lin, Wang, & Masland, 2004). Mice with a targeted disruption of Brn3b lose a majority of their ganglion cells and have a significant thinning of the inner plexiform layer and nerve fibre layer (Camp et al., 2011). In humans, the thickness of the ganglion cell complex is measured clinically to aid in the diagnosis of early glaucoma and to track the progression of disease (Choi, Jeoung, Park, & Kim, 2013). The ganglion cell complex is the sum of the three innermost retinal layers of the retina: the nerve fibre layer, ganglion cell layer and inner plexiform layer (Garas, Vargha, & Holló, 2011). Given that the retinal ganglion cell layer is one cell layer thick in mice and that the nerve fibre layer is comparatively thinner in mice than in humans, it was expected that changes in these layers would be challenging to detect histologically. The thinning of the inner plexiform layer in the retinas of AP-2 β NCC KO is a strong indicator of

glaucomatous changes and is consistent with the remodeling seen in glaucomatous retinas, as previously reported in the literature (Camp et al., 2011).

When the inner and outer nuclear layers were examined for their nuclear densities, there were no significant changes in the number of nuclei comprising either of the layers between control and AP-2 β NCC KO. Combined with the knowledge that the thickness of these layers did not vary significantly between control and AP-2 β NCC KO mice, it demonstrates that there was no cell loss in either of these layers in AP-2 β NCC KO mice. The loss of cell bodies was specific to the retinal ganglion cell layer. Martino et al. reported that in addition to retinal ganglion cell loss, there was a quantifiable loss of displaced amacrine cells within the retinal ganglion cell layer. The selective loss of RGCs and their axons without involving neurons in the outer or inner nuclear retinal layers has been considered a classic hallmark of glaucomatous optic neuropathy but it is unclear whether the damage caused by glaucoma is restricted to RGCs and their axons (Vidal-Sanz et al., 2012). Several studies in humans have reported a loss of neurons in the outer nuclear layer (Vidal-Sanz et al., 2012). A loss of photoreceptors was reported in human eyes with secondary angle-closure glaucoma (Panda & Jonas, 1992). Swelling of red and green sensitive cones, as well as their patchy loss was observed in human primary open angle glaucoma (Nork et al., 2000). Analysis of images obtained using *in vivo* retinal imaging of patients with chronic glaucoma demonstrated losses in cone density that corresponded to retinal locations with reduced visual sensitivity (Choi et al.,

2011). Multiphoton imaging of DAPI labeled human glaucomatous retinas was used to demonstrate significant neuronal loss in the outer nuclear layer as well as the inner nuclear layer (Lei et al., 2008). It is possible that 8-12 week old AP-2 β NCC KO mice may be too early in glaucomatous disease progression for the loss of cells beyond those in the retinal ganglion cell layer. Future studies could examine the loss of cells in the inner nuclear layer and outer nuclear layer to gain an understanding of the changes in the retina of later stages of disease in this model of glaucomatous injury. The data collected here in AP-2 β NCC KO mice is in line with the classical understanding of cellular loss associated with glaucoma (Vidal-Sanz et al., 2012).

Retinal neurons and glia interact with the vasculature under normal conditions (Saint-Geniez & D'amore, 2004). Functional impairment of the vasculature, as seen in branch vein occlusion, is known to damage the retina (Alshareef et al., 2016). Conversely, the apoptosis of neuroglial cells, as seen in diabetes, is thought to contribute to the degeneration of retinal capillaries (Barber, 2003; Fletcher, Phipps, & Wilkinson-Berka, 2005). Retinal ischemia can lead to visual impairment in conditions like diabetic retinopathy (Bresnick, Engerman, Davis, de Venecia, & Myers, 1976), as well glaucoma (Osborne et al., 1999). AP-2 β NCC KO mice exhibit a closed iridocorneal angle and develop high intraocular pressure. It was hypothesized that elevated intraocular pressure might lead to ischemia, and subsequent changes in the retinal blood vessels. The microvasculature of AP-2 β NCC KO mice was investigated to visualize any

potential changes in response to the glaucomatous neurodegeneration exhibited in this model. FITC-Dextran injections revealed changes in each of the retinal microvascular plexuses. There was a significant decrease in the area covered by each layer of capillaries. This decrease in area may have resulted as a consequence of changes in the diameters of the vessels themselves so the average capillary diameter was calculated in each plexus. There were no differences in capillary diameter when examining each of the capillary layers and comparing them between AP-2 β NCC KO mice and their control littermates. A confocal microscopy study found that the mean inner diameter of deep layer capillaries was reported as $4.98 \pm 0.96 \mu\text{m}$ in wild type C57 BLKS mice (Paques et al., 2003). The findings here consistent with that measurement, at $4.161 \pm 0.404 \mu\text{m}$ in control mice, and $3.806 \pm 0.35 \mu\text{m}$ in AP-2 β NCC KOs.

Since the diameter of the capillaries did not change, this consequently suggested that there was an actual decrease in the number of capillaries in each of the layers. When the capillary density was calculated, it was only in the intermediate and deep layers that there was a significant change in the number of capillaries. Although capillary density significantly changes in both the intermediate and deep layers, it was only the intermediate layer that had a dramatic change in the intercapillary distance. This indicates that there was a dramatic drop in the number of capillaries in the intermediate capillary plexus and that the distance separating the capillaries was dramatically increased. A study of normal human eyes found a correlation between the intercapillary distance of the

peripapillary capillaries and retinal nerve fibre layer thickness (Yu, Cringle, & Yu, 2014). The authors concluded that this relationship was a reflection of the significance of neurovascular co-patterning and mechanisms of functional cross talk involved in retinal homeostasis (Yu et al., 2014). Given the adjacency of the intermediate capillary plexus to the inner plexiform layer it was hypothesized that there might be cross talk between the thinning of the inner plexiform layer and the changes in the intermediate capillary plexus. When plotted together it was revealed that there was a strong negative correlation between the thickness in the inner plexiform layer and increase in intercapillary distance in the intermediate capillary plexus. It is unclear exactly how these two changes are related. Did the remodeling of the inner plexiform layer result in degeneration of the capillaries, vice versa, or are these events coincidental to another phenomenon? A study using a model of ischemia reperfusion injury that used the acute elevation of intraocular pressure in both mice and rats found that it was only after a significant loss of retinal ganglion cells that the degeneration of retinal capillaries occurred (Zheng, Gong, Hatala, & Kern, 2007). This model shows that temporally, neurodegeneration precedes the loss of capillaries. It is suggested that the vascular degeneration seen in the retinas of AP-2 β NCC KO mice is a response preceded by the neurodegeneration caused by chronic elevated intraocular pressure. The snapshot in time this study provides is only at a timepoint 8-12 weeks into the lives of the mice. It is unknown what the earlier structure of the capillary plexus in AP-2 β NCC KO mice was. It is possible that the differences observed in the

microvasculature of AP-2 β NCC KO mice are congenital, but this is unlikely as the knockout of AP-2 β in the neural crest is not expected to have any effect on the retinal vasculature (Martino et al., 2016). Future investigations into the vasculature of the AP-2 β NCC KO retina should examine the earlier time points leading up to 8 weeks to characterize the changes in the retinal vasculature temporally in association with the thickness of the retinal layers and the survival of retinal ganglion cells.

There have been studies on both human eyes and in animal models that have implicated an immune component in the response to retinal ganglion cell death in glaucoma (Kamat, Gregory, & Pasquale, 2016). This evidence for immunological involvement in glaucoma has included autoantibodies (Wax et al., 1994), complement activation (Ohlsson et al., 2003), as well as immune cell recruitment (Garcia-Valenzuela & Sharma, 1999). It was hypothesized that the systemic immune system would be involved in the response to retinal ganglion cell death in AP-2 β NCC KO mice as a response to the injury of retinal ganglion cells and their axons. It was confirmed that blood-borne macrophages responded to the death of retinal ganglion cells by examining their presence on the vitreal surface of the retina. Iba-1 staining, combined with the round morphology of these cells and their location, verified the identity of the adherent immune cells as macrophages and not microglia (Imai, Ibata, Ito, Ohsawa, & Kohsaka, 1996). The density of macrophages on the surface of the retina was the same, regardless of their location, suggesting that their response was widespread and not targeting a

specific location on the vitreal surface of the retina. The location of these macrophages, on the vitreal surface of the retina, combined with the absence of vascular leakage observed following FITC-Dextran injection suggests that these cells did not enter the eye through the retinal vasculature, but rather that they entered the eye through another location. It is hypothesized that their point of entry could be ciliary body through the blood-aqueous barrier (Schwartz & Shechter, 2010), but more evidence would be required before making any conclusion. It is suggested that these cells play a role late in the injury process as most of the retinal ganglion cells were absent by the timepoint studied. The role of the immune system in retinal injury is controversial and while some studies suggest the systemic immune system plays a supportive role to injured tissue (Steinsapir et al., 2000; Tsai, Chang, & Wang, 2008; Yin et al., 2006), others suggest that it is detrimental to cell survival after injury (Baptiste et al., 2005; Shimazawa, Yamashima, Agarwal, & Hara, 2005; Thanos, Mey, & Wild, 1993). Given that the data in Chapter 4 suggests that systemic immune cells have a minimal influence on neurodegeneration early in acute optic nerve injury, it is suggested that the infiltrated immune cells in AP-2 β NCC KO mice also play a minimal role in initial neurodegeneration. Studies in DBA/2J mice indicate that monocyte infiltration may be an early event in response to high intraocular pressure (Howell et al., 2002), so studying a younger group of mice would be helpful to clarify this uncertainty. Future studies should elucidate the temporal relationship between retinal ganglion cell death and the infiltration of systemic

macrophages into the eye to gain a better understanding of their influence on neurodegeneration. Using immunomodulatory compounds to investigate the effect of macrophages on retinal ganglion cell survival could provide insight into their role in retinal ganglion cell death in AP-2 β NCC KO mice.

5.3 Figures

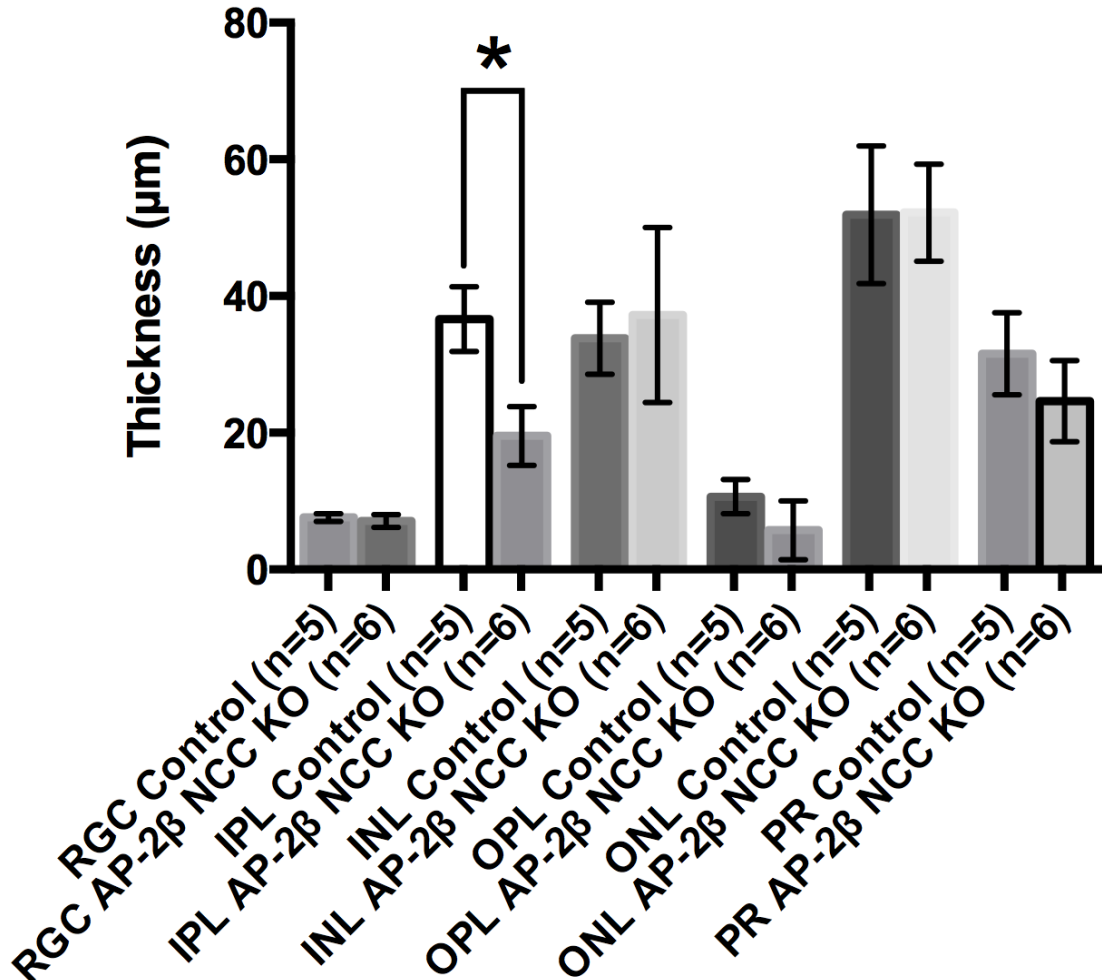


Figure 5.1 Retinal layer thicknesses in control and AP-2β NCC KO retinas. The retinal ganglion cell layer (RGC: control = $7.608 \pm 0.87 \mu\text{m}$, AP-2β NCC KO = $7.097 \pm 1.0 \mu\text{m}$), inner plexiform layer (IPL: control = $36.63 \pm 4.74 \mu\text{m}$, AP-2β NCC KO = $19.39 \pm 4.62 \mu\text{m}$), inner nuclear layer (INL: control = $33.81 \pm 5.28 \mu\text{m}$, AP-2β NCC KO = $37.24 \pm 12.82 \mu\text{m}$), outer plexiform layer (OPL: control = $10.66 \pm 2.48 \mu\text{m}$, AP-2β NCC KO = $5.74 \pm 4.306 \mu\text{m}$), outer nuclear layer (ONL: control = $51.9 \pm 10.05 \mu\text{m}$, AP-2β NCC KO = $52.2 \pm 7.09 \mu\text{m}$), and the photoreceptors (PR: control = $31.57 \pm 6.01 \mu\text{m}$, AP-2β NCC KO = $24.63 \pm 5.92 \mu\text{m}$) were measured in control (n=5) and AP-2β NCC KO (n=6) retinal sections. There was a statistically significant decrease (ANOVA/Tukey’s post hoc tests, p=0.0005) in thickness of the inner plexiform layer (IPL) in AP-2β NCC KO mice compared to controls.

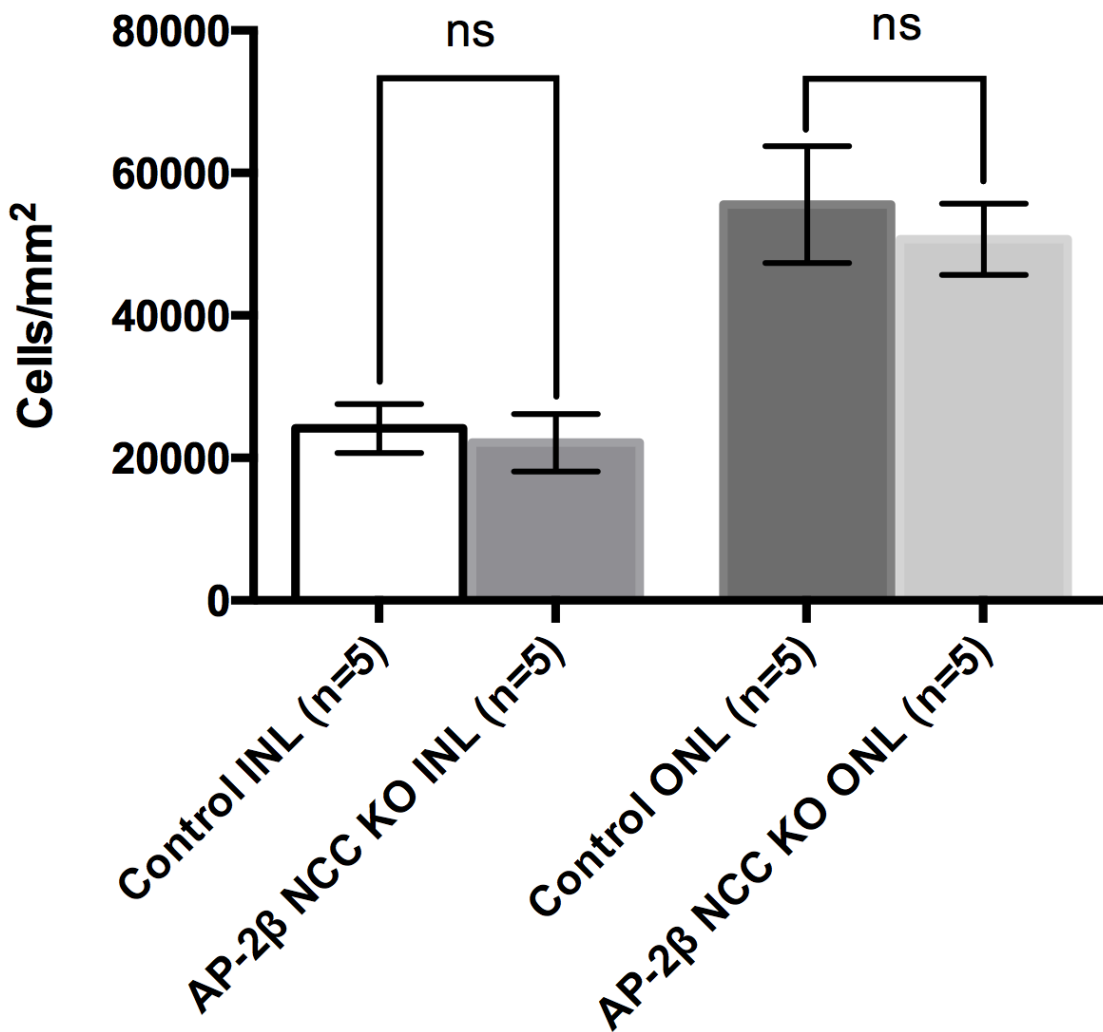


Figure 5.2 Nuclear density of the inner and outer nuclear layers in control mice and AP-2β NCC KOs. DAPI labeled cell density of the inner nuclear layer (INL: control = 24145 ± 3414 cells/mm², AP-2β NCC KO = 22137 ± 4034 cells/mm²) and outer nuclear layer (ONL: control = 55592 ± 8201 cells/mm², AP-2β NCC KO = 50709 ± 4988 cells/mm²) was quantified in retinal sections in controls (n=5) and AP-2β NCC KOs (n=5). There were no statistically significant differences (ANOVA) in the nuclear density when comparing homologous layers in control and AP-2β NCC KO mice.

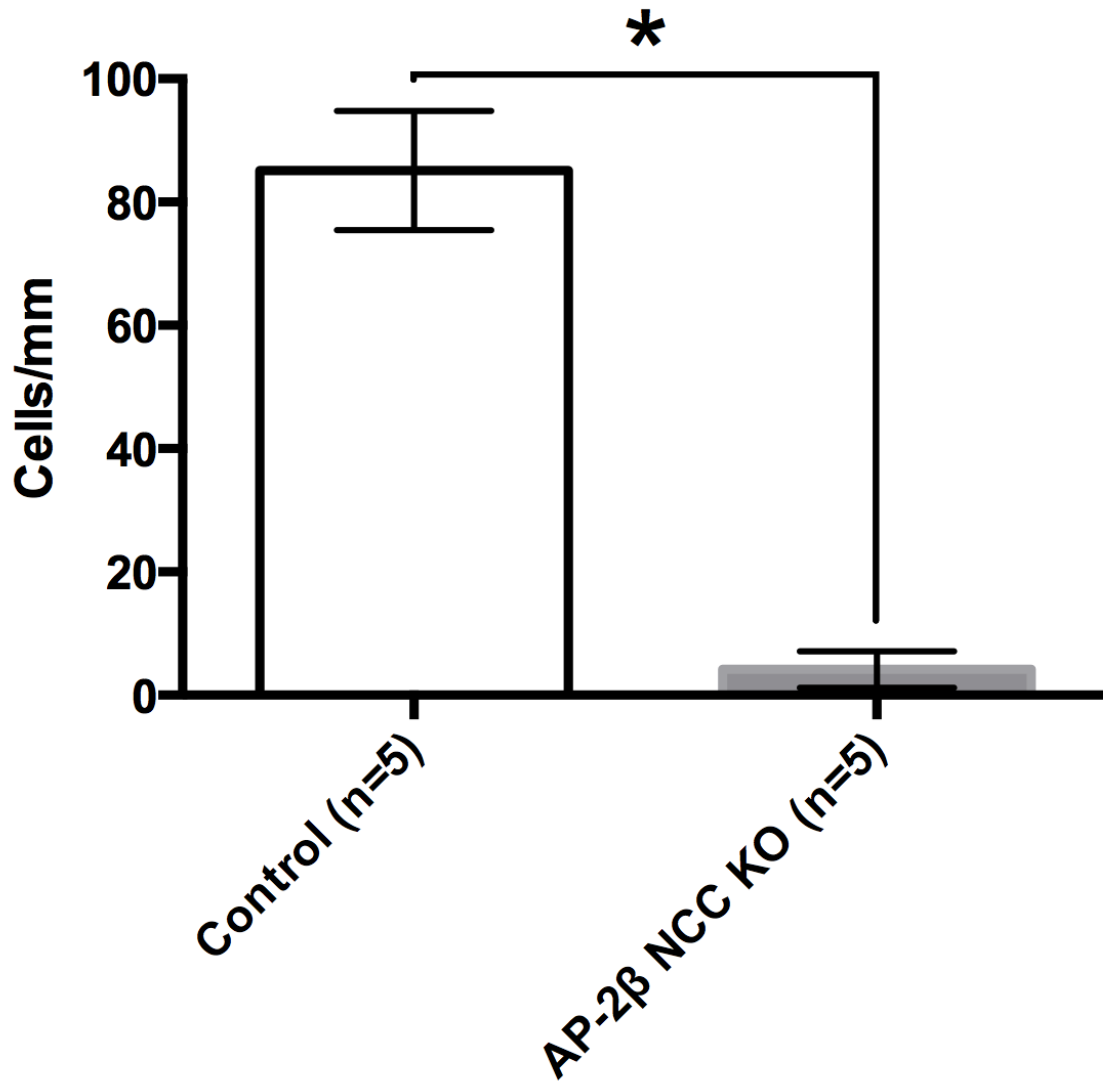


Figure 5.3 Quantification of Brn3a cell density in control and AP-2β NCC KO retinas. Brn3a cell density was quantified in 12 μm thick frozen transverse retinal sections in control (n=5, 85.1 ± 9.66 cells/mm) and AP-2β NCC KO mice (n=5, 4.089 ± 2.968 cells/mm). There was a significant decrease (t test, p<0.0001) in the density of Brn3a cell labeling in AP-2β NCC KOs.

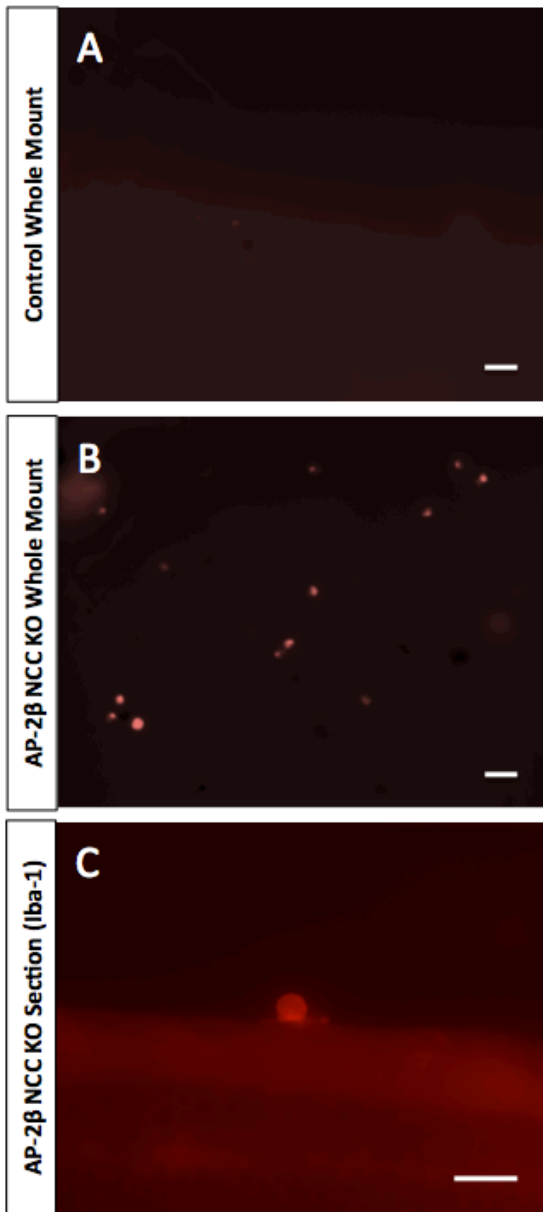


Figure 5.4 Fluorescent immune cells on the vitreal surface of the retina of controls versus AP-2 β NCC KOs. There are no immune cells on the surface of the (A) control (n=6) mice, while fluorescent cells are visible on the surface of (B) AP-2 β NCC KO (n=6) mice. (C) Iba-1 staining in 12 μ m thick frozen transverse retinal sections showing cell adherent to the retinal surface. Scale Bar = 50 μ m.

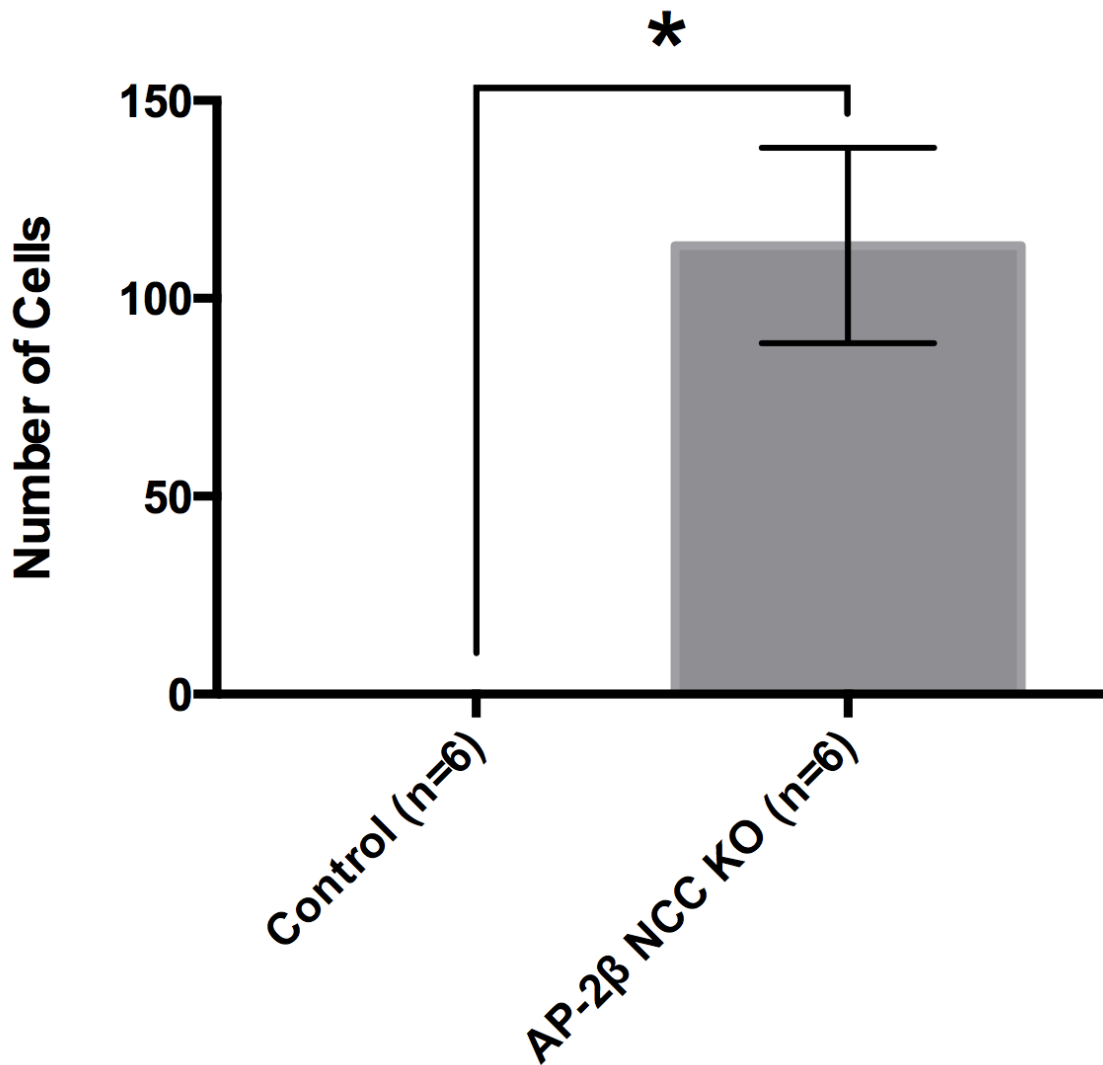


Figure 5.5 Quantification of fluorescent cells on the retinal surface. There was a significant increase in the number of fluorescent cells on the retinal surface of AP-2β NCC KOs (n=6, 71.5 ± 56.31 cells) compared to controls (n=6, 0 cells).

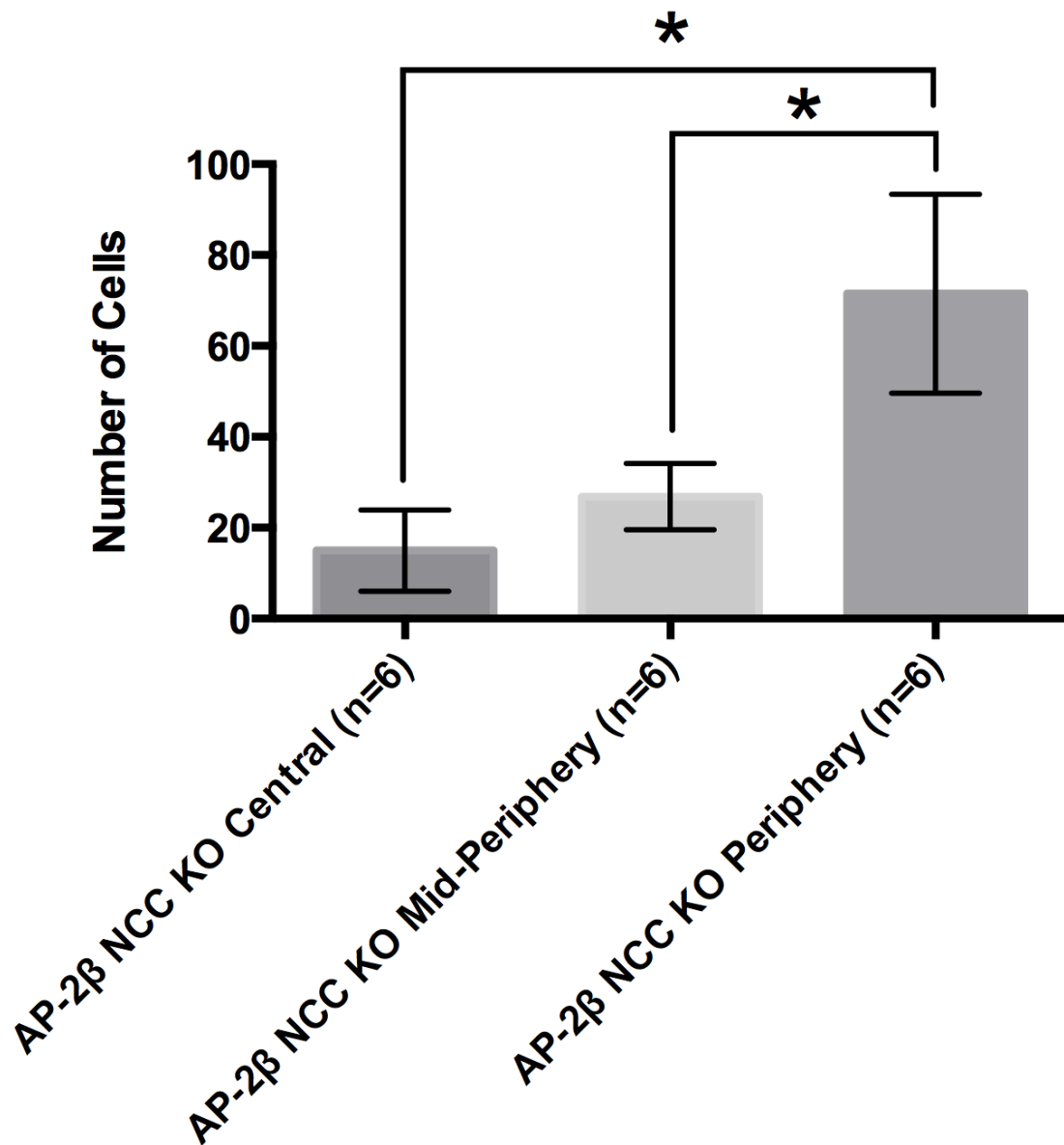


Figure 5.6 Fluorescent cells based on location on the retina. Fluorescent cells were quantified in the central (15 ± 8.95 cells), mid-peripheral (26.83 ± 7.28 cells), and peripheral (71.5 ± 56.31 cells) retina of AP-2β NCC KOs ($n=6$). There was a significantly larger (ANOVA/Tukey's post-hoc test; $p=0.0191$) number of cells in the retinal periphery compared to the central retina.

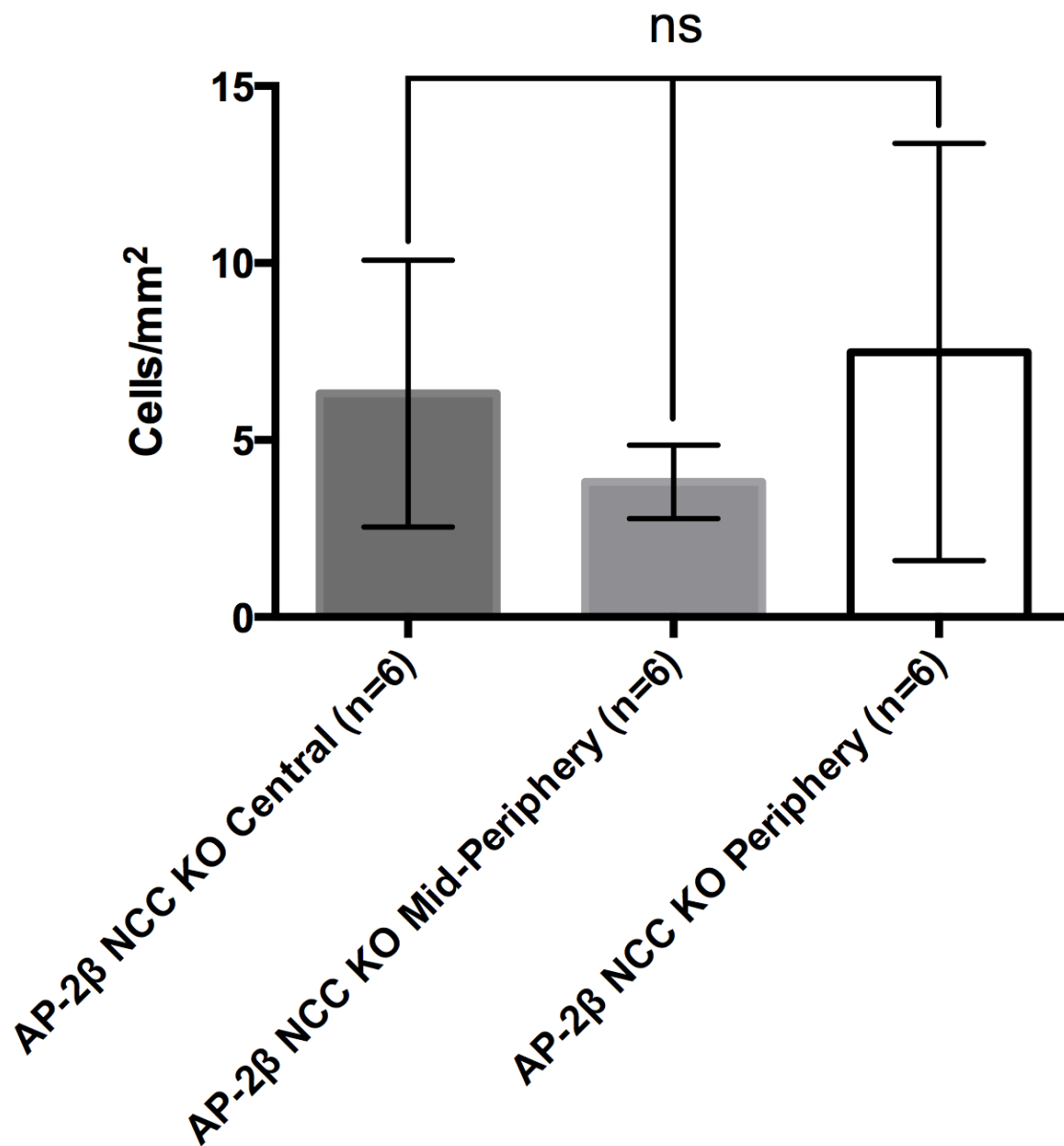


Figure 5.7 Fluorescent cell density on the retinal surface of AP-2β NCC KOs. The density of fluorescent cells on the retinal surface of AP-2β NCC KOs (n=6) does not vary (ANOVA) when comparing the central (6.312 ± 3.77 cells/mm²), mid-peripheral (3.82 ± 1.04 cells/mm²), and peripheral (7.48 ± 5.89 cells/mm²) surfaces.

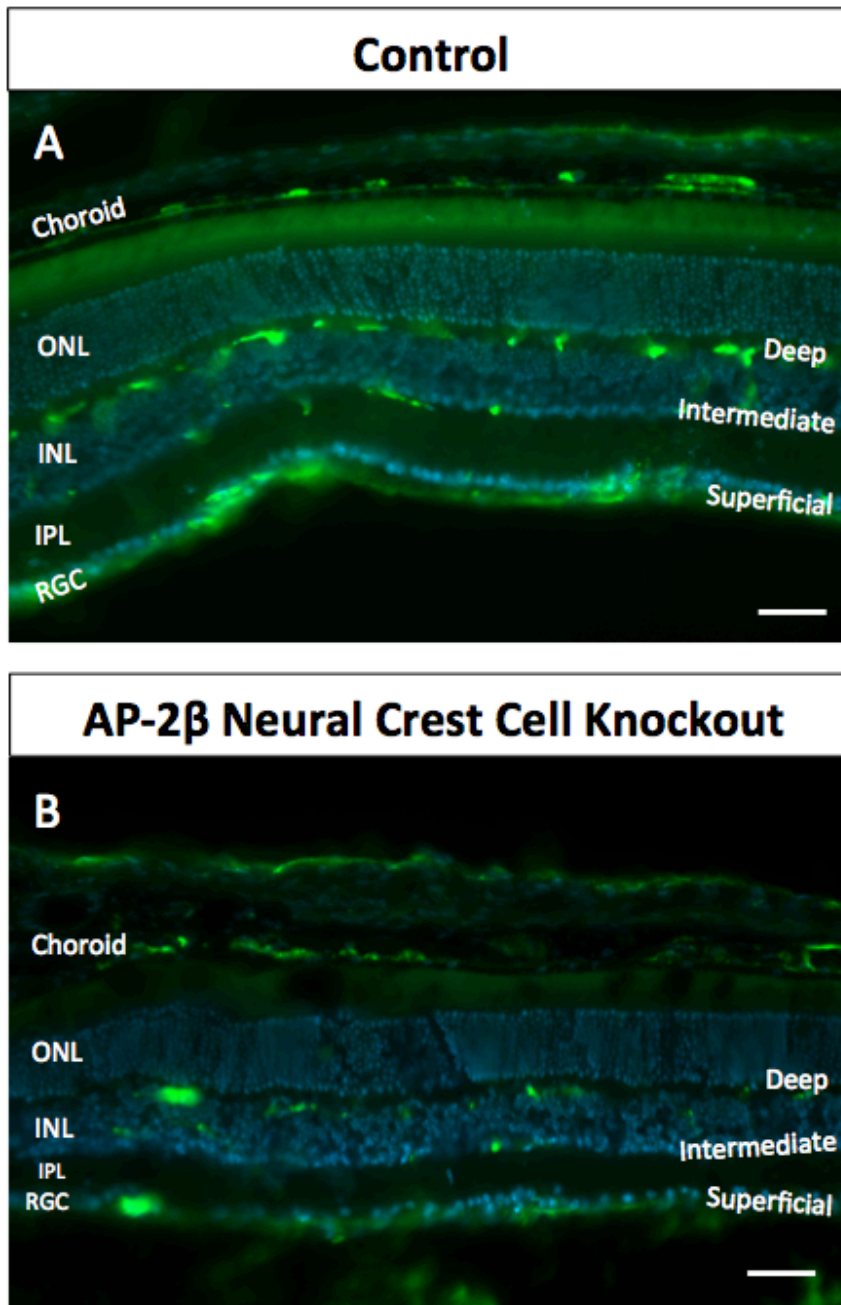


Figure 5.8 DAPI labeled nuclei and FITC-Dextran filled blood vessels in control and AP-2β NCC KO retinas. (A) Control (n=5) and (B) AP-2β NCC KO (n=5) mice were intravenously injected with FITC-Dextran (green) and frozen 12 μm thick transverse retinal sections were processed from the eyes. The sections were then stained with DAPI (blue). Scale bar = 50 μm.

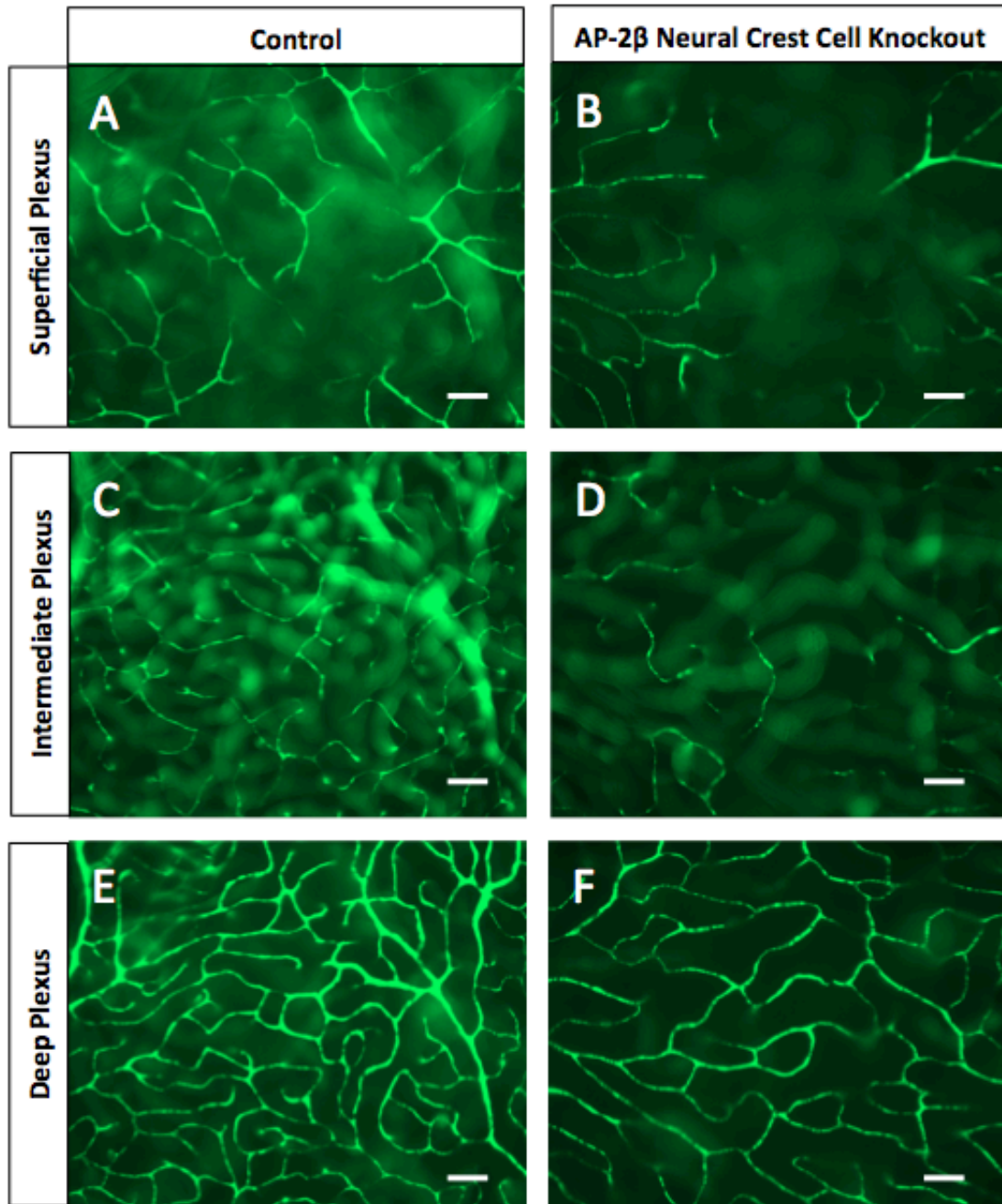


Figure 5.9 Whole mounts of retinas labeled intravascularly with FITC-Dextran in control and AP-2 β NCC KO mice. FITC-Dextran blood vessel labeling in the (A) superficial capillary plexus of controls (n=5) and (B) AP-2 β NCC KOs (n=5), the (C) middle capillary plexus of controls (n=5) and (D) AP-2 β NCC KOs (n=5), the (E) deep capillary plexus of controls (n=5) and (F) AP-2 β NCC KOs (n=5). Scale Bar = 50 μ m.

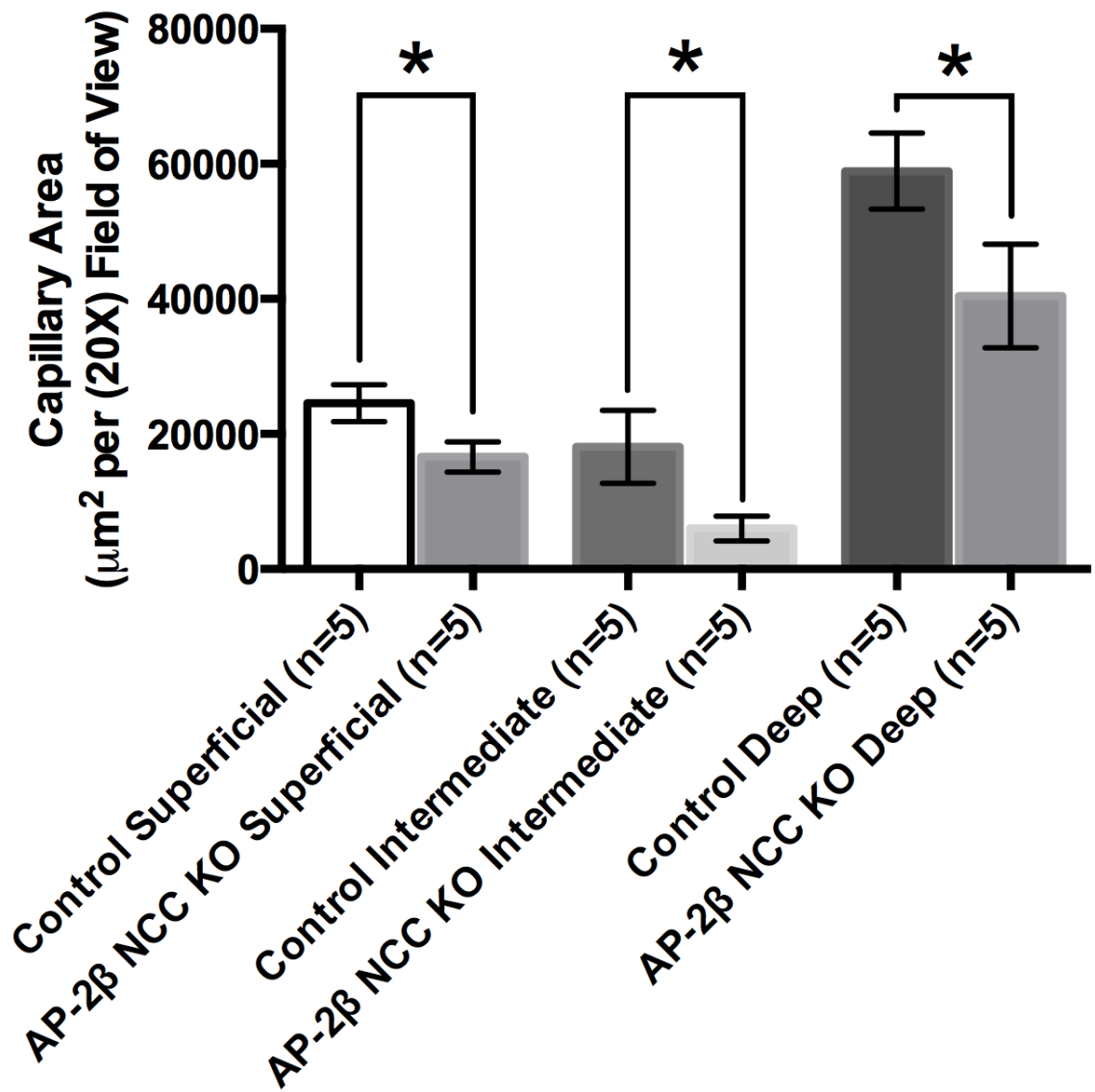


Figure 5.10 Change in capillary plexus areas in control mice versus AP-2β NCC KOs. There was a significant decrease in capillary area observed in each of the three capillary plexuses. Areas are expressed as area per 20X field of view. The area of the superficial capillary plexus was $24550 \pm 2729 \mu\text{m}^2$ in control (n=5) animals, and $16619 \pm 2239 \mu\text{m}^2$ in AP-2β NCC KOs (n=5) (p=0.0334). In controls (n=5) the area of the intermediate capillary plexus was $18084 \pm 5401 \mu\text{m}^2$ and $5396 \pm 1862 \mu\text{m}^2$ in AP-2β NCC KOs (n=5) (p=0.0005). The area of the deep capillary plexus was $58919 \pm 5636 \mu\text{m}^2$ in control (n=5) animals while in AP-2β NCC KOs (n=5) it was $40433 \pm 7662 \mu\text{m}^2$ (p<0.001).

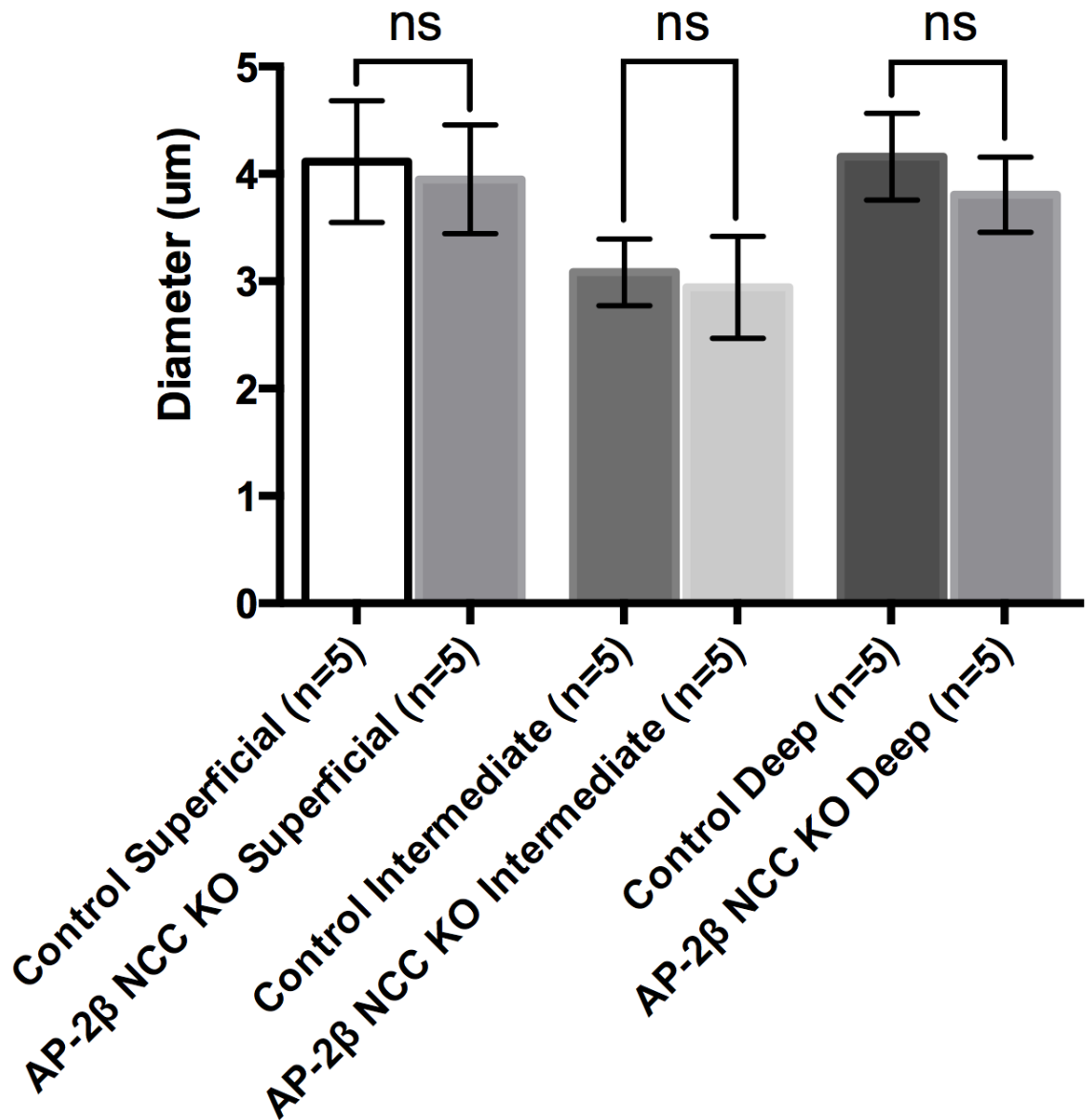


Figure 5.11 Capillary diameter in the capillary plexuses of control versus AP-2β NCC KO mice. There were no statistically significant differences in capillary diameter in each of the capillary plexuses in control (n=5) and AP-2β NCC KO (n=5) mice. (Superficial plexus, controls = 4.114 ± 0.567 µm, AP-2β NCC KOs = 3.949 ± 0.507 µm. Intermediate plexus, controls = 3.084 ± 0.31 µm, AP-2β NCC KOs = 2.943 ± 0.475 µm. Deep plexus, controls = 4.161 ± 0.404 µm, AP-2β NCC KOs = 3.806 ± 0.35 µm)

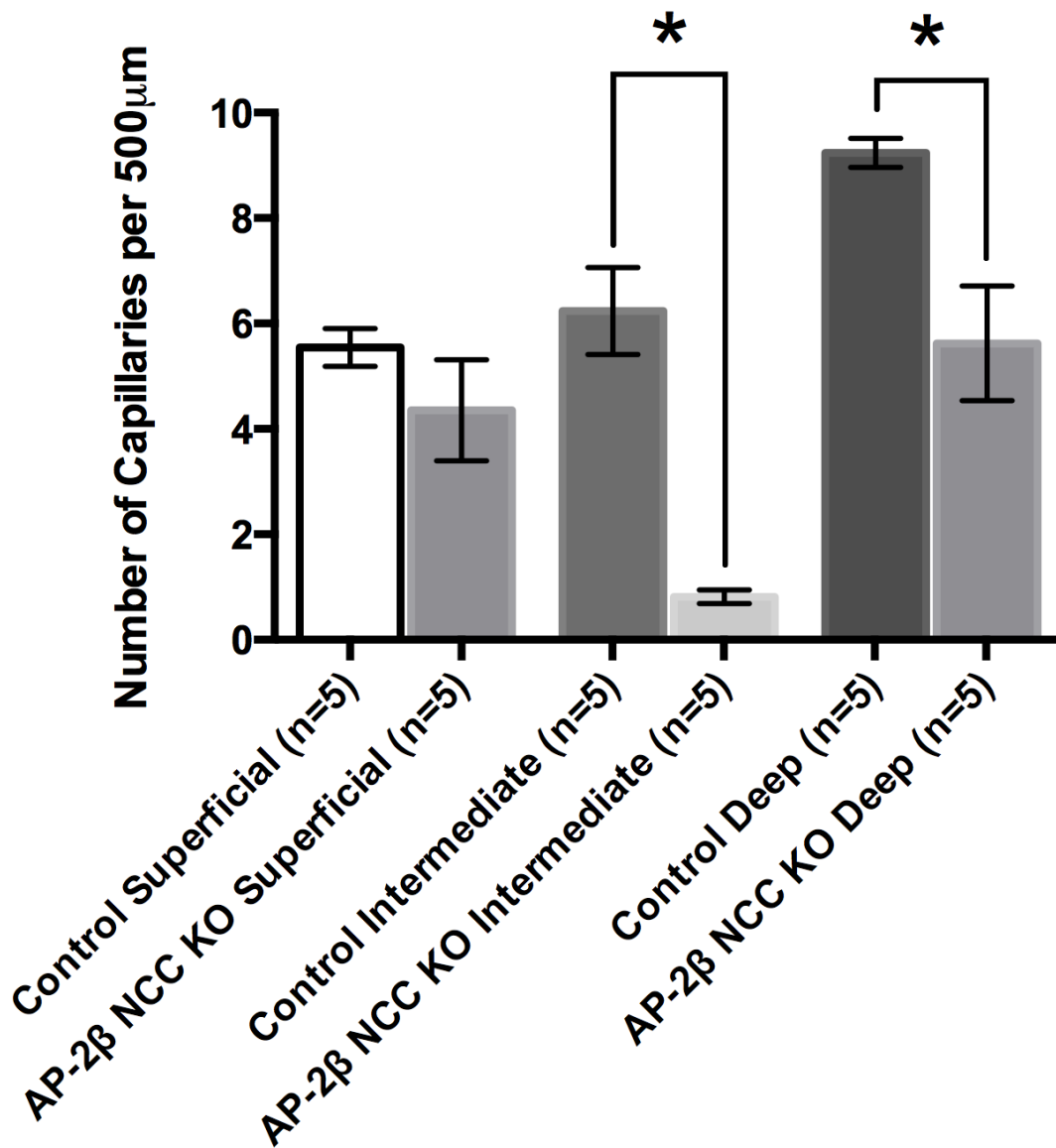


Figure 5.12 Capillary density in the capillary plexuses of control versus AP-2β NCC KO mice. There were no significant changes in capillary density in the superficial capillary plexus. There was a significant decrease in the number of capillaries in the intermediate (ANOVA/Tukey's post hoc test, $p < 0.0001$) and deep plexuses ($p < 0.0001$) of AP-2β NCC KO (n=5) mice compared to controls (n=5). (Superficial plexus, controls = 5.547 ± 0.246 capillaries/500 µm, AP-2β NCC KOs = 4.353 ± 1.188 capillaries/500 µm. Intermediate plexus, controls = 6.240 ± 1.025 capillaries/500 µm, AP-2β NCC KOs = 1.302 ± 1.412 capillaries/500 µm. Deep plexus, controls = 9.237 ± 0.342 capillaries/500 µm, AP-2β NCC KOs = 5.623 ± 1.35 capillaries/500 µm)

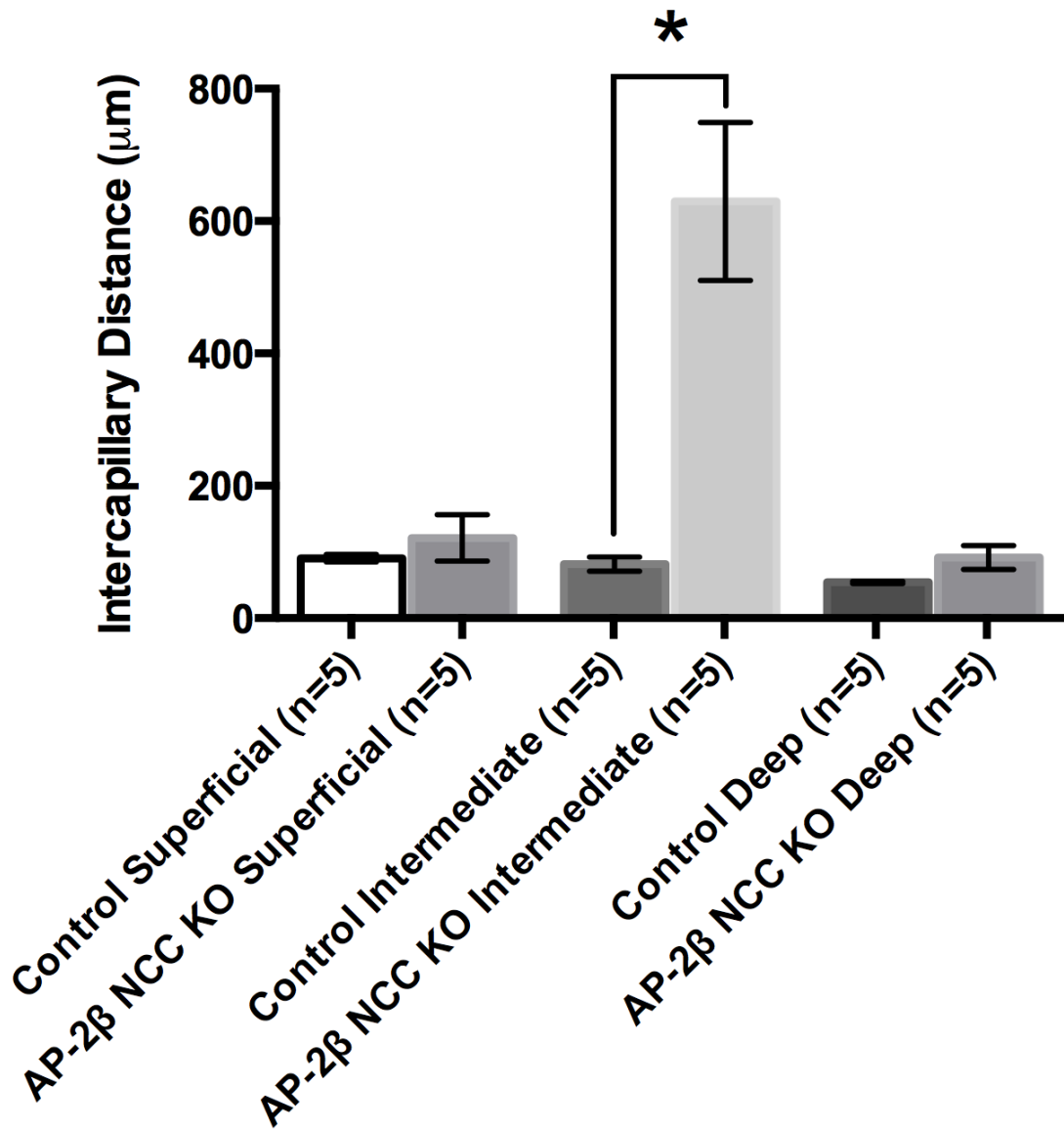


Figure 5.13 Intercapillary distance in the capillary plexuses of control and AP-2β NCC KO mice. There was a significant increase in intercapillary distance in the intermediate capillary plexus in AP-2β NCC KO (n=5) mice compared to controls (n=5). There were no significant differences in intercapillary distance found in the superficial and deep capillary plexuses. (Superficial plexus, controls = 90.60 ± 6.71 µm, AP-2β NCC KO = 121.1 ± 43.27 µm. Intermediate plexus, controls = 81.41 ± 13.27 µm, AP-2β NCC KO = 547.6 ± 309.3 µm. Deep plexus, controls = 54.28 ± 2.04 µm, AP-2β NCC KO = 91.86 ± 22.43 µm)

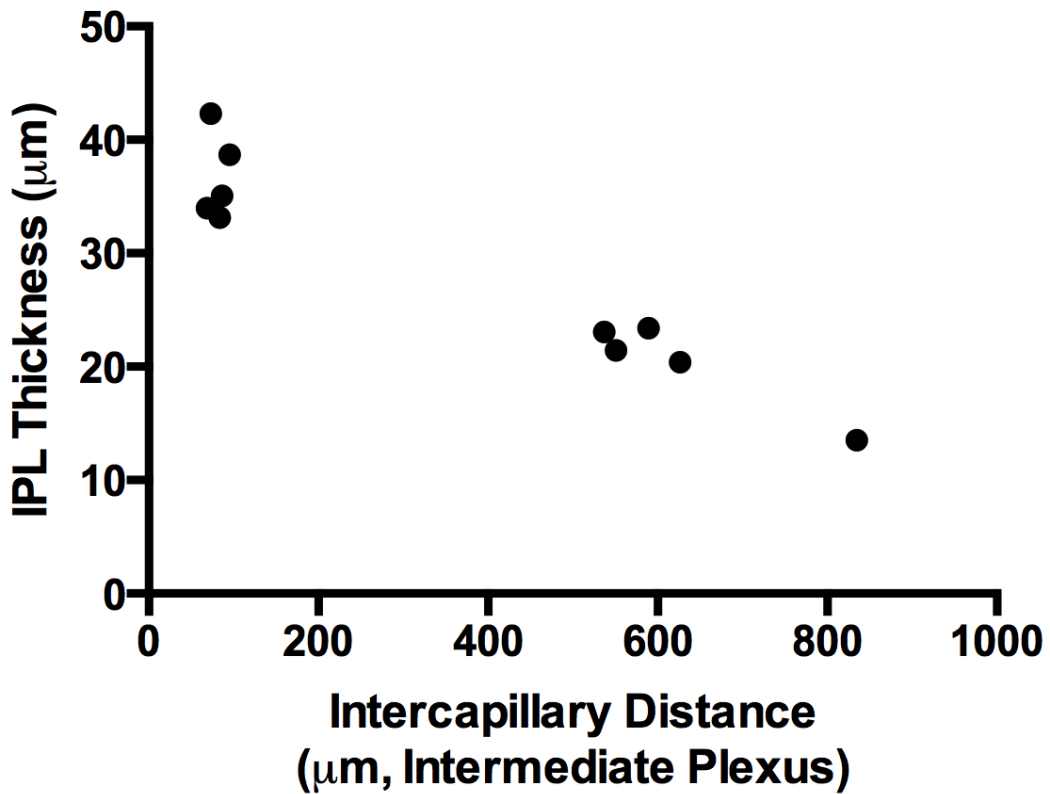


Figure 5.14 Correlation between inner plexiform layer thickness and intercapillary distance in the intermediate capillary plexus. There is a strong negative correlation ($r(8) = -0.9583$, $p < 0.0001$) between the thickness of the inner plexiform layer (IPL) and the intercapillary distance of the intermediate capillary plexus.

CHAPTER 6: THE ROLE OF THE OPTIC NERVE HEAD IN AP-2 β NCC KO MICE

6.1 Results

6A: Structural changes in the optic nerve head of AP-2 β NCC KO mice

6.1.1 Retinal thickness at the optic disc decreases in AP-2 β NCC KO mice

The thickness of the retina at the optic disc of control animals was $175.6 \pm 19.8 \mu\text{m}$, while in AP-2 β NCC KOs it was $87.11 \pm 25.45 \mu\text{m}$ (**Figure 6.1, Figure 6.2**). In control animals, when comparing the thickness of the retina at the mid-periphery ($198.7 \pm 18.7 \mu\text{m}$) versus at the optic disc, there were no significant differences in thickness. When comparing the thickness of the retina in AP-2 β NCC KOs at the mid-periphery ($155.7 \pm 25.2 \mu\text{m}$) versus at the optic disc, there was a significant decrease in thickness at the optic disc compared to the midperiphery (ANOVA/Tukey's post hoc test, $p < 0.0001$).

6.1.2 The optic nerve is displaced below the level of the sclera in AP-2 β NCC KO mice

The maximum displacement of optic nerve tissue in relationship to the level of the sclera was $186.1 \pm 30.7 \mu\text{m}$ in control animals ($n=6$) (**Figure 6.3**). In AP-2 β NCC KO animals ($n=6$) the maximum displacement of the optic nerve tissue in relationship to the level of the sclera was $-53.12 \pm 19.72 \mu\text{m}$. There was a

significant displacement in optic nerve tissue below the level of the sclera in AP-2 β NCC KO animals compared to controls (t test, $p < 0.0001$).

6.1.3 The optic nerve head is excavated below the level of the sclera in AP-2 β NCC KO mice

In control animals (n=6) there was no area of excavation ($0 \mu\text{m}^2$) of optic nerve tissue below the level of the sclera (**Figure 6.4**). In AP-2 β NCC KOs (n=6), the area excavated below the level of the sclera was $10119 \pm 6438 \mu\text{m}^2$. There was a significant increase in the area excavated below the level of the sclera in AP-2 β NCC KOs compared to control animals (t test, $p = 0.0024$).

6B: Glial reactivity in the optic nerve head of AP-2 β NCC KO mice

6.1.4 Iba-1 expression in the retinas and optic nerve head of AP-2 β NCC KO mice

The density of Iba-1 expressing cells in the retinal sections control animals (n=5) was $60.65 \pm 11.95 \text{ cells/mm}^2$ while in AP-2 β NCC KOs (n=5) it was $166.1 \pm 82.82 \text{ cells/mm}^2$ (**Figure 6.5**). There was a significant increase in the density of Iba-1 expressing cells (t test, $p = 0.0081$) in AP-2 β NCC KOs compared to control animals. The intensity of Iba-1 fluorescence expressed as mean gray value was 5182 ± 655 in control animals, while it was 6613 ± 872 in AP-2 β NCC KOs (**Figure 6.6**). There was a significant increase (t test, $p = 0.0066$) in the intensity of Iba-1 fluorescence in the retinas of AP-2 β NCC KO mice compared to controls.

These findings are consistent with the original study done by Martino et al. in a cohort of younger mice.

In the optic nerve head of control animals (n=6) the density of Iba-1 labeled cells was 189.1 ± 33.7 cells/mm² (**Figure 6.7, Figure 6.8**). In AP-2 β NCC KOs (n=6) the density of Iba-1 labeled cells was 423.6 ± 85.1 cells/mm². There was a significant increase in the density of Iba-1 labeled cells in AP-2 β NCC KOs compared to controls at the optic nerve head (t test, p<0.0001).

6.1.5 GFAP expression in the retinas and optic nerve head of AP-2 β NCC KO mice

GFAP fluorescence in the retinal ganglion cell layer was expressed as mean gray value. The mean GFAP fluorescence intensity in control mice (n=5) was 4095 ± 683 . In AP-2 β NCC KOs (n=5) the GFAP fluorescence intensity was 9275 ± 1357 (**Figure 6.9**). There was a significant increase in the fluorescence of GFAP in the retinal ganglion cell layer in AP-2 β NCC KOs compared to controls (t test, p<0.0001).

There was a significant increase in the number of Müller cells expressing GFAP in the retinas of control animals compared to AP-2 β NCC KOs (t test, p<0.0001) (**Figure 6.10**). In controls (n=5) there were 0 Müller cells/mm expressing GFAP. This is in contrast to AP-2 β NCC KOs (n=5) where 167.8 ± 22 cells/mm GFAP expressing Müller cells were observed. The data obtained in this study are in line with the observations made by Martino et al.

At the location of the optic nerve head in control animals (n=4), GFAP fluorescence intensity, expressed as mean gray value, was 26.27 ± 5.27 (**Figure 6.11, Figure 6.12**). In AP-2 β NCC KO mice (n=4), GFAP fluorescence at the optic nerve head was 31.11 ± 4.49 . There were no significant differences detected in GFAP fluorescence at the optic nerve head between control and AP-2 β NCC KO animals (t test; p=0.0679).

6.2 Discussion

“Cupping” of the optic nerve head is a clinical term used to describe structural changes in optic neuropathies of all types (Bianchi-Marzoli, Rizzo, Brancato, & Lessell, 1995; Greenfield, Siatkowski, Glaser, Schatz, & Parrish, 1998; Schwartz, Reuling, & Garrison, 1975). It has been an important characteristic used in the diagnosis of glaucoma and measured as an indicator of disease progression (Hasnain, 2016). The centre “cup” of the optic nerve is measured and compared to the margin of the optic nerve, referred to as the “disc” (Casson et al., 2012). As the ratio of the disc increases, so does the progression of disease (Jung, Jeon, & Park, 2016). “Cupping” is also used synonymously for the pathophysiology of glaucomatous optic nerve head damage (Anderson & Cynader, 1997; Kalvin & Hamasaki, 1966; Quigley & Green, 1979; Vrabc, 1976), and hereinafter the term “cupping” will refer to these pathophysiological changes. AP-2 β NCC KO mice have a complete closure of the iridocorneal angle and elevated intraocular pressure, as seen in closed-angle glaucoma (Leske,

1983). It was expected that there would be a significant deformity of the optic nerve head, “cupping,” as a result of the significant intraocular pressure caused by inadequate drainage of aqueous humor in the anterior chamber. Within the eye the optic nerve head is considered the structure most susceptible to damage, as it is located at a discontinuity of the corneo-scleral shell (Crawford Downs, Roberts, & Sigal, 2011). A discontinuity such as this is considered a weak spot in a mechanically loaded system as it may be the site of considerable concentrations of stress (Crawford Downs et al., 2011). Given that this weak point is where all 1.2-2.0 million retinal ganglion cell axons turn and coalesce to form the optic nerve, it is (Burgoyne, 2011), and has historically been (Zimmerman, de Venecia, & Hamasaki, 1967), an important site to study in glaucoma. There is an abundance of evidence suggesting that damage to the optic nerve axons happens at the level of the optic nerve head in glaucoma (Hernandez & Pena, 1997; Quigley, Addicks, Green, & Maumenee, 1981). Compression, stretching, and remodeling of the connective tissue optic nerve head is a feature of human glaucomatous eyes (Hernandez, Andrzejewska, & Neufeld, 1990), and appears in animal models of elevated intraocular pressure (Johnson et al., 1996). Excavation of the optic nerve head as well as thinning of the neuroretinal rim are associated with pressure-induced damage (Mao et al., 2011). The current study sought to determine if characteristics of pressure-induced damage were present in 12-16 week old AP-2 β NCC KO mice and to provide a quantification of such changes. When frozen sections through the optic nerve head were cut and examined there were stark

changes in AP-2 β NCC KO mice compared to their control littermates. The level of the sclera was chosen as a reference point in the quantification of changes in the optic nerve head. Previous studies using primate eyes showed the scleral canal wall to be the insertion point for the lamina cribosa and that experimentally induced glaucoma caused the outward migration of the lamina cribosa below the level of the sclera (Yang et al., 2010). Although the optic nerve heads of mice do not have a lamina cribosa, the level of the sclera provides a reference point that allows for the comparison of changes in “cupping” across models and species (May & Lütjen-Drecoll, 2002). When measuring the maximum displacement of tissue at the optic nerve head, control animals had thick nerve fibres displaced above the level of the sclera, as expected in healthy, uninjured eyes. AP-2 β NCC KO mice displayed a clear recession of tissue below the level of the sclera compared to controls. This demonstrates that there is pressure-induced damage at the optic nerve head of AP-2 β NCC KO mice. There was a significant area excavated below the level of the sclera in all AP-2 β NCC KO optic nerve heads examined. This is a characteristic of advanced glaucomatous damage (Yang et al., 2011). There was a concave shape associated to the excavation, matching the expected structure of an optic nerve head that was cupped due to remodeling from elevated intraocular pressure (Hasnain, 2016). There was also a statistically significant decrease in the thickness of the retina at the optic nerve head of AP-2 β NCC KO in relation to the thickness of the mid-periphery when compared to the decrease in thickness of control littermates. Thinning of the neuroretinal rim in

human glaucoma is associated with corresponding visual defects (Hitchings & Spaeth, 1977). The excavation of the optic nerve head in AP-2 β NCC KO mice and the thinning of the retina at the optic nerve head provide strong evidence to suggest that the optic nerve head is the site of damage resulting in the death of retinal ganglion cells and that AP-2 β NCC KO mice represent an animal model of glaucoma that closely mimics the changes at the optic nerve head observed in human disease. The precise cause of retinal ganglion cell death and the role of elevated intraocular pressure remains controversial, although lowering intraocular pressure remains the only method proven to delay the onset and progression of glaucomatous disease (Crawford Downs et al., 2011). Impingement of the retinal ganglion cell axons at the optic nerve head may cause a decrease in the transport of neurotrophic factors (Almasieh, Wilson, Morquette, Cueva Vargas, & Di Polo, 2012), that results in the death of the retinal ganglion cells. Alternative theories suggest that retinal ganglion cells die by pressure-induced axotomy at the optic nerve head (Hasnain, 2016). Future studies should delve deeper into the precise mechanisms of injury involved in the death of retinal ganglion cells using the AP-2 β NCC KO mouse model. For example, a temporal study of retinal ganglion cell death using a fluorescent tracer, such as Neurobiotin, could examine the patterning, if any, associated with retinal ganglion cell death. Given that the visual defects in glaucoma begin with an arcuate shaped loss in the periphery and progress peripherally and centrally (Leske & Rosenthal, 1979), there may be a predictable order to the loss of retinal ganglion cells in AP-2 β NCC KO mice.

Additionally, tracking the structure of the optic nerve head over time and studying it in both younger and older mice may reveal more information about its role in retinal ganglion cell death.

The clear structural changes in the optic nerve head in AP-2 β NCC KO mice lend credence to the notion that there would be glial reactions in cells of the optic nerve head. Astrocytes play an important role in central nervous system injury (Aschner, 1998; Buffo et al., 2010; Ridet et al., 1997). In reaction to injury astrocytes become activated, proliferate, and upregulate intermediate filaments that are comprised of vimentin, nestin, and glial fibrillary acidic protein (GFAP) (Pekny & Nilsson, 2005). There is evidence to suggest that astrocytes can be beneficial or detrimental for neuroprotection and tissue regeneration (Buffo et al., 2010). Reactive astrocytes can upregulate and express a variety of supportive growth factors including brain-derived neurotrophic factor and nerve growth factor in response to injury (Schwartz & Nishiyama, 1994). On the other hand, reactive astrocytes in the optic nerve head of a rat model of elevated intraocular pressure have been shown to upregulate inducible nitric oxide synthase, NOS-2 (Neufeld, Hernandez, & Gonzalez, 1997), a powerful enzyme generating large amounts of nitric oxide that can be neurotoxic to the axons of retinal ganglion cells (Neufeld, 1999). Martino et al. originally demonstrated GFAP reactivity in astrocytes and Müller cells in the retinas of 8-12 week old AP-2 β NCC KO mice. A cohort of 12-16 week old mice was used in this study to examine and quantify glial reactivity in the optic nerve head and its relationship to the changes in the

retina. There was a clear upregulation of GFAP in the retinal ganglion cell layer. This suggests that there is an astrocytic response to retinal injury in AP-2 β NCC KO mice. Additionally there was widespread upregulation of GFAP in the Müller cells of the retina, reaffirming the findings of Martino et al. Retinal Müller glial reactivity is a classic indicator of many different types of retinal injury (Bringmann et al., 2006). There were no changes in astrocytic GFAP reactivity in the optic nerve head of AP-2 β NCC KO mice compared to littermate controls. This is in line with previously reported findings in a model of elevated intraocular pressure induced using injections of hypertonic saline into the episcleral veins of Brown Norway rats (Johnson, Deppmeier, Wentzien, Hsu, & Morrison, 2000). After 1 and 2 weeks of elevated intraocular pressure, GFAP labeling in the optic nerve head was found to decrease dramatically in this model (Johnson et al., 2000). It was only after 33 days that optic nerve head GFAP labeling was restored (Johnson et al., 2000). GFAP immunoreactivity has been shown to initially decrease at the site of optic nerve crush injury (Gocht & Löhler, 1993; Sagaties Farmer et al., 1997). Given that AP-2 β NCC KO animals were 12-16 weeks old, and have a chronic form of early-onset congenital glaucoma, it is most plausible that the timepoint studied is a very late stage in the disease process. It does not rule out the notion that the optic nerve head is the site of injury in this model of glaucoma and suggests that GFAP optic nerve head expression should be studied earlier in the lifespan of the animals.

Martino et al. showed microglial reactivity using Iba-1 staining in 8-12 week old AP-2 β NCC KO mice. Microglia play a major role in mediating phagocytosis during the degeneration of retinal ganglion cells (Thanos, Moore, & Hong, 1996). In this study the number of microglia were quantified in both the retina and optic nerve head in 12-16 week old mice. There was a clear increase, approximately 2-fold, in the number of microglia in both the retina and optic nerve in AP-2 β NCC KO mice compared to their littermates. Microgliosis has been documented following optic nerve crush and after acute intraocular pressure elevation in the retina (Liu et al., 2012). Between 7 and 21 days after optic nerve crush, microglia increase in number by about 2-fold in the retina (Liu et al., 2012). After 60 minutes of acute intraocular pressure elevation, the number of microglia increase 2-fold after 7 days, but return to baseline by 28 days (Liu et al., 2012). The findings here in the retinas of AP-2 β NCC KO mice are consistent with findings in the other models of injury (Wohl, Schmeer, Witte, & Isenmann, 2010). In response to retinal ganglion cell death, microglia proliferate and double in number (Liu et al., 2012; Wohl et al., 2010). Although the number of microglia in injured retinas return to baseline after acute injury (Liu et al., 2012), AP-2 β NCC KO mice represent a chronic injury, potentially explaining the persistence of microgliosis observed in 12-16 old mice, after the death of almost all retinal ganglion cells. The doubling in number of microglia was also observed in the optic nerve head, showing that microglial response plays an important role at that site. The proliferation of microglial cells in the optic nerve head is likely in

response to the degeneration of retinal ganglion cell axons. These findings show that microglial cells play a role in both the retina and optic nerve head with similar increases in cell density that are associated with retinal ganglion cell degeneration. Understanding more about microglial responses in models of elevated intraocular pressure could provide mechanistic insights into retinal ganglion cell death and also neuroprotection. Microglia have the ability to provide support to dying retinal ganglion cells by removing cellular debris and secreting neurotrophic factors (Liao, Zhao, Beers, Henkel, & Appel, 2012). As well microglia can play a more sinister role in neurodegeneration releasing damaging molecules like tumor necrosis factor α and nitric oxide (Cao & He, 2013). Given that microglia proliferate in this model, their dynamic profiles should be investigated as a target to augment the survival of retinal ganglion cells and provide further mechanistic insights into their death.

6.3 Figures

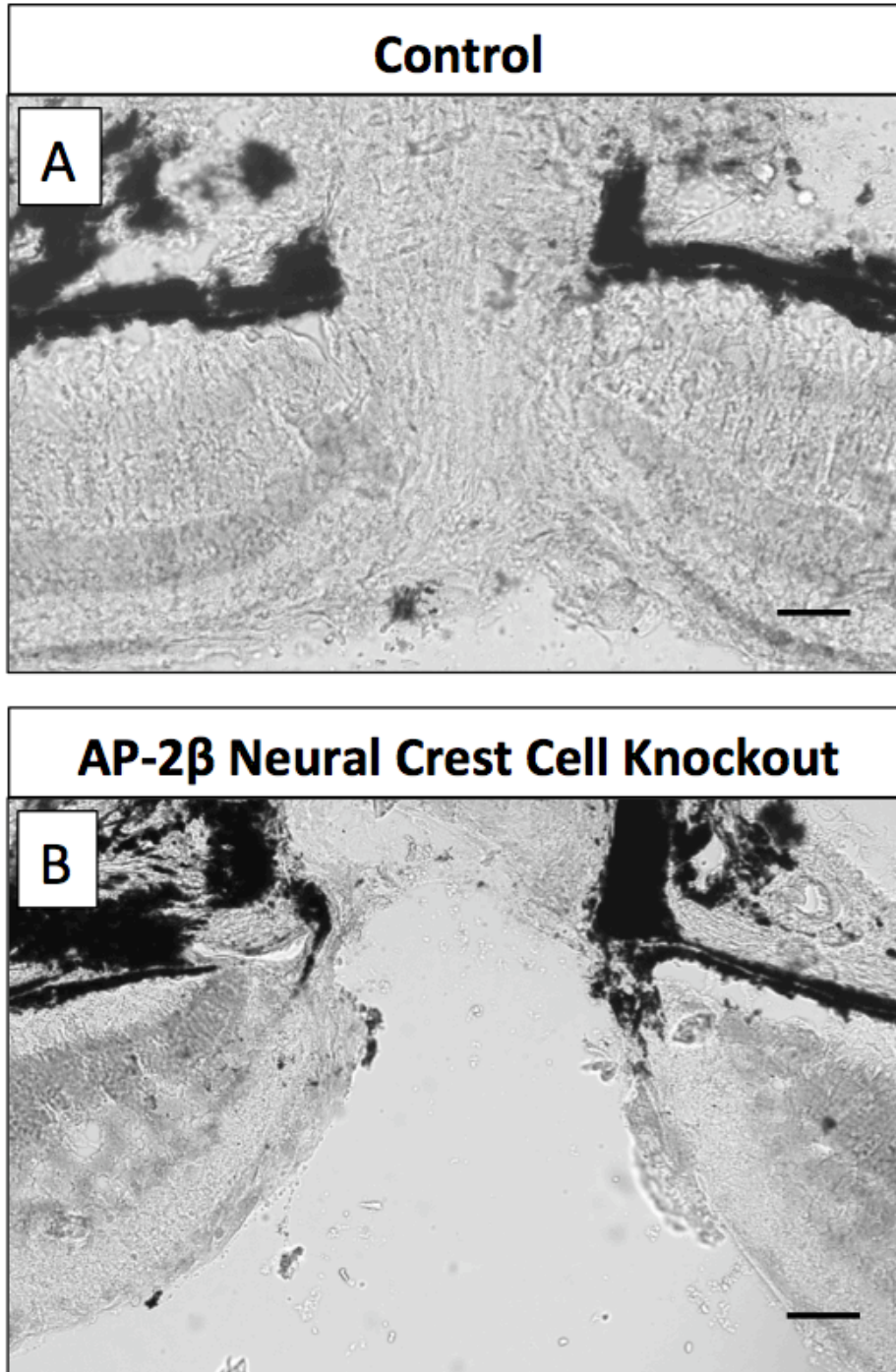


Figure 6.1 Toluidine blue staining of the optic nerve head in control and AP-2β NCC KO mice. (A) Control (n=6) optic nerve head stained with toluidine blue. (B) AP-2β NCC KO (n=6) optic nerve head stained with toluidine blue demonstrating excavation of the optic nerve. Scale Bar = 50 μm.

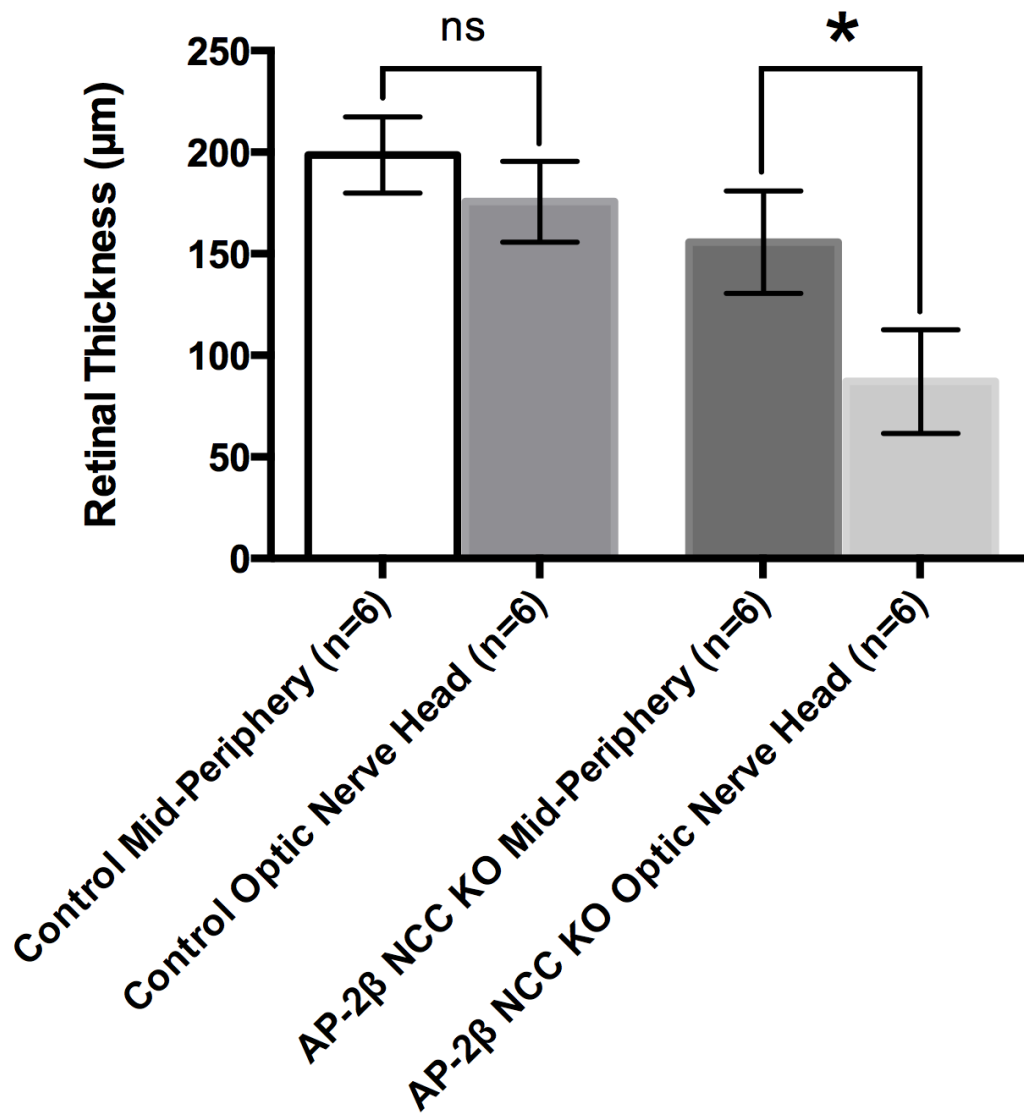


Figure 6.2 Retinal thicknesses at the optic nerve head in control versus AP-2β NCC KO mice. There is a significant (ANOVA/Tukey's post hoc test, $p < 0.0001$) decrease in the thickness of the retina at the optic disc in AP-2β NCC KOs ($n=6$, $87.11 \pm 25.45 \mu\text{m}$) compared to the midperiphery ($n=6$, $155.7 \pm 25.2 \mu\text{m}$). In control animals, there were no changes in the thickness of the retina at the optic disc ($n=6$, $175.6 \pm 19.8 \mu\text{m}$) compared to the mid-periphery ($n=6$, $198.7 \pm 18.7 \mu\text{m}$).

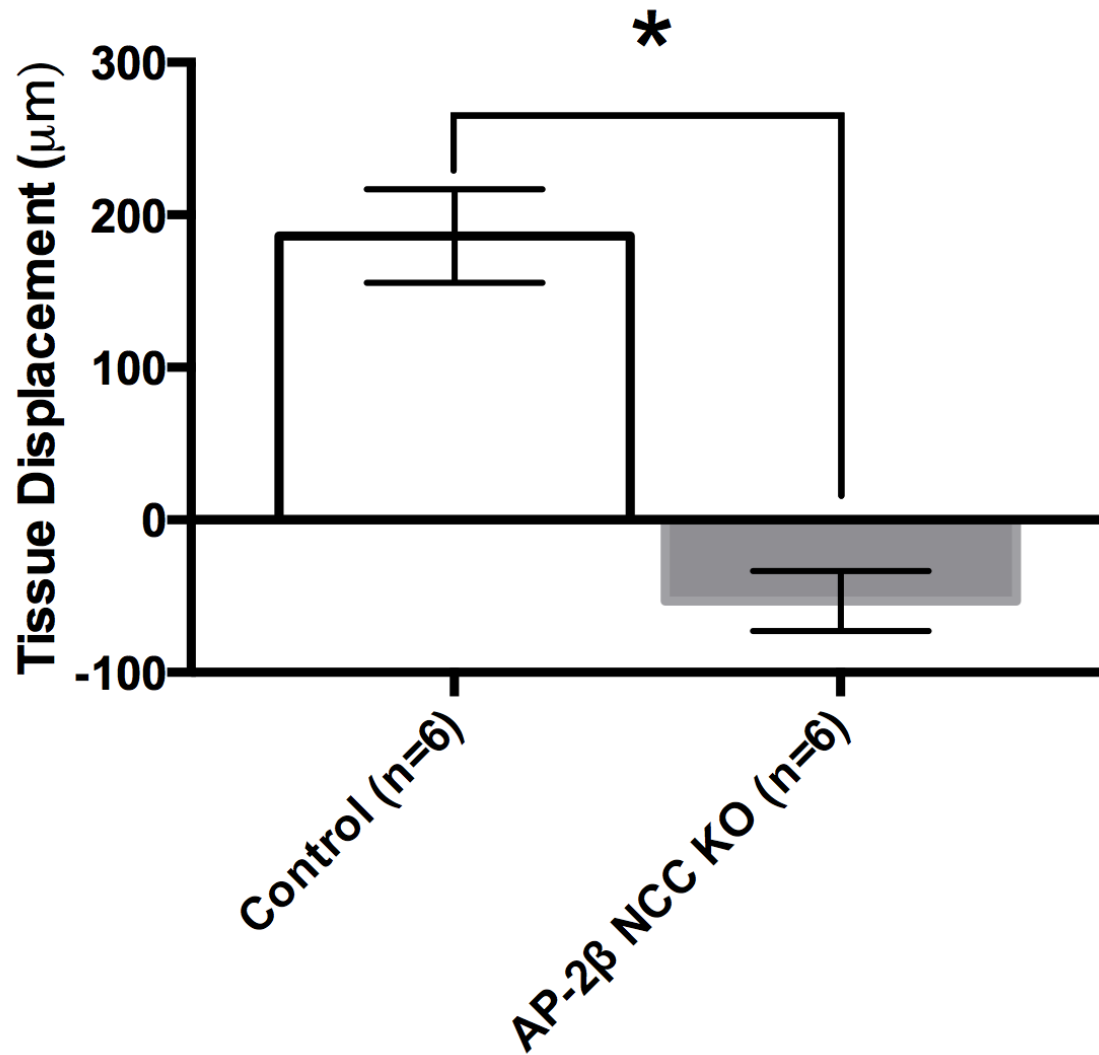


Figure 6.3 Tissue displacement from the sclera at the optic nerve head in control and AP-2β NCC KO mice. There was a significant difference in the displacement of tissue from the sclera when comparing AP-2β NCC KOs and animals. The tissue at the optic nerve head is above the level of the sclera in controls (n=6, 186.1 ± 30.7 μm), while in AP-2β NCC KOs it is displaced below the level of the sclera (n=6, -53.12 ± 19.72 μm).

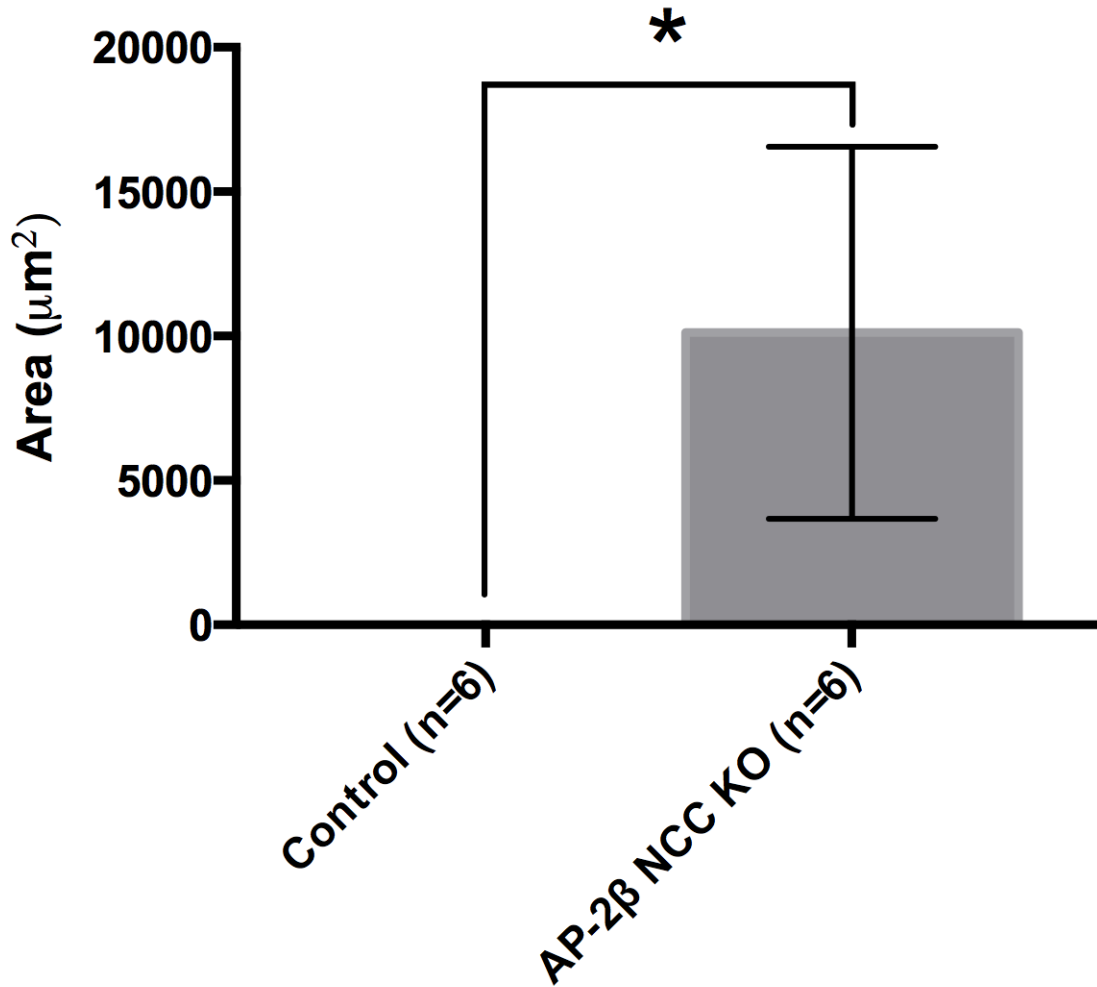


Figure 6.4 Area of optic nerve head excavation below the level of the sclera in control and AP-2β NCC KO mice. There is a significant difference in area excavated below the level of the sclera in AP-2β NCC KO (n=6, 10119 ± 6438 µm²) mice compared to control (n=6, 0 µm²) mice (t test, p=0.0024).

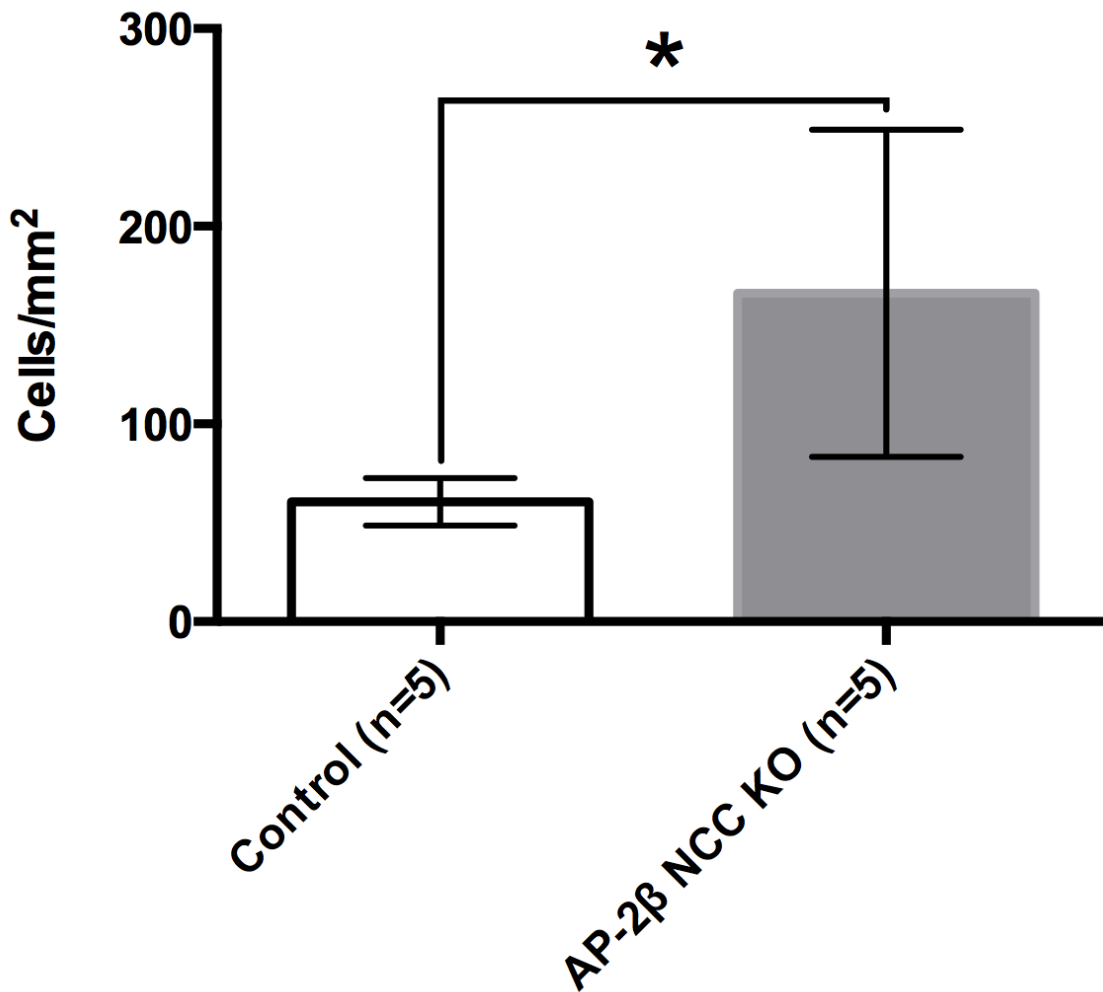


Figure 6.5 Iba-1 cell density in the retinas of AP-2β NCC KO and control mice. There was a significant increase (t test, $p=0.0081$) in the density of cells expressing Iba-1 in AP-2β NCC KO mice ($n=5$, 166.1 ± 82.82 cells/mm²) when compared to controls ($n=5$, 60.65 ± 11.95 cells/mm²).

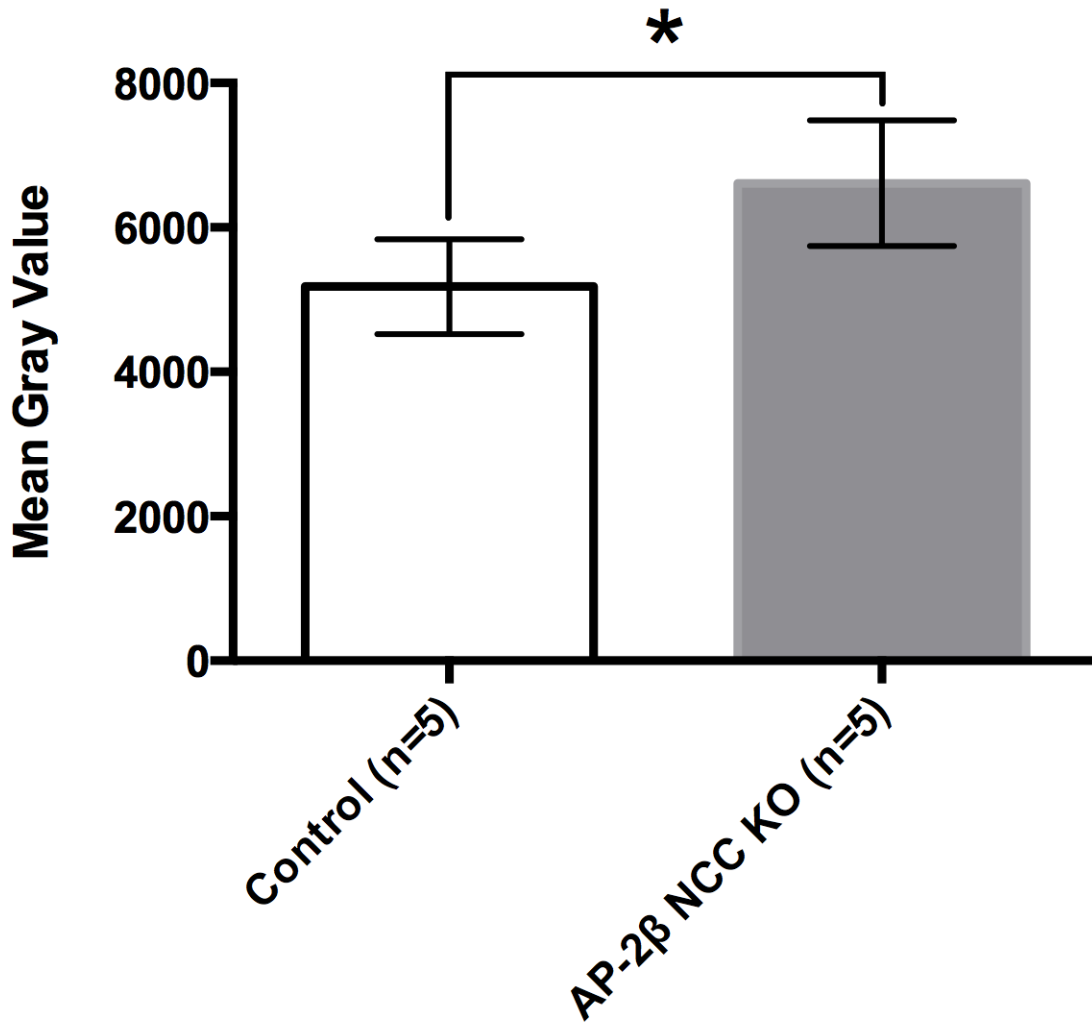


Figure 6.6 Iba-1 fluorescence intensity in the retinas of control mice versus AP-2β NCC KOs. There was a significant increase (t test, $p=0.0066$) detected in Iba-1 fluorescence intensity in AP-2β NCC KOs ($n=5$, mean gray value = 6613 ± 872) when compared to controls ($n=5$, mean gray value = 5182 ± 655).

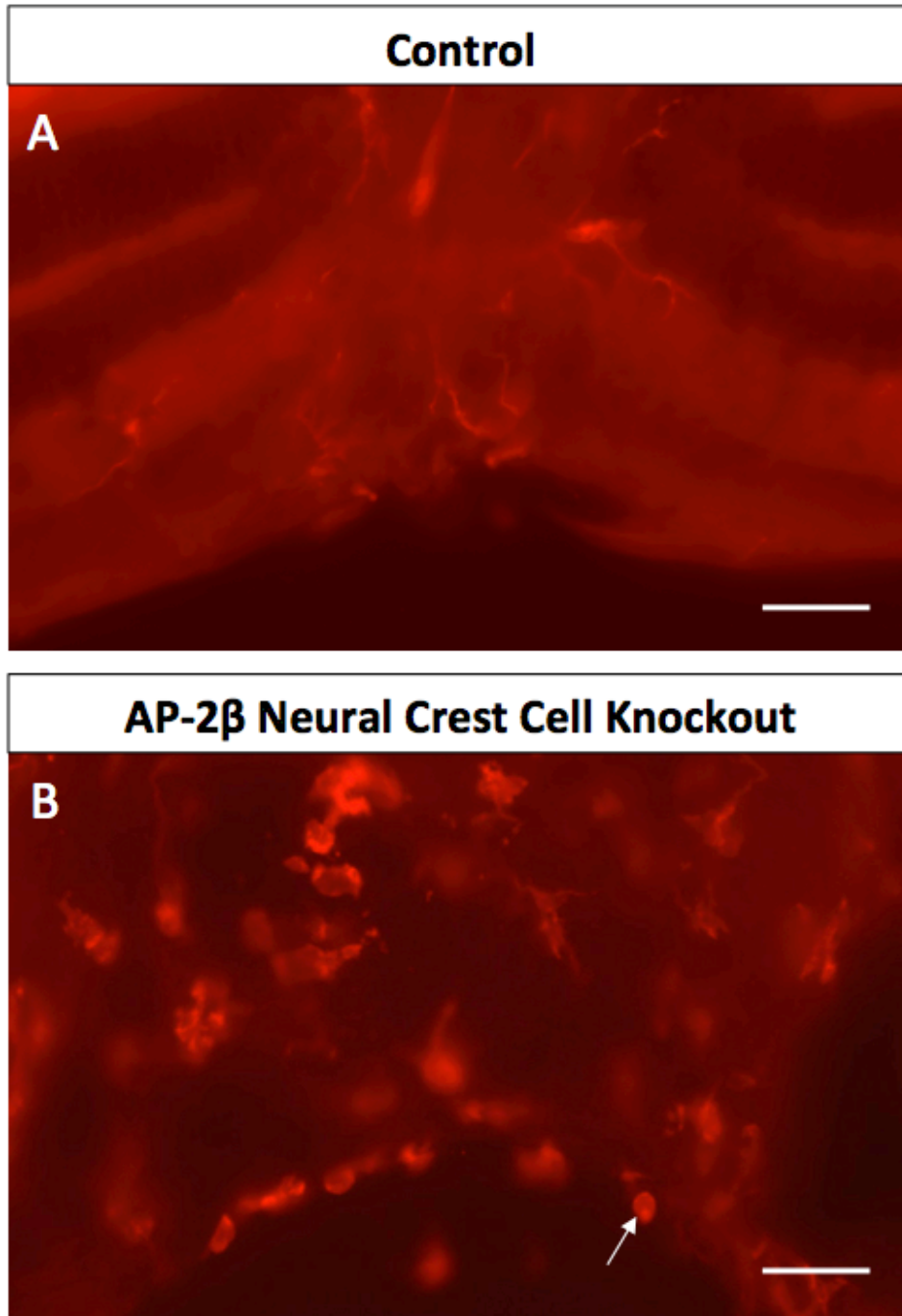


Figure 6.7 Iba-1 fluorescence in the optic nerve heads of control and mice. Iba-1 (red) is expressed in microglia in the optic nerve head of (A) control (n=6) mice. In the optic nerve head of (B) AP-2 β NCC KOs (n=6), Iba-1 is expressed in reactive microglia as well as macrophages (arrow) on the surface of the optic nerve head. Scale Bar = 50 μ m.

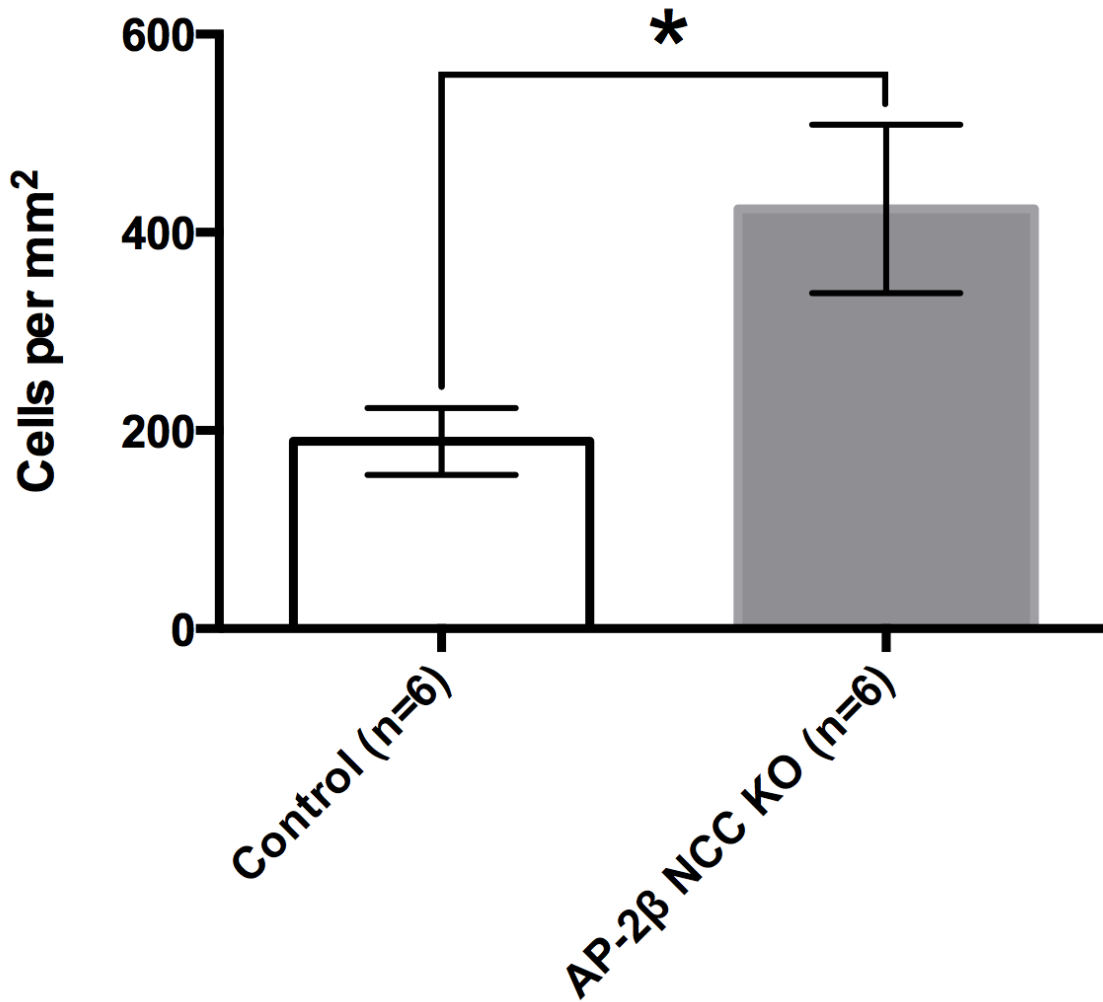


Figure 6.8 Iba-1 cell density in the optic nerve head of AP-2β NCC KO and control mice. There was a significant increase (t test, $p < 0.0001$) in the density of cells expressing Iba-1 in the optic nerve head of AP-2β NCC KO ($n=6$, 423.6 ± 85.1 cells/mm²) mice when compared to controls ($n=6$, 189.1 ± 33.7 cells/mm²).

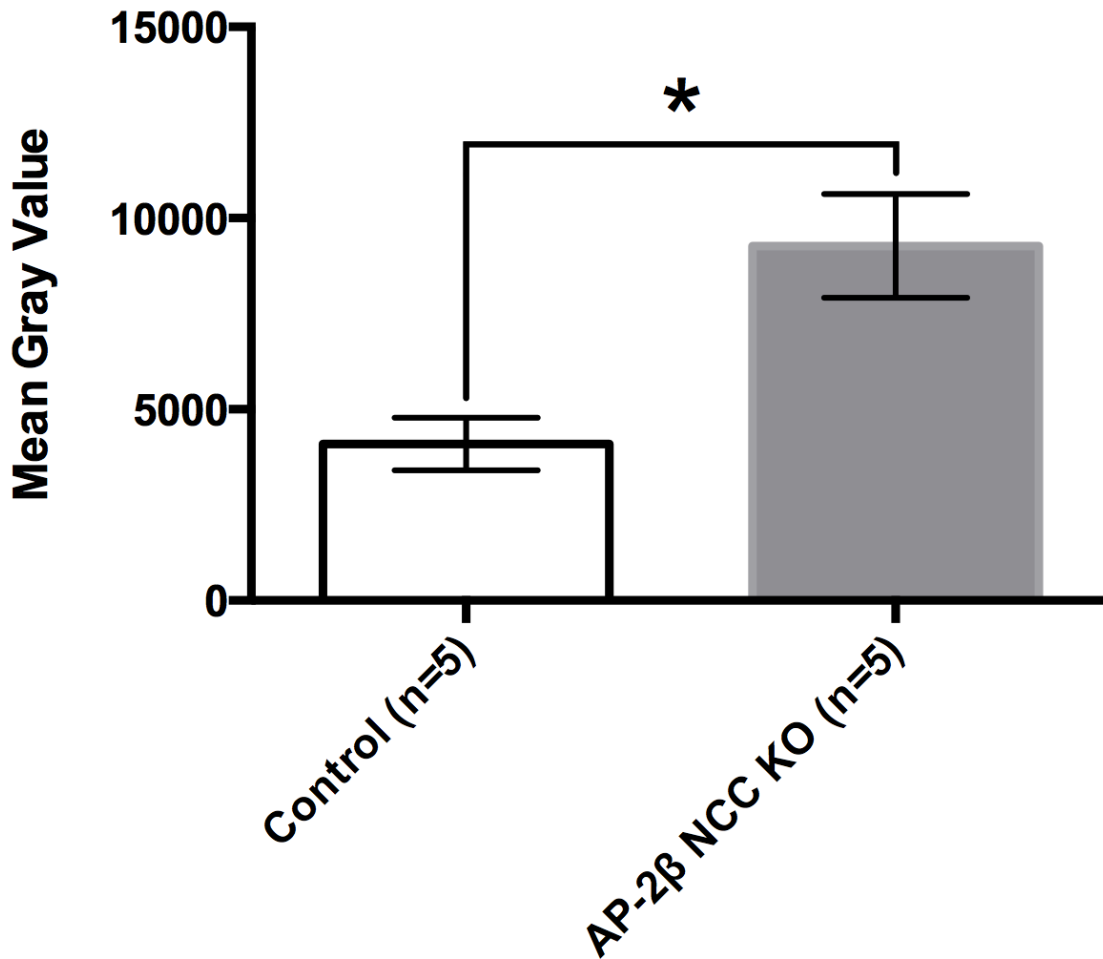


Figure 6.9 GFAP fluorescence intensity of the retinal ganglion cell layer in control versus AP-2β NCC KO mice. There was a significant increase (t test, $p < 0.0001$) in the fluorescence of the retinal ganglion cell layer in AP-2β NCC KO (n=5, mean gray value = 9275 ± 1357) mice compared to controls (n=5, mean gray value = 4095 ± 683).

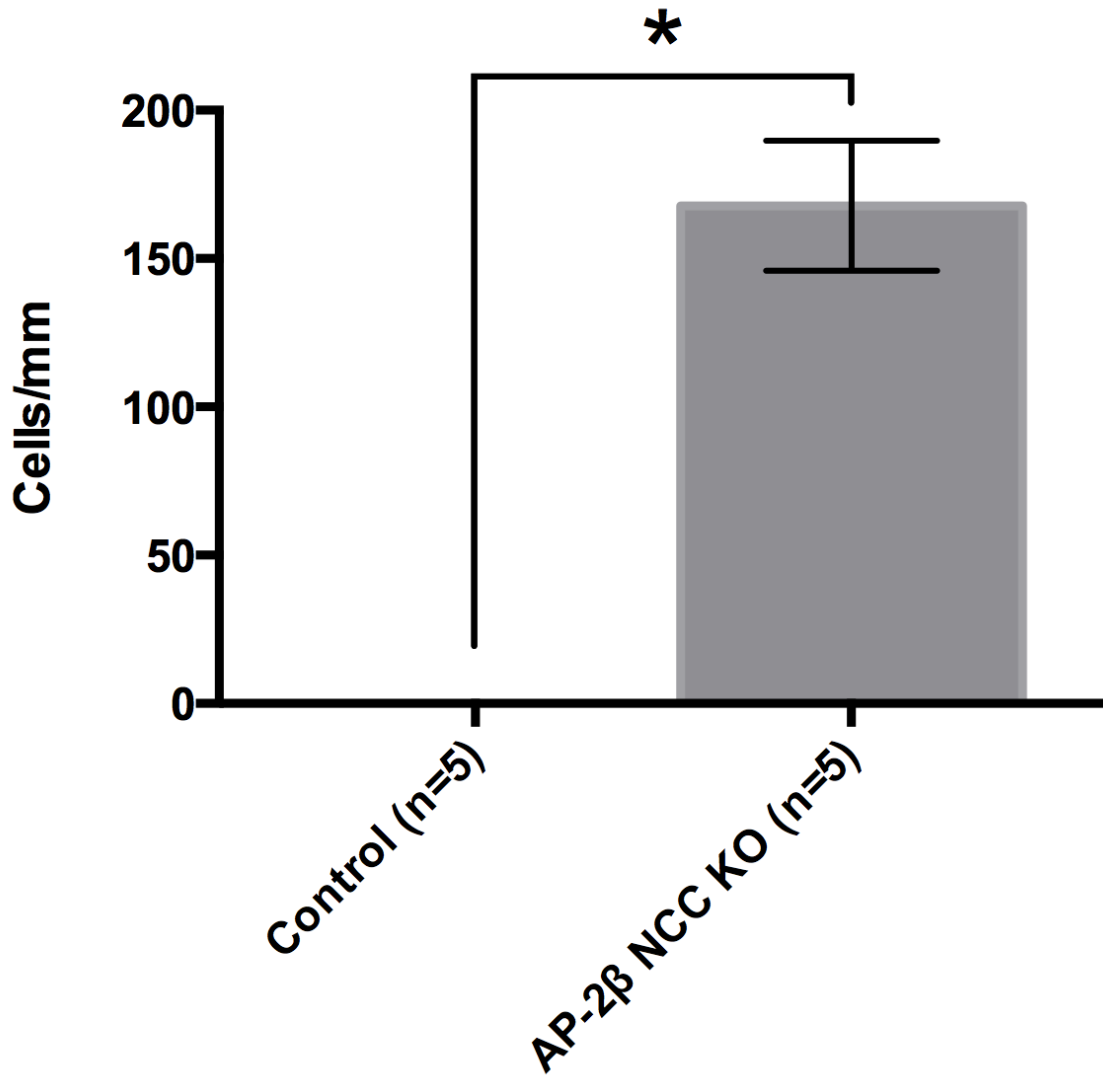


Figure 6.10 GFAP expression in Müller cells in control mice versus AP-2β NCC KOs. There were no Müller cells detected expressing GFAP in control mice. Müller cell expression of GFAP increased significantly (t test, $p < 0.0001$) in AP-2β NCC KO ($n=5$, 167.8 ± 22 cells/mm) mice compared to controls.

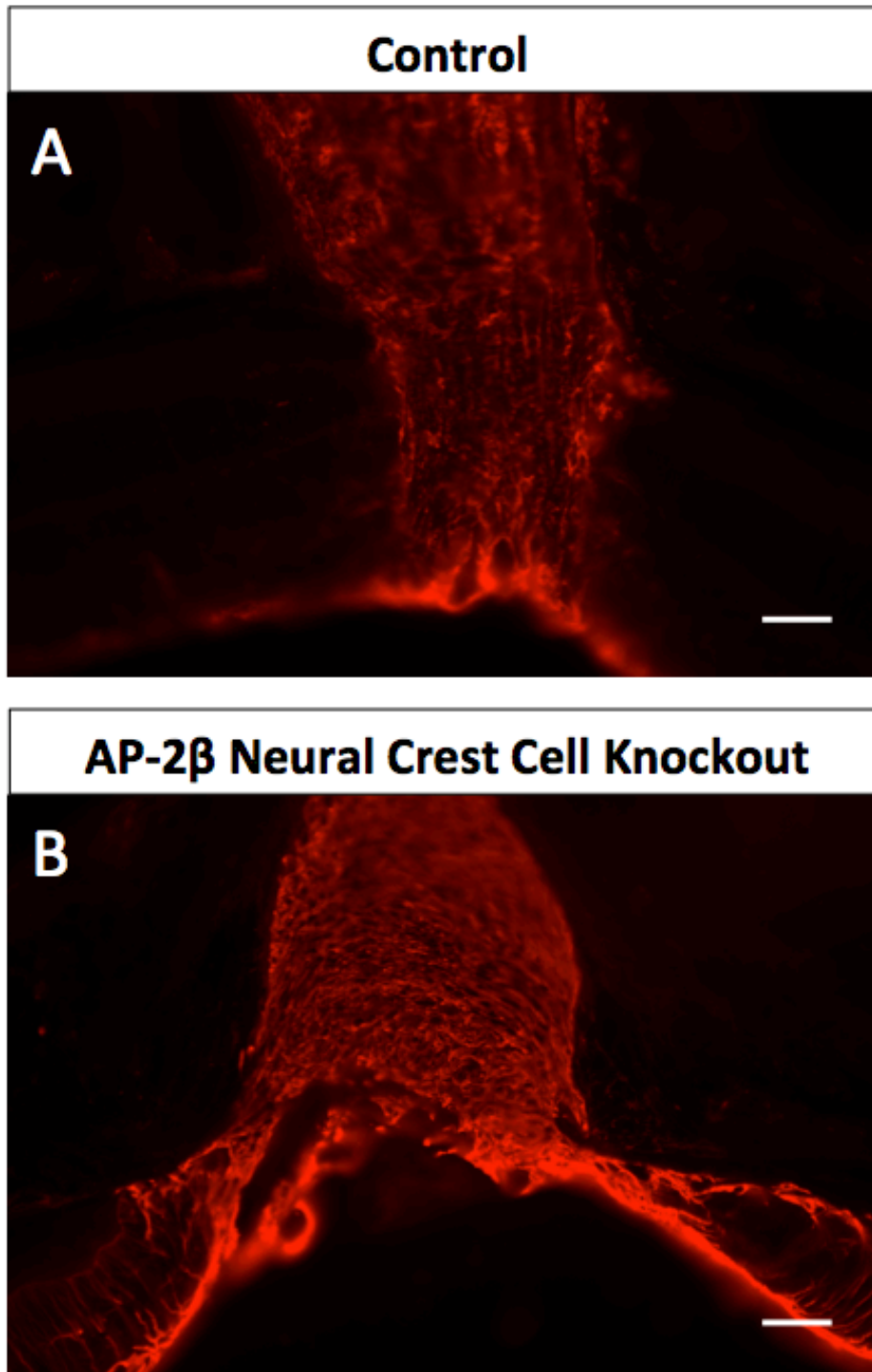


Figure 6.11 GFAP staining in the optic nerve head of control versus AP-2 β NCC KO mice. GFAP (red) staining in the optic nerve head astrocytes of (A) control (n=4) versus (B) AP-2 β NCC KO (n=4) mice. Scale Bar = 50 μ m.

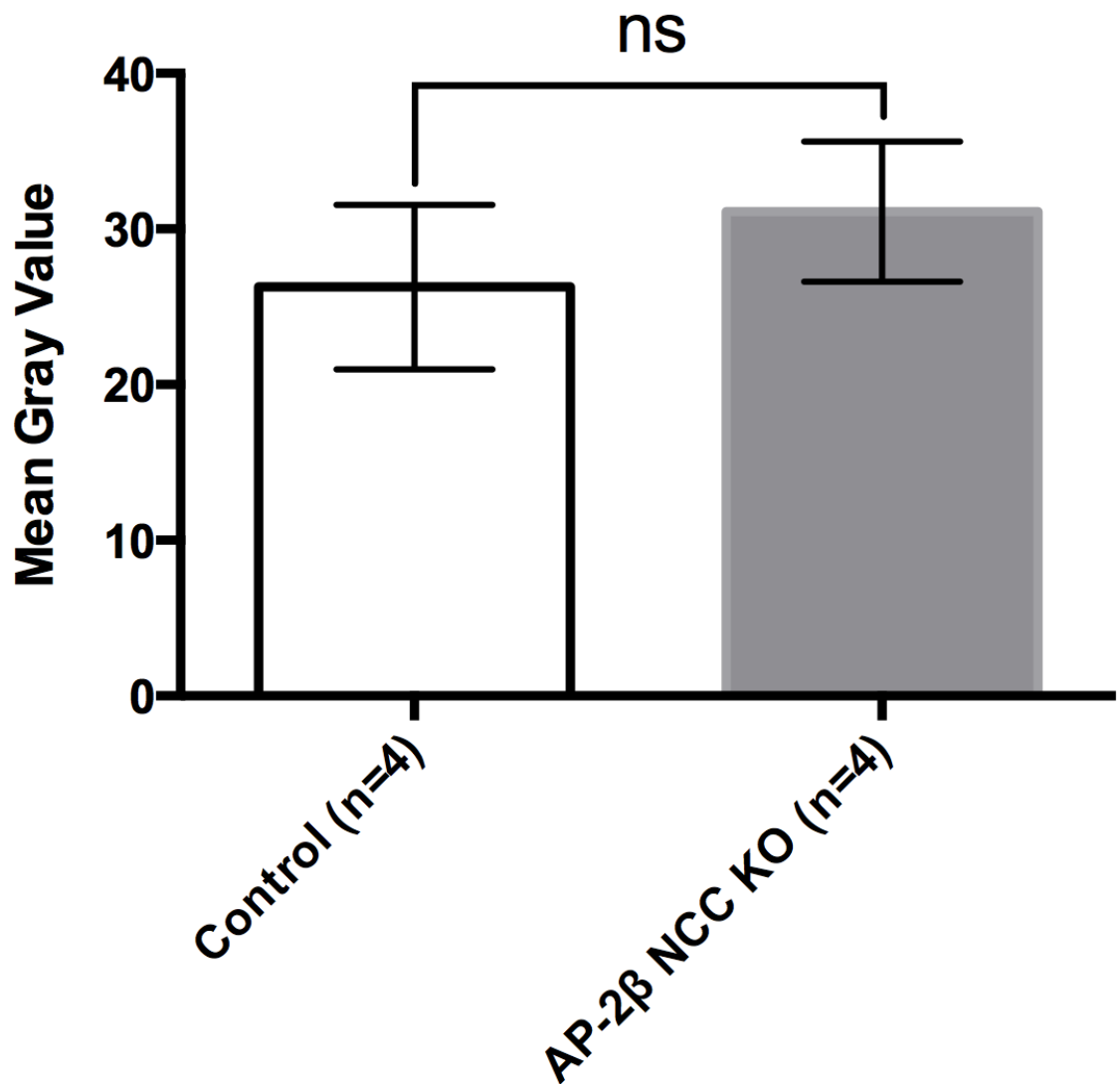


Figure 6.12 GFAP fluorescence intensity in the optic nerve head of control versus AP-2β NCC KO mice. GFAP fluorescence intensity does not change significantly (t test) when comparing AP-2β NCC KOs (n=4, mean gray value = 31.11 ± 4.49) and control (n=4, mean gray value = 26.27 ± 5.27) mice.

CHAPTER 8: CONCLUSION

The overall hypothesis of this study was that the immune system and vasculature played a role in the retinal response to injury in models of glaucoma. Based on the data collected here it can be concluded that indeed the vasculature and immune system do play a role in the retinal response to injury, but to varying degrees in different models and different points in time after retinal ganglion cell injury.

Early on after optic nerve crush, it was demonstrated in that the systemic immune system did not play a significant role in the response to crush injury up to 7 days. The retinal vasculature did not show signs of permeability while the optic nerve showed a significant breach in vessel integrity and subsequent leakage after crush. Slit2 administration did not have any measurable effect on the death of retinal ganglion cells after optic nerve crush injury, supporting the idea that vasculature and immune system do not play a significant role in the response to retinal ganglion cell injury.

Experiments conducted on AP-2 β NCC KO mice demonstrated that the immune system and vasculature play role following widespread retinal ganglion cell degeneration. Microgliosis was observed in both the retina as well as the optic nerve head. There were dramatic changes in structure in the optic nerve head as well, suggesting that this is the site of injury due to elevated intraocular pressure in AP-2 β NCC KO mice. Blood-borne macrophages were discovered on the

vitreal surface of the retina, adherent across the entire retinal surface including at the optic nerve head. There were changes in the microvasculature in each of the retinal capillary plexuses. Decreases in capillary density affected the intermediate and deep capillary plexuses, and there was a significant increase in intercapillary distance in the intermediate plexus. There was a correlation between the changes in the intermediate capillary plexus and the remodeling in the inner plexiform layer. Since there were no changes in retinal thickness after significant cell loss 7 days after optic nerve crush it is suggested that both the retinal remodeling and microvascular degeneration occurred after significant neurodegeneration in the AP-2 β NCC KO mouse model. The data gathered from these mice suggests that the immune system and vasculature play a role late in the response to retinal injury.

Further studies into the role of the immune system and vasculature can help us to better understand the mechanisms underlying disease in glaucoma in the hope that therapeutic targets can be identified to treat patients with this condition and potentially reverse the blindness associated with it.

REFERENCES

- Abcouwer, S. F., Lin, C. M., Shanmugam, S., Muthusamy, A., Barber, A. J., & Antonetti, D. A. (2013). Minocycline prevents retinal inflammation and vascular permeability following ischemia-reperfusion injury. *Journal of Neuroinflammation*, *10*, 149.
- Ahmed, F., Brown, K. M., Stephan, D. A., Morrison, J. C., Johnson, E. C., & Tomarev, S. I. (2004). Microarray analysis of changes in mRNA levels in the rat retina after experimental elevation of intraocular pressure. *Investigative Ophthalmology & Visual Science*, *45*, 1247–1258.
- Almasieh, M., Wilson, A. M., Morquette, B., Cueva Vargas, J. L., & Di Polo, A. (2012). The molecular basis of retinal ganglion cell death in glaucoma. *Progress in Retinal and Eye Research*, *31*, 152–181.
- Alshareef, R. A., Barteselli, G., You, Q., Goud, A., Jabeen, A., Rao, H. L., et al. (2016). In vivo evaluation of retinal ganglion cells degeneration in eyes with branch retinal vein occlusion. *British Journal of Ophthalmology*, *bjophthalmol-2015-308106*.
- Altay, T., McLaughlin, B., Wu, J. Y., Park, T. S., & Gidday, J. M. (2007). Slit modulates cerebrovascular inflammation and mediates neuroprotection against global cerebral ischemia. *Experimental Neurology*, *207*, 186–194.
- Alward, W. L. M. (2000). Axenfeld-Rieger syndrome in the age of molecular genetics. *American Journal of Ophthalmology*, *130*, 107–115.

- Anderson, D. R., & Cynader, M. S. (1997). Glaucomatous optic nerve cupping as an optic neuropathy. *Clinical Neuroscience (New York, N.Y.)*, 4, 274–278.
- Anderson, D. R., Hoyt, W. F., & Hogan, M. J. (1967). The fine structure of the astroglia in the human optic nerve and optic nerve head. *Transactions of the American Ophthalmological Society*, 65, 275.
- Anderson, M. G., Smith, R. S., Hawes, N. L., Zabaleta, A., Chang, B., Wiggs, J. L., & John, S. W. M. (2001a). Mutations in genes encoding melanosomal proteins cause pigmentary glaucoma in DBA/2J mice. *Nature Genetics*, 30, 81–85.
- Anderson, M. G., Smith, R. S., Savinova, O. V., Hawes, N. L., Chang, B., Zabaleta, A., et al. (2001b). Genetic modification of glaucoma associated phenotypes between AKXD-28/Ty and DBA/2J mice. *BMC Genetics*, 2, 1.
- Aschner, M. (1998). Astrocytic functions and physiological reactions to injury: the potential to induce and/or exacerbate neuronal dysfunction--a forum position paper. *Neurotoxicology*, 19, 7–17– discussion 37–8.
- Balabanov, R., & Dore-Duffy, P. (1998). Role of the CNS microvascular pericyte in the blood-brain barrier. *Journal of Neuroscience Research*, 53, 637–644.
- Balda, M. S., González-Mariscal, L., Contreras, R. G., Macias-Silva, M., Torres-Marquez, M. E., Sáinz, J. A. G., & Cerejido, M. (1991). Assembly and sealing of tight junctions: Possible participation of G-proteins, phospholipase C, protein kinase C and calmodulin. *The Journal of Membrane Biology*, 122, 193–202.

- Baptiste, D. C., Powell, K. J., Jollimore, C. A. B., Hamilton, C., Levatte, T. L., Archibald, M. L., et al. (2005). Effects of minocycline and tetracycline on retinal ganglion cell survival after axotomy. *Neuroscience*, *134*, 575–582.
- Barber, A. J. (2003). A new view of diabetic retinopathy: a neurodegenerative disease of the eye. *Progress in Neuro-Psychopharmacology & Biological Psychiatry*, *27*, 283–290.
- Battisti, W. P., Wang, J., Bozek, K., & Murray, M. (1995). Macrophages, microglia, and astrocytes are rapidly activated after crush injury of the goldfish optic nerve: A light electron microscopic analysis. *Journal of Comparative Neurology*, *354*, 306–320.
- Bayer, A. U., Neuhardt, T., May, A. C., Martus, P., Maag, K. P., Brodie, S., et al. (2001). Retinal morphology and ERG response in the DBA/2NNia mouse model of angle-closure glaucoma. *Investigative Ophthalmology & Visual Science*, *42*, 1258–1265.
- Belecky-Adams, T. L., Chernoff, E. C., & Wilson, J. M. (2013). Reactive muller glia as potential retinal progenitors. In L. Bonfanti, *Neural Stem Cells - New Perspectives*.
- Berkelaar, M., Clarke, D. B., Wang, Y. C., Bray, G. M., & Aguayo, A. J. (1994). Axotomy results in delayed death and apoptosis of retinal ganglion cells in adult rats. *Journal of Neuroscience*, *14*, 4368–4374.
- Bernstein, M. H., & Hollenberg, M. J. (1965). Fine structure of the choriocapillaris and retinal capillaries. *Investigative Ophthalmology*, *4*, 1016–

1025.

- Berry, M., Ahmed, Z., Lorber, B., Douglas, M., & Logan, A. (2008).
Regeneration of axons in the visual system. *Restorative Neurology and Neuroscience*, *26*, 147–174.
- Bianchi-Marzoli, S., Rizzo, J. F., Brancato, R., & Lessell, S. (1995). Quantitative analysis of optic disc cupping in compressive optic neuropathy. *Ophthalmology*, *102*, 436–440.
- Bignami, A., Eng, L. F., Dahl, D., & Uyeda, C. T. (1972). Localization of the glial fibrillary acidic protein in astrocytes by immunofluorescence. *Brain Research*, *43*, 429–435.
- Bora, N. S., Gobleman, C. L., Atkinson, J. P., Pepose, J. S., & Kaplan, H. J. (1993). Differential expression of the complement regulatory proteins in the human eye. *Investigative Ophthalmology & Visual Science*, *34*, 3579–3584.
- Bosco, A., Crish, S. D., Steele, M. R., Romero, C. O., Inman, D. M., Horner, P. J., et al. (2012). Early reduction of microglia activation by irradiation in a model of chronic glaucoma. *PloS One*, *7*, e43602.
- Bosco, A., Steele, M. R., & Vetter, M. L. (2011). Early microglia activation in a mouse model of chronic glaucoma. *The Journal of Comparative Neurology*, *519*, 599–620.
- Bresnick, G. H., Engerman, R., Davis, M. D., de Venecia, G., & Myers, F. L. (1976). Patterns of ischemia in diabetic retinopathy. *Transactions. Section on Ophthalmology. American Academy of Ophthalmology and Otolaryngology*,

81, OP694–709.

- Bringmann, A., Iandiev, I., Pannicke, T., Wurm, A., Hollborn, M., Wiedemann, P., et al. (2009). Cellular signaling and factors involved in Müller cell gliosis: neuroprotective and detrimental effects. *Progress in Retinal and Eye Research*, 28, 423–451.
- Bringmann, A., Pannicke, T., Grosche, J., Francke, M., Wiedemann, P., Skatchkov, S. N., et al. (2006). Müller cells in the healthy and diseased retina. *Progress in Retinal and Eye Research*, 25, 397–424.
- Bringmann, A., Skatchkov, S. N., Pannicke, T., Biedermann, B., Wolburg, H., Orkand, R. K., & Reichenbach, A. (2000). Müller glial cells in anuran retina. *Microscopy Research and Technique*, 50, 384–393.
- Brose, K., & Tessier-Lavigne, M. (2000). Slit proteins: key regulators of axon guidance, axonal branching, and cell migration. *Current Opinion in Neurobiology*, 10, 95–102.
- Brose, K., Bland, K. S., Wang, K. H., Arnott, D., Henzel, W., Goodman, C. S., et al. (1999). Slit proteins bind Robo receptors and have an evolutionarily conserved role in repulsive axon guidance. *Cell*, 96, 795–806.
- Buffo, A., Rolando, C., & Ceruti, S. (2010). Astrocytes in the damaged brain: Molecular and cellular insights into their reactive response and healing potential. *Biochemical Pharmacology*, 79, 77–89.
- Burgoyne, C. F. (2011). A biomechanical paradigm for axonal insult within the optic nerve head in aging and glaucoma. *Experimental Eye Research*, 93,

120–132.

Cahoon, J. M., Olson, P. R., Nielson, S., Miya, T. R., Bankhead, P., McGeown, J.

G., et al. (2014). Acridine orange leukocyte fluorography in mice.

Experimental Eye Research, 120, 15–19.

Camp, A. S., Ruggeri, M., Munguba, G. C., Tapia, M. L., John, S. W. M.,

Bhattacharya, S. K., & Lee, R. K. (2011). Structural correlation between the

nerve fiber layer and retinal ganglion cell loss in mice with targeted

disruption of the Brn3b gene. *Investigative Ophthalmology & Visual Science*,

52, 5226–5232.

Cao, L., & He, C. (2013). Polarization of macrophages and microglia in

inflammatory demyelination. *Neuroscience Bulletin*, 29, 189–198.

Carson, M. J., Doose, J. M., Melchior, B., Schmid, C. D., & Ploix, C. C. (2006).

CNS immune privilege: hiding in plain sight. *Immunological Reviews*, 213,

48–65.

Casson, R. J., Chidlow, G., Wood, J. P., Crowston, J. G., & Goldberg, I. (2012).

Definition of glaucoma: clinical and experimental concepts. *Clinical &*

Experimental Ophthalmology, 40, 341–349.

Chan-Ling, T. (2006). The Blood Retinal Interface: Similarities and Contrasts

with the Blood-Brain Interface. *Blood-Brain Barriers* (Vol. 1, pp. 701–724).

Weinheim, Germany: Wiley-VCH Verlag GmbH & Co. KGaA.

Chan-Ling, T., & Stone, J. (1992). Degeneration of astrocytes in feline

retinopathy of prematurity causes failure of the blood-retinal barrier.

Investigative Ophthalmology & Visual Science, 33, 2148–2159.

Chang, B., Smith, R. S., Hawes, N. L., Anderson, M. G., Zabaleta, A., Savinova, O., et al. (1999). Interacting loci cause severe iris atrophy and glaucoma in DBA/2J mice. *Nature Genetics*, 21, 405–409.

Choi, S. S., Zawadzki, R. J., Lim, M. C., Brandt, J. D., Keltner, J. L., Doble, N., & Werner, J. S. (2011). Evidence of outer retinal changes in glaucoma patients as revealed by ultrahigh-resolution in vivo retinal imaging. *British Journal of Ophthalmology*, 95, 131–141.

Choi, Y. J., Jeoung, J. W., Park, K. H., & Kim, D. M. (2013). Glaucoma Detection Ability of Ganglion Cell-Inner Plexiform Layer Thickness by Spectral-Domain Optical Coherence Tomography in High Myopia Ganglion Cell-Inner Plexiform Layer in High Myopia. *Investigative Ophthalmology & Visual Science*, 54, 2296–2304.

Chong, R. S., & Martin, K. R. (2015). Glial cell interactions and glaucoma. *Current Opinion in Ophthalmology*, 26, 73–77.

Crawford Downs, J., Roberts, M. D., & Sigal, I. A. (2011). Glaucomatous cupping of the lamina cribrosa: A review of the evidence for active progressive remodeling as a mechanism. *Experimental Eye Research*, 93, 133–140.

Cristini, G. (1951). Common pathological basis of the nervous ocular symptoms in chronic glaucoma. *British Journal of Ophthalmology*, 35, 11–20.

- Cunha-Vaz, J. G. (1976). The blood-retinal barriers. *Documenta Ophthalmologica. Advances in Ophthalmology*, 41, 287–327.
- Dallasta, L. M., Pizarov, L. A., Esplen, J. E., Werley, J. V., Moses, A. V., Nelson, J. A., & Achim, C. L. (1999). Blood-brain barrier tight junction disruption in human immunodeficiency virus-1 encephalitis. *The American Journal of Pathology*, 155, 1915–1927.
- Danias, J., Lee, K. C., Zamora, M.-F., Bin Chen, Shen, F., Filippopoulos, T., et al. (2003). Quantitative Analysis of Retinal Ganglion Cell (RGC) Loss in Aging DBA/2NNia Glaucomatous Mice: Comparison with RGC Loss in Aging C57/BL6 Mice. *Investigative Ophthalmology & Visual Science*, 44, 5151–5162.
- de A Moura, A. L., Raza, A. S., Lazow, M. A., De Moraes, C. G., & Hood, D. C. (2012). Retinal ganglion cell and inner plexiform layer thickness measurements in regions of severe visual field sensitivity loss in patients with glaucoma. *Eye*, 26, 1188–1193.
- Diaz-Araya, C. M., Provis, J. M., Penfold, P. L., & Billson, F. A. (1995). Development of microglial topography in human retina. *The Journal of Comparative Neurology*, 363, 53–68.
- Dickson, B. J. (2002). Molecular Mechanisms of Axon Guidance. *Science*, 298, 1959–1964.
- Distler, C., & Dreher, Z. (1996). Glia Cells of the Monkey Retina—II. Müller Cells. *Vision Research*, 36, 2381–2394.

- Do Carmo, A., Ramos, P., Reis, A., Proenca, R., & Cunha-Vaz, J. G. (1998). Breakdown of the Inner and Outer Blood Retinal Barrier in Streptozotocin-Induced Diabetes. *Experimental Eye Research*, *67*, 569–575.
- Dorrell, M. I., Aguilar, E., & Friedlander, M. (2002). Retinal Vascular Development Is Mediated by Endothelial Filopodia, a Preexisting Astrocytic Template and Specific R-Cadherin Adhesion. *Investigative Ophthalmology & Visual Science*, *43*, 3500–3510.
- Dorrell, M. I., Friedlander, M., & Smith, L. E. H. (2007). Retinal Vascular Development. In *Retinal Vascular Disease* (pp. 24–37). Berlin, Heidelberg: Springer Berlin Heidelberg.
- Dreher, Z., Robinson, S. R., & Distler, C. (1992). Müller cells in vascular and avascular retinae: a survey of seven mammals. *The Journal of Comparative Neurology*, *323*, 59–80.
- Drubin, D. G., & Nelson, W. J. (1996). Origins of Cell Polarity. *Cell*, *84*, 335–344.
- Duh, E. J., Yang, H. S., Suzuma, I., Miyagi, M., Youngman, E., Mori, K., et al. (2002). Pigment epithelium-derived factor suppresses ischemia-induced retinal neovascularization and VEGF-induced migration and growth. *Investigative Ophthalmology & Visual Science*, *43*, 821–829.
- Duvdevani, R., Rosner, M., Belkin, M., Sautter, J., Sabel, B. A., & Schwartz, M. (1990). Graded crush of the rat optic nerve as a brain injury model: combining electrophysiological and behavioral outcome. *Restorative*

- Neurology and Neuroscience*, 2, 31–38.
- Eaton, S., & Simons, K. (1995). Apical, basal, and lateral cues for epithelial polarization. *Cell*, 82, 5–8.
- Ebner, A., Casson, R. J., Wood, J. P. M., & Chidlow, G. (2010). Microglial activation in the visual pathway in experimental glaucoma: spatiotemporal characterization and correlation with axonal injury. *Investigative Ophthalmology & Visual Science*, 51, 6448–6460.
- Ehinger, B. (1966). Adrenergic Nerves to the Eye and to Related Structures in Man and in the Cynomolgus Monkey (*Macaca Iru*s). *Investigative Ophthalmology & Visual Science*, 5, 42–52.
- Ehrlich, P. (1885). Das Sauerstoff-Bedürfnis des Organismus: Eine farbenanalytische Studie. Berlin: August Hirschwald.
- Eichler, W., Yafai, Y., Kuhrt, H., Gräter, R., Hoffmann, S., Wiedemann, P., & Reichenbach, A. (2001). Hypoxia: modulation of endothelial cell proliferation by soluble factors released by retinal cells. *NeuroReport*, 12, 4103.
- Eichler, W., Kuhrt, H., Hoffmann, S., Wiedemann, P., & Reichenbach, A. (2000). VEGF release by retinal glia depends on both oxygen and glucose supply. *NeuroReport*, 11, 3533.
- Elschnig, A. (1928). Über Glaukom. *Graefe's Archive for Clinical and Experimental Ophthalmology*, 120, 94–116.
- Fernandes, A., Miller-Fleming, L., & Pais, T. F. (2014). Microglia and inflammation: conspiracy, controversy or control? *Cellular and Molecular*

Life Sciences CMLS, 71, 3969–3985.

Fischer, A. J., & Bongini, R. (2010). Turning Müller glia into neural progenitors in the retina. *Molecular Neurobiology*, 42, 199–209.

Fischer, D., Hauk, T. G., Müller, A., & Thanos, S. (2008). Crystallins of the β/γ -superfamily mimic the effects of lens injury and promote axon regeneration. *Molecular and Cellular Neuroscience*, 37, 471–479.

Fletcher, E. L., Phipps, J. A., & Wilkinson-Berka, J. L. (2005). Dysfunction of retinal neurons and glia during diabetes. *Clinical & Experimental Optometry*, 88, 132–145.

Frank, R. N., Turczyn, T. J., & Das, A. (1990). Pericyte coverage of retinal and cerebral capillaries. *Investigative Ophthalmology & Visual Science*, 31, 999–1007.

Fujikawa, K., Iwata, T., Inoue, K., Akahori, M., Kadotani, H., Fukaya, M., et al. (2010). VAV2 and VAV3 as Candidate Disease Genes for Spontaneous Glaucoma in Mice and Humans. *PloS One*, 5, e9050.

Furuse, M., Fujita, K., Hiragi, T., Fujimoto, K., & Tsukita, S. (1998). Claudin-1 and -2: novel integral membrane proteins localizing at tight junctions with no sequence similarity to occludin. *The Journal of Cell Biology*, 141, 1539–1550.

Furuyoshi, N., Furuyoshi, M., May, C. A., Hayreh, S. S., Alm, A., & Lütjen-Drecoll, E. (2000). Vascular and Glial Changes in the Retrolaminar Optic Nerve in Glaucomatous Monkey Eyes. *Ophthalmologica*, 214, 24–32.

- Garas, A., Vargha, P., & Holló, G. (2011). Diagnostic accuracy of nerve fibre layer, macular thickness and optic disc measurements made with the RTVue-100 optical coherence tomograph to detect glaucoma. *Eye*, *25*, 57–65.
- Garcia-Valenzuela, E., & Sharma, S. C. (1999). Laminar restriction of retinal macrophagic response to optic nerve axotomy in the rat. *Journal of Neurobiology*, *40*, 55–66.
- Garcia-Valenzuela, E., Gorczyca, W., Darzynkiewicz, Z., & Sharma, S. C. (1994). Apoptosis in adult retinal ganglion cells after axotomy. *Journal of Neurobiology*, *25*, 431–438.
- Gardner, T. W. (1995). Histamine, ZO-1 and increased blood-retinal barrier permeability in diabetic retinopathy. *Transactions of the American Ophthalmological Society*, *93*, 583.
- Gardner, T. W., Lieth, E., Khin, S. A., Barber, A. J., Bonsall, D. J., Leshner, T., et al. (1997). Astrocytes increase barrier properties and ZO-1 expression in retinal vascular endothelial cells. *Investigative Ophthalmology & Visual Science*, *38*, 2423–2427.
- Gertig, U., & Hanisch, U.-K. (2014). Microglial diversity by responses and responders. *Frontiers in Cellular Neuroscience*, *8*, 131.
- Giebel, J., Woenckhaus, C., Fabian, M., & Tost, F. (2005). Age-related differential expression of apoptosis-related genes in conjunctival epithelial cells. *Acta Ophthalmologica Scandinavica*, *83*, 471–476.
- Ginhoux, F., Greter, M., Leboeuf, M., Nandi, S., See, P., Gokhan, S., et al.

- (2010). Fate Mapping Analysis Reveals That Adult Microglia Derive from Primitive Macrophages. *Science*, *330*, 841–845.
- Gocht, A., & Löhler, J. (1993). Microenvironmental changes during axonal regrowth in the optic nerve of the myelin deficient rat. Immunocytochemical and ultrastructural observations. *Journal of Neurocytology*, *22*, 461–479.
- Goldblum, D., & Mittag, T. (2002). Prospects for relevant glaucoma models with retinal ganglion cell damage in the rodent eye. *Vision Research*, *42*, 471–478.
- Gong, H., Tripathi, R. C., & Tripathi, B. J. (1996). Morphology of the aqueous outflow pathway. *Microscopy Research and Technique*, *33*, 336–367.
- Gottanka, J., Kuhlmann, A., Scholz, M., Johnson, D. H., & Lütjen-Drecoll, E. (2005). Pathophysiologic Changes in the Optic Nerves of Eyes with Primary Open Angle and Pseudoexfoliation Glaucoma. *Investigative Ophthalmology & Visual Science*, *46*, 4170–4181.
- Gould, D. B., & John, S. W. M. (2002). Anterior segment dysgenesis and the developmental glaucomas are complex traits. *Human Molecular Genetics*, *11*, 1185–1193.
- Gramlich, O. W., Beck, S., Thun und Hohenstein-Blaul, von, N., Boehm, N., Ziegler, A., Vetter, J. M., et al. (2013). Enhanced Insight into the Autoimmune Component of Glaucoma: IgG Autoantibody Accumulation and Pro-Inflammatory Conditions in Human Glaucomatous Retina. *PloS One*, *8*, e57557.
- Gräfe, von, A. (1857). Ueber die Iridectomie bei Glaucom und über den

- glaucomatösen Process. *Archiv Für Ophthalmologie*, 3, 456–555.
- Greenfield, D. S., Siatkowski, R. M., Glaser, J. S., Schatz, N. J., & Parrish, R. K., II. (1998). The cupped disc. *Ophthalmology*, 105, 1866–1874.
- Guan, H., Zu, G., Xie, Y., Tang, H., Johnson, M., Xu, X., et al. (2003). Neuronal repellent Slit2 inhibits dendritic cell migration and the development of immune responses. *Journal of Immunology*, 171, 6519–6526.
- Guthrie, S. (2004). Axon guidance: mice and men need Rig and Robo. *Current Biology : CB*, 14, R632–4.
- Hanisch, U.-K., & Kettenmann, H. (2007). Microglia: active sensor and versatile effector cells in the normal and pathologic brain. *Nature Neuroscience*, 10, 1387–1394.
- Harris, A., Lerner, S. F., Costa, V. P., Martinez, A., & Siesky, B. (2013). Vascular Considerations in Glaucoma: Current Perspective.
- Hasnain, S. S. (2016). The Missing Piece in Glaucoma? *Open Journal of Ophthalmology*, 6, 56–62.
- Hauk, T. G., Leibinger, M., Müller, A., Andreadaki, N., Knippschild, U., & Fischer, D. (2009). Intravitreal application of the Toll-like receptor 2 agonist Pam3Cys stimulates axon regeneration in the mature optic nerve. *Investigative Ophthalmology & Visual Science*, 51, 459–464.
- Hayhow, W. R., Sefton, A., & Webb, C. (1962). Primary optic centers of the rat in relation to the terminal distribution of the crossed and uncrossed optic nerve fibers. *Journal of Comparative Neurology*, 118, 295–321.

- Hayreh, S. S. (1978). Ischemic optic neuropathy. *International Ophthalmology*, *1*, 9–18.
- Hayreh, S. S. (1994). Progress in the understanding of the vascular etiology of glaucoma. *Current Opinion in Ophthalmology*, *5*, 26–35.
- Hayreh, S. S., & Weingeist, T. A. (1980). Experimental occlusion of the central artery of the retina. I. Ophthalmoscopic and fluorescein fundus angiographic studies. *British Journal of Ophthalmology*, *64*, 896–912.
- Hazlett, L. D., & Stein-Streilein, J. (2012). The Eye as a Model for Immune Privilege. In J. Stein-Streilein, *Infection, Immune Homeostasis and Immune Privilege* (pp. 1–29). Basel: Springer Basel.
- Hernandez, M. R., & Pena, J. D. O. (1997). The Optic Nerve Head in Glaucomatous Optic Neuropathy. *Archives of Ophthalmology (Chicago, Ill. : 1960)*, *115*, 389–395.
- Hernandez, M. R., Andrzejewska, W. M., & Neufeld, A. H. (1990). Changes in the Extracellular Matrix of the Human Optic Nerve Head in Primary Open-Angle Glaucoma. *American Journal of Ophthalmology*, *109*, 180–188.
- Hernández, M., Pearce-Kelling, S. E., Rodriguez, F. D., Aguirre, G. D., & Vecino, E. (2010). Altered expression of retinal molecular markers in the canine RPE65 model of Leber congenital amaurosis. *Investigative Ophthalmology & Visual Science*, *51*, 6793–6802.
- Hernández, M., Urcola, J. H., & Vecino, E. (2008). Retinal ganglion cell neuroprotection in a rat model of glaucoma following brimonidine,

- latanoprost or combined treatments. *Experimental Eye Research*, 86, 798–806.
- Herrmann, J. E., Imura, T., Song, B., Qi, J., Ao, Y., Nguyen, T. K., et al. (2008). STAT3 is a critical regulator of astrogliosis and scar formation after spinal cord injury. *The Journal of Neuroscience : the Official Journal of the Society for Neuroscience*, 28, 7231–7243.
- Hickey, T. L., & Spear, P. D. (1976). Retinogeniculate projections in hooded and albino rats: an autoradiographic study. *Experimental Brain Research*, 24, 523–529.
- Hippel, von, P. E. (1910). Über die Schnabelsche Lehre von der Entstehung der glaukomatösen Excavation. *Albrecht Von Graefes Archiv Fur Klinische Und Experimentelle Ophthalmologie*, 74, 101–167.
- Hitchings, R. A., & Spaeth, G. L. (1977). The optic disc in glaucoma II: correlation of the appearance of the optic disc with the visual field. *British Journal of Ophthalmology*, 61, 107–113.
- Hogan, M. J., & Feeney, L. (1963). The Ultrastructure of the Retinal Vessels. III. Vascular-Glial Relationships. *Journal of Ultrastructure Research*, 49, 47–64.
- Hogan, M. J., Moschini, G. B., & Zardi, O. (1971). Effects of Toxoplasma gondii toxin on the rabbit eye. *American Journal of Ophthalmology*, 72, 733–742.
- Hollows, F. C., & Graham, P. A. (1966). Intra-ocular pressure, glaucoma, and glaucoma suspects in a defined population. *British Journal of Ophthalmology*, 50, 570–586.

- Howell, G. R., Macalinao, D. G., Sousa, G. L., Walden, M., Soto, I., Kneeland, S. C., et al. (2011). Molecular clustering identifies complement and endothelin induction as early events in a mouse model of glaucoma. *The Journal of Clinical Investigation*, *121*, 1429–1444.
- Howell, G. R., Soto, I., Zhu, X., Ryan, M., Macalinao, D. G., Sousa, G. L., et al. (2012). Radiation treatment inhibits monocyte entry into the optic nerve head and prevents neuronal damage in a mouse model of glaucoma. *The Journal of Clinical Investigation*, *122*, 1246–1261.
- Huang, T. L., Chang, C. H., Lin, K. H., Sheu, M. M., & Tsai, R. K. (2011). Lack of protective effect of local administration of triamcinolone or systemic treatment with methylprednisolone against damages caused by optic nerve crush in rats. *Experimental Eye Research*, *92*, 112–119.
- Hughes, S., Yang, H., & Chan-Ling, T. (2000). Vascularization of the Human Fetal Retina: Roles of Vasculogenesis and Angiogenesis. *Investigative Ophthalmology & Visual Science*, *41*, 1217–1228.
- Ikram, M. K., de Voogd, S., Wolfs, R. C. W., Hofman, A., Breteler, M. M. B., Hubbard, L. D., & de Jong, P. T. V. M. (2005). Retinal vessel diameters and incident open-angle glaucoma and optic disc changes: the Rotterdam study. *Investigative Ophthalmology & Visual Science*, *46*, 1182–1187.
- Imai, Y., Iбата, I., Ito, D., Ohsawa, K., & Kohsaka, S. (1996). A Novel Geneiba1 in the Major Histocompatibility Complex Class III Region Encoding an EF Hand Protein Expressed in a Monocytic Lineage. *Biochemical and*

- Biophysical Research Communications*, 224, 855–862.
- Ito, D., Imai, Y., Ohsawa, K., Nakajima, K., Fukuuchi, Y., & Kohsaka, S. (1998). Microglia-specific localisation of a novel calcium binding protein, Iba1. *Brain Research. Molecular Brain Research*, 57, 1–9.
- Ito, Y. A., & Walter, M. A. (2013). Genomics and anterior segment dysgenesis: a review. *Clinical & Experimental Ophthalmology*, 42, 13–24.
- Jaeger, E. (1858). Ueber glaucom und seine Heilung durch Iridectomie. Nabu Press.
- Jakobs, T. C., Libby, R. T., Ben, Y., John, S. W. M., & Masland, R. H. (2005). Retinal ganglion cell degeneration is topological but not cell type specific in DBA/2J mice. *The Journal of Cell Biology*, 171, 313–325.
- Jamieson, R. V., Perveen, R., Kerr, B., Carette, M., Yardley, J., Héon, E., et al. (2002). Domain disruption and mutation of the bZIP transcription factor, MAF, associated with cataract, ocular anterior segment dysgenesis and coloboma. *Human Molecular Genetics*, 11, 33–42.
- Jin, M., Barron, E., He, S., Ryan, S. J., & Hinton, D. R. (2002). Regulation of RPE Intercellular Junction Integrity and Function by Hepatocyte Growth Factor. *Investigative Ophthalmology & Visual Science*, 43, 2782–2790.
- Jin, M., Chen, Y., He, S., Ryan, S. J., & Hinton, D. R. (2004). Hepatocyte growth factor and its role in the pathogenesis of retinal detachment. *Investigative Ophthalmology & Visual Science*, 45, 323–329.
- John, S. W., Smith, R. S., Savinova, O. V., Hawes, N. L., Chang, B., Turnbull, D.,

- et al. (1998). Essential iris atrophy, pigment dispersion, and glaucoma in DBA/2J mice. *Investigative Ophthalmology & Visual Science*, *39*, 951–962.
- Johnson, E. C., Deppmeier, L. M., Wentzien, S. K., Hsu, I., & Morrison, J. C. (2000). Chronology of optic nerve head and retinal responses to elevated intraocular pressure. *Investigative Ophthalmology & Visual Science*, *41*, 431–442.
- Johnson, E. C., Morrison, J. C., Farrell, S., Deppmeier, L., Moore, C. G., & McGinty, M. R. (1996). The effect of chronically elevated intraocular pressure on the rat optic nerve head extracellular matrix. *Experimental Eye Research*, *62*, 663–674.
- Jonas, J. B., Nguyen, X. N., & Naumann, G. O. (1989). Parapapillary retinal vessel diameter in normal and glaucoma eyes. I. Morphometric data. *Investigative Ophthalmology & Visual Science*, *30*, 1599–1603.
- Jones, C. A., London, N. R., Chen, H., Park, K. W., Sauvaget, D., Stockton, R. A., et al. (2008). Robo4 stabilizes the vascular network by inhibiting pathologic angiogenesis and endothelial hyperpermeability. *Nature Medicine*, *14*, 448–453.
- Jones, C. A., Nishiya, N., London, N. R., Zhu, W., Sorensen, L. K., Chan, A. C., et al. (2009). Slit2–Robo4 signalling promotes vascular stability by blocking Arf6 activity. *Nature*, *461*, 1331.
- Jung, K. I., Jeon, S., & Park, C. K. (2016). Lamina Cribrosa Depth is Associated With the Cup-to-Disc Ratio in Eyes With Large Optic Disc Cupping and Cup-

- to-Disc Ratio Asymmetry. *Journal of Glaucoma*, 25, e536–e545.
- Junglas, B., Kuespert, S., Seleem, A. A., Struller, T., Ullmann, S., Bösl, M., et al. (2012). Connective Tissue Growth Factor Causes Glaucoma by Modifying the Actin Cytoskeleton of the Trabecular Meshwork. *The American Journal of Pathology*, 180, 2386–2403.
- Kalvin, N. H., & Hamasaki, D. I. (1966). Experimental glaucoma in monkeys: I. Relationship between intraocular pressure and cupping of the optic disc and cavernous atrophy of the optic nerve. *Archives of Ophthalmology*, 76, 82–93.
- Kamat, S. S., Gregory, M. S., & Pasquale, L. R. (2016). The Role of the Immune System in Glaucoma: Bridging the Divide Between Immune Mechanisms in Experimental Glaucoma and the Human Disease. *Seminars in Ophthalmology*, 31, 147–154.
- Kanellis, J., Garcia, G. E., Li, P., Parra, G., Wilson, C. B., Rao, Y., et al. (2004). Modulation of inflammation by slit protein in vivo in experimental crescentic glomerulonephritis. *The American Journal of Pathology*, 165, 341–352.
- Kaur, C., Foulds, W., & Ling, E. (2008). Blood–retinal barrier in hypoxic ischaemic conditions: Basic concepts, clinical features and management. *Progress in Retinal and Eye Research*, 27, 622–647.
- Kaur, C., Sivakumar, V., & Foulds, W. S. (2006). Early response of neurons and glial cells to hypoxia in the retina. *Investigative Ophthalmology & Visual Science*, 47, 1126–1141.
- Kawasaki, R., Wang, J. J., Rohtchina, E., Lee, A. J., Wong, T. Y., & Mitchell, P.

- (2013). Retinal Vessel Caliber Is Associated with the 10-year Incidence of Glaucoma. *Ophthalmology*, *120*, 84–90.
- Kettenmann, H., & Verkhratsky, A. (2008). Neuroglia: the 150 years after. *Trends in Neurosciences*, *31*, 653–659.
- Kidd, M. N., & O'Connor, M. (1985). Progression of field loss after trabeculectomy: a five-year follow-up. *British Journal of Ophthalmology*, *69*, 827–831.
- Kidd, T., Bland, K. S., & Goodman, C. S. (1999). Slit Is the Midline Repellent for the Robo Receptor in *Drosophila*. *Cell*, *96*, 785–794.
- Kidd, T., Brose, K., Mitchell, K. J., Fetter, R. D., Tessier-Lavigne, M., Goodman, C. S., & Tear, G. (1998). Roundabout controls axon crossing of the CNS midline and defines a novel subfamily of evolutionarily conserved guidance receptors. *Cell*, *92*, 205–215.
- Kiel, J. W. (2011). The Ocular Circulation. *Colloquium Series on Integrated Systems Physiology: From Molecule to Function*, *3*, 1–81.
- Kim, J. H., Kim, J.-H., Park, J. A., Lee, S.-W., Kim, W.-J., Yu, Y.-S., & Kim, K.-W. (2006). Blood-neural Barrier: Intercellular Communication at Glial-Vascular Interface. *Journal of Biochemistry and Molecular Biology*, *39*, 339–345.
- Kivelä, T., & Uusitalo, M. (1998). Structure, development and function of cytoskeletal elements in non-neuronal cells of the Human Eye. *Progress in Retinal and Eye Research*, *17*, 385–428.

- Koeberle, P. D., & Ball, A. K. (1998). Effects of GDNF on retinal ganglion cell survival following axotomy. *Vision Research*, *38*, 1505–1515.
- Kolb, H. (1979). The inner plexiform layer in the retina of the cat: electron microscopic observations. *Journal of Neurocytology*, *8*, 295–329.
- Kreutzberg, G. W. (1996). Microglia: a sensor for pathological events in the CNS. *Trends in Neurosciences*, *19*, 312–318.
- Kuehn, M. H., Kim, C. Y., Ostojic, J., Bellin, M., Alward, W. L. M., Stone, E. M., et al. (2006). Retinal synthesis and deposition of complement components induced by ocular hypertension. *Experimental Eye Research*, *83*, 620–628.
- Kupfer, C., & Kaiser-Kupfer, M. I. (1979). Observations on the development of the anterior chamber angle with reference to the pathogenesis of congenital glaucomas. *American Journal of Ophthalmology*, *88*, 424–426.
- Kupfer, C., & Kaiser-Kupfer, M. I. (1977). New hypothesis of developmental anomalies of the anterior chamber associated with glaucoma. *Transactions of the Ophthalmological Societies of the United Kingdom*, *98*, 213–215.
- LaGrange, F., & Beauvieux, J. (1925). Anatomie de l'excavation glaucomateuse. *Arch F Ophth*, *42*, 129–140.
- Lamb, T. D., Collin, S. P., & Pugh, E. N. (2007). Evolution of the vertebrate eye: opsins, photoreceptors, retina and eye cup. *Nature Reviews Neuroscience*, *8*, 960–976.
- Laquis, S., Chaudhary, P., & Sharma, S. C. (1998). The patterns of retinal ganglion cell death in hypertensive eyes. *Brain Research*, *784*, 100–104.

- Laties, A. M. (1967). Central retinal artery innervation. Absence of adrenergic innervation to the intraocular branches. *Archives of Ophthalmology (Chicago, Ill. : 1960)*, *77*, 405–409.
- Lei, Y., Garrahan, N., Hermann, B., Becker, D. L., Hernandez, M. R., Boulton, M. E., & Morgan, J. E. (2008). Quantification of retinal transneuronal degeneration in human glaucoma: a novel multiphoton-DAPI approach. *Investigative Ophthalmology & Visual Science*, *49*, 1940–1945.
- Leino, R. L., Gerhart, D. Z., Duelli, R., Enerson, B. E., & Drewes, L. R. (2001). Diet-induced ketosis increases monocarboxylate transporter (MCT1) levels in rat brain. *Neurochemistry International*, *38*, 519–527.
- Leon, S., Yin, Y., Nguyen, J., Irwin, N., & Benowitz, L. I. (2000). Lens injury stimulates axon regeneration in the mature rat optic nerve. *The Journal of Neuroscience*, *20*, 4615–4626.
- Leske, M. C. (1983). The epidemiology of open-angle glaucoma: a review. *American Journal of Epidemiology*, *118*, 166–191.
- Leske, M. C., & Rosenthal, J. (1979). Epidemiologic aspects of open-angle glaucoma. *American Journal of Epidemiology*, *109*, 250–272.
- Leung, H., Wang, J. J., Rohtchina, E., Tan, A. G., Wong, T. Y., Klein, R., et al. (2003). Relationships between age, blood pressure, and retinal vessel diameters in an older population. *Investigative Ophthalmology & Visual Science*, *44*, 2900–2904.
- Levin, L. A. (2001). Models of neural injury. *Journal of Glaucoma*, *10*, S19–21.

- Ley, K., Laudanna, C., Cybulsky, M. I., & Nourshargh, S. (2007). Getting to the site of inflammation: the leukocyte adhesion cascade updated. *Nature Reviews Immunology*, *7*, 678–689.
- Liao, B., Zhao, W., Beers, D. R., Henkel, J. S., & Appel, S. H. (2012). Transformation from a neuroprotective to a neurotoxic microglial phenotype in a mouse model of ALS. *Experimental Neurology*, *237*, 147–152.
- Liesegang, T. J. (1996). Glaucoma: changing concepts and future directions. *Mayo Clinic Proceedings*, *71*, 689–694.
- Lin, B., Wang, S. W., & Masland, R. H. (2004). Retinal ganglion cell type, size, and spacing can be specified independent of homotypic dendritic contacts. *Neuron*, *43*, 475–485.
- Liu, S., Li, Z.-W., Weinreb, R. N., Xu, G., Lindsey, J. D., Ye, C., et al. (2012). Tracking Retinal Microgliosis in Models of Retinal Ganglion Cell Damage. *Investigative Ophthalmology & Visual Science*, *53*, 6254–6262.
- Liu, Y., & Vollrath, D. (2004). Reversal of mutant myocilin non-secretion and cell killing: implications for glaucoma. *Human Molecular Genetics*, *13*, 1193–1204.
- London, N. R., & Li, D. Y. (2011). Robo4-dependent Slit signaling stabilizes the vasculature during pathologic angiogenesis and cytokine storm. *Current Opinion in Hematology*, *18*, 186–190.
- London, N. R., Zhu, W., Bozza, F. A., Smith, M. C. P., Greif, D. M., Sorensen, L. K., et al. (2010). Targeting Robo4-Dependent Slit Signaling to Survive the

- Cytokine Storm in Sepsis and Influenza. *Science Translational Medicine*, 2, 23ra19–23ra19.
- Lotan, M., Solomon, A., Ben-Bassat, S., & Schwartz, M. (1994). Cytokines Modulate the Inflammatory Response and Change Permissiveness to Neuronal Adhesion in Injured Mammalian Central Nervous System. *Experimental Neurology*, 126, 284–290.
- Lütjen-Drecoll, E. (2006). Choroidal innervation in primate eyes. *Experimental Eye Research*, 82, 357–361.
- Lye-Barthel, M., Sun, D., & Jakobs, T. C. (2013). Morphology of astrocytes in a glaucomatous optic nerve. *Investigative Ophthalmology & Visual Science*, 54, 909–917.
- Lynch, S., Yanagi, G., DelBono, E., & Wiggs, J. L. (2002). DNA sequence variants in the tyrosinase-related protein 1 (TYRP1) gene are not associated with human pigmentary glaucoma. *Molecular Vision*, 8, 127–129.
- Malhotra, A., Minja, F. J., Crum, A., & Burrowes, D. (2011). Ocular Anatomy and Cross-Sectional Imaging of the Eye. *Seminars in Ultrasound, CT and MRI*, 32, 2–13.
- Mao, M., Hedberg-Buenz, A., Koehn, D., John, S. W. M., & Anderson, M. G. (2011). Anterior segment dysgenesis and early-onset glaucoma in nee mice with mutation of *Sh3pxd2b*. *Investigative Ophthalmology & Visual Science*, 52, 2679–2688.
- Martino, V. B., Sabljic, T., Deschamps, P., Green, R. M., Akula, M., Peacock, E.,

- et al. (2016). Conditional deletion of AP-2 β in mouse cranial neural crest results in anterior segment dysgenesis and early-onset glaucoma. *Disease Models & Mechanisms*, 9, 849–861.
- Mason, C. A., Sparrow, N., & Lincoln, D. W. (1977). Structural features of the retinohypothalamic projection in the rat during normal development. *Brain Research*, 132, 141–148.
- May, C. A., & Mittag, T. (2004). Neuronal nitric oxide synthase (nNOS) positive retinal amacrine cells are altered in the DBA/2NNia mouse, a murine model for angle-closure glaucoma. *Journal of Glaucoma*, 13, 496–499.
- May, C. A., & Lütjen-Drecoll, E. (2002). Morphology of the murine optic nerve. *Investigative Ophthalmology & Visual Science*, 43, 2206–2212.
- May, C. A., & Lütjen-Drecoll, E. (2004). Choroidal ganglion cell changes in human glaucomatous eyes. *Journal of Glaucoma*, 13, 389–395.
- Medawar, P. B. (1948). Immunity to homologous grafted skin. III. The fate of skin homografts transplanted to the brain, to subcutaneous tissue, and to the anterior chamber of the eye. *British Journal of Experimental Pathology*, 29, 58–69.
- Mey, J., & Thanos, S. (2000). Development of the visual system of the chick. *Brain Research Reviews*, 32, 343–379.
- Midwood, K., Sacre, S., Piccinini, A. M., Inglis, J., Trebaul, A., Chan, E., et al. (2009). Tenascin-C is an endogenous activator of Toll-like receptor 4 that is essential for maintaining inflammation in arthritic joint disease. *Nature*

Medicine, 15, 774–780.

Mitic, L. L., & Anderson, J. M. (1998). Molecular architecture of tight junctions.

Annual Review of Physiology, 60, 121–142.

Miyahara, T., Kikuchi, T., Akimoto, M., Kurokawa, T., Shibuki, H., &

Yoshimura, N. (2003). Gene microarray analysis of experimental glaucomatous retina from cynomolgous monkey. *Investigative Ophthalmology & Visual Science*, 44, 4347–4356.

Miyamoto, K., Hiroshiba, N., Tsujikawa, A., & Ogura, Y. (1998). In vivo

demonstration of increased leukocyte entrapment in retinal microcirculation of diabetic rats. *Investigative Ophthalmology & Visual Science*, 39, 2190–2194.

Mo, J.-S., Anderson, M. G., Gregory, M., Smith, R. S., Savinova, O. V., Serreze,

D. V., et al. (2003). By Altering Ocular Immune Privilege, Bone Marrow-derived Cells Pathogenically Contribute to DBA/2J Pigmentary Glaucoma. *The Journal of Experimental Medicine*, 197, 1335–1344.

Moore, D. L., & Goldberg, J. L. (2010). Four steps to optic nerve regeneration.

Journal of Neuro-Ophthalmology, 30, 347–360.

Morrison, J. C., Moore, C. G., Deppmeier, L. M., Gold, B. G., Meshul, C. K., &

Johnson, E. C. (1997). A rat model of chronic pressure-induced optic nerve damage. *Experimental Eye Research*, 64, 85–96.

Nadal-Nicolas, F. M., Jimenez-Lopez, M., Sobrado-Calvo, P., Nieto-Lopez, L.,

Canovas-Martinez, I., Salinas-Navarro, M., et al. (2009). Brn3a as a Marker

- of Retinal Ganglion Cells: Qualitative and Quantitative Time Course Studies in Naïve and Optic Nerve–Injured Retinas. *Investigative Ophthalmology & Visual Science*, 50, 3860–3868.
- Nadarajah, B. (2003). Neuronal Migration in the Developing Cerebral Cortex: Observations Based on Real-time Imaging. *Cerebral Cortex*, 13, 607–611.
- Nag, S. (Ed.). (2011). *The Blood-Brain and Other Neural Barriers*. New York: Springer.
- Nair, K. S., Hmani-Aifa, M., Ali, Z., Kearney, A. L., Ben Salem, S., Macalinao, D. G., et al. (2011). Alteration of the serine protease PRSS56 causes angle-closure glaucoma in mice and posterior microphthalmia in humans and mice. *Nature Genetics*, 43, 579–584.
- Nakahara, T., Mori, A., Kurauchi, Y., Sakamoto, K., & Ishii, K. (2013). Neurovascular Interactions in the Retina: Physiological and Pathological Roles. *Journal of Pharmacological Sciences*, 123, 79–84.
- Nakazawa, T. (2016). Ocular Blood Flow and Influencing Factors for Glaucoma. *The Asia-Pacific Journal of Ophthalmology*, 5, 38–44.
- Nataf, S., Stahel, P. F., Davoust, N., & Barnum, S. R. (1999). Complement anaphylatoxin receptors on neurons: new tricks for old receptors? *Trends in Neurosciences*, 22, 397–402.
- Neufeld, A. H. (1999). Nitric oxide: a potential mediator of retinal ganglion cell damage in glaucoma. *Survey of Ophthalmology*, 43 Suppl 1, S129–35.
- Neufeld, A. H., Hernandez, M. R., & Gonzalez, M. (1997). Nitric oxide synthase

- in the human glaucomatous optic nerve head. *Archives of Ophthalmology (Chicago, Ill. : 1960)*, 115, 497–503.
- Newman, E. A., Frambach, D. A., & Odette, L. L. (1984). Control of extracellular potassium levels by retinal glial cell K⁺ siphoning. *Science*, 225, 1174–1175.
- Nguyen-Ba-Charvet, K. (2001). Sensory Axon Response to Substrate-Bound Slit2 Is Modulated by Laminin and Cyclic GMP. *Molecular and Cellular Neuroscience*, 17, 1048–1058.
- Niclou, S. P., Jia, L., & Raper, J. A. (2000). Slit2 is a repellent for retinal ganglion cell axons. *Journal of Neuroscience*, 20, 4962–4974.
- Nikolskaya, T., Nikolsky, Y., Serebryiskaya, T., Zvereva, S., Sviridov, E., Dezso, Z., et al. (2009). Network analysis of human glaucomatous optic nerve head astrocytes. *BMC Medical Genomics*, 2, 1.
- Nimmerjahn, A., Kirchhoff, F., & Helmchen, F. (2005). Resting Microglial Cells Are Highly Dynamic Surveillants of Brain Parenchyma in Vivo. *Science*, 308, 1314–1318.
- Nork, T. M., Ver Hoeve, J. N., Poulsen, G. L., Nickells, R. W., Davis, M. D., Weber, A. J., et al. (2000). Swelling and loss of photoreceptors in chronic human and experimental glaucomas. *Archives of Ophthalmology (Chicago, Ill. : 1960)*, 118, 235–245.
- Ohlsson, M., Bellander, B.-M., Langmoen, I. A., & Svensson, M. (2003). Complement Activation following Optic Nerve Crush in the Adult Rat. *Journal of Neurotrauma*, 20, 895–904.

- Ohlsson, M., Westerlund, U., Langmoen, I. A., & Svensson, M. (2004). Methylprednisolone treatment does not influence axonal regeneration or degeneration following optic nerve injury in the adult rat. *Journal of Neuro-Ophthalmology*, *24*, 11–18.
- Oliver, G., & Gruss, P. (1997). Current views on eye development. *Trends in Neurosciences*, *20*, 415–421.
- Osborne, N. N., Ugarte, M., Chao, M., Chidlow, G., Bae, J. H., Wood, J. P. M., & Nash, M. S. (1999). Neuroprotection in Relation to Retinal Ischemia and Relevance to Glaucoma. *Survey of Ophthalmology*, *43*, S102–S128.
- Ozaki, H., Seo, M.-S., Ozaki, K., Yamada, H., Yamada, E., Okamoto, N., et al. (2000). Blockade of Vascular Endothelial Cell Growth Factor Receptor Signaling Is Sufficient to Completely Prevent Retinal Neovascularization. *The American Journal of Pathology*, *156*, 697–707.
- Palczewski, K. (2012). Chemistry and biology of vision. *Journal of Biological Chemistry*, *287*, 1612–1619.
- Panda, S., & Jonas, J. B. (1992). Decreased photoreceptor count in human eyes with secondary angle-closure glaucoma. *Investigative Ophthalmology & Visual Science*, *33*, 2532–2536.
- Paques, M., Tadayoni, R., Sercombe, R., Laurent, P., Genevois, O., Gaudric, A., & Vicaut, E. (2003). Structural and Hemodynamic Analysis of the Mouse Retinal Microcirculation. *Investigative Ophthalmology & Visual Science*, *44*, 4960–4967.

- Park, K. W., Morrison, C. M., Sorensen, L. K., Jones, C. A., Rao, Y., Chien, C.-B., et al. (2003). Robo4 is a vascular-specific receptor that inhibits endothelial migration. *Developmental Biology*, *261*, 251–267.
- Pederson, J. E. (2006). Fluid physiology of the subretinal space. In C. P. Wilkinson, *Retina* (4 ed., Vol. 3, pp. 1955–1968). Elsevier Mosby.
- Pekny, M., & Nilsson, M. (2005). Astrocyte activation and reactive gliosis. *Glia*, *50*, 427–434.
- Petty, M. A., & Lo, E. H. (2002). Junctional complexes of the blood-brain barrier: permeability changes in neuroinflammation. *Progress in Neurobiology*, *68*, 311–323.
- Piper, M., & Little, M. (2003). Movement through Slits: cellular migration via the Slit family. *BioEssays : News and Reviews in Molecular, Cellular and Developmental Biology*, *25*, 32–38.
- Plange, N., Kaup, M., Huber, K., Remky, A., & Arend, O. (2006). Fluorescein filling defects of the optic nerve head in normal tension glaucoma, primary open-angle glaucoma, ocular hypertension and healthy controls. *Ophthalmic & Physiological Optics : the Journal of the British College of Ophthalmic Opticians (Optometrists)*, *26*, 26–32.
- Plange, N., Kaup, M., Weber, A., Remky, A., & Arend, O. (2004). Fluorescein Filling Defects and Quantitative Morphologic Analysis of the Optic Nerve Head in Glaucoma. *Archives of Ophthalmology (Chicago, Ill. : 1960)*, *122*, 195–201.

- Prasad, A., Qamri, Z., Wu, J., & Ganju, R. K. (2007). Slit-2/Robo-1 modulates the CXCL12/CXCR4-induced chemotaxis of T cells. *Journal of Leukocyte Biology*, *82*, 465–476.
- Qu, J., & Jakobs, T. C. (2013). The Time Course of Gene Expression during Reactive Gliosis in the Optic Nerve. *PloS One*, *8*, e67094.
- Quigley, H. A. (1999). Neuronal death in glaucoma. *Progress in Retinal and Eye Research*, *18*, 39–57.
- Quigley, H. A., & Broman, A. T. (2006). The number of people with glaucoma worldwide in 2010 and 2020. *British Journal of Ophthalmology*, *90*, 262–267.
- Quigley, H. A., & Green, W. R. (1979). The Histology of Human Glaucoma Cupping and Optic Nerve Damage: Clinicopathologic Correlation in 21 Eyes. *Ophthalmology*, *86*, 1803–1827.
- Quigley, H. A., Addicks, E. M., Green, W. R., & Maumenee, A. E. (1981). Optic Nerve Damage in Human Glaucoma: II. The Site of Injury and Susceptibility to Damage. *Archives of Ophthalmology (Chicago, Ill. : 1960)*, *99*, 635–649.
- Quigley, H. A., Hohman, R. M., Addicks, E. M., & Green, W. R. (1984). Blood vessels of the glaucomatous optic disc in experimental primate and human eyes. *Investigative Ophthalmology & Visual Science*, *25*, 918–931.
- Ramírez, A. I., Salazar, J. J., de Hoz, R., Rojas, B., Gallego, B. I., Salobarra-García, E., et al. (2015). Macro- and microglial responses in the fellow eyes contralateral to glaucomatous eyes. In *New Trends in Basic and Clinical Research of Glaucoma: A Neurodegenerative Disease of the Visual System*,

Part A (Vol. 220, pp. 155–172). Elsevier.

- Ransohoff, R. M., & Brown, M. A. (2012). Innate immunity in the central nervous system. *The Journal of Clinical Investigation*, *122*, 1164–1171.
- Reddy, D. V., & Kinsey, V. E. (1960). Composition of the vitreous humor in relation to that of plasma and aqueous humors. *Archives of Ophthalmology (Chicago, Ill. : 1960)*, *63*, 715–720.
- Reichenbach, A., Hagen, E., Schippel, K., Brückner, G., Reichelt, W., & Leibnitz, L. (1988). Cytotopographical specialization of enzymatically isolated rabbit retinal Müller (glial) cells: structure, ultrastructure, and 3H-ouabain binding sites. *Zeitschrift Für Mikroskopisch-Anatomische Forschung*, *102*, 897–912.
- Reichenbach, A., Siegel, A., Rickmann, M., Wolff, J. R., Noone, D., & Robinson, S. R. (1995). Distribution of Bergmann glial somata and processes: implications for function. *Journal Für Hirnforschung*, *36*, 509–517.
- Reichenbach, A., Stolzenburg, J. U., Eberhardt, W., Chao, T. I., Dettmer, D., & Hertz, L. (1993). What do retinal müller (glial) cells do for their neuronal 'small siblings'? *Journal of Chemical Neuroanatomy*, *6*, 201–213.
- Reichenbach, A., Wurm, A., Pannicke, T., Iandiev, I., Wiedemann, P., & Bringmann, A. (2007). Müller cells as players in retinal degeneration and edema. *Graefe's Archive for Clinical and Experimental Ophthalmology*, *245*, 627–636.
- Rezaie, T., Child, A., Hitchings, R., Brice, G., Miller, L., Coca-Prados, M., et al. (2002). Adult-Onset Primary Open-Angle Glaucoma Caused by Mutations in

- Optineurin. *Science*, 295, 1077–1079.
- Ricklin, D., Hajishengallis, G., Yang, K., & Lambris, J. D. (2010). Complement: a key system for immune surveillance and homeostasis. *Nature Immunology*, 11, 785–797.
- Ridet, J. L., Privat, A., Malhotra, S. K., & Gage, F. H. (1997). Reactive astrocytes: cellular and molecular cues to biological function. *Trends in Neurosciences*, 20, 570–577.
- Ritter, M. R., Aguilar, E., Banin, E., Scheppke, L., Uusitalo-Järvinen, H., & Friedlander, M. (2005). Three-dimensional in vivo imaging of the mouse intraocular vasculature during development and disease. *Investigative Ophthalmology & Visual Science*, 46, 3021–3026.
- Rizzolo, L. J. (1997). Polarity and the development of the outer blood-retinal barrier. *Histology and Histopathology*, 12, 1057–1067.
- Rodriguez-Boulan, E., & Nelson, W. J. (1989). Morphogenesis of the polarized epithelial cell phenotype. *Science*, 245, 718–725.
- Rosenzweig, S., Raz-Prag, D., Nitzan, A., Galron, R., Paz, M., Jeserich, G., et al. (2010). Sema-3A indirectly disrupts the regeneration process of goldfish optic nerve after controlled injury. *Graefe's Archive for Clinical and Experimental Ophthalmology*, 248, 1423–1435.
- Rothberg, J. M., & Artavanis-Tsakonas, S. (1992). Modularity of the slit protein. Characterization of a conserved carboxy-terminal sequence in secreted proteins and a motif implicated in extracellular protein interactions. *Journal*

of Molecular Biology, 227, 367–370.

- Rothberg, J. M., Hartley, D. A., Walther, Z., & Artavanis-Tsakonas, S. (1988). slit: An EGF-homologous locus of *D. melanogaster* involved in the development of the embryonic central nervous system. *Cell*, 55, 1047–1059.
- Rothberg, J. M., Jacobs, J. R., Goodman, C. S., & Artavanis-Tsakonas, S. (1990). slit: an extracellular protein necessary for development of midline glia and commissural axon pathways contains both EGF and LRR domains. *Genes & Development*, 4, 2169–2187.
- Rungger-Brändle, E., Dosso, A. A., & Leuenberger, P. M. (2000). Glial reactivity, an early feature of diabetic retinopathy. *Investigative Ophthalmology & Visual Science*, 41, 1971–1980.
- Russ, P. K., Davidson, M. K., Hoffman, L. H., & Haselton, F. R. (1998). Partial characterization of the human retinal endothelial cell tight and adherens junction complexes. *Investigative Ophthalmology & Visual Science*, 39, 2479–2485.
- Sagaties Farmer, M. J., Schwartz, B., & Takamoto, T. (1997). Computerized measurement of the three-dimensional distribution of optic disc pallor. *Current Eye Research*, 16, 1096–1101.
- Sagaties, M. J., Raviola, G., Schaeffer, S., & Miller, C. (1987). The structural basis of the inner blood-retina barrier in the eye of *Macaca mulatta*. *Investigative Ophthalmology & Visual Science*, 28, 2000–2014.
- Saint-Geniez, M., & D'amore, P. A. (2004). Development and pathology of the

- hyaloid, choroidal and retinal vasculature. *International Journal of Developmental Biology*, 48, 1045–1058.
- Sarthy, V., & Ripps, H. (2002). Role in retinal pathophysiology. In C. Blakemore, (pp. 181–215). New York: Kluwer Academic/Plenum Publishers.
- Schnabel, J. (1905). I. Die Entwicklungsgeschichte der glaukomatösen Exkavation. *Ophthalmologica*, 14, 1–22.
- Schnitzer, J. (1987). Retinal astrocytes: their restriction to vascularized parts of the mammalian retina. *Neuroscience Letters*, 78, 29–34.
- Schulz, C., Perdiguero, E. G., Chorro, L., Szabo-Rogers, H., Cagnard, N., Kierdorf, K., et al. (2012). A Lineage of Myeloid Cells Independent of Myb and Hematopoietic Stem Cells. *Science*, 336, 86–90.
- Schwartz, J. P., & Nishiyama, N. (1994). Neurotrophic factor gene expression in astrocytes during development and following injury. *Brain Research Bulletin*, 35, 403–407.
- Schwartz, J. T., Reuling, F. H., & Garrison, R. J. (1975). Acquired cupping of the optic nerve head in normotensive eyes. *British Journal of Ophthalmology*, 59, 216–222.
- Schwartz, M., & Shechter, R. (2010). Systemic inflammatory cells fight off neurodegenerative disease. *Nature Reviews. Neurology*, 6, 405–410.
- Shastry, B. S. (1997). Signal transduction in the retina and inherited retinopathies. *Cellular and Molecular Life Sciences CMLS*, 53, 419–429.
- Shechter, R., London, A., & Schwartz, M. (2013). Orchestrated leukocyte

- recruitment to immune-privileged sites: absolute barriers versus educational gates. *Nature Reviews Immunology*, *13*, 206–218.
- Shepro, D., & Morel, N. M. (1993). Pericyte physiology. *The FASEB Journal*, *7*, 1031–1038.
- Sherchan, P., Huang, L., Wang, Y., Akyol, O., Tang, J., & Zhang, J. H. (2016). Recombinant Slit2 attenuates neuroinflammation after surgical brain injury by inhibiting peripheral immune cell infiltration via Robo1-srGAP1 pathway in a rat model. *Neurobiology of Disease*, *85*, 164–173.
- Shiau, C. E., & Bronner-Fraser, M. (2009). N-cadherin acts in concert with Slit1-Robo2 signaling in regulating aggregation of placode-derived cranial sensory neurons. *Development (Cambridge, England)*, *136*, 4155–4164.
- Shields, M. B., Buckley, E., Klintworth, G. K., & Thresher, R. (1985). Axenfeld-Rieger syndrome. A spectrum of developmental disorders. *Survey of Ophthalmology*, *29*, 387–409.
- Shimazawa, M., Yamashima, T., Agarwal, N., & Hara, H. (2005). Neuroprotective effects of minocycline against in vitro and in vivo retinal ganglion cell damage. *Brain Research*, *1053*, 185–194.
- Sims, D. E. (1991). Recent advances in pericyte biology--implications for health and disease. *The Canadian Journal of Cardiology*, *7*, 431–443.
- Sisk, D. R., & Kuwabara, T. (1985). Histologic changes in the inner retina of albino rats following intravitreal injection of monosodiuml-glutamate. *Graefe's Archive for Clinical and Experimental Ophthalmology*, *223*, 250–

258.

- Smerdon, D. (2000). Anatomy of the eye and orbit. *Current Anaesthesia & Critical Care*, *11*, 286–292.
- Snodderly, D. M., Weinhaus, R. S., & Choi, J. C. (1992). Neural-vascular relationships in central retina of macaque monkeys (*Macaca fascicularis*). *Journal of Neuroscience*, *12*, 1169–1193.
- Sofroniew, M. V., & Vinters, H. V. (2010). Astrocytes: biology and pathology. *Acta Neuropathologica*, *119*, 7–35.
- Sohn, J. H., Kaplan, H. J., Suk, H. J., Bora, P. S., & Bora, N. S. (2000). Chronic low level complement activation within the eye is controlled by intraocular complement regulatory proteins. *Investigative Ophthalmology & Visual Science*, *41*, 3492–3502.
- Sommer, A., Tielsch, J. M., Katz, J., Quigley, H. A., Gottsch, J. D., Javitt, J., & Singh, K. (1991). Relationship Between Intraocular Pressure and Primary Open Angle Glaucoma Among White and Black Americans: The Baltimore Eye Survey. *Archives of Ophthalmology (Chicago, Ill. : 1960)*, *109*, 1090–1095.
- Soto, I., & Howell, G. R. (2014). The Complex Role of Neuroinflammation in Glaucoma. *Cold Spring Harbor Perspectives in Medicine*, *4*, a017269–a017269.
- Soto, I., Oglesby, E., Buckingham, B. P., Son, J. L., Roberson, E. D. O., Steele, M. R., et al. (2008). Retinal Ganglion Cells Downregulate Gene Expression

- and Lose Their Axons within the Optic Nerve Head in a Mouse Glaucoma Model. *Journal of Neuroscience*, 28, 548–561.
- Stasi, K., Nagel, D., Yang, X., Wang, R.-F., Ren, L., Podos, S. M., et al. (2006). Complement Component 1Q (C1Q) Upregulation in Retina of Murine, Primate, and Human Glaucomatous Eyes. *Investigative Ophthalmology & Visual Science*, 47, 1024–1029.
- Steinsapir, K. D., Goldberg, R. A., Sinha, S., & Hovda, D. A. (2000). Methylprednisolone exacerbates axonal loss following optic nerve trauma in rats. *Restorative Neurology and Neuroscience*, 17, 157–163.
- Stone, E. M., Fingert, J. H., Alward, W. L. M., Nguyen, T. D., Polansky, J. R., Sunden, S. L. F., et al. (1997). Identification of a Gene That Causes Primary Open Angle Glaucoma. *Science*, 275, 668–670.
- Stone, J., Itin, A., Alon, T., Pe'er, J., Gnessin, H., Chan-Ling, T., & Keshet, E. (1995). Development of retinal vasculature is mediated by hypoxia-induced vascular endothelial growth factor (VEGF) expression by neuroglia. *Journal of Neuroscience*, 15, 4738–4747.
- Streilein, J. W. (2003). Ocular immune privilege: therapeutic opportunities from an experiment of nature. *Nature Reviews Immunology*, 3, 879–889.
- Streit, W. J., Walter, S. A., & Pennell, N. A. (1999). Reactive microgliosis. *Progress in Neurobiology*, 57, 563–581.
- Sun, D., Qu, J., & Jakobs, T. C. (2013). Reversible reactivity by optic nerve astrocytes. *Glia*, 61, 1218–1235.

- Tanigami, H., Okamoto, T., Yasue, Y., & Shimaoka, M. (2012). Astroglial Integrins in the Development and Regulation of Neurovascular Units. *Pain Research and Treatment*, 2012, 1–10.
- Taylor, A. W. (2007). Ocular immunosuppressive microenvironment. *Chemical Immunology and Allergy*, 92, 71–85.
- Taylor, S., Calder, C. J., Albon, J., Erichsen, J. T., Boulton, M. E., & Morgan, J. E. (2011). Involvement of the CD200 receptor complex in microglia activation in experimental glaucoma. *Experimental Eye Research*, 92, 338–343.
- Templeton, J. P., & Geisert, E. E. (2012). A practical approach to optic nerve crush in the mouse. *Molecular Vision*.
- Tezel, G., & Wax, M. B. (2004). The immune system and glaucoma. *Current Opinion in Ophthalmology*, 15, 80.
- Tezel, G., Tezel, G., Thornton, I. L., Thornton, I. L., Tong, M. G., Tong, M. G., et al. (2012). Immunoproteomic Analysis of Potential Serum Biomarker Candidates in Human Glaucoma. *Investigative Ophthalmology & Visual Science*, 53, 8222–8231.
- Tezel, G., Yang, X., Luo, C., Kain, A. D., Powell, D. W., Kuehn, M. H., & Kaplan, H. J. (2010). Oxidative Stress and the Regulation of Complement Activation in Human Glaucoma. *Investigative Ophthalmology & Visual Science*, 51, 5071–5082.
- Tham, Y. C., Li, X., Wong, T. Y., Quigley, H. A., Aung, T., & Cheng, C.-Y.

- (2014). Global Prevalence of Glaucoma and Projections of Glaucoma Burden through 2040: A Systematic Review and Meta-Analysis. *Ophthalmology*, *121*, 2081–2090.
- Thanos, S., Mey, J., & Wild, M. (1993). Treatment of the adult retina with microglia-suppressing factors retards axotomy-induced neuronal degradation and enhances axonal regeneration in vivo and in vitro. *Journal of Neuroscience*, *13*, 455–466.
- Thanos, S., Moore, S., & Hong, Y.-M. (1996). Retinal microglia. *Progress in Retinal and Eye Research*, *15*, 331–361.
- Thompson, H., Camand, O., Barker, D., & Erskine, L. (2006). Slit proteins regulate distinct aspects of retinal ganglion cell axon guidance within dorsal and ventral retina. *Journal of Neuroscience*, *26*, 8091.
- Tole, S., Mukovozov, I. M., Huang, Y. W., Magalhaes, M. A. O., Yan, M., Crow, M. R., et al. (2009). The axonal repellent, Slit2, inhibits directional migration of circulating neutrophils. *Journal of Leukocyte Biology*, *86*, 1403–1415.
- Tout, S., Chan-Ling, T., Holländer, H., & Stone, J. (1993). The role of müller cells in the formation of the blood-retinal barrier. *Neuroscience*, *55*, 291–301.
- Trainor, P. A., & Tam, P. P. (1995). Cranial paraxial mesoderm and neural crest cells of the mouse embryo: co-distribution in the craniofacial mesenchyme but distinct segregation in branchial arches. *Development (Cambridge, England)*, *121*, 2569–2582.
- Tretiach, M., Madigan, M. C., Wen, L., & Gillies, M. C. (2005). Effect of Müller

- cell co-culture on in vitro permeability of bovine retinal vascular endothelium in normoxic and hypoxic conditions. *Neuroscience Letters*, 378, 160–165.
- Tsai, R. K., Chang, C. H., & Wang, H. Z. (2008). Neuroprotective effects of recombinant human granulocyte colony-stimulating factor (G-CSF) in neurodegeneration after optic nerve crush in rats. *Experimental Eye Research*, 87, 242–250.
- Tserentsoodol, N., Shin, B.-C., Suzuki, T., & Takata, K. (1998). Colocalization of tight junction proteins, occludin and ZO-1, and glucose transporter GLUT1 in cells of the blood-ocular barrier in the mouse eye. *Histochemistry and Cell Biology*, 110, 543–551.
- Tsujikawa, A., & Ogura, Y. (2012). Evaluation of leukocyte-endothelial interactions in retinal diseases. *Ophthalmologica*, 227, 68–79.
- Tsukita, S., Furuse, M., & Itoh, M. (2001). Multifunctional strands in tight junctions. *Nature Reviews. Molecular Cell Biology*, 2, 285–293.
- Uga, S., & Smelser, G. K. (1973). Electron microscopic study of the development of retinal Müllerian cells. *Investigative Ophthalmology*, 12, 295–307.
- Vecino, E., Rodriguez, F. D., Ruzafa, N., Pereiro, X., & Sharma, S. C. (2016). Glia-neuron interactions in the mammalian retina. *Progress in Retinal and Eye Research*, 51, 1–40.
- Vidal-Sanz, M., Salinas-Navarro, M., Nadal-Nicolás, F. M., Alarcón-Martínez, L., Valiente-Soriano, F. J., Miralles de Imperial, J., et al. (2012). Understanding glaucomatous damage: Anatomical and functional data from ocular

- hypertensive rodent retinas. *Progress in Retinal and Eye Research*, 31, 1–27.
- Vinores, S. A., Derevjanik, N. L., Ozaki, H., Okamoto, N., & Campochiaro, P. A. (1999). Cellular mechanisms of blood-retinal barrier dysfunction in macular edema. *Documenta Ophthalmologica*, 97, 217–228.
- Vrabec, F. (1976). Glaucomatous cupping of the human optic disk. *Albrecht Von Graefes Archiv Fur Klinische Und Experimentelle Ophthalmologie*, 198, 223–234.
- Wang, L., Cioffi, G. A., Cull, G., Dong, J., & Fortune, B. (2002). Immunohistologic Evidence for Retinal Glial Cell Changes in Human Glaucoma. *Investigative Ophthalmology & Visual Science*, 43, 1088–1094.
- Wang, S., Xu, L., Wang, Y., Wang, Y., & Jonas, J. B. (2007). Retinal vessel diameter in normal and glaucomatous eyes: the Beijing eye study. *Clinical & Experimental Ophthalmology*, 35, 800–807.
- Waring, G. O., Rodrigues, M. M., & Laibson, P. R. (1975). Anterior chamber cleavage syndrome. A stepladder classification. *Survey of Ophthalmology*, 20, 3–27.
- Watanabe, T., & Raff, M. C. (1988). Retinal astrocytes are immigrants from the optic nerve. *Nature*, 332, 834–837.
- Wax, M. B., Barrett, D. A., & Pestronk, A. (1994). Increased incidence of paraproteinemia and autoantibodies in patients with normal-pressure glaucoma. *American Journal of Ophthalmology*, 117, 561–568.
- Weitzman, M., Bayley, E. B., & Naik, U. P. (2008). Robo4: a guidance receptor

- that regulates angiogenesis. *Cell Adhesion & Migration*, 2, 220–222.
- Werner, E. B., Drance, S. M., & Schulzer, M. (1977). Trabeculectomy and the Progression of Glaucomatous Visual Field Loss. *Archives of Ophthalmology (Chicago, Ill. : 1960)*, 95, 1374–1377.
- Wiggs, J. L. (2013). Glaucoma. In *EMERY AND RIMOIN'S PRINCIPLES AND PRACTICE OF MEDICAL GENETICS E-DITION - 3 VOLUME SET, 5TH EDITION* (6 ed., pp. 1–15). Elsevier.
- Williams, C. D., & Rizzolo, L. J. (1997). Remodeling of junctional complexes during the development of the outer blood-retinal barrier. *The Anatomical Record*, 249, 380–388.
- Willis, C. L., Leach, L., Clarke, G. J., Nolan, C. C., & Ray, D. E. (2004). Reversible disruption of tight junction complexes in the rat blood-brain barrier, following transitory focal astrocyte loss. *Glia*, 48, 1–13.
- Wilson, C. A., Berkowitz, B. A., Funatsu, H., Metrikin, D. C., Harrison, D. W., Lam, M. K., & Sonkin, P. L. (1995). Blood-retinal barrier breakdown following experimental retinal ischemia and reperfusion. *Experimental Eye Research*, 61, 547–557.
- Wilson, M. R. (1997). The Myth of "21". *Journal of Glaucoma*, 6, 75.
- Wohl, S. G., Schmeer, C. W., Witte, O. W., & Isenmann, S. (2010). Proliferative Response of Microglia and Macrophages in the Adult Mouse Eye after Optic Nerve Lesion. *Investigative Ophthalmology & Visual Science*, 51, 2686–2696.

- Wu, J. Y., Feng, L., Park, H. T., Havlioglu, N., Wen, L., Tang, H., et al. (2001). The neuronal repellent Slit inhibits leukocyte chemotaxis induced by chemotactic factors. *Nature*, *410*, 952.
- Xu, Q., Qaum, T., & Adamis, A. P. (2001). Sensitive Blood–Retinal Barrier Breakdown Quantitation Using Evans Blue. *Investigative Ophthalmology & Visual Science*, *42*, 789–794.
- Yang, H., Williams, G., Downs, J. C., Sigal, I. A., Roberts, M. D., Thompson, H., & Burgoyne, C. F. (2011). Posterior (Outward) Migration of the Lamina Cribrosa and Early Cupping in Monkey Experimental Glaucoma. *Investigative Ophthalmology & Visual Science*, *52*, 7109–7121.
- Yang, H., Williams, G., Downs, J., Sigal, I., Roberts, M., Grimm, J., et al. (2010). Optic Nerve Head (ONH) Lamina Cribrosa Insertion Migration and Pialization in Early Non-Human Primate (NHP) Experimental Glaucoma. *Investigative Ophthalmology & Visual Science*, *51*, 1631–1631.
- Ye, B.-Q., Geng, Z. H., Ma, L., & Geng, J.-G. (2010). Slit2 regulates attractive eosinophil and repulsive neutrophil chemotaxis through differential srGAP1 expression during lung inflammation. *Journal of Immunology*, *185*, 6294–6305.
- Ye, X. D., Laties, A. M., & Stone, R. A. (1990). Peptidergic innervation of the retinal vasculature and optic nerve head. *Investigative Ophthalmology & Visual Science*, *31*, 1731–1737.
- Yin, Y., Henzl, M. T., Lorber, B., Nakazawa, T., Thomas, T. T., Jiang, F., et al.

- (2006). Oncomodulin is a macrophage-derived signal for axon regeneration in retinal ganglion cells. *Nature Neuroscience*, *9*, 843–852.
- Yu, P. K., Cringle, S. J., & Yu, D.-Y. (2014). Correlation between the radial peripapillary capillaries and the retinal nerve fibre layer in the normal human retina. *Experimental Eye Research*, *129*, 83–92.
- Zallen, J. A., Yi, B. A., & Bargmann, C. I. (1998). The Conserved Immunoglobulin Superfamily Member SAX-3/Robo Directs Multiple Aspects of Axon Guidance in *C. elegans*. *Cell*, *92*, 217–227.
- Zhang, C., & Tso, M. O. M. (2003). Characterization of activated retinal microglia following optic axotomy. *Journal of Neuroscience Research*, *73*, 840–845.
- Zhang, Y., & Stone, J. (1997). Role of astrocytes in the control of developing retinal vessels. *Investigative Ophthalmology & Visual Science*, *38*, 1653–1666.
- Zhao, D. Y. (2002). Peripapillary microvascular study of human eyes with primary open-angle glaucoma. *Annals of Ophthalmology*, *34*, 215–221.
- Zhao, H., Anand, A. R., & Ganju, R. K. (2014). Slit2–Robo4 Pathway Modulates Lipopolysaccharide-Induced Endothelial Inflammation and Its Expression Is Dysregulated during Endotoxemia. *Journal of Immunology*, *192*, 385–393.
- Zheng, L., Gong, B., Hatala, D. A., & Kern, T. S. (2007). Retinal Ischemia and Reperfusion Causes Capillary Degeneration: Similarities to Diabetes. *Investigative Ophthalmology & Visual Science*, *48*, 361–367.

Zimmerman, L. E., de Venecia, G., & Hamasaki, D. I. (1967). Pathology of the optic nerve in experimental acute glaucoma. *Investigative Ophthalmology*, 6, 109–125.